Tools for Evaluating Fault Detection and Diagnostic Methods for HVAC Secondary Systems

A Thesis

Submitted to the Faculty

Of

Drexel University

By

Shokouh Pourarian

in partial fulfillment of the
requirements for the degree
of
Doctor of Philosophy
December, 2015

Dissertation approval form

ACKNOWLEDGMENTS

Ostensibly, this dissertation represents the consummation of my PhD work. In reality, it represents thirty years of patient and thoughtful support from family, friends and all my teachers and mentors. In this regard I would like to acknowledge all who contributed to this journey for such a long time. In particular, I must express my appreciation to Dr. Jin Wen who granted me the opportunity to pursue the doctoral degree at Drexel University. In the last five years, she has emerged as a trusted guide and invaluable mentor for this work.

To Dr. Daniel A. Veronica, Dr. Anthony José Kearsley and Dr. Amanda Pertzborn from National Institute of Standard and Technology: I extend special appreciation for their dependable, serious, and accurate guidance, input and support during the accomplishment of this work.

To members of my committee, Dr. Amanda Pertzborn (National Institute of Standard and Technology), Dr. Xiaohui Zhou (Iowa Energy Center), Dr. Patrick L. Gurian and Dr. Michael Waring (Drexel- Civil, Architectural and Environmental Engineering): thank you for reviewing my dissertation and your valuable inputs.

The developed testbeds in this thesis were validated using experimental data provided by Iowa Energy Center. I would like to thank Dr. Xiaohui Zhou and Dr. Ran Liu from this center for their support, help as well as patience in answering the questions.

I would like to express my gratitude to the U.S. National Institute of Standard and Technology for financially sponsoring my researches and providing this wonderful opportunity to pursue my PhD.

I appreciate all my BSEG lab mates specially Xiwang Li for his generous collaboration and Jared Langevin for his perpetual company and encouragement. I am

particularly indebted to many wonderful and intimate friends who make my stay in beloved Philadelphia an enjoyable, pleasant and unforgettable experience.

I must express my deepest gratitude and warmest appreciation to my parents, Mohamadali Pourarian and Nasrin Razzagh Rostami and to my sisters, Dr. Shohreh, Shahla and Nasim for the tireless support and unconditional love offered in forms that only a family can provide. I am eternally indebted to them for their continuous and unwavering source of energy. I am further grateful to Mehdi Mohebi-Moghadam and Jila Shapouri, my parents-in-law, who managed to help me and taking care of my little son during the last months of my PhD.

Finally, to my lovely husband, Mahyar Mohebi-Moghadam: Indeed, I owe this work to you. You have been the continuous source of energy, enthusiasm, intellectual support and studied advice, most particularly appreciated at those fragile moments when the path appeared the most difficult and the obstacles insurmountable.

Shokouh Pourarian,

December 2015

Drexel University, Philadelphia, PA

TABLE OF CONTENTS

LIST OF TABLES

LIST OF FIGURES

ABSTRACT

Tools for Evaluating Fault Detection and Diagnostic Methods for HVAC Secondary Systems

Shokouh Pourarian
Jin Wen, advisor, PhD

Although modern buildings are using increasingly sophisticated energy management and control systems that have tremendous control and monitoring capabilities, building systems routinely fail to perform as designed. More advanced building control, operation, and automated fault detection and diagnosis (AFDD) technologies are needed to achieve the goal of net-zero energy commercial buildings. Much effort has been devoted to develop such technologies for primary heating ventilating and air conditioning (HVAC) systems, and some secondary systems. However, secondary systems, such as fan coil units and dual duct systems, although widely used in commercial, industrial, and multifamily residential buildings, have received very little attention. This research study aims at developing tools that could provide simulation capabilities to develop and evaluate advanced control, operation, and AFDD technologies for these less studied secondary systems.

In this study, HVACSIM+ is selected as the simulation environment. Besides developing dynamic models for the above-mentioned secondary systems, two other issues related to the HVACSIM+ environment are also investigated. One issue is the nonlinear equation solver used in HVACSIM+ (Powell's Hybrid method in subroutine SNSQ). It has been found from several previous research projects (ASRHAE RP 825 and 1312) that SNSQ is especially unstable at the beginning of a simulation and sometimes unable to converge to a solution. Another issue is related to

the zone model in the HVACSIM+ library of components. Dynamic simulation of secondary HVAC systems unavoidably requires an interacting zone model which is systematically and dynamically interacting with building surrounding. Therefore, the accuracy and reliability of the building zone model affects operational data generated by the developed dynamic tool to predict HVAC secondary systems function. The available model does not simulate the impact of direct solar radiation that enters a zone through glazing and the study of zone model is conducted in this direction to modify the existing zone model.

In this research project, the following tasks are completed and summarized in this report:

1. Develop dynamic simulation models in the HVACSIM+ environment for common fan coil unit and dual duct system configurations. The developed simulation models are able to produce both fault-free and faulty operational data under a wide variety of faults and severity levels for advanced control, operation, and AFDD technology development and evaluation purposes;
2. Develop a model structure, which includes the grouping of blocks and superblocks, treatment of state variables, initial and boundary conditions, and selection of equation solver, that can simulate a dual duct system efficiently with satisfactory stability;
3. Design and conduct a comprehensive and systematic validation procedure using collected experimental data to validate the developed simulation models under both fault-free and faulty operational conditions;
4. Conduct a numerical study to compare two solution techniques: Powell's Hybrid (PH) and Levenberg-Marquardt (LM) in terms of their robustness and accuracy.

5. Modification of the thermal state of the existing building zone model in HVACSIM+ library of component. This component is revised to consider the transmitted heat through glazing as a heat source for transient building zone load prediction

In this report, literature, including existing HVAC dynamic modeling environment and models, HVAC model validation methodologies, and fault modeling and validation methodologies, are reviewed. The overall methodologies used for fault free and fault model development and validation are introduced. Detailed model development and validation results for the two secondary systems, i.e., fan coil unit and dual duct system are summarized. Experimental data mostly from the Iowa Energy Center Energy Resource Station are used to validate the models developed in this project. Satisfactory model performance in both fault free and fault simulation studies is observed for all studied systems.

INTRODUCTION

Over the past three decades, various computer software applications have been developed to simulate the dynamic interactions between the shell, internal loads, ambient conditions, and the heating, ventilating, and air conditioning (HVAC) systems of buildings. Building and HVAC system simulation techniques provide convenient and low-cost tools for predicting energy and environment performance of building and HVAC system in their design, commissioning, operation and management (Lebrun et al, 1999 & Kusuda et al, 1999), and testing and evaluating the control strategies and algorithm in energy management and control systems (Lebrun et al, 1993 & Wang et al, 1999).

Software packages offering dynamic simulations of the actual physics of buildings are clearly distinct from software able only to simulate fictitious equilibrium quantities presumed to be static for significant periods of time, as in the hourly averaged simulations used to evaluate energy conservation options. By generating values that realistically simulate the transient physical quantities observable by real system instrumentation, dynamic simulation software serves as a platform -or, as called here, a tool- for research and development of HVAC operations, optimal controls, and automated fault detection and diagnosis (AFDD). Faulty operation of HVAC systems might be caused by component degradation, malfunction or improper control strategy, leading to waste of energy and lack of comfort for building occupants. Early detection and diagnosis of faults through AFDD technologies development may result in energy savings as much as 30% (Ardehali et al, 2003). To achieve the goal of realizing net-zero energy commercial building by 2025, advanced building control, operation and AFDD technologies need to be developed and tested.

Various faults including design faults, installation faults, sensor faults, equipment faults and control faults often exist in the building HVAC system and associated energy management and control systems (EMCSs) without being noticed for a long time. A study of 60 commercial buildings found that more than one half of them suffered from control problems, 40 percent had problems with the HVAC equipment and one third had sensors that were not operating properly (PECI 1998). Such faults cause increased energy consumption and utility cost, uncomfortable and unhealthy indoor environment, as well as equipment failures. The problems associated with identifying and isolating faults in HVAC systems are more severe than those occur in the most process applications (Katipamula et al, 2001; Dexter and Ngo, 2001). Dynamic simulation of HVAC systems thus not only opens ways to synthesize operational data under different control strategies, but also makes it possible to predict the symptoms associated with various faulty conditions and their effects on system performance and occupant comfort.

This study aims at developing necessary tools for building performance, control, operation and AFDD technologies development and evaluation. Its focus is mostly on dynamic model development for secondary HVAC systems which have not been studied thoroughly although are widely used, such as fan coil unit, (FCU) and dual duct system. For this purpose, the HVACSIM+ (Park et al, 1985) dynamic simulation software package developed by the U.S. National Institute of Standards and Technology (NIST) is used. It employs a unique hierarchical computation approach. HVACSIM+ is a component based modelling package which is comprised of a collection of programs belonging to one of three categories: pre-processing, simulation, and post-processing. During the pre-processing stage, a simulation work file is created by the interactive front-end program. The essence of HVACSIM+ lies

in MODSIM known as the solver. The MODSIM program consists of a main drive program and many subprograms for input/output operation, block and state variable status control, integrating differential equations, solving a system of simultaneous non-linear algebraic equations, component models (HVAC, controls, building shell, etc.), and supporting utilities (Clark and May, 1985). The simulation work file is constructed in the hierarchical structure, comprising super blocks, blocks, and units for the purpose of saving the required time for simulation execution while retaining the highest level of accuracy.

Individual simulation elements (called “units”) are first grouped by the user into “blocks” for simultaneous solution. Blocks are then similarly grouped into “superblocks” for simultaneous solution. Each superblock is a numerically independent subsystem of the overall simulation; its time evolution and internal solutions are propagated independently of other superblocks. The time step in a superblock is a variable that is automatically and continuously adjusted by a solver subroutine to maintain numerical stability. Each individual unit is an instance of a specifically serialized equipment or device “TYPE” (written all caps, to distinguish from the common use of the word), requiring the user to link inputs and outputs between all units and assign unit parameters. A subroutine solves the resulting sets of nonlinear algebraic and differential equations to determine system state at each time step (Clark, 1985). This hierarchical approach makes even complex simulations solvable. HVACSIM+ has been experimentally validated and improved (Dexter et al., 1987), and proven appropriate for fault modelling (Bushby et al. 2001, Dexter, 1995, and Peitsman et al. 1997). Fault symptoms of varying severity are represented by a fault flag system that changes the values of relevant unit parameters.

A subroutine (SNSQ) with its associated subprograms is used in MODSIM to solve the resulting sets of nonlinear algebraic and differential equations to determine system state at each time step (Clark, 1985). The method used in the SNSQ is based on Powel's Hybrid (PH) method (Park et.al 1986). During the simulation of the mentioned secondary systems, it was found out that in some cases, PH method fails to converge to a solution. Thus it is necessary to examine alternatives to PH or to investigate problem formulation. Efficiently, robustly and accurately solving large sets of structured, non-linear algebraic and differential equations is computationally expensive requirement for dynamic simulation of building energy systems. In this study, a straight-forward replacement of PH with the commonly employed Levenberg-Marquardt method (LM) is suggested to be investigated for the cases with convergence failure of PH method.

Another problem specifically observed during FCU and dual duct system model validation which needs to be addressed in this research study is the 2C3R zone model available in the HVACSIM+ library of components. The dynamic simulation of FCU and dual duct system unavoidably requires an interacting zone model including systemic interactions with the building's surroundings. Therefore the accuracy and dynamic of modelled zone will affect dynamic response of HVAC systems. The 2C3R model for zone does not simulate well the impact of direct solar radiation that enters a zone through glazing. This causes a discrepancy between the model predicted results and experimental data during the validation process. Besides the mentioned purposes, this research will address modification of building zone model considering the direct solar radiation through transparent surfaces of the building.

More specifically, this research study has been conducted in three directions:

Firstly, it seeks to develop and validate a dynamic simulation tool for FCU and dual duct system under faulty and fault-free conditions;

Secondly, it seeks to study the solver of HVACSIM+ to replace the existing one with a more robust, reliable and efficient method;

Thirdly, it seeks to modify the existing building zone model in HVACSIM+ library of component to include the radiation heat transfer received by the zone through the glazing.

In support of the proposed general aims, five chapters have been developed to describe the tasks and taken directions as follows:

Chapter 1: provides the literature related to this project and the overall methodology used to simulate and validate the dynamic model.

Chapter 2: describes development and validation procedure of dynamic simulation model in HVACSIM+ environment for common FCU configuration. The developed model is capable of generating operational data under fault-free and replicate fault symptoms under various faults with different severities.

Chapter 3: describes development and validation procedure of dynamic simulation model in HVACSIM+ environment for dual duct double fan system. The developed model is capable of generating operational data under fault-free and replicate fault symptoms under various faults with different severities.

Chapter 4: describes the conducted study to investigate and comparison of the efficiency, robustness and accuracy of the two commonly employed solution methods, PH & LM.

Chapter 5: describes the required modifications to the building zone model to include the transmitted radiation energy through the glazing and to improve its accuracy.

Conclusion and summary: summarizes the work and key outcomes of the work presented in this dissertation. Furthermore, it proposes some direction for future works to enrich the studies and researches accomplished in this project.

1. CHAPTER ONE: PROBLEM STATEMENT

1.1 Background

Although modern buildings are using increasingly sophisticated Energy Management and Control Systems (EMCSs) that have tremendous control and monitoring capabilities, building systems routinely fail to perform as designed (CEC, 1999). Various faults including design faults, installation faults, sensor faults, equipment faults and control faults often exist in the building Heating, Ventilation and Air Conditioning (HVAC) system and associated EMCS without being noticed for long periods of time. A study of 60 commercial buildings found that more than one half of them suffered from control problems, 40 percent had problems with the HVAC equipment and one-third had sensors that were not operating properly (PECI, 1998). Such faults cause increased energy consumption and utility cost, uncomfortable and unhealthy indoor environment, as well as equipment failures.

Early detection of faults prevents energy wastage and equipment damage. The problems associated with identifying and isolating faults in HVAC systems are more severe than those occur in most process control applications (Katipamula et al., 2001; Dexter and Ngo, 2001). The behavior of HVAC plants and buildings are more difficult to predict. Accurate numerical and mathematical models cannot be produced because most of HVAC designs are unique and financial considerations restrict the amount of time and effort that can be put in deriving a model. Detailed design information is seldom available, and measured data from actual plant are often inadequate indicator of the overall behavior, since test signals cannot be injected during normal operation due to the occupant discomfort and possibly the equipment damage. Another problem is that many variables cannot be measures accurately, and some measurements, needed for proper modelling, are not even available. Finally, the

issue of fault diagnosis can be problematic since several faults may have the same symptoms.

Extensive research has been conducted during the past decades in the AFDD area to identify different technologies that are suitable for building HVAC systems (a good review is provided by Katipamula et al., 2001, 2005a, and 2005b). Physical redundancy, heuristics or statistical bands, including control chart approach, pattern recognition techniques, and innovation-based methods or hypothesis testing on physical models are usually used to detect faults. Information flow charts, expert systems, semantic networks, artificial neural network, and parameter estimation methods are commonly used to isolate faults. Heuristics rules and probabilistic approaches are used for evaluate faults. Based on the research, a series of AFDD products including software and hardware products have been or being developed. However, efficiently evaluating different AFDD technologies and products is not an easy task, and is well appreciated by professionals in this area.

To assist in the development and evaluation of chiller system AFDD methods, American Society of Heating Refrigeration and Air-conditioning Engineers (ASHRAE) 1043-RP "Fault Detection and Diagnostic Requirement and Evaluation Tools for Chillers" (Comstock and Braun,1999a,b; Bendapudi and Braun, 2002) produced several experimental data sets of chiller operation under fault-free as well as faulty data (under different faults and four severity levels each) as well as a dynamic simulation model for centrifugal chillers. A similar project, ASHRAE 1312-RP "Tools for Evaluating Fault Detection and Diagnostic Methods for Air-Handling Units" (Li and Wen, 2010, Li et al., 2010, and Wen, 2010), produced extensive experimental data sets and a dynamic simulation testbed, which was developed using HVACSIM+ environment, for single duct dual fan air handling unit (AHU) AFDD

study. Several studies conducted by National Institute of Standard and Technology (NIST) (Schein and Bushby, 2005 and Schein, 2006) generated simulation programs (using HVACSIM+ environment) and laboratory and field data for variable air volume terminal system AFDD study.

However, for other typical secondary systems, such as dual duct system and fan coil unit, there are very limited AFDD development and evaluation tools. Very limited experimental data exist for developing these tools as well. These typical but less studied secondary systems are widely used in the commercial, industrial, hospital and multifamily residential buildings. The operation of these secondary systems greatly affects building energy consumption and occupant comfort. To achieve the goal of marketable net zero energy buildings by 2025, dynamic simulation models to help developing and evaluating control, operation and AFDD strategies for these typical but less studied secondary systems are needed. Moreover, such dynamic simulation models need to be properly validated with experimental data for both fault-free and faulty operation.

Dynamic simulation using the developed model for the proposed secondary HVAC systems unavoidably requires an interacting building zone model, including systemic interactions with the building's surroundings. Building zone models are fundamental tools used to investigate the thermal performance and energy use of a HVAC system. Real time monitoring of building thermal performance and control play a significant role in operating HVAC equipment. The dynamics of temperature evolution in a building is one of the most important aspects of the overall building dynamics. The complexity in the dynamics of temperature evolution comes from the thermal interaction among rooms and the outside. This interaction can be either through conduction through various building elements such as walls, roof, ceiling,

floor, etc., or through convective air exchange among rooms and radiation from different surfaces. Besides, solar radiation is transmitted through transparent windows and is absorbed by the internal surfaces of the building. Heat is also added to the space due to the presence of human occupants and the use of lights and equipment.

Therefore, to capture the dynamic of HVAC secondary systems under fault-free and faulty conditions the building zone model accuracy and effectiveness is a matter of importance. Currently several building simulators exist which are able to model most of the physical phenomena affecting buildings (Crawley et al., 2008). However, these simulators need a substantial computational time to perform a long run simulation. When the user requires running a large number of simulations, these tools might not be ideal, as their use might render the study unfeasible due to prohibitive overall computational times. Some authors have faced this and used surrogate models to reduce the computational times (such as Magnier et al., 2010) but others have used simpler simulators to represent building zones (such as Coley et al., 2002; Kampf et al., 2009 or Kershaw et al., 2011). This research study not only briefly investigates the effectiveness of the models for building thermal response but also attempt to modify the available model for building zone in HVACSIM+ library of component. The available building zone model in the HVACSIM+ library does not consider transmitted thermal radiation through the glazing. The large discrepancy of the simulation results from experimental data during the FCU and dual duct model validation especially for the transient seasons certify the deficiency of this model.

The essence of simulation is to solve the differential and algebraic equations resulted from mathematical modelling of the building and HVAC equipment. Efficiently, robustly and accurately solving large sets of structured, non-linear algebraic and differential equations is one of the most computationally expensive

steps in the dynamic simulation of building energy systems. In this study, besides development and validation of dynamic models for the three proposed secondary systems, the efficiency, robustness and accuracy of two commonly employed solution methods are compared. More specifically, the following tasks performed in this project:

1 Develop dynamic simulation models in the HVACSIM+ environment for common fan coil unit and dual duct system configurations. The developed simulation models is able to produce both fault-free and faulty operational data under a wide variety of faults and severity levels for advanced control, operation, and AFDD technology development and evaluation purposes;

2 Analyze experimental data provided by Energy Resource Center Iowa Energy Center (ERS) to validate the developed simulation models under both fault-free and faulty conditions;

3 Design and conduct a comprehensive and systematic validation procedure using provided experimental data to validate the developed simulation models under both fault-free and faulty operational conditions;

4 Conduct a study to compare two solution methods for solving the system of nonlinear algebraic equations arising from the developed dynamic models in the HVACSIM+ environment;

5 Modify the existing building zone model in HVACSIM+ component library in order to consider the transmitted part of solar radiation through glazing as a heat source received by the zone ; and

6 Document the model development and validation process

1.2 Literature review

The scope of this research is not to develop or evaluate AFDD methods but to develop and validate tools that are capable of predicting performance data for the proposed HVAC systems under fault-free condition and replicating faulty symptoms under various faulty conditions with different fault severities. In addition, the robustness and accuracy of the available solution technique, namely Powell's hybrid, in the HVACSIM+ is studied against a common method, namely Levenberg-Marquardt. This research also focuses on modelling thermal response of building zones and the issues associated with the current model in the HVACSIM+ library of components. Hence the literature review focuses on:

1) Existing HVAC dynamic modelling environment
2) Existing dynamic models for fan coil unit and dual duct system
3) HVAC dynamic model validation
4) Fault modelling and validation
5) Existing dynamic models for thermal performance of building zone model
6) Various solution techniques employed in common building energy performance tools

1.2.1 Existing HVAC dynamic modelling environment

Various building HVAC simulators have been developed during the past decade for different purposes (Reddy et al., 2005): 1) Simplified Spreadsheet Programs, such as BEST (Waltz, 2000); 2) Simplified System Simulation Method, such as SEAM and ASEAM (Knebel, 1983 and ASEAM, 1991); 3) Fixed Schematic Hourly Simulation Program, such as DOE-2 (Winkelmann et al., 1993, and BLAST (BSL, 1999); 4) Modular Variable Time-Step Simulation Program, such as TRNSYS (SEL, 2000),

SPARK (SPARK, 2003), ESP (Clarke and McLean, 1998), Energy Plus (Crawley et al., 2004), ASHRAE Primary and Secondary Toolkits (Bourdouxhe et al., 1998 and Brandemuehl, 1993); and 5) Specialized Simulation Program, such as HVACSIM+ (Park et al., 1985), GEMS (Shah, 2001), and other CFD programs (Broderick and Chen, 2001). Detailed building and HVAC simulation model reviews can also be found in Kusuda (1991 and 2001), Bourdouxhe et al. (1998), Shavit (1995), Ayres and Stamper (1995), and Yuill and Wray (1990).

Among all available HVAC simulation models, HVACSIM+ (Park et al.,1985) developed by the U.S. National Institute of Standard and Technology (NIST), is of interest in this study. It is a component based modelling package which employs a unique hierarchical computation approach. Individual simulation elements (called "units") are first grouped by the user into "blocks" for simultaneous solution. Blocks are then similarly grouped into "superblocks" for simultaneous solution. Each superblock is a numerically independent subsystem of the overall simulation; its time evolution and internal solutions are propagated independently of other superblocks. The time step in a superblock is a variable that is automatically and continuously adjusted by a solver subroutine to maintain numerical stability. Each individual unit is an instance of a specifically serialized equipment or device "TYPE" (written all caps, to distinguish from the common use of the word), requiring the user to link inputs and outputs between all units and assign unit parameters. A subroutine solves the resulting sets of nonlinear algebraic and differential equations to determine system state at each time step. This hierarchical approach makes even complex simulations solvable. HVACSIM+ has been experimentally validated and improved (Dexter et al., 1987), and proven appropriate for fault modeling (Bushby et al. 2001, Dexter, 1995, and Peitsman et al. 1997).

Results from several ASHRAE research projects have enriched the HVACSIM+ simulation capability. ASHREA 825-RP (Norford and Haves, 1997) extended the ability of HVACSIM+ and TRNSYS in the following areas:

1) New models such as those for controller, sensor, and air flow related components were developed
2) Component models of the building fabric and mechanical equipment were enriched
3) A real building, including the AHU system, was simulated and documented in detail to demonstrate the use of the component models.

An ASHRAE project 1194-RP (Braun and Zhou, 2004) developed and validated a dynamic cooling coil model in great detail, which was generally not available from other discussed HVAC simulation programs.

ASHRAE 1312-RP (Li and Wen, 2012, Li et al., 2010, and Wen, 2012) developed a four zone building simulation testbed based on the model developed for ASHRAE 825-RP using HVACSIM+. The 1312 model also included the cooling coil model developed in ASHRAE 1194-RP. The 1312 model was capable of simulating fault-free and faulty AHU operational data. It was validated using experimental data for both faulty and fault-free operations.

In Summary, HVACSIM+ is a simulation environment that provides its user flexibility to develop comprehensive dynamic simulation models for building and HVAC systems. Several ASHRAE research projects have developed various sybsystem models and enriched the HVACSIM+ library of component and its simulation capability. Therefore, HVACSIM+ is selected as the simulation environment for this project.

1.2.2 Existing dynamic models for the proposed secondary systems

The above discussed HVAC dynamic modelling environments, including HVACSIM+, have mostly focused on single AHU and VAV terminal systems. Very few studies and dynamic simulation models have focused on other secondary HVAC systems, including fan coil unit and dual duct system although they are widely used in the buildings.

Publications discuss fuzzy logic control of FCUs (Chu et al., 2005, Ghiaus, 2000), but there has been no prior work specifically about dynamic simulation and validation of FCUs, as evidenced by the lack of any dynamic model by which FCU performance can be simulated to generate data for study. Joo and Liu (2002) used a model to simulate energy performance of dual duct AHU and Salsbury et al. (2000) discussed the potential of simulation as a performance validation tool to evaluate a dual duct single fan system installed in an office in San Francisco. But there has been no prior work specifically about dynamic simulation and model validation for dual duct systems. The development of advanced control, operation, and automated fault detection and diagnosis techniques requires reliable simulation tools, therefore there is a need to develop a simulation tool that is capable of simulating realistic fault free and faulty operational data for fan coil units and dual duct systems.

1.2.3 HVAC dynamic model validation

Validation of A HVAC and building simulation model is not a trivial issue. There are publications in the literature that discuss HVAC system dynamic model verification and validation, such as those focus on a) component models (Clark et al., 1985, Braun and Zhou, 2004); b) primary systems (Wang et al., 2004) ; and c) air conditioning process and its interaction with building zones (Brandemuehl et al.,

1993). Detailed review about simulation code verification and validation has been provided by Reddy et al. (2005) as part of an ASHRAE Research Project 1051-RP. Bloomfield (1999) provides a good review of work done on validation of computer programs for predicting the thermal performance of buildings. A more recent and more complete document is the draft addition to Chapter 31 of ASHRAE Handbook Fundamental. Major conceptual issues are described along with outstanding problems, both pragmatic and philosophical. Finally, Bloomfield, based on several previous papers categorized validation techniques as follows:

(i) *Code checking*, which involves a series of activities designed to test the operation of the code against specified functionalities and expected behavior;

(ii) *Analytical validation tests*, in which outputs from the program, subroutines, or algorithm are compared against results from a generally accepted numerical method for isolated heat transfer mechanisms under very simple and highly constrained boundary conditions;

(iii) *Inter-model (or comparative) comparisons*, where the results of one program are checked against those of another which may be considered better validated or more detailed, or presumably, more physically correct; and

(iv) *Empirical validation*, which entails comparing simulation predictions with measurements or monitored data from real building, test cell or laboratory experiments.

Though, several papers can be found in the literature on verification and validation of building energy analysis programs, the first systematic and complete study was undertaken by researchers from National Renewable Energy

Laboratory (NREL) called the BESTEST inter-model comparison method which provides both systematic model testing and diagnosing the source of predictive disagreement (Judkoff and Neymark, 1999). The NREL methodology as it pertains to empirical validation distinguishes between different levels, depending on the degree of control exercised over the possible sources of error during the simulation. The error sources were divided into:

(a) External error types due to differences/discrepancies between actual and simulation inputs:

1. In weather data,
2. In building operational data (such as schedules, control strategies, effect of occupant behavior,…),
3. In physical properties (thermal, optical,…) of the various building envelope and equipment components, and
4. Due to the user error in deriving model input files.

(b) Internal error types having to do with accuracy of the models and algorithms:

1. Due to the model simplifications in how the heat, mass and fluid flow processes are modelled,
2. From improper numerical resolution of the models, and
3. Due to coding errors.

A systematic validation strategy, including system level steady state validation, system level validation dynamic and component model calibration was recommended by Li et al. (2010) as part of ASHRAE 1312-RP project. Li et al. indicated that the key for the validation process was to separate different component dynamics and parameter from each other. During a system level validation, if a component model

was found to be unacceptable, experimental data specifically for that component were then sought to modify the component model.

1.2.4 Fault modelling and validation

In general, models of faulty component and process are used either as part of AFDD method or used as part of the simulation to develop or evaluate an AFDD method (Haves, 1997). None of the simulation models discussed in section 1.2.1 and 1.2.2 directly provides the capability to simulate faulty operation except those developed at NIST (Bushby et al., 2001) and in ASHRAE 1312-RP. Although many AFDD studies simulate various faults for their own methodology development, few supplies detailed information about how the faults are modelled. Fewer studies describe how their simulated faulty operation data are validated.

Haves (1997) provides a general discussion about fault modelling methodology, in which faults are grouped into design, installation, abrupt and degradation categories. He suggests that faults can be modelled in two different ways, i.e., by 1) changing parameter values in a fault-free model, such as reducing UA value to model a fouled coil in a simple coil model; 2) extending the structure of a fault-free model to treat faults explicitly, such as adding a new parameter that specifies the thermal resistance of the deposit for a detailed coil model when modelling coil fouling fault. Furthermore, it is noted that if a fault is such that a basic assumption of the model is no longer valid, a major change in the fault-free model is needed, such as poor sensor placement, which invalidates the perfect mixing assumption. Examples on cooling coil and valve faults modelling are also provided.

As part of the scope for ASHRAE project 1043-RP, a simulation model was developed for a vapor compression centrifugal liquid chiller (Bendapudi and Braun,

2002). The model is based on first principals and is able to capture start-up and other transient caused by changes in steady state operation. Four faults, namely, 1) 20% reduced condenser and evaporator water flow rates; 2) 20% reduced refrigerant charge; 3) 20% refrigerant overcharge; and 4) 45% fouling in condenser, are modelled in the simulation tool. The fault-free and four faulty simulation data sets are validated using experimental data under steady state, start-up, and other transient states. System pressure, power, and various temperatures are generally used to compare the simulation model against real system. Large deviation in the model predictions have been observed for evaporator pressure prediction under both fault-free and faulty operations. Furthermore, it is hard to judge what are the criteria used to claim that the model is "validated". Different levels of difference exist between model prediction and real measurements especially under transient states. For example, the model over-predicts the motor power by nearly 30% and over-predicts the sub-cooling by nearly 100% under load charge (LC9) for 20% excess refrigerant fault simulation.

Bushby et al. (2001) describes two tools, namely an AFDD test shell and the Virtual Cybernetic Building Testbed (VCBT), used for AFDD tool development. The VBCT employs HVACSIM+ as the simulation program and is able to emulate the characteristics and performance of a cybernetic building system. Twelve faults associated with VAV AHU are modelled using VCBT, which include supply, return, mixed, and outdoor air temperature sensor offset faults; stuck open, closed, or partially open outdoor air damper; leaking outdoor air damper; stuck closed cooling coil valve; leaking cooling coil valve; stuck closed heating coil valve and leaking heating coil valve. The fault modelling details are provided in Bushby et al. (2001). Experiments also have been conducted at the Iowa Energy Centre Energy resource Station (ERS) testing facility to examine the simulated faults. However, differences

exist between the simulation and testing conditions, like during simulation, historic weather data are used which are different from the testing weather conditions. Such differences prevent a rigorous validation comparison. Hence, only the trends between faulty operation and fault-free operation displayed in the simulation results are compared with those shown in the real measurements. It is noted that during the tests, two identical AHUs have been employed at the ERS. One AHU serves as fault-free AHU while another serves as the faulty AHU. A large variety of faults which are typical for a single duct AHU have been modelled in the ASHREA 1312-RP (Wen, 2009). Similar strategies as those described by Haves (1997) have been used to model faults. Extensive experiments were conducted at ERS test facility to validate the fault models. It has been concluded that because fault models are often a much simplified representation of the real phenomena, the objective of the validation process for the faulty operation simulation should be in the direction of replicating fault symptoms associated with the given fault and severity. Most faults have been modelled by adding parameters or changing values of existing parameters, which did not involve new component model development. In order to ideally validate a fault model simulation, a parallel fault-free system running side by side is necessary. Comparison of the operational data of both parallel systems is a good indication of fault presence in the faulty operating system and reflecting the fault symptoms associated with each fault. Fault model simulation results in 1312-RP project have been validated based on the described rule having two parallel and similar system running side by side one under faulty and another under fault-free condition.

1.2.5 Existing dynamic models for building thermal response

Much effort has been devoted to modelling building thermal response in order to provide techniques for a range of building design and analysis problems including building energy demands, passive design, environmental comfort and the response of plant and control. Much of the early effort throughout the 1970s and 1980s concentrated on the development of a group of three contrasting thermal modelling methodologies: the impulse response factor method (Mitalas et al., 1967); the finite difference method (Clarke, 1985) and the lumped parameter method (Crabb et al., 1987). As a result, a significant number of commercially available and public domain codes have become available most of which are based on the first two of the three methods mentioned (for a review of the principles see Wright et al., 1992; for a comparison of available codes see Bunn, 1995). The impulse response factor method is based on the theoretical response of building elements to a unit pulse in some input excitation (e.g. heat flux) and can be expressed as a time series of multiplying factors that can be applied independently to the actual input excitations experienced by the element. This means that the response factors need be computed once only at the outset of a simulation. This led to substantial economies in computational effort which at the time of development of the method (1960s/1970s) was a crucial consideration but is much less so today due to major advances in computer power. The time series are usually of one hour interval whereas when plant and control system analyses is required a much shorter time interval is needed for satisfactory solution. This led to the need to pre-process the time series data and then post-process the plant model in order to capture the economies of computational effort necessitating the introduction of weighting factors for building response in order to match the quicker response of the plant for a sequential solution. Accuracy then

became an issue and the method has never generally been suitable for fully dynamic simulations where the simulation time step is necessarily low (e.g. where control system response is of interest).

The finite difference method simply seeks to solve the Fourier conduction equation using difference equations in which the layering of construction elements and time interval can be independently fixed with reference to model stability criteria. In principle, the method is accurate especially at high construction element layering resolutions and low time intervals but the large number of simultaneous calculations renders the method computationally demanding especially at time intervals relevant to plant and control system simulations.

The lumped parameter method has probably received least attention of all three methods and yet is the simplest method of building thermal response modelling involving the break-up of construction elements into a (usually small) number of temperature-uniform elements about which an energy balance can be expressed. The resulting linear differential equation for each element can be solved analytically in principle making the method very computationally efficient. Model orders as low as 5^{th} order are possible (4 describing construction element balances and the 5th describing room air) but accuracy is limited. However, accuracy can be improved by increasing the model order (i.e. describing each construction element by a larger number of temperature-uniform elements). This method is therefore suitable for full simulations including plant and control since it offers economies of computational effort at the time intervals involved.

In order to analyze the control system, short-time-horizon modelling of the building thermal response is of interest in this research. Therefore, the lumped parameter method is used to simulate building zones interacting with FCU and dual

duct system. The available 2nd order model for zone modelling does not include the radiation heat transfer through the glazing which input inaccuracy in the simulation results. Therefore, there is a potential to modify the available model in this direction.

1.2.6 Various solution techniques employed in common building energy performance tools

Efficiently, robustly and accurately solving large sets of structured, non-linear algebraic and differential equations is one of the most computationally expensive steps in the dynamic simulation of building energy systems. The building engineering software packages employ mathematical models of real systems, so a common challenge encountered by software developers is selecting numerical solution methods appropriate for the mathematical structures inherent to the dynamic modeling of energy in buildings. The goal is an accurate, stable and globally convergent solution at each step of the time sequence being simulated.

Development of building energy simulation tools during the recent four decades resulted in a wide range of currently available products (DOE 2009, Crawley et al, 2008). These products range (complexity-wise) from spread-sheet tools to more advanced special-purpose simulation tools, and (integration-wise) from tools that handle a single aspect of the building design, to tools that integrate multiple aspects of the building design (Hensen, 2009, Trcka et al, 2010). The evolution of using analytical solution as well as simplifying assumptions to numerical solution considering the real building dynamic is observable in various generations of building energy simulation tools (Trcka et al, 2010). The current tools can capture reality much better than earlier tools, but are more complex to use. Currently, publically available simulation tools used to simulate dynamic behavior of building and HVAC system as

a fully integrated model include SPARK, EnergyPlus, MODELICA, TRNSYS, HVACSIM+, etc. They employ different solution techniques to solve the equations resulting from mathematical modeling of the constitutive components. In the following a brief review of the solution techniques employed in the above mentioned simulation tools is presented.

SPARK (SPARK, 2003):

It is similar to a general differential/algebraic equation solver, which is an object-oriented software system that can be used to simulate physical systems described in differential and algebraic equations. By object-oriented we mean that components and subsystems are modeled as objects that can be interconnected to specify the model of the entire system. In another word, in SPARK, components and subsystems are modeled as objects that can be interconnected to specify the model of the entire system. Models are expressed as systems of interconnected objects, either created by the user or selected from a library. The integrator classes in the SPARK library are used for numerical solution of differential equations. All of the implemented integration methods in SPARK include, the Euler explicit and implicit methods, the Backward-Forward difference method, the 4th -Order Backward-Forward difference method, the Adams-Bashforth-Moulton method, the PC Euler method and the PC Trapezoidal method. The interested reader is referred to SPARK manual to distinguish the differences and pros and cons of each integrator.

Systems of algebraic equations often have to be solved iteratively. In SPARK, in the problem setup phase, it determines if iteration is required by detecting cycles in the problem graph. If cycles are detected, a graph algorithm is used to find a small set of variables (nodes in the graph) that “cut” the cycles. In another words, graph-theoretic methods are used to decompose the problem into a series of smaller

problems, called components that can be solved independently. The associated problem variables, called break variables, are placed in a vector to act as the unknown vector x in a multi-dimensional Newton-Raphson (N-R) solution scheme as the default method. Normally, this process converges to the solution quite rapidly (quadratically). However, it is well known that the Newton-Raphson process, like all methods for solving general sets of nonlinear equations, can fail to converge under certain circumstances. Failure occurs when the residual functions have particular kinds of non-linearities and the starting values are not sufficiently close to the actual solution. Other available numerical methods for the user in the case of N-R method failure are Perturbed Newton and Secant methods.

EnergyPlus (EnergyPlus, 2005):

The Building Systems Laboratory together with Lawrence Berkeley National Laboratory and the Department of Energy has combined two programs: BLAST and DOE-2 (EnergyPlus, 2005). With this program, the heating, cooling, lighting, ventilation and other energy related flows in a building can be simulated. It uses a heat balance-based zone simulation method to perform calculations. When analyzing buildings, EnergyPlus can account for moisture adsorption and desorption within the building elements. Calculated loads at a user-specified time step are passed to the building systems simulation module to calculate heating and cooling system and plant and electrical system response. EnergyPlus provides three different solution algorithms to solve the energy and moisture balance equations. These are 3rd order backward difference, Euler method and analytical solution. The first two methods use the finite difference approximation while the third uses an analytical solution. The use of numerical integration in a long time simulation is a cause for some concern due to the potential build-up of truncation error over many time steps. In this case, the finite

difference approximation is of low order that further aggravates the problem. To improve on this, higher order expressions for the first derivative, with corresponding higher-order truncation errors, is used. The goal of this approach is to allow for the use of larger time steps in the simulation than would be possible using the first order Euler form, without experiencing instabilities. Approximations from second through fifth order have been tried with the conclusion that the third order finite difference approximation gave the best result. The analytical solution algorithm provides a possible way to obtain solutions without truncation errors and independent of time step length (EnergyPlus, 2014).

MODELICA (LBNL, 2011):

MODELICA, is an object-oriented, equation based language to conveniently model complex physical systems containing, e.g., mechanical, electrical, electronic, hydraulic, thermal, control, electric power or process-oriented subcomponents. It is the newest dynamic building models library currently being developed and supported by the LBNL. Two versions of the MODELICA building library were released by the LBNL in March and May 2011. MODELICA allows the separation of the "modeling (i.e., defining the model equations) and simulation (i.e., computing a numerical solution to the equations)" (LBNL, 2011). Such a separation allows (LBNL, 2011): "1) a high degree of model reuse; 2) graphical "plug and play" modeling since modular models can be connected in an arbitrary way; 3) the integration of models from different domains (controls, thermodynamics, heat and mass transfer, fluid flow, electrical systems, etc.); 4) the coupling of models with fast dynamics in the order of seconds (local loop control) and slow dynamics (energy storage); 5) the coupling of models whose evolution is described by continuous time equations (for the physics and local loop control), discrete time equations (for supervisory control) and state

events (for control that switches when a threshold is reached); 6) the exchange of models with other simulation platforms; and 7) the use of state-of-the art numerical solvers."

There are three different kinds of equation systems resulting from the translation of MODELICA model to a flat set of equations, from the simplest to the most complicated and powerful (Frtitzson, 2004):

ODEs- Ordinary differential equations for continues-time problems.

DAEs- differential algebraic equations for continuous-time problems.

Hybrid DAEs- Hybrid differential algebraic equations for mixed continues-discrete problems.

Since the focus of this study is modeling continues-time problem, in the following a short review of the methods to solve these kinds of equation systems is presented. However, these representations are strongly interrelated: an ODE is a special case of DAE without algebraic equations, whereas a DAE is a special case of hybrid DAEs without discrete or conditional equations. We should also point out that in certain cases a MODELICA model results in one of the following two forms of purely algebraic equation systems, which can be viewed as DAEs without a differential equation part: a) Linear algebraic equation systems; and b) Nonlinear algebraic equation systems

The purpose of solving an ordinary differential equation (ODE) problem is to compute, i.e., to integrate, the continues-time state variables from their derivatives. Some well-known methods for solving ODEs used in MODLEICA are:

- The explicit and implicit Euler methods
- Multistep methods
- The Runge-Kutta methods

- The Adams-Bashforth methods

When the simulation problem is a DAE the method of choice is differential algebraic system solver by Petzold 1982, and continuously improved.

TRNSYS:

The TRaNsient SYstems Simulation (TRNSYS) program was developed by the Solar Energy Laboratory at the University of Wisconsin Madison since 1975 (SEL, 2007). It is a flexible simulation tool that can simulate the transient performance of thermal energy systems. The simulation program uses component based methodology in which: 1) a building is decomposed into components each of which is described by a FORTRAN subroutine, 2) the user assembles the arbitrary system by linking component inputs and outputs and by assigning component performance parameters, and 3) the program solves the resulting non-linear algebraic and differential equations to determine system response at each time step. The three numerical integration algorithms that allow TRNSYS to solve the differential equations comprising the system model each time step are:

1. Modified-Euler method (a 2nd order Runge-Kutta method)
2. Non-self-starting Heun's method (a 2nd order Predictor-Corrector method)
3. Fourth-order Adams method (a 4th order Predictor-Corrector method)

TRNSYS is outfitted with two methods for solving the coupled system of algebraic and differential equations that model a given system: the “successive substitution” method and “Powell’s” method. With successive substitution, the outputs of a given model are substituted for the inputs of the next model in the system. The performance of that next model is recomputed and its outputs are then substituted for the inputs of the next model. This substitution continues at a given time step until all connected outputs have stopped changing. At that point simulation

proceeds on to simulate the next time step. Although the successive substitution computational scheme has proven to be reliable and efficient for simulating systems with coupled differential equations and nearly-linear algebraic equations; the limitations of the computational scheme become apparent when TRNSYS is used to solve sets of non-linear algebraic equations without differential equations. The successive substitution solution method does not efficiently solve non-linear algebraic equations and may, in fact, not be able to find a solution if the equations are highly non-linear. Another option of TRYNSYS for those cases is Powel's method.

HVACSIM+ (Park et al, 1985):

The HVACSIM+ dynamic simulation software package developed at NIST is a component based modeling package that is comprised of a collection of programs belonging to one of three categories: preprocessing, simulation, and post-processing. During the preprocessing stage, a simulation work file is created by the interactive front-end program. The equation solving routines of HVACSIM+ reside in the core program, MODSIM. The MODSIM program consists of a main driving routine and many subprograms for input/output operation, block and state variable status control, integrating differential equations, solving a system of simultaneous non-linear algebraic equations, component models (HVAC, controls, building shell, etc.), and supporting utilities (Clark and May, 1985). A simulation run essentially involves the MODSIM program operating upon a simulation model representing the real system, with that model being in the form of a text file defining a hierarchical composition of units, blocks, and superblocks.

Each unit, represented by a TYPE, in the simulation model is an individual instance of a generic component model representing a specific piece of equipment, envelope element, or control device. A TYPE is comprised of one or more nonlinear

differential or nonlinear algebraic equations as a FORTRAN 90 routine expressing the component dynamics. Instantiating a TYPE as a unit in the simulation model requires the HVACSIM+ user to link its input and output quantities to those of other, functionally-related units, which contributes equations to the overall system-level set of simultaneous equations that must be solved Closely-coupled units are first grouped by the user into blocks for simultaneous solution. Blocks are then similarly grouped into a superblock for simultaneous solution. Superblocks are weakly coupled through the state variables and the solver treats each superblock as an independent subsystem of the overall simulation (Park et al, 1986). In each superblock, time evolution and internal solutions are propagated independently of other superblocks. A subroutine (SNSQ) with its associated subprograms is used in MODSIM to solve the resulting sets of nonlinear algebraic and differential equations to determine the system state at each time step (Clark, 1985). The method used in SNSQ is based on Powell's Hybrid (PH) method (Park et al, 1986).

In some simulated cases in HVACSIM+, the PH method fails to converge to a solution. There is another study performed by Shterenlikht and Alexander (2012) to investigate the performance of Powell's method in fracture simulation. It ended up the same conclusion that Powell's method is unable to converge in some studied cases. Thus it is necessary to examine alternatives to this method or to investigate problem formulation.

1.3 Objectives and Approach

Based on the literature review, there is a need to develop and validate simulation tools for those less studied secondary HVAC systems in the HVACSIM+ environment. The developed tools should be able to generate operational data under

fault-free condition and replicate fault symptoms under various faulty conditions with different fault severities. Unavoidable dynamic interactions of the secondary HVAC systems with an interacting building zone requires a close look at the available building zone model and fix the deficiencies associated with that. Furthermore, the solution technique employed in the HVACSIM+ needs to be studied in order to examine the robustness and accuracy of a substitute method of solution. In this section, the overall objectives and the scope of the research tasks are discussed.

1.3.1 Overall objectives

The objectives of the research project are to:

1) Develop dynamic simulation model in the HVACSIM+ environment for the following secondary HVAC systems: a) fan coil unit with four pipe and outdoor air damper configuration; b) dual duct system with double supply fan and one return fan and variable air volume configuration.
2) Identify the typical faults associated with the above secondary systems and extend the simulation ability of the developed models to replicate fault symptoms under faulty conditions of various categories of faults with different severities. The generated faulty operational data can be used for the purpose of AFDD methods evaluation for the mentioned systems.
3) Design and identify validation process for the developed dynamic models under both fault-free and faulty conditions (under different types of fault and severity levels) using collected experimental data provided by ERS.
4) Collect and analyze experimental data for the proposed secondary HVAC systems at different seasons provided by ERS for validation purposes.

5) Modify the building zone model in the HVACSIM+ library in order to reflect the transmitted radiation through glazing.
6) Validate the modified model for building zone using the collected experimental data at ERS.
7) Conduct a numerical study to compare two solution techniques: Powell's Hybrid (PH) and Levenberg-Marquardt (LM) in terms of their robustness and accuracy. In this study, the PH algorithm, as implemented in SNSQ, is replaced by the LM algorithm to solve the identical problem.

1.3.2 Scope

This project includes five major areas: 1) fault-free dynamic models development; 2) fault-free dynamic model validation; 3) fault identification and model development; 4) fault model validation; 5) modify and validate building zone model; and 6) study two different solution techniques in HVACSIM+.

1.3.2.1 Fault-free dynamic model development

To simulate the dynamic behavior of the proposed secondary systems, new HVACSIM+ subroutines and new component models is developed. Moreover, a model structure, which includes the grouping of blocks and superblocks, initial and boundary conditions, needs to be examined.

As summarized by the ASHRAE handbook (HVAC systems and equipment, chapter 3, 2008), a large variety of fan coil unit configurations exist. A FCU consists of at least one air-water heat exchanger coil for heating or cooling its air flow and a fan. To condition its space, hot or cold water is circulated through the FCU coil to add or remove heat from the airstream discharged to the space by the fan. The amount of heating or cooling is regulated primarily by control of the water flow and secondarily

by control of the speed of the fan. Unit configurations include horizontal (ceiling mounted) or vertical (floor mounted). There are also two distinct configurations with regard to the water side. Two-pipe FCUs have one supply pipe, providing hot or cold water to the coil depending on the season, and one return pipe. Four-pipe FCUs have two supply pipes and two return pipes. This allows either hot or cold water to enter the unit at any given time. Since it is often necessary to heat and cool different areas of a building at the same time, due to differences in internal heat loss or heat gain, the four-pipe fan coil unit is the most commonly used (ASHRAE Handbook, 2008).

The purpose of this research is to develop a dynamic simulation model for a typical fan coil unit. The modelled FCU is characterized as a vertical four pipe hydronic FCU with three fans running by two electric motors of triple speeds: low, medium and high. The existing HVACSIM+ library of component models does not include a FCU as a single, integrated TYPE. With this work, new necessary TYPEs are added to the library as Fortran subroutines representing the control logic, mass flows, and thermal states of a FCU.

ASHRAE Handbook (HVAC systems and equipment, chapter 2, 2008) summarized typical configurations for dual duct AHUs. In a dual duct system, hot and cold air flows are separately carried by two parallel duct systems. The hot deck is equipped with a heating coil and the cold deck is equipped with a cooling coil. The two decks run in a parallel configuration throughout the building. In a terminal unit, the proper proportions of hot and cold air streams are modulated by cold air and hot air dampers before proceeding downstream to the space. The simultaneous availability of hot and cold air enriches the flexibility of this system to handle zones with widely varying loads. Meanwhile, energy could be saved by utilizing outside air directly as hot air or cold air in different seasons. The dual duct systems may be

designed as constant air volume (CAV) or variable air volume (VAV). In a CAV dual duct system, the supply air flow rate through the supply fan and to each zone is constant. However, the flow rates through the cold and hot decks vary depending on the requirements to satisfy the individual zone load. In a VAV dual duct system, the supply air flow rate through the supply fan is not constant and is dependent on the zone temperature control and ventilation needs. Similar to single duct VAV terminal units, VAV dual duct terminal units can also be categorized as pressure-dependent or pressure-independent units. More details about how dual duct systems are controlled can be found in (Kreider et al. 2002). This project specifically focuses on simulating a pressure-independent VAV dual duct double fan system serving four zones that have various orientations. To simulate this system besides using the available TYPES in HVACSIM+ library of components, new TYPES are developed to simulate VAV dual duct terminal units and represent control strategy. Simulation model for dual duct system is generated based on ASHRAE 1312 model to include dual duct terminal units and four building zones. In comparison with single duct systems, dual duct systems present unique challenges, especially regarding air flow simulations. Since the cold and hot air flow network are strongly coupled, how to simulate them simultaneously and robustly is a key obstacle. In this research, the focus is to model the constituent components of a dual duct system in terms of their governing equations, as well as the arrangement of these equations to achieve a stable and efficient simulation.

1.3.2.2 Fault-free dynamic model validation

According to ASHRAE 1312-RP project, a well validated fault-free dynamic model is the basis for fault model development and validation. Li et al. (2010) also showed that a HVAC system constitutive component parameters identified from

experimental data lead to much better simulation results than those calculated using manufacturer data/ catalogue. When validating a dynamic model, performance indexes of a simulation model need to be in close agreement to those from experimental data. Performance indexes include: 1) energy consumptions; 2) key measurements; 3) model dynamic response time. Key measurements are those measurements that are commonly available for control, operation and AFDD purposes. The magnitude of closeness, however, could vary due to the sensor accuracy, data quality, and the nature of a model.

Extensive experiments are conducted at ERS on real FCUs and full scale dual duct double fan system in three different seasons to generate operational data under a wide variety of fault-free and faulty operational conditions used in validation of the developed model for this study. The ERS has been described in at least three earlier studies (Norford et al. 2000, Castro et al. 2003, Li et al. 2010). Of the several rooms of the ERS having exterior exposures, the east, south and west-facing rooms were equipped with FCUs of a common configuration, serving as the prototype for the FCU simulation model. Besides, the major feature of this test facility is two identical air handling units (AHU A and B). In order to provide experimental data for dual duct system, significant modifications have been made to the two identical single duct AHU systems to convert them from two single duct systems to one dual duct double fan system with one return duct.

Validation of the dynamic model for the mentioned secondary systems is accomplished by a separate procedure at each of two levels: at the component level and at the system level. At each level of validation, the model parameters or structures are adjusted to achieve good agreement between simulated and experimental data. For each UNIT, the values for the parameters need to be determined. These parameter

values are determined either through manufacturer's catalogue data or a component test (especially for critical components). Where manufacturer catalogues include parameters for key components, component level validation is still conducted to ensure realistic model behavior. Because as mentioned earlier parameters identified from experimental data lead to much better simulation results than those calculated using manufacturer catalogue data.

At the component level validation, the key components which strongly affect system behaviour such as fan, valves, and dampers undergo experiment as an isolated equipment or component. Component test results with focus just on a specific equipment/part provide important data to determine the physical parameters representing component behavior which affects overall system dynamic model. Therefor the first step in fault-free model validation is to tune the constitutive component parameters with the available experimental data. Then, the entire system level validation is performed under real operational conditions applying the control strategies and weather conditions of the test facility. Finally, dynamic behavior of the model is validated by comparing simulation results with corresponding experimental data. A well validated fault-free dynamic model is the foundation for faulty model validation.

1.3.2.3 Faults modelling

To achieve the goal of assessing the performance of AFDD methods, the proposed simulation models should be able to simulate large variety of faults likely to occur in those two secondary systems. As discussed in the literature, very few studies exist in the literature that discusses faults specifically related to the proposed secondary systems. Based on the literature of other typical secondary systems and

logical analysis, a comprehensive and categorized list of faults for these three subsystems are proposed in the following chapters.

Theoretically, all devices including control software could develop faults. Therefore, the faults are categorized based on the specific device corrupted by a fault, with the devices grouped into four categories: equipment, sensor, controlled device, and controller. Such categories are mostly used among control engineers. It is noted that some devices, such as fans and pumps can be either grouped into the controlled device category or the equipment category.

Although the simulation tool should be able to simulate fault with any user-defined level of severity, it is impossible for all of them to be validated through designed experiments. In general, the nonlinear characteristic of HVAC components results in nonlinear impact for a fault severity on HVAC measurements. For example, a 10°F supply air temperature sensor offset may yield similar system measurements as a 4°F offset. Furthermore, when the severity levels exceed certain values, the system measurements may asymptote (or be saturated). Therefore, the fault severity levels should be selected so that they are between the minimum and maximum values that would saturate the system measurements.

Faults can be modelled in two different ways (Haves, 1997): 1) by changing parameter values in a fault-free model, such as reducing the UA value (heat conductance coefficient) to model a fouled coil in a simple coil model; and 2) by extending the structure of a fault-free model to treat faults explicitly, such as modelling a coil fouling fault by adding a new parameter that specifies the thermal resistance of the deposit in a detailed coil model. In this study, faults are modelled by changing values of existing parameters, avoiding the need to develop new model components explicitly replicating faults. A fault flag arrangement is employed to

allow the user to select a fault type and severity. Given the simulation system model has been validated under fault-free conditions, the only further validations require to ensure realistic representation of faults are those on the altered parameter values. The developed dynamic model simulates the faults with varying severity, which projects proportionally to the fault symptoms observable in data.

1.3.2.4 Fault model validation

The objective of faulty operation simulation is to assure that the fault symptoms produced from the simulation system models are consistent with those in a real system when faults exist. During the validation of fault modelling, it is more important to compare fault symptoms rather than regenerating the dynamics of each variable. This is due to the complex impacts of faults under real world conditions, and the difficulty of simulating such impacts precisely. In order to ideally validate the system under faulty condition, two identical systems operating side by side, with one system implemented with a fault and the other one without fault is necessary. Fault symptoms can be identified easily by comparing measurements from these two systems. Both simulation results and experimental data are used to validate the modelling of faults, involving simulation results under both faulty and fault-free conditions (to identify simulated fault symptoms), and similarly for experimental real data (to identify the real fault symptoms). Once fault symptoms are identified, it is easy to validate fault models. Based on the experimental data provided by ERS for FCU and dual duct system, there is a lack of experimental data under fault-free conditions for the same test day and exterior rooms undergoing the faulty test. Thus in this research project, a normal test day with close or more severe weather condition (that is, a condition that will cause system variables to change similarly as the tested fault) is picked as a reference day to confirm that the system behavior and the

observed symptoms in real data have resulted from the fault and not the weather. The fault-free and faulty simulation results are generated by adjusting fault flags.

1.3.2.5 Modification and validation of building zone model

Dynamic simulation using the FCU and dual duct system model unavoidably requires an interacting zone model, including systemic interactions with the building's surroundings. Physical characteristics of zone interactions also needed to be assigned. The 2C3R model (TYPE 403) that has been used in ASHRAE 825 and 1312-RP is used in dynamic model development of FCU and dual duct system. Therefore, parameters from the ASHRAE 1312 research project (Li et al., 2010) are used to represent the thermal characteristics and zone mass interaction properties between ambient conditions and adjacent zones. However, it is found that the 2C3R model does not properly simulate the impact of direct solar radiation that enters a zone through glazing, which causes a discrepancy between simulation data and experimental results during the validation process especially for transient seasons. ERS exterior rooms have large uncovered windows which allow a significant amount of radiation heat transmitted to the zone. This deficiency of the available component model for simulating thermal state of the zone is addressed and validated against experimental data for each orientation and various seasons.

1.3.2.6 Study two different solution techniques in HVACSIM+

Efficiently, robustly and accurately solving large sets of structured, non-linear algebraic and differential equations is one of the most computationally expensive steps in the dynamic simulation of building energy systems. Here, the efficiency, robustness and accuracy of two commonly employed solution methods are compared. The HVACSIM+ software presently employs Powell's Hybrid method to solve

systems of nonlinear algebraic equations that model the dynamics of energy states and interactions within buildings. It is shown here that the Powell's method does not always converge to a solution. Since a myriad of other numerical methods are available, the question arises as to which method is most appropriate for building energy simulation. This research finds considerable computational benefits result from replacing the Powell's Hybrid method solver in HVACSIM+ with a solver more appropriate for the challenges particular to numerical simulations of buildings. Evidence is provided that a variant of the Levenberg-Marquardt solver has superior accuracy and robustness compared to the Powell's Hybrid method presently used in HVACSIM+.

1.4 Overall methodology

The overall methodology followed in this project to develop dynamic model under fault-free and faulty conditions and also to validate these models is described in this section. The following validation strategy is especially crucial for large systems like dual duct system which has its own complications and made up of various components. This section is composed of two subsections the overall methodology for fault-free model development and validation and the overall methodology for fault model development and validation.

1.4.1 Fault-free model development and validation methodology

In order to develop the dynamic model of every HVAC system well in the HVACSIM+ environment, it is necessary to decompose the system into the constituent states. Generally for the systems under study in this project, there are five distinct constitutive processes including: control logic, actuator, air flow, thermal and sensor states. They can be described with independent subsystems whose time

evolution in the process of numerical calculation is independent of other subsystems. Therefore, the first step of fault-free model development is to develop the subsystems describing the overall system. If the existing HVACSIM+ library of component models does not include the components (TYPEs) to represent the system, the new required TYPEs are added to the library. Determining the parameters representative the operational condition and physical characteristic of each component (TYPE) is a matter of importance. So validation of the developed dynamic model is accomplished by a separate procedure at each of two levels: at the component level and at the system level. During model development, nominal parameters for system performance within each TYPE are assigned only when suitable parameters from manufacturer data are not available. Assignment of nominal parameters is accomplished by an experimental procedure. Where manufacturer catalogs included parameters for key components, component level validation is still conducted to ensure realistic model behavior.

Finally, dynamic behavior of the model is validated by comparing simulation results with corresponding experimental data provided by ERS at different seasons. At the system level validation the interaction of the system with the environment and its own various constituent processes are examined. The representative variables like control signals, air flow rates and temperatures of different points of the system are used to examine the developed model in system level validation.

1.4.1.1 Fault-free model performance evaluation

At system level validation the developed fault-free model is compared against the provided experimental data. In order to quantify the accuracy of the developed model in predicting the dynamic of the system, coefficient of determination, R^2 (Eq. (1-1)) is used (Devore, 2004).

$$R^2 = \left(\frac{\sum_{i=1}^{n}(x_i - \bar{x})(\hat{x}_i - \bar{\hat{x}})}{\sqrt{\sum_{i=1}^{n}(x_i - \bar{x})^2 \sum_{i=1}^{n}(\hat{x}_i - \bar{\hat{x}})^2}} \right)^2 \quad (1\text{-}1)$$

Where x_i is the experimentally measured variable like control signals (heating/ cooling coil valves, dampers,…), temperature, flow rate and etc., $\hat{x}_i$ is the corresponding variable predicted by the model, $\bar{x}$ and $\bar{\hat{x}}$ are their average.

Root-mean-square error (Eq. (1-2)) is also used to evaluate the model performance.

$$\text{RMSE} = \sqrt{\frac{\sum_{i=1}^{n}(x_i - \hat{x}_i)^2}{n}} \quad (1\text{-}2)$$

Where x_i and $\hat{x}_i$ has the same definition as mentioned earlier.

1.4.2 Fault model development and validation methodology

Faults can be modeled in two different ways (Haves, 1997): 1) by changing parameter values in a fault-free model, such as reducing the UA value (heat conductance coefficient) to model a fouled coil in a simple coil model; and 2) by extending the structure of a fault-free model to treat faults explicitly, such as modeling a coil fouling fault by adding a new parameter that specifies the thermal resistance of the deposit in a detailed coil model. In this study, faults are modeled by changing values of existing parameters, avoiding the need to develop new model components explicitly replicating faults. A fault flag arrangement is employed to allow the user to select a fault type and severity. The category of potential faults which may occur in every HVAC system and the devices affected by these faults are listed and tested at ERS in different seasons. Given the simulation system model had been validated under fault-free conditions, the only further validations required to ensure realistic representation of faults are those on the altered parameter values.

During the validation of fault modeling, it is more important to compare fault symptoms rather than regenerating the dynamics of each variable. This is due to the complex impacts of faults under real world conditions, and the difficulty of simulating such impacts precisely. Therefore, faulty operation validation does not need a comprehensive process as described for fault-free validation. Therefore, we don't define evaluation index for the performance of fault model as the purpose is just to replicate the fault symptoms rather than regenerating the exact value of variables.

Both simulation results and experimental data are used to validate the modeling of faults, involving simulation results under both faulty and fault-free conditions (to identify simulated fault symptoms), and similarly for experimental real data (to identify the real fault symptoms). The fault-free and faulty simulation results are generated by adjusting fault flags. In order to ideally validate the system under faulty condition; fault-free experimental data of a similar system running in parallel with the faulty system is necessary. For the studied HVAC systems, there is a lack of experimental data under fault-free conditions for the same test day and exterior rooms undergoing the faulty test. Thus, a normal test day with close or more severe weather condition (that is, a condition that will cause system variables to change similarly as the tested fault) is picked as a reference day to confirm that the system behavior and the observed symptoms in real data are resulted from the fault and not the weather.

2. CHAPTER TWO: FAN COIL UNIT DYNAMIC MODEL DEVELOPMENT IN HVACSIM+ AND VALIDATION- FAULTY AND FAULT FREE

2.1 Introduction

Fan coil units (FCU) are simple, economical devices used extensively in the HVAC systems of commercial, institutional and multifamily residential buildings. However, very little has been reported in the literature to improve their design and operation. There has also been a lack of dynamic simulation tool development focusing on FCUs. The work documented here models a vertical four pipe hydronic FCU as an integrated component to be run within the HVACSIM+ dynamic simulation software package. Dynamic simulation of FCU not only opens ways to synthesize operational data under fault-free conditions, but also makes it possible to predict the symptoms associated with various faulty conditions and their effects on system performance and occupant comfort. A comprehensive and systematic validation procedure, using data collected experimentally from real FCUs at ERS laboratory, is used to validate the tool under both faulty and fault-free operating conditions in three different seasons. The validated tool not only predicts real-world FCU behavior under different control strategies, but it also predicts symptoms associated with various faults, as well as the effects those faults have on system performance at various severities. Fault symptoms of varying severity are represented by a fault flag system that changes the values of relevant unit parameters. This chapter describes the procedure of model development from the new added TYPEs to HVACSIM+ library of components to validation of the model at both component and system levels. It also spends on fault modeling by designing fault flag and validation of fault model.

2.2 Test Facility and Experimental Set up

Extensive experiments were conducted at ERS on real FCUs in three different seasons to generate operational data under a wide variety of fault-free and faulty operational conditions. As Figure 2-1 demonstrates, of the several rooms of the ERS having exterior exposures, the east B, south B and west B-facing rooms are equipped with FCUs of a common configuration, serving as the prototype for the FCU simulation model. To generate FCU data under normal conditions all rooms were operated without imposed faults. To establish data under faulty conditions, the east and west-facing rooms were operated with deliberately imposed faults while the south room ran normally. The zones have identical construction and details about the zone envelop structure are provided by Price and Smith (2003).

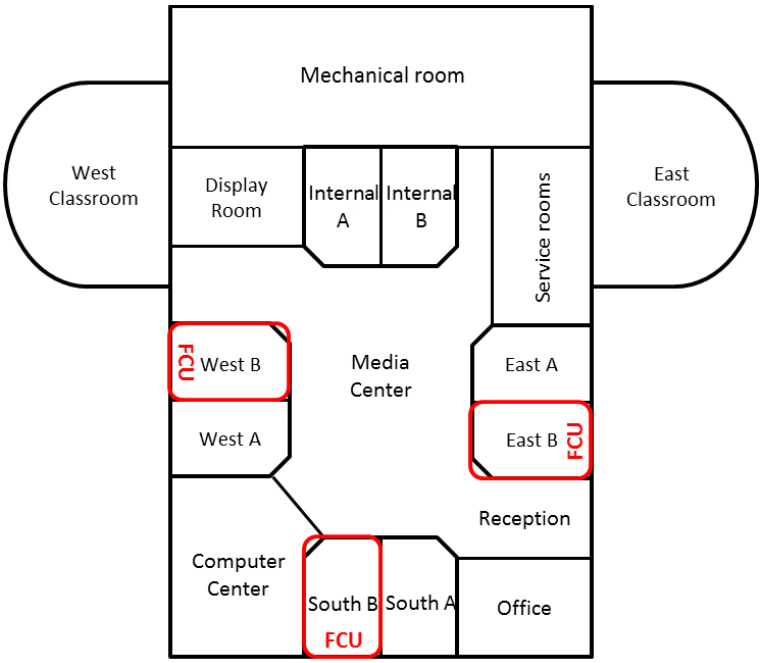

Figure 2-1. The schematic of Energy resource station building zones equipped with FCU

Each FCU modulated the amount of ventilation supplied to its zone by way of a motorized damper over the outside air connection at the back of the unit. The FCUs are vertical four pipe hydronic ones with three fans running by two electric motors of triple speeds: high, medium and low. Figure 2-2 shows the schematic of the FCU at ERS.

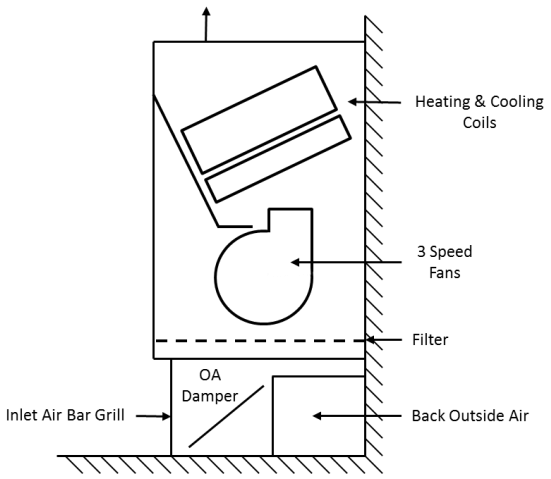

Figure 2-2. The ERS fan coil unit schematic

The control mode of the FCU can be selected as either “Unoccupied” or “Occupied”. In “Unoccupied” mode, the fan is off, the mixed air damper and heating and cooling coil valves are fully closed, and the test room temperature floats. In “Occupied” mode, the fan coil unit is controlled to maintain test room thermostat heating and cooling setpoints, with the 3-speed fan in one of three modes of operation: “Automatic On/Off” with different fan speed control, “Always On” at predetermined speed, and “Cycle On/Off” at a predetermined speed. The mixed air damper is modulated by a proportional-integral-derivative (PID) control loop, maintaining at least a minimum damper position in both cooling and heating modes. When room demand calls for cooling, the mixed air damper will modulate automatically to meet a mixed air temperature setpoint. When the FCU is in

"Occupied" mode, the controller compares room temperature to the cooling setpoint (72 F (22.22 ^{o}C) in fall and winter, 74 F (23.33 ^{o}C) in summer) and heating setpoint (68 F (20 ^{o}C) in fall and winter, 70 F (21.11 ^{o}C) in summer). If the actual room temperature is greater than (cooling setpoint - 1F (0.56 ^{o}C)), the FCU is in "cooling" mode and if it is less than (heating setpoint + 1F (0.56 ^{o}C)), the FCU is in "heating" mode. A dedicated PID loop is enabled for each mode to control cooling or heating valve position. As long as room temperature lies between the heating and cooling setpoints, the PID loops are disabled and the corresponding valves are fully closed. It is worth mentioning that, during fault-free tests, FCUs were run with a fixed outside air damper position (0% open) in summer and (30% Open) in fall and winter with "Always ON" mode to run the fan at high speed. The mixed air temperature was not controlled. Detailed description about FCU control sequence, algorithm and point names can be found in APPENDIX A.

2.3 Fault-Free Dynamic Model Development

This section presents the structure of the FCU model in HVACSIM+. Publications discuss fuzzy logic control of FCUs (Chu et al., 2005, Ghiaus, 2000), but there has been no prior work specifically about dynamic simulation and validation of FCUs, as evidenced by the lack of any dynamic model by which FCU performance can be simulated to generate data for study. The FCU model developed here is validated by comparing the data from simulated operation under faulty and fault–free conditions with the corresponding experimental data from ERS.

As mentioned earlier, there are different configurations, types and operational strategies for fan coil units. Since the purpose of this project is to develop FCU dynamic model and validate it by experimental data representing real operational data,

the simulated FCU has the characteristic of FCU at ERS test facility. In this study, the dynamic behavior of a vertical four pipe hydronic FCU in conjunction with the affiliated zone is simulated using a component based approach by HVACSIM+.

Prior to this work, the existing HVACSIM+ library of component models did not include a FCU as a single, integrated TYPE. In this project, different TYPEs representing control logic, mass flows, and thermal states of FCU has been added to HVACSIM+ library to give the user the ability of FCU modeling with no concern about the constitutive components. In order to dynamic simulation of FCU, user can input parameters, provide weather information and zone interior loads. The user is allowed to alter the parameters of the model but it is worth mentioning that just FCUs which have parameters similar to those at the test facility can be considered as a validated model. The scope of this project does just include development and validation of FCU dynamic model and validation of building zone model is out of the project scope. Building zone model affect FCU model result by providing values for the return air temperature. In the following the required TYPEs which should be added to HVACSIM+ library to model FCU are discussed. In addition, the process of key components validation including mixed air damper, fan as well as heating and cooling coil valves is discussed. Furthermore, the characteristic of test facility and the experimental tests procedure are described in the following sections.

2.3.1 New TYPEs added to HVACSIM+ to model FCU

In order to include FCU as a single, integrated TYPE to HVACSIM+ library of component, new TYPEs 479, 307 and 314 are added to the library as Fortran subroutines representing, respectively, the control logic, mass flows, and thermal states of a FCU. The inputs, outputs and parameters required for new TYPEs are

presented in APPENDIX B. Modeling any HVAC device well in HVACSIM+ requires all of the constitutive processes represented by the model to be divided among multiple constituent TYPEs, each TYPE expressing separately one category of process states that is both physically and numerically independent from- or at most, coupled only weakly to- any other category of the process states in the device. In the case of the FCU, five distinct categories of states- (1) sensors, (2) actuators, (3) control logic, (4) fluid (i.e., mass flow and pressure), and (5) thermal (temperature and humidity)- are each modeled by a dedicated TYPE. The user groups each of these TYPEs into a block with corresponding TYPEs of the same state category representing other devices (i.e., units) in the HVAC system. That block may or may not be grouped with other blocks of the same category, depending upon the extent of the overall HVAC system being represented. In any case, the result is a system simulation having at least one superblock dedicated specifically to each of the five state categories mentioned. Figure 2-3 illustrates this HVACSIM+ structure in the case of the FCU model.

In this Figure, T represents the TYPE model and SB stands for superblock. C, N, TMA and TROOM represent control signals, fan rotational speed, mixed air temperature and room air temperature respectively. Figure 2-3 shows the mixed air and room air temperature signals, sent from a sensors superblock (SB5) to a controls superblock (SB1), result in positioning of the heating and cooling coil valves and outdoor air damper. Valve and damper positions determined in the control superblock are passed to other superblocks as appropriate. Simultaneous solution of mass-pressure equations occurs in the fluid superblock (SB3), while energy balance equations are solved simultaneously in the thermal superblock (SB4).

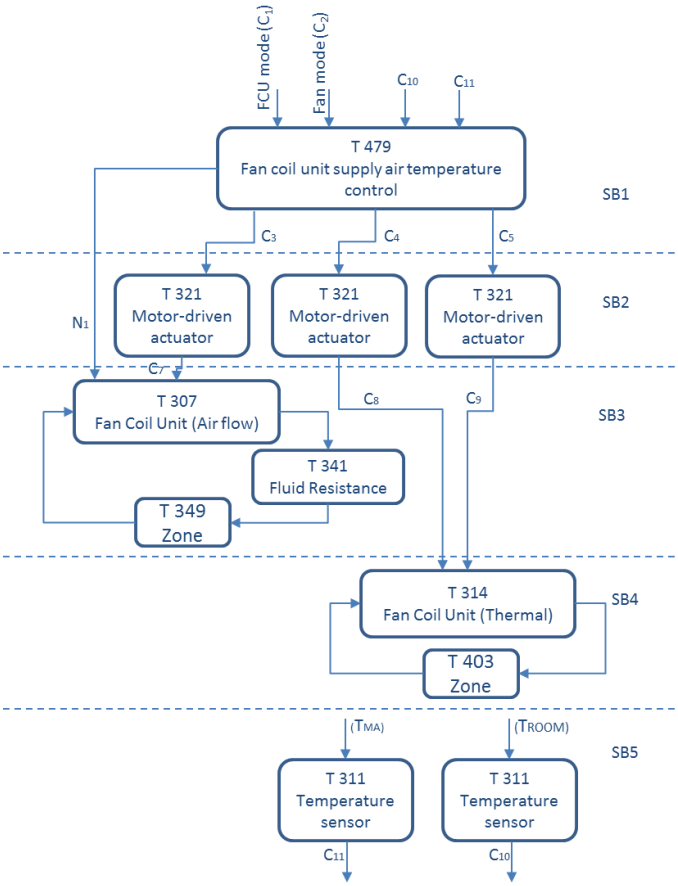

Figure 2-3. Fan coil unit model structure in HVACSIM+

2.3.2 Model parameters

There are too many parameters needed to be determined for simulation to represent the FCU at the test facility. Some of the parameters are identified directly from the manufacturer catalog data or calculated based on the catalog information. Some other parameters, which could not be easily calculated based on catalog information, are determined through a designed experiment. The designed experiment concentrates on a specific piece of equipment/component to obtain the necessary data required for predicting its dynamic behavior. Where manufacturer catalogs included parameters for key components like mixed air damper, heating and cooling coil,

component level validation is still conducted to ensure realistic model behavior. Therefore, validation of the FCU model is accomplished by a separate procedure at each of two levels: at the component level and at the system level. For instance damper and valves dynamic behavior need to be tested separately in component level validation which is different from fault-free and faulty system level validation.

In the following section the process of determining model parameters for the components of each superblock including control, air flow and thermal superblocks is reviewed.

2.3.2.1 Control network parameters determination

In the control superblock the FCU control mode (occupied or unoccupied) and fan control mode (auto/ on or cycle) are determined. The adjustment of mixed air damper, heating and cooling coil valves is performed by three separate Proportional-Integral-Derivative (PID) loops fed by signals coming from mixed air and room air temperature sensors. The parameters for each PID control loop including proportional band, integral time and derivative time are the required parameters in TYPE 479 representing the FCU control sequence. Although PID algorithm parameters are obtained from ERS but they might be changed during PID loops tuning at system level validation to provide stable control action. Since dynamic of the real system is different form simulation model; control loop parameters for model are not necessarily identical with the real system. Detailed description about FCU control sequence, algorithm and point names can be found in APPENDIX A and the parameters values are listed in APPENDIX B.

2.3.2.2 Air flow network parameters determination

In the air flow network, TYPE 307 represents the air flow-pressure equations of FCU. Therefore, parameters representing fan performance curves and damper dynamic behavior need to be determined. The governing equations of fan and procedure of defining fan parameters are described in section 2.3.2.2.1. Determining mixed air damper parameters require designing an experiment to measure pressure drop by mixed air damper at different openings. In section 2.3.2.2.2 the experiment conducted for damper component validation and the approach of identifying its parameters is discussed. Since the test facility is identical with 1312 project the needed parameters for building zones, TYPE 349, can be derived from this project.

2.3.2.2.1 Coefficients of fan

TYPE 307 representing the air flow state of FCU calls fan model, TYPE 355, as a subroutine. The fan model in TYPE 355 uses a dimensionless fourth order polynomial equation, Eq. (2-1), to represent the correlation of static pressure rise, air flow rate, fan diameter and rotational speed. Furthermore, Eq. (2-2) represents the correlation of fan efficiency, air flow rate, fan diameter and rotational speed in a dimensionless fourth order polynomial format.

$$\Delta P'(\dot{M}) = a_4\dot{M}^4 + a_3\dot{M}^3 + a_2\dot{M}^2 + a_1\dot{M} + a_0 \quad (2\text{-}1)$$

$$\eta_f(\dot{M}) = e_4\dot{M}^4 + e_3\dot{M}^3 + e_2\dot{M}^2 + e_1\dot{M} + e_0 \quad (2\text{-}2)$$

where $\Delta P'$ is the dimensionless pressure rise expressed in Eq. (2-3), $\dot{M}$ is the dimensionless mass flow rate defined in Eq. (2-4) and η_f is the fan efficiency. Based on the fan similarity laws (ASHRAE, 2008), $\Delta P'$and $\dot{M}$ are independent of fan speed and fan diameter.

$$\Delta P'(\dot{M}) = \frac{1000\,\Delta P}{\rho N^2 D^2} \tag{2-3}$$

$$\dot{M} = \frac{\dot{m}}{\rho N D^3} \tag{2-4}$$

where ΔP is the fan pressure rise (Kpa); ρ is the fluid density (Kg/m^3); N is the rotational speed (rev/s); D is the fan diameter and $\dot{m}$ is air mass flow rate (Kg/s).

ERS fan coil units provider catalog does not include fan characteristic curves to determine fan coefficient for FCU model. Pressure measurement at different flow rates corresponding to various damper positions is needed to determine the fan operational point at each fan speed. As Figure 2-4 demonstrates, the performed experiment measurements cover a narrow range of the performance curve of the employed fans. Therefore, the fan performance curve provided by the other manufacturers with similar operational conditions was used to determine the coefficients in Eqs. (2-1) and (2-2). The calculated coefficients for normalized fan performance curve can be found in APPENDIX B.

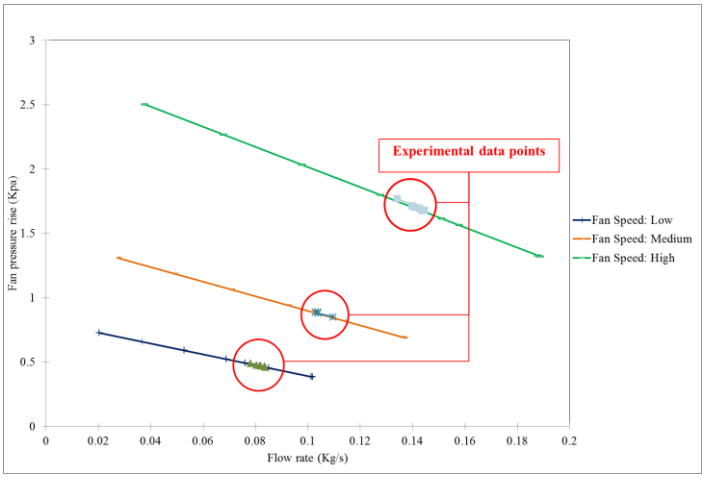

Figure 2-4. Fan performance curves at different speeds

2.3.2.2.2 Pressure resistance for mixed air damper

Outdoor air damper in the FCU is a single piece counter balance damper adjusting the proportion of outdoor and return air in supply air flow rate. In general, damper resistances are modeled by Eq. (2-5) (Legg, 1986):

$$\Delta P = K_\theta \frac{\rho v^2}{2} \tag{2-5}$$

where ΔP is the pressure drop across damper (Pa or Psf) ρ is air density (kg/m^3 or lbm/ft^3), v is mean air velocity (m/s or fpm), and K_θ is the loss coefficient calculated by:

$$log_e K_\theta = a + b\theta \quad \{15 < \theta < 55 \text{ for opposed, } 15 < \theta < 65 \text{ for parallel blades}\} \tag{2-6}$$

$$log_e K_\theta = A_1\theta^2 + B_1\theta + C_1 \quad \{0 < \theta < 15 \text{ for both opposed and parallel blades}\} \tag{2-7}$$

$$log_e K_\theta = A_2\theta^2 + B_2\theta + C_2 \quad \{55 < \theta < 90 \text{ for opposed, } 65 < \theta < 90 \text{ for parallel blades}\} \tag{2-8}$$

where θ is the angle between damper blade and the direction of air flow. a and b are constants. For opposed and single blades, a = -1.51 and b = 0.105 deg^{-1} and for parallel blades, a = -1.51 and b= 0.0842 deg^{-1}. A1, B1, C1, A2, B2, and C2 are parameters whose values need to be determined with the method introduce later.

Flow resistance, R (1/kg.m or 1/lbm.ft) for dampers are calculated from Eq. (2-9) (Norford and Haves, 1997).

$$R = \frac{\Delta P}{m^2} \tag{2-9}$$

where m is the air mass flow rate (kg/s or lbm/hr) and is calculated by:

$$m = \rho A_f v \tag{2-10}$$

where A_f is the face area of the damper (m^2 or ft^2). Combining Eqs. (2-5), (2-9) and (2-10), flow resistance for damper is calculated by:

$$R = \frac{K_\theta}{2\rho A_f^2} \tag{2-11}$$

The loss coefficient K_0 at fully open damper position (θ=0) is given by Eq. (2-12)

$$K_{\theta=0} = K_0 = 2\rho A_f^2 R_0 \tag{2-12}$$

where R_0 is the resistance of a fully open damper (1/kg·m or1/lbm·ft). The resistance of a fully closed damper, R_{90} (1/kg·m or 1/lbm·ft) is calculated by Eq. (2-13):

$$R_{90} = f_1^{-2} R_0 \tag{2-13}$$

where f_1 is flow leakage ratio, which is the ratio of the flow with a fully closed damper to the flow with a fully open damper. Therefore the loss coefficient $K_{\theta=90} = K_{90}$ at θ=90 (fully closed damper position) is expressed by Eq. (2-14)

$$K_{90} = 2\rho A_f^2 R_{90} = 2\rho A_f^2 f_1^{-2} R_0 \tag{2-14}$$

Parameters in Eqs. (2-6)-(2-8) including A_1, B_1, C_1, A_2, B_2, and C_2 are determined so that:

1) The gradients at points of θ=15 and θ=55/65 are continuous.

2) K_θ for θ=0 and 90 agree with those calculated from Eqs. (2-12) and (2-14)

The governing equations to obtain the parameters for damper model are given below (refer to INTERPAR subroutine in HVACSIM+)

$$@\ \theta = 15 \quad \frac{d(\log K_\theta)}{d\theta} = b = 2A_1\theta + B_1 \tag{2-15}$$

$$@\ \theta = 55 \quad \frac{d(\log K_\theta)}{d\theta} = b = 2A_2\theta + B_2 \tag{2-16}$$

$$@\ \theta = 15 \quad a + b\theta = A_1\theta^2 + B_1\theta + C_1 \tag{2-17}$$

$$@\ \theta = 55 \quad a + b\theta = A_2\theta^2 + B_2\theta + C_2 \tag{2-18}$$

$$@\ \theta = 0 \quad K_0 = 2\rho A_f^2 R_0 = C_1 \tag{2-19}$$

$$@\ \theta = 90 \quad K_{90} = 2\rho A_f^2 f_1^{-2} R_0 = A_2\theta^2 + B_2\theta + C_2 \tag{2-20}$$

Now there are 6 unknowns and 6 equations to calculate the required parameters estimating damper dynamic. Moreover, resistance for a fully open damper R_0 and a damper flow leakage ratio f_l are also needed.

2.3.2.2.2.1 Least square method application for damper dynamic validation

In order to accurately estimate damper dynamic, it is necessary to measure the pressure drop across the damper and corresponding outdoor air flow rate at different damper positions during a component test. In the designed experiment, the pressure difference across the damper was measured at different damper positions and fan speeds. Experimental data were used to obtain the unknown outdoor air damper parameters. In addition, coefficients a and b and the linear range region in Eq.(2-6) need to be validated using the experimental data because for outdoor air damper in FCU the angle for 0% open position is 65 and for totally open (100%) position is 0 degree.

In the conducted experiment, damper pressure drop and supply air flow rate was measured varying damper position. The proportion of outdoor air flow rate at every damper position is calculated using mixed air law. Although, there are some predicted inaccuracies in the calculation of $\frac{m_{RA}}{m_{SA}}$ and $\frac{m_{OA}}{m_{SA}}$ based on the return air, fresh air and mixed air temperatures; outdoor air flow rate measurement incorporates more inaccuracies. The assumptions associated with using this law are:

1- The location of mixed air sensor is so that it feels the temperature of air stream after two air streams including outdoor air and return air get thoroughly blend.
2- Room air temperature is used as return air temperature.

3- During the experiment, the adequate time span of changing damper position has been considered by the operator. Due to changes in damper position air stream regime alters and it takes time to reach to the steady state situation.

$\frac{m_{RA}}{m_{SA}}$ and $\frac{m_{OA}}{m_{SA}}$ are calculate by:

$$\frac{m_{OA}}{m_{SA}} = \frac{T_{RA} - T_{MA}}{T_{OA} - T_{RA}} \tag{2-21}$$

$$\frac{m_{RA}}{m_{SA}} = \frac{T_{MA} - T_{OA}}{T_{OA} - T_{RA}} \tag{2-22}$$

where T_{RA}, T_{MA} and T_{OA} are return air, mixed air and outdoor air temperatures (F or C) respectively and are automatically recorded at the test facility. The calculated ratios are demonstrated in Figure 2-5.

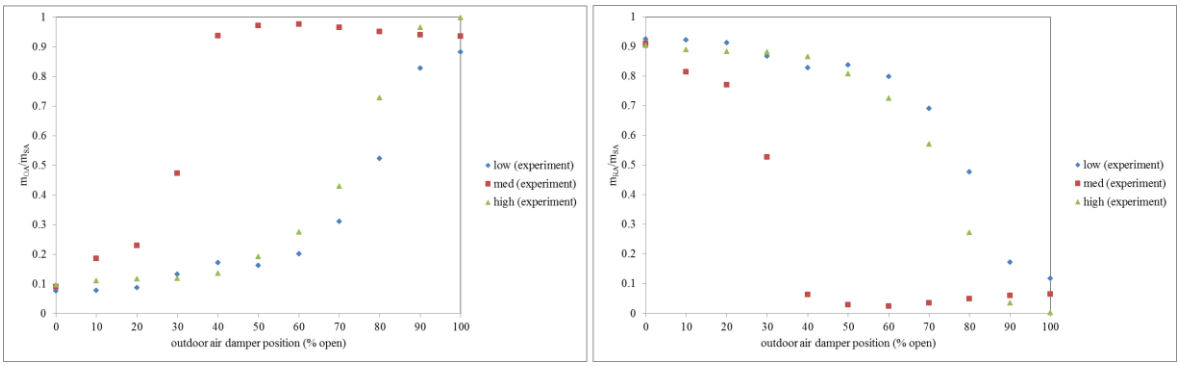

a) m_{OA}/m_{SA} vs. outdoor air damper positions b) m_{RA}/m_{SA} vs. outdoor air damper positions

Figure 2-5. The proportions of return air and outdoor air mass flow rate in supply air

As Figure 2-5 shows the calculated proportions at medium speed of the fan has a totally different trend from low and high speeds. The experiment shows that for low and high speeds of fan, damper position opens up gradually from fully closed to fully open but for medium speed the process is reverse. In the medium speed, transition occurs form turbulent flow to laminar. In other words, transition is from higher

entropy to lower which is in the reverse direction of natural phenomena and takes more time for the air stream to reach to the steady state situation. It is the reason behind totally different trend of m_{OA}/m_{SA} vs. damper position for medium speed of the fan.

Here, experimental data corresponding to high speed of fan are used to validate damper dynamic. The reason is that return air and outdoor air streams have enough kinetic energy to mix together and it is most probable that mixed air temperature sensor shows the well mixed air streams temperature. The calculated ratio of m_{OA}/m_{SA} for high speed of fan at 100% open outdoor air damper position given temperatures provides adequate evidence for this reasoning.

$log_e K_\theta$ is calculated form experimental data using Eq. (2-5).

$$log_e K_\theta = log_e \left(\frac{2\,\Delta P_\theta}{\rho v^2{}_\theta}\right) \tag{2-23}$$

where ΔP_θ is the pressure drop across damper (Pa or Psf) corresponding to the damper angle θ, and v_θ is the mean air velocity (m/s or fpm) calculated using:

$$v_\theta = \frac{Q_\theta}{A_f} \tag{2-24}$$

Where Q_θ is the measured volumetric flow rate (m^3/s or CFM) corresponding to the damper angle θ.

Figure 2-6 shows the calculated $log_e K_\theta$ from experimental data and the best fit model. Different try and errors show that the proper range of linear region for $log_e K_\theta$ is $7< \theta < 40$ and the new set of a and b coefficient were determined using least square method. To obtain the coefficients of lower and upper regions, $0< \theta <7$ and $40< \theta < 65$, INTERPAR subroutine in HVACSIM+ is used having $log_e K_\theta$ at fully open damper position for low end point of Eq. (2-7) and $log_e K_\theta$ at fully closed damper position for high end point of Eq. (2-8). Finally the required parameters for modeling

damper dynamic refer to Eqs. ((2-6)-(2-8)) and K_0 and f_1 are obtained and summarized in Table 2-1. The R^2 for damper model is 0.97.

Table 2-1. Calculated coefficients in Eqs. (2-6)-(2-8), K_0 and f_1 for damper model

Mixed air damper	a	b	A_1	B_1	C_1	A_2	B_2	C_2	K_0	f_1
	0.4877	0.0715	0.0118	−0.0942	1.0676	0.0156	−1.176	25.43	2.91	0.001

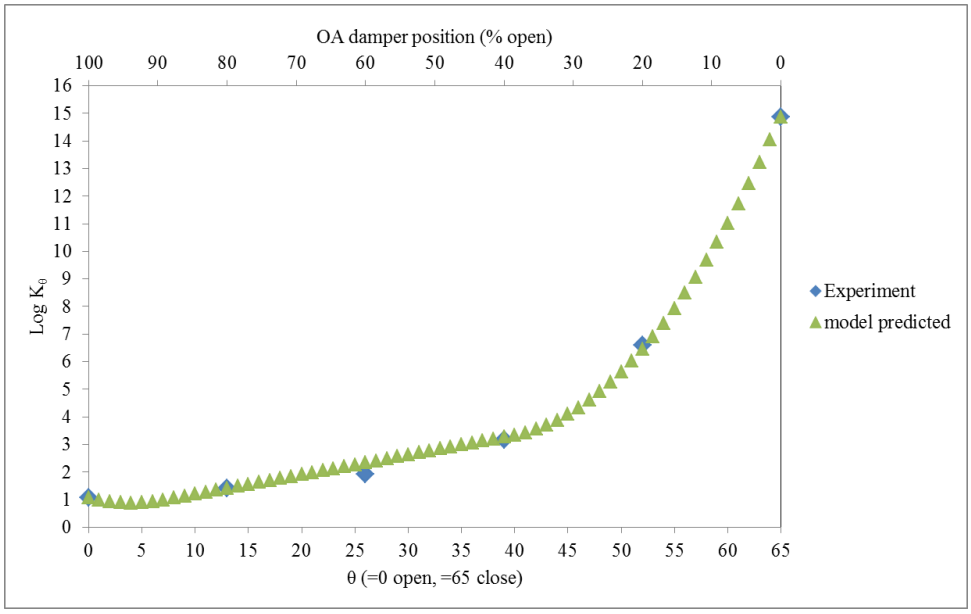

Figure 2-6. Experimentally calculated and model predicated Log K_θ vs. damper angle θ

2.3.2.3 Thermal network parameters determination

In the thermal network, the thermal interaction of FCU with the building zone is simulated. The FCU thermal state is represented by TYPE 314, a new TYPE added to HVACSIM+ library, and TYPE 403 represents the building zone thermal state. The thermal calculation of heating and cooling coils is performed base on the parameters representing their physical characteristics and water flow rate through the coil.

Cooling and heating water flow rate is adjusted by mean of two way valve for each coil. The physical parameters of coils are determined based on the manufacturer catalog or some simple measurements. While heating and cooling coil valve parameters determination is accomplished through component validation. Two experiments conducted for valve dynamic validation.

Section 2.3.2.3.1 briefly describes the procedure of zone parameters calculation and their values are presented in APPENDIX B. In section 2.3.2.3.2 the experiment conducted for cooling and heating coil valves component validation and the approach of identifying their parameters is discussed.

2.3.2.3.1 Building Zones thermal parameters

As is shown in Figure 2-1, ERS test facility consists of eight zones which exterior B-rooms are equipped with vertical four pipe fan coil units. Details about the zone envelope structure are provided by (Price and Smith, 2003) and like air flow parameters thermal parameters for zones are derived from 1312 project.

Building zones characterized by a uniform temperature and a perfectly mixed volume (supposed to be thermally homogeneous) are modeled by TYPE 403 in HVACSIM+ library of components. In TYPE 403, each building zone is composed of two sets of Two-Capacitor–Three-Resistor (2C3R) model (Norford and Haves, 1997, DeSimone, 1996). One set of 2C3R model represents the occupied space and the contents of the zone and the other set represents the corresponding plenum or unoccupied space and its contents (Figure 2-7). The two sets of 2C3R models are coupled together with a connecting resistance (R) which represents the ceiling separating the two spaces. As Figure 2-7 illustrates for each building zone, there are eleven parameters which need to be determined.

In Figure 2-7 the upper 2C3R network is representative of plenum and the lower one is room model the connecting resistance of the two networks (R11) is representative of ceiling. The constitutive resistances and capacitances of plenum 2C3R network are:

R21 represents light external wall and R22 and R23 are representative of proportioned structural resistances. C22 and C23 are internal and structural capacitance respectively.

Zone 2C3R network is composed of:

R01 represents light external wall and R02 and R03 are representative of proportioned structural resistances. C02 and C03 are internal and structural capacitance respectively.

Heat sources for zone directly added to the internal air node of zone network are lighting and equipment (Q_r) and occupant (Q_o) and HVAC heat gain (Q_v). Similarly heat gain in the plenum (Q_p) is added to the internal air node of the plenum network.

T_{pa} and T_{ra} are temperatures of the internal air and all light structures in the plenum and room model which are calculated in TYPE 403 as a weighted average, taking into account the influences of surrounding walls, the outside ambient air, leakage and infiltration from adjacent zones, and the supply air (Norford and Haves, 1997, DeSimone, 1996). T_p and T_r are plenum and zone structure temperature and T_{sa} is sol-air temperature.

To determine the global parameters of 2C3R network, the resistances and capacitances of all individually identifiable walls, floor and ceiling components of the zone including internal, external and connecting walls are needed to be defined. The global model is an attempt to bring together a large number of individual systems in order to render a complex system into a simple network replicating the real behavior

of the building zones. The details about the procedure and equations used to determine the resistance and capacitance of different constitutive components of the zone which consequently lead to determine the parameters for 2C3R global model are provided by DeSimone (1996) and are not reproduced here.

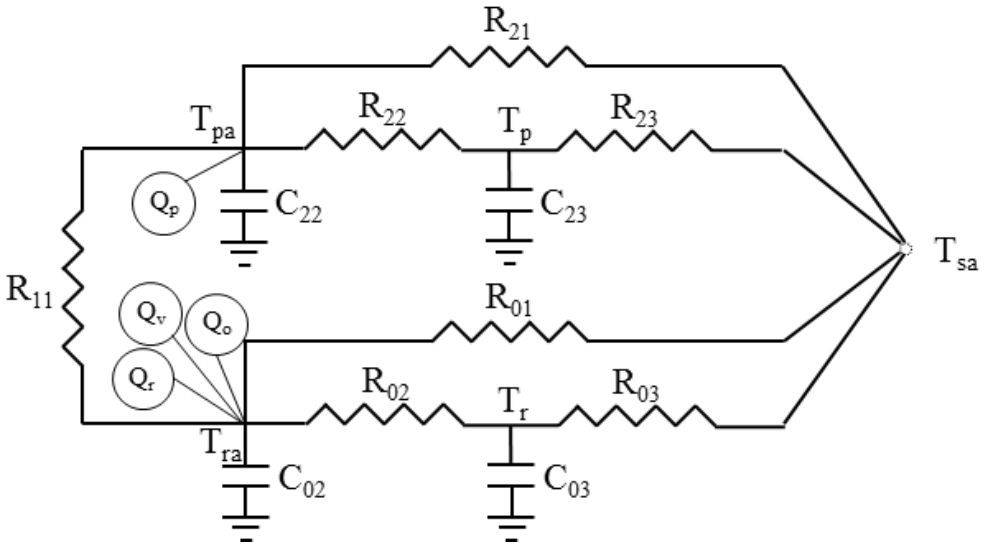

Figure 2-7. Illustration of a 2C3R model for a building zone (DeSimone,1996)

2.3.2.3.2 Cooling and heating coil valves model

HVACSIM+ provides a two port valve model (used in TYPE 522) which is illustrated in Figure 2-8. The provided valve model can have either linear or nonlinear behavior. When valve position varies, valve resistance changes and results in the change of water flow rates through the coil. As demonstrated in Figure 2-8, two resistances are used for two port valve model: coil flow resistance (R_{coil}) and valve resistance that controls the coil water flow rate (R_{valve}).

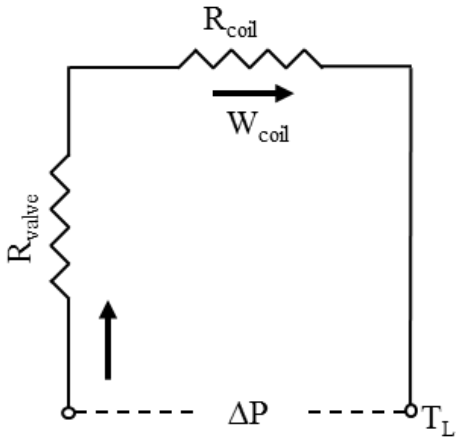

Figure 2-8. Diagram of a two port valve model

The two resistances are calculated based on valve position and valve characteristics. The following equation is used to calculate valve resistances (Norford and Haves, 1997):

$R_{valve} = 1296\ {K_v}^{-2} f^{-2}$ (SI unit) or $R_{valve} = 66.94\ {K_v}^{-2} f^{-2}$ (IP unit) (2-25)

Where K_v is valve capacity (m^3/hr or GPM) and f is fractional flow (%). f is a function of valve position x (ranging from 0 to 1). The procedure of calculating f is discussed in the following. Water flow rate through the coil is finally calculated by:

$$W = \sqrt{\frac{\Delta P}{R}} \quad (2\text{-}26)$$

Where W is the coil water flow rate (kg/s or GPM), ΔP is the pressure drop across the coil and valve (Kpa or in.w.c) and R is the total flow resistance (0.001 Kg.m or 0.001 lbm.ft) which is calculated by:

$$R = R_{coil} + R_{valve} \quad (2\text{-}27)$$

According to the manufacturer information cooling and heating coil valves are equal percentage. But component test for both valves show that their behavior is

different from equal percentage valves. For this reason, HVACSIM+ two port valve model with nonlinear behavior is not applicable to simulate cooling and heating coil valves properly. A new valve model is required to have the ability of simulating valve dynamic at different valve openings. To test valve dynamic, valve position is systematically varied from 0% to 100% open and the flow rates through the valve is measured while pressure drop across the cooling and heating coil kept constant. Analyses of experimental data indicate that both heating and cooling valves characteristics should be divided into three ranges:

For cooling coil valve: range1 (0% to 10% open), range 2 (10% to 80% open) and range 3 (80% to 100% open).

For heating coil valve: range1 (0% to 10% open), range 2 (10% to 70% open) and range 3 (70% to 100% open).

Valves behave differently over these three ranges. Therefore, valve is divided into three regions namely cut off region ($0 < x < x_l$); linear region ($x_l < x < x_h$) and high-end region ($x_h < x < 1$). Fractional flow is calculated using the following equation:

$$F=ax+b \tag{2-28}$$

Where a and b are:

For cut-off region ($0 < x < x_l$):

$$a= 0 \text{ and } b= C_L \tag{2-29}$$

(for cooling valve b=0.0001 and for heating valve b=0.00019)

For linear region ($x_l < x < x_h$):

$$a = \frac{C_H - C_L}{x_h - x_l} \; and \; b = \frac{x_h C_L - x_l C_H}{x_h - x_l} \tag{2-30}$$

For high end region ($x_h < x < 1$):

$$a = \frac{1-C_H}{1-x_h} \; and \; b = \frac{C_H - x_h}{1-x_h} \tag{2-31}$$

C_L and C_H are parameters representing fractional flow rate corresponding to valve positions at x_l and x_h respectively. As Figure 2-9 demonstrate for cooling valve C_L = 0.0001 and C_H = 0.9834 and based on Figure 2-10 for heating valve C_L = 0.00019 and C_H = 0.9703

Experimental data are used to estimate unknown parameters in the new valve model. Eqs. (2-25) to (2-27) are combined to obtain the following model equation:

$$\frac{1}{W^2} = \frac{1296}{\Delta P \; {K_v}^2} \; (ax+b)^{-2} + \frac{R_{coil}}{\Delta P} \text{ (SI unit)} \quad \text{or}$$
$$\frac{1}{W^2} = \frac{66.94}{\Delta P \; {K_v}^2} \; (ax+b)^{-2} + \frac{R_{coil}}{\Delta P} \text{ (IP unit)} \tag{2-32}$$

This equation can be rewritten into the linear form:

$$y = \theta_1 \emptyset_1 + \theta_2 \emptyset_2 \tag{2-33}$$

where $y = \frac{1}{W^2}$, $\emptyset_1 = (ax+b)^{-2}$, $\emptyset_2 = 1$, $\theta_1 = \frac{1296}{\Delta P \; {K_v}^2}$ and $\theta_2 = \frac{R_{coil}}{\Delta P}$. The calculated values for fractional flow f form Eqs. (2-29)-(2-31) are used to calculate $\emptyset_1$ at different regions and consequently applying least square method results in the values of unknown parameters. Table 2-2 summarizes the parameters for heating and cooling coil valves. Figure 2-9 & Figure 2-10 demonstrate the comparison between simulated heating and cooling coil water flow rate at different valve positions and corresponding experimentally measured values. Although, predicted flow rates by model does not exactly match with experimental values but it is representing the best fit model and yields to satisfactory results. The R^2 for cooling coil valve model is 0.62 and for heating coil valve model is 0.84.

Table 2-2. Cooling and heating coil valves parameters estimated from experimental data

Parameters	Explanation	Value
$R_{cooling\ coil}$	Cooling coil water flow resistance, 0.001 kg-m	90.18
$K_{V\text{-}cooling\ coil}$	Cooling coil valve capacity, m^3/hr	0.93
$C_{L\text{-}cooling\ coil}$	Cooling coil valve leakage (fractional flow), %	0.0001
$C_{H\text{-}cooling\ coil}$	Cooling coil high-end fractional flow, %	0.9834
$R_{heating\ coil}$	Heating coil water flow resistance, 0.001 kg-m	9584.4
$K_{V\text{-}heating\ coil}$	Heating coil valve capacity, m^3/hr	0.45
$C_{L\text{-}heating\ coil}$	Heating coil valve leakage (fractional flow), %	0.0002
$C_{H\text{-}heating\ coil}$	Heating coil high-end fractional flow, %	0.9703

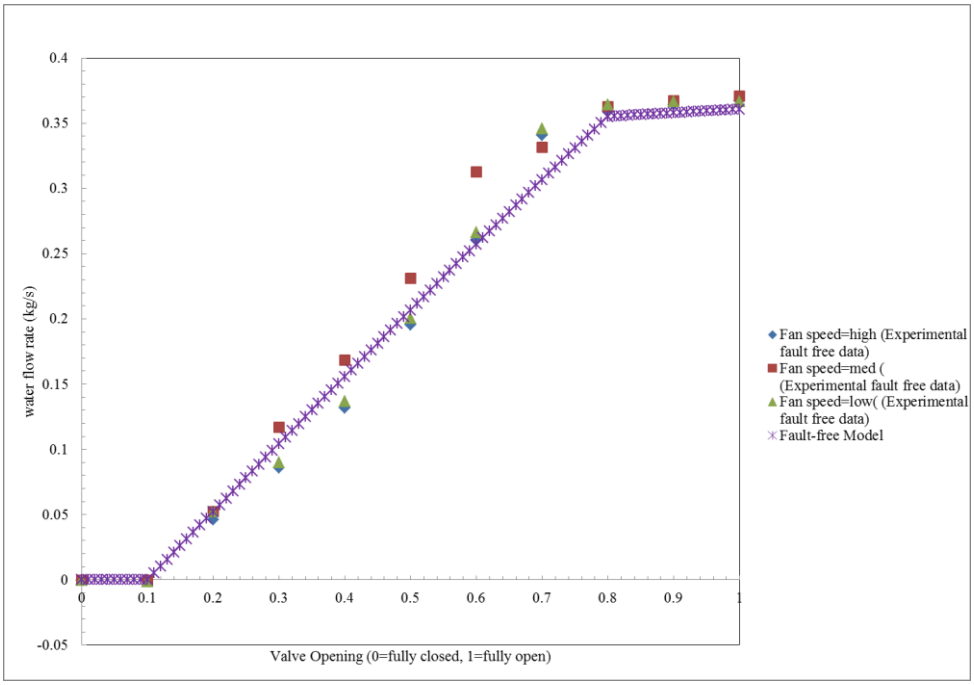

Figure 2-9. Experimental and simulated water flow rates vs. valve opening for cooling coil

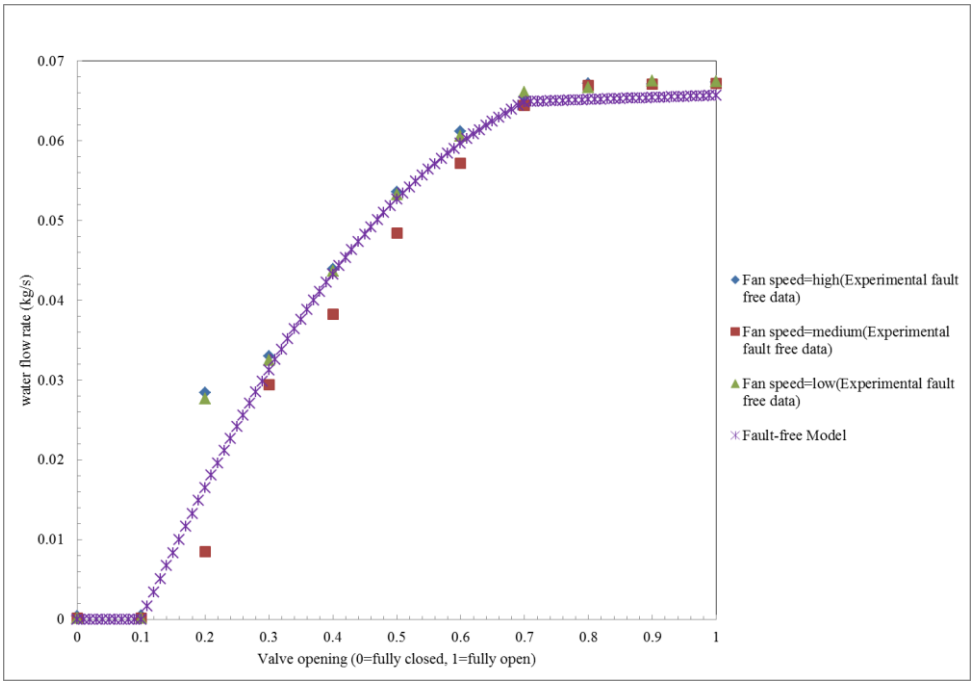

Figure 2-10. Experimental and simulated water flow rates vs. valve opening for heating coil

2.4 Boundary File Generation

The essence of HVACSIM+ simulation package can be found in MODSIM which contains the solver of this package. In order to solve the system of governing equations; it calls model definition file and boundary data files. Model definition file contains structure of the model, physical and geometric characteristics of each component, state variables initial value and state variables comprising time dependent boundary variables. Therefore, the FCU model is influenced directly or indirectly by both steady and time dependent factors that are included in the overall system simulation: device performance parameters, zone interior loads, outdoor air temperature and humidity, room and plenum temperatures, and inlet cooling and heating water temperatures. The three types of controllable internal loads in each test room are: lighting loads, sensible heat loads from people and false thermal loads generated by the baseboard heaters. The values of these boundary conditions are

directly determined from the test facility measurements. Internal gain profiles are provided to the model as time dependent boundary condition on the fractional basis according to ERS schedule for various zones. Figure 2-11 is representing the actual schedule of the internal gain profile. External gains consist of effective sol-air temperatures based on ambient air temperature, solar flux and external wall properties (DeSimone, 1996).

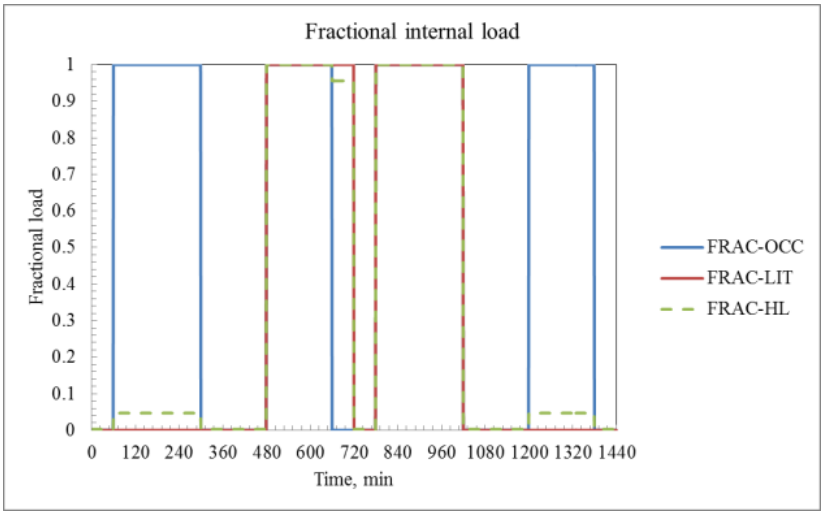

Figure 2-11. Fractional internal loads as time dependent boundary conditions

The ambient air physical properties and solar radiation effective on room heating and cooling loads as well as internal heat gains are defined as time variant boundary conditions.

2.5 Fault-free Model Validation

According to the literature there has been no prior work specifically about dynamic simulation and validation of FCUs. As evidenced by the lack of any dynamic model by which FCU performance can be simulated to generate data to assist further

research in their control and operation, as well as automatic fault detection and diagnosis. The comprehensive FCU dynamic model developed here is validated by comparing the data from simulated operation under fault-free condition with the corresponding experimental data from ERS. Validation of the FCU model is accomplished by a separate procedure at each of two levels: at the component level and at the system level. The component level validation described in the previous sections was accomplished to obtain the representative parameters of the corresponding components. During model development, nominal parameters for FCU performance within each TYPE were assigned only when suitable parameters from manufacturer data were not available. Assignment of nominal parameters was accomplished by an experimental procedure. Where manufacturer catalogs included parameters for key components like fan, mixed air damper, heating and cooling coil, component level validation was still conducted to ensure realistic model behavior. Despite all of the efforts have been to validate the components accurately there are some unavoidable uncertainty/error associated with measurement and data fitting. Therefore, system level performance may not be in a very close agreement with experimental data due to error propagation and problems with numerical stability and convergence in the calculations. In this section the system level validation procedure of fault-free dynamic simulation model for FCU is summarized.

2.5.1 Validation procedure

After component level validation to obtain FCU parameters, system level validation is accomplished to evaluate the performance of the integrated components all together. Furthermore, validation involves solving the right governing equations of the system under simulation and comparing model predicted results against field or

experimental data. For FCU system level validation, dynamic behavior of the model is validated by comparing simulation results with corresponding experimental data generated by ERS. ERS has generated experimental data under fault-free operation of FCUs interacting with exterior zones (east, west and south) for winter, summer and fall seasons. Dynamic simulation using the FCU model unavoidably requires an interacting zone model, including systemic interactions with the building's surroundings. Physical characteristics of zone interactions also needed to be assigned. Parameters from the ASHRAE 1312 research project (Li et al., 2010) were used to represent the thermal characteristics and zone mass interaction properties between ambient conditions and adjacent zones.

Variables examined for system level validation included cooling and heating coil valve positions, room air temperature, outdoor air damper position and hot water flow rate. Although discharge (supply) and mixed air temperatures are measured in the test facility, they are not used for validation due to very large experimental uncertainty caused by uneven flow profiles around sensors. Thermal network validation as an isolated superblock fed by supply air flow rate, outdoor air damper position, heating and cooling coil valve positions from experimental data as well as corresponding time dependent boundary condition raised this problem. The observations from thermal network validation showed large disagreement between the model predicted supply air and mixed air temperatures and the experimental ones (examined for couple days in different seasons). Figure 2-12 (a-c) illustrates the result of isolated validation of thermal network for a winter test day (Dec 22nd 2011). The corresponding control signals and supply air flow rate are provided to the model from experimental data.

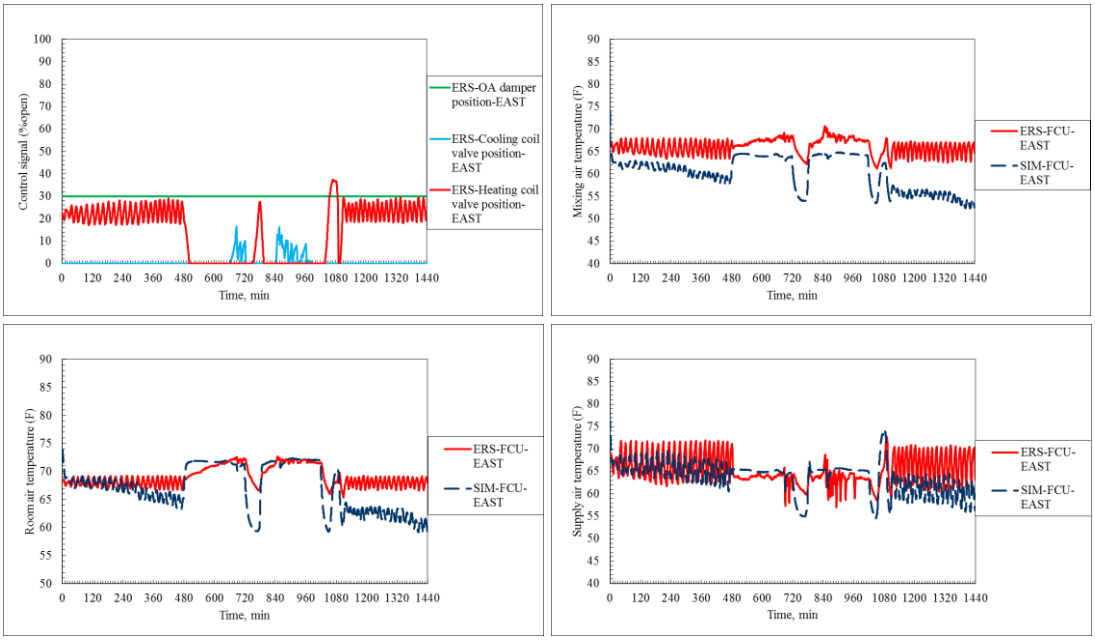

(a) East room FCU thermal network validation

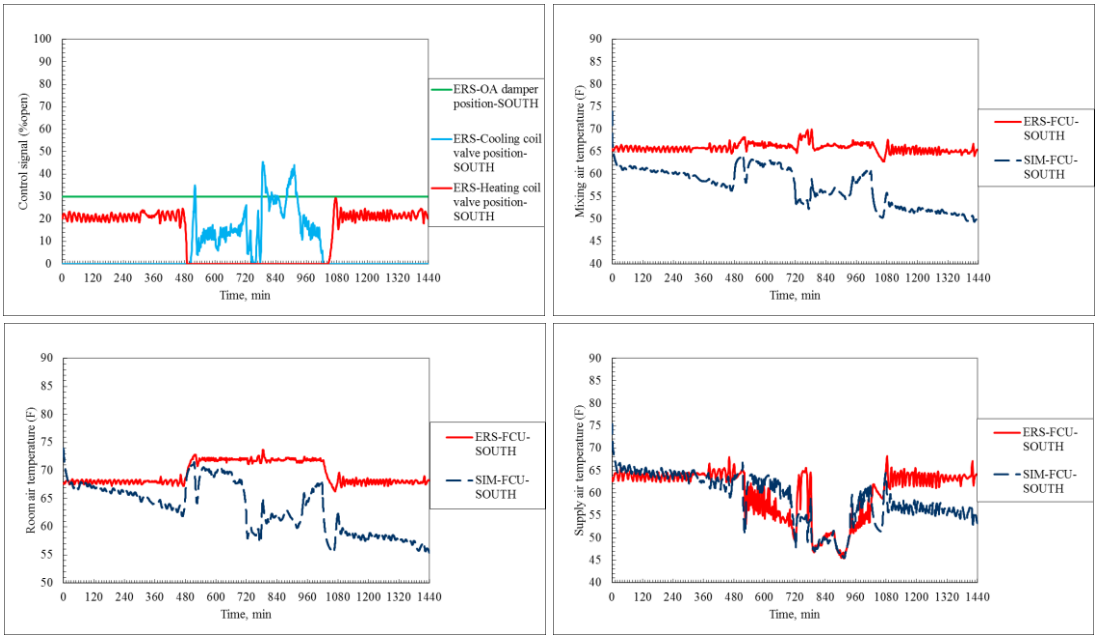

(b) South room FCU thermal network validation

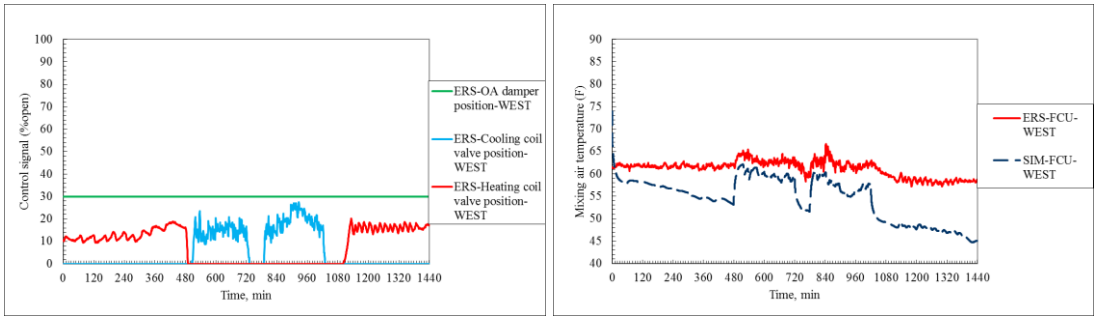

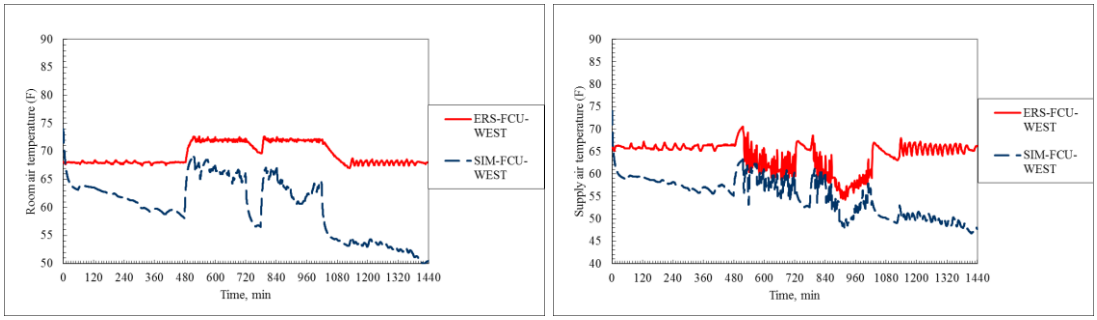

(c) West room FCU thermal network validation

Figure 2-12. FCU thermal network validation fed by control signals from experimental data

In order to narrow down the problem, further analysis was accomplished focusing on the coil model. Inlet air and water temperatures, inlet water and air flow rates were provided to the model from experimental data. In Figure 2-13 the observations of heating coil analysis on a winter test day (Jan 13th 2012) for east, south and west-facing rooms are illustrated. This analysis was done for a couple of test days but we suffice to illustrate the results of one day. As Figure 2-13 (a-c) demonstrates the model predicted results for supply air temperatures do not match with experimental data. The following evidences ended up to the conclusion that mixed and supply air temperature sensor reading are unreliable:

1) For south room and partially east room mixed air temperature which is the inlet air temperature of the heating coil is less than supply air temperature while FCU is in heating mode.
2) For all rooms there is large discrepancy between heat transfer rate for water side and air side for experimental data

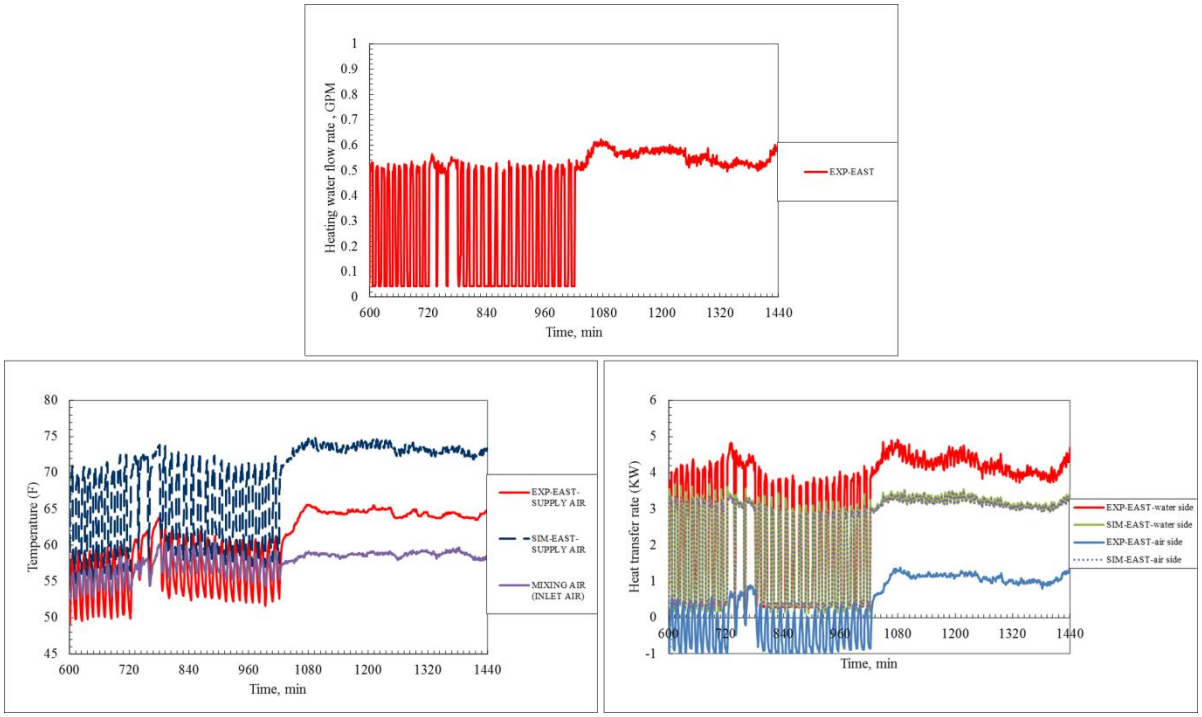

(a) East room

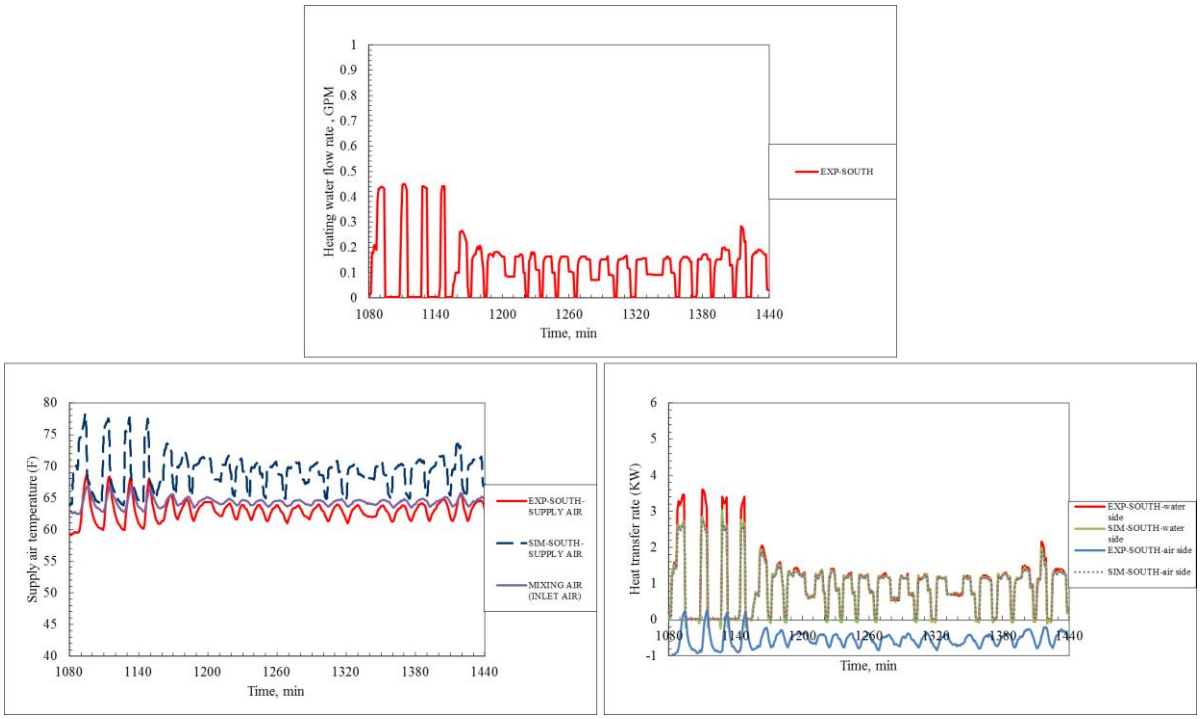

(b) South room

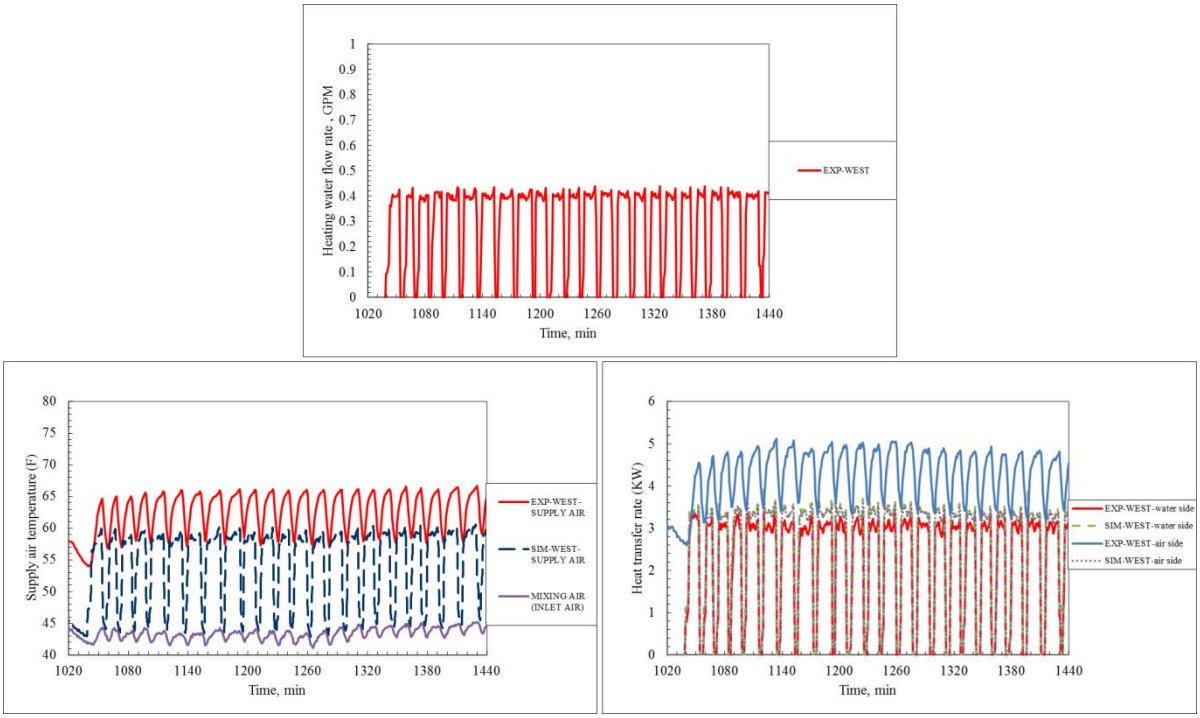

(c) West room

Figure 2-13. FCU heating coil performance for east, south and west-facing rooms

Those weird observed evidences called for more analysis. In order to further study this matter, the cases with no call for heating and cooling under the conditions of 0% open and 100% open outdoor air damper (26th & 29th Oct 2011) underwent investigation. Figure 2-14(a) illustrates comparison of supply, mixing and room air temperatures for east and west- facing rooms and Figure 2-14(b) demonstrates those temperatures comparison with ambient temperature for east, south and west-facing rooms. The uncertainty associated with mixing air and supply air temperature sensor can be clearly observed from the graphs. Especially Figure 2-14(b) illustrates uneven temperature profile for supply and mixing air temperatures while they are expected to be equal. In addition, the significant difference between ambient temperature and both supply and mixing air temperatures imply to the uncertainty associated with those temperature sensors.

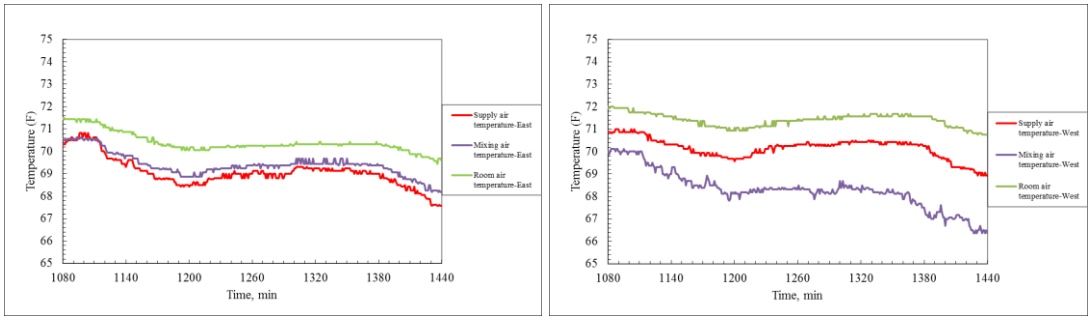

(a) Comparison of supply, mixing and room air temperatures (outdoor air damper=0% open, no call for heating and cooling)

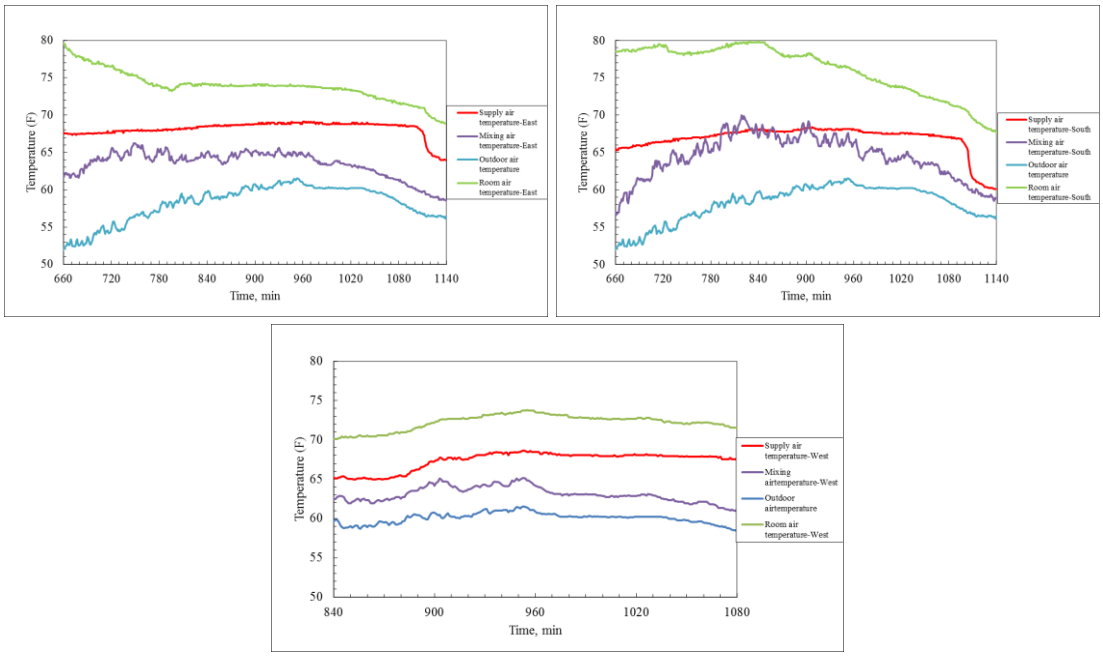

(b) Comparison of supply, mixing, ambient and room air temperatures (outdoor air damper=100% open, no call for heating and cooling)

Figure 2-14. Comparison of supply, mixing, ambient and room air temperatures with OA damper=% open & 100% open

The mixed air temperature sensor located in the mixing chamber/box of FCU does not reflect the well mixed temperature caused by mixture of fresh air and return air due to the limited space of mixing chamber. The error/uncertainty in temperature reading of mixed air propagates to supply air temperature profile too. In spite of uneven supply air temperature profile alongside the FCU, its sensor reflects a local point reading. All of these analyses and studies led us to ignore the mixed and supply

air temperatures for validation of FCU at system level. In the following sections the results of normal validation are illustrated and discussed.

2.5.2 Fault –free model validation results

Validation of the FCU model under fault-free condition is accomplished by a separate procedure at each of two levels: at the component level and at the system level. During model development, nominal parameters for FCU performance within each TYPE were assigned only when suitable parameters from manufacturer data were not available. Assignment of nominal parameters was accomplished by an experimental procedure. Where manufacturer catalogs included parameters for key components like mixed air damper, heating and cooling coil, component level validation was still conducted to ensure realistic model behavior. Although not detailed here, dynamic simulation using the FCU model unavoidably requires an interacting zone model, including systemic interactions with the building's surroundings. Physical characteristics of zone interactions also needed to be assigned. Parameters from the ASHRAE 1312 research project (Li et al., 2010) were used to represent the thermal characteristics and zone mass interaction properties between ambient conditions and adjacent zones. Finally, dynamic behavior of the model is validated by comparing simulation results with corresponding experimental data. Variables examined for system level validation include cooling and heating coil valve positions, room air temperature, outdoor air damper position and hot water flow rate. Although discharge and mixed air temperatures are measured in the test facility, they are not used for validation due to very large experimental uncertainty caused by uneven flow profiles around sensors. Validation of FCU fault-free model has been done on various days of three different seasons: fall, winter and summer. Figure 2-15

and Figure 2-16 show the simulation results comparison against experimental data on a summer test day (July 30th 2011) and winter test day (January 8th 2012) for east, south and west- facing rooms.

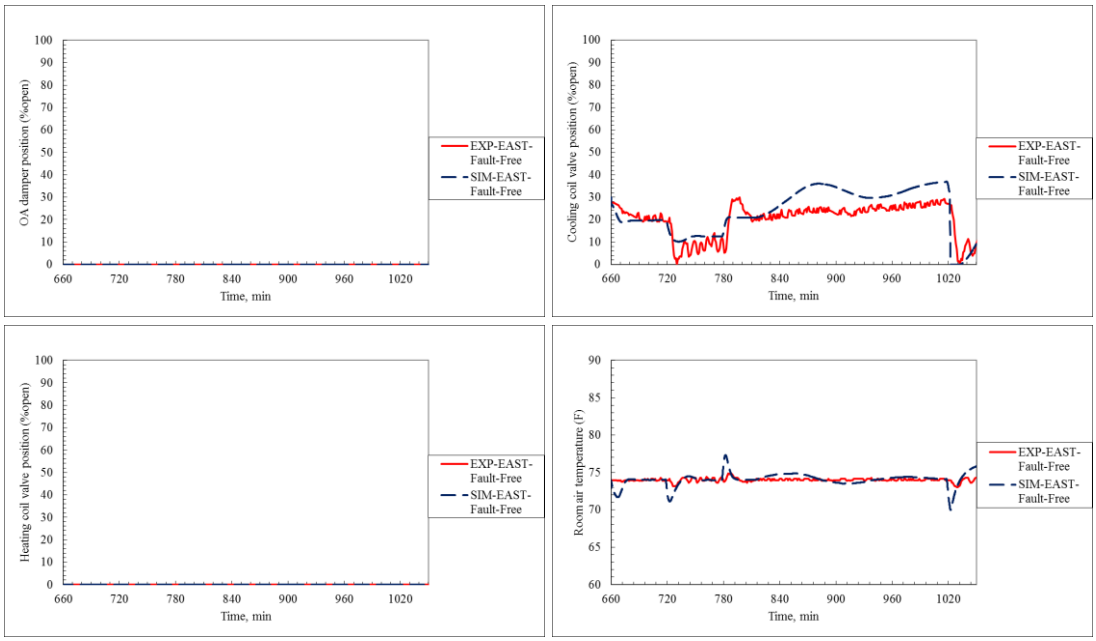

(a) East-facing room validation results

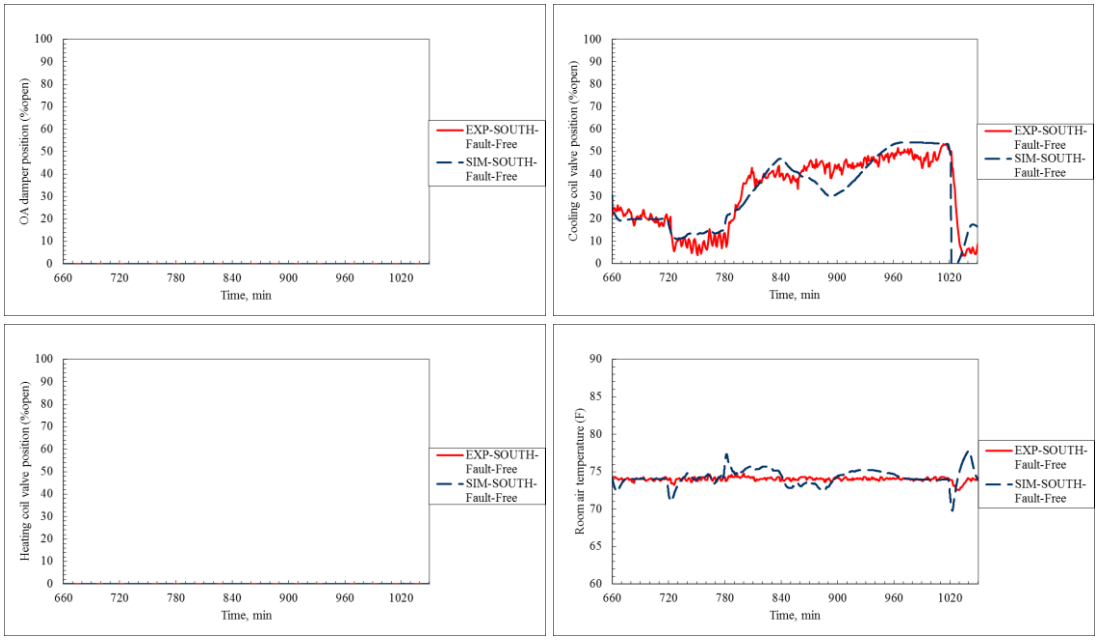

(b) South-facing room validation results

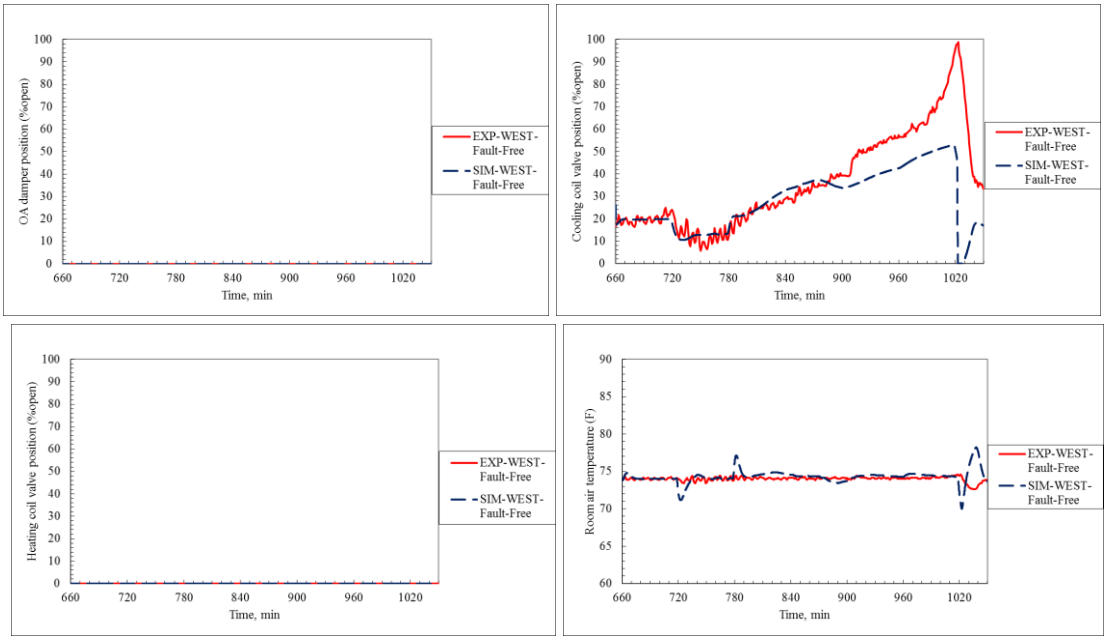

(c) West-facing room validation results

Figure 2-15. The results of FCU fault-free model validation in summer (07.30.2011)

In the presented graphs, the red line is representative of experimental data and navy blue line is representative of simulation results. In summer operation, the outdoor air minimum damper position is set to zero and the mixed air temperature set-point is set to 100 F so that it is always closed. Fan mode is in "On" mode which always runs at preset speed set at High during the normal test days, regardless the cooling or heating PID output. As the heating coil valve position graph shows, there is no need for heating and the FCU is operating in cooling mode in the depicted time window. In the beginning of the simulation especially for east and west-facing rooms, the cooling coil valve position tracks the value and trend of the experimental data but as it gets closer to the evening the discrepancy between the two cases emerges. The discrepancy between the simulated cooling coil valve position and the real position arises from two factors. First, component tests for valve model validation were only performed in the south facing room. Although ERS FCUs in the exterior rooms are

the same, there might be some differences that were neglected here. Secondly, the simulated zone is more sensitive to changes in internal load and ambient air fluctuations than the actual zone. The simulated room air temperature is representative of well mixed air within the room, but in reality the room temperature sensor may reflect a local temperature that is not necessarily reflective of a bulk room temperature. For these reasons, the dynamics of the modeled FCU display some deviation from the real FCU due in part to unavoidable simplifications to the zone model that were necessary to keep the zone model tractable.

The performance of the developed model in predicting the dynamic variables for FCU is evaluated using the R^2 and RMSE defined in Eqs. (1-1) & (1-2)) and is tabulated in Table 2-3.

Table 2-3. FCU model performance for summer test day (07.30.2011)

Variable		R^2	RMSE
Cooling coil valve position	East Room	0.56	8.173
	South Room	0.33	18.586
	West Room	0.67	9.237
Room air temperature	East Room	0.65	0.75
	South Room	0.45	1.053
	West Room	0.68	1.292

To show the performance of the developed model in different weather condition a winter test day (01.08.2012) is picked. Figure 2-16 demonstrates the simulation result compare with the real one for this day.

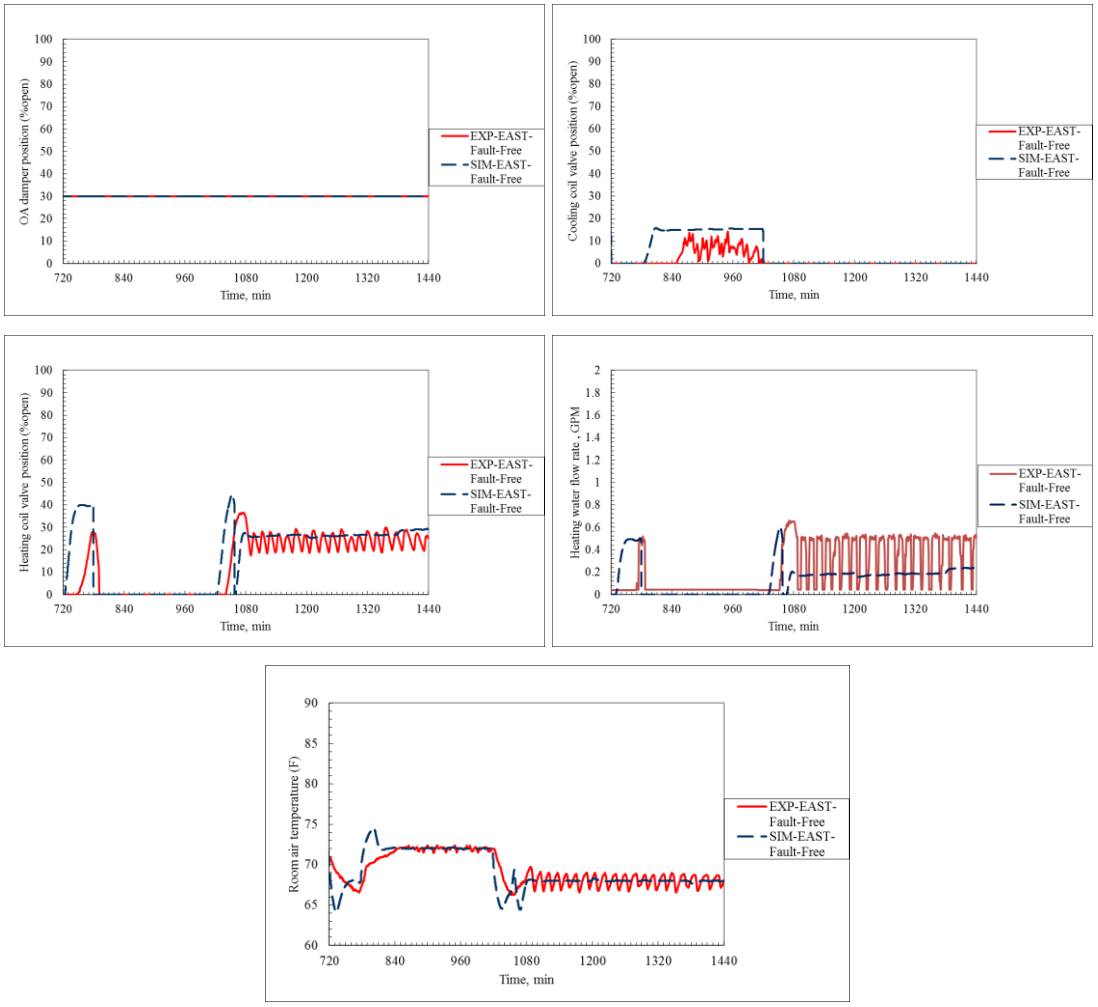

(a) East-facing room validation results

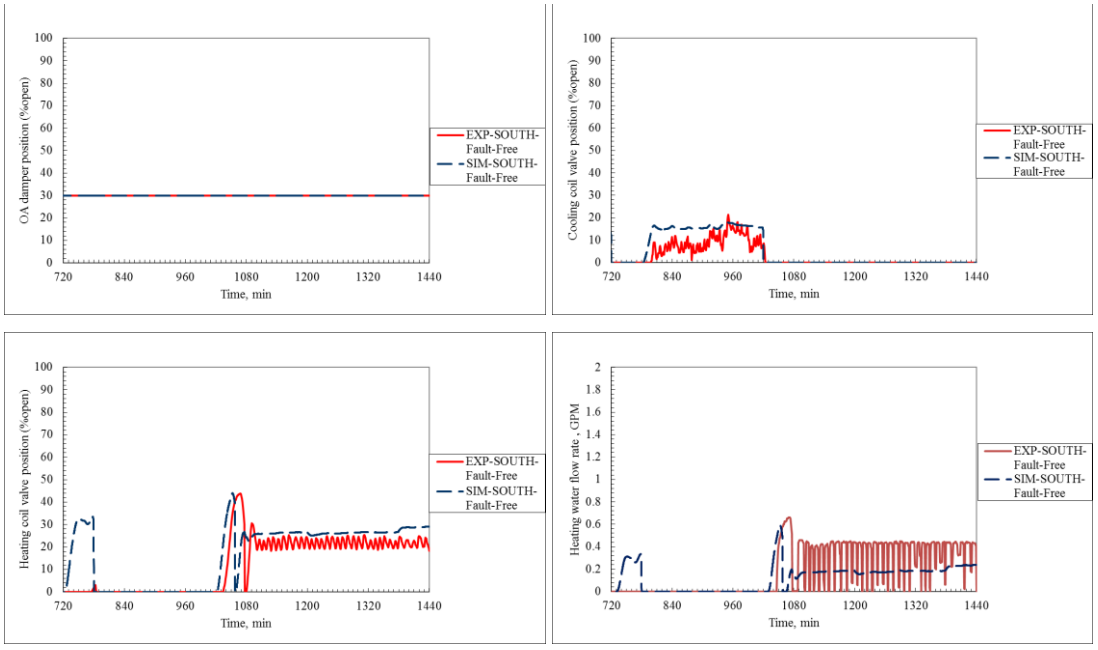

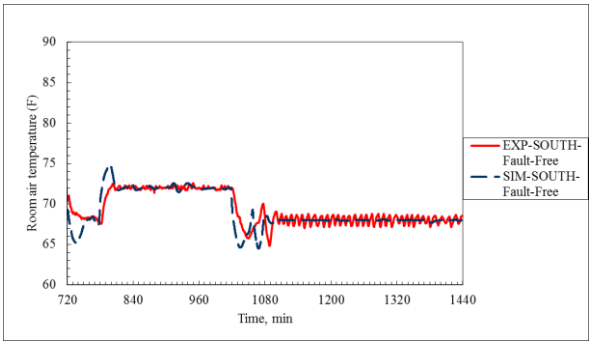

(b) South-facing room validation results

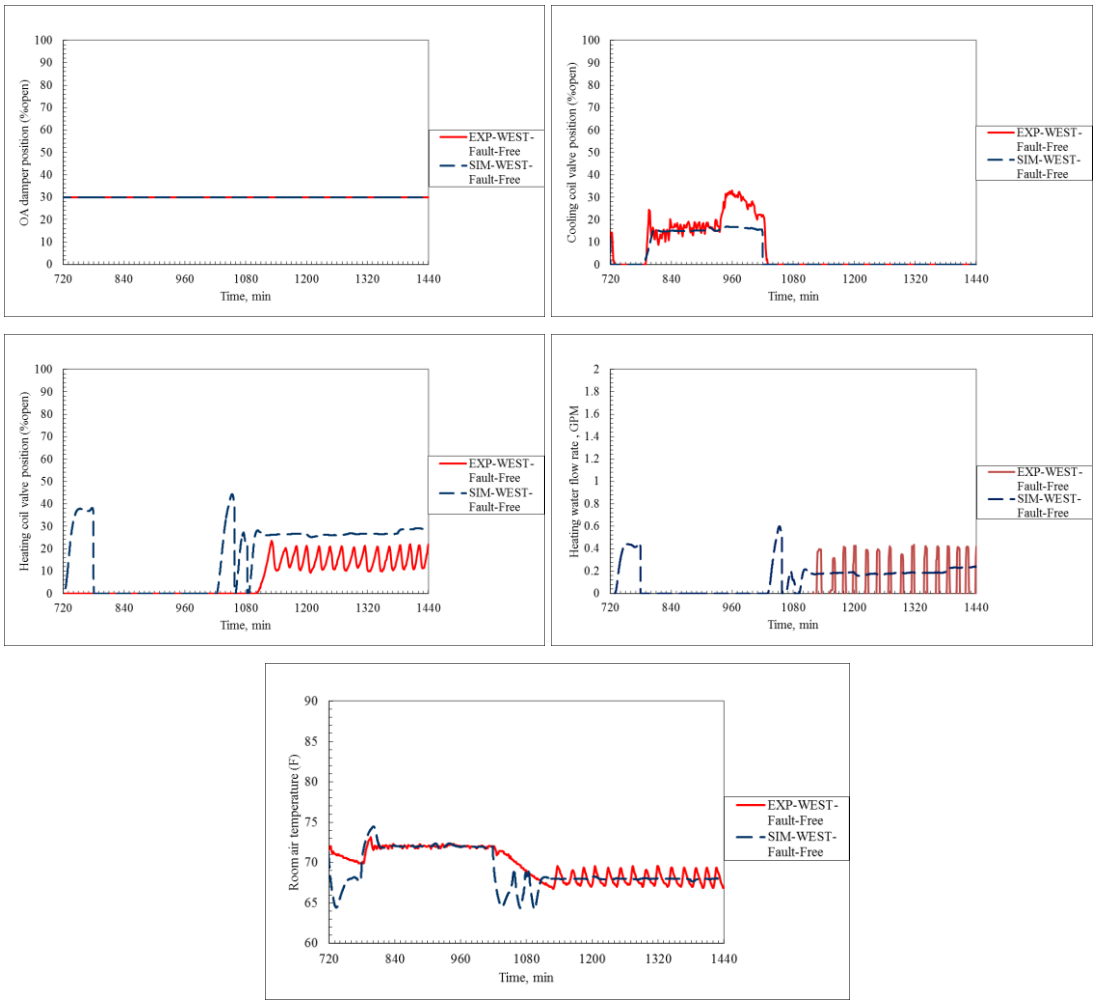

(c) West-facing room validation results

Figure 2-16. The results of FCU fault-free model validation in winter (01.08.2012)

Validation of the FCU model for winter also demonstrates the same trend and led to the same conclusion. As Figure 2-16 demonstrates as soon as turning off the

internal loads in 720-780 and 1020-1200 time frames; the modeled room calls for heating while the real room either has lag or no call for heating. In addition, the room model in TYPE 403 using 2C-3R model does not consider the solar beam radiation transferred trough glazing. Considering the fact that ERS exterior rooms are facilitated with large windows without any covering; the amount of solar radiation transmitted to the room can't be negligible. This evidenced the lag of the real room response to the absence of internal load. Table 2-4 represents the performance of the model for the winter test day.

Table 2-4. FCU model performance for winter test day (01.08.2012)

Variable		R^2	RMSE
Cooling coil valve position	East Room	0.53	6.017
	South Room	0.79	4.337
	West Room	0.86	4.695
Heating coil valve position	East Room	0.51	10.698
	South Room	0.52	10.536
	West Room	0.36	15.152
Room air temperature	East Room	0.63	1.388
	South Room	0.75	1.15
	West Room	0.45	1.891

2.6 Fault Model Development

Faults can be modeled in two different ways (Haves, 1997): 1) by changing parameter values in a fault-free model, such as reducing the UA value (heat conductance coefficient) to model a fouled coil in a simple coil model; and 2) by extending the structure of a fault-free model to treat faults explicitly, such as modeling a coil fouling fault by adding a new parameter that specifies the thermal resistance of the deposit in a detailed coil model. In this study, faults are modeled by

changing values of existing parameters, avoiding the need to develop new model components explicitly replicating faults. A fault flag arrangement is employed to allow the user to select a fault type and severity. The category of faults which may occur in FCUs and the devices affected by these faults are listed in Table 2-5. The FCU model simulates those faults with varying severity, which projects proportionally to the fault symptoms observable in data. As Table 2-5 demonstrates, various fault categories associated with FCU are listed in four different categories: equipment, sensor, controlled devices and controllers. In the following sections a brief review of various categories of potential faults for FCU and the type of faults which are artificially implemented to different devices are described. Furthermore, the fault flag arrangement imposing the fault type and severity to the simulation model is discussed.

Table 2-5. FCU fault summary

Category	Device	Fault Name	Fault Type	Summer Test Days	Fall Test Days	Winter Test days
Equipment	Fan	Failure	Abrupt		1	
		Outlet Blockage	Abrupt		1	
	Heating Coil	Fouling-Airside	Degradation			2
		Fouling-Waterside	Degradation			1
	Cooling Coil	Fouling-Airside	Degradation	2		
		Fouling-Waterside	Degradation	2		
	Filter	Filter Restriction	Degradation	1		1
	Economizer	Restricted Airflow	Opening Blockage		1	1
		Leaking OA/RA DMPR	Degradation		1	1
Sensor	Room Temp	Offset	Degradation	2		2
	MA Temp	Offset	Degradation		2	2
Controlled Device	Heating Valve	Stuck	Full Open			1
			Full Closed			1
			Partial Open			1
		Leaking	Degradation			1
	Cooling Valve	Stuck	Full Open	1		
			Full Closed	1		
			Partial Open	1		
		Leaking	Degradation	1		
	OA/RA Damper	Stuck	Full Open	1	1	
			Full Closed		1	
			Partial Open	1	1	1
Control	FCU Cycle I Control	Unstable Control	Degradation	1	1	
	FCU Cycle II Control	Unstable Control	Degradation	1	1	
	FCU Cycle III Control	Unstable Control	Degradation		1	1
	Heating Control	Reverse Acting	Implementation		1	1
	Cooling Control	Reverse Acting	Implementation	1	1	

2.6.1 Equipment Fault

The components of FCU may undergo faulty condition where faults could occur in fan, coil (heating or cooling) filter and economizer. For fan, two types of faults, namely, fan motor failure/ fan bearing seized and discharge outlet blockage are modeled. Complete failure fault is modeled by outputting zero fan movement and outlet blockage fault is modeled by adding a user specified bias to the simulated pressure drop in FCU.

Two types of faults, namely, air side fouling and water side fouling are modeled for coils. The studies in the literature shows that heat exchanger fouling can be implemented by altering the heat-transfer coefficients (Bendapudi and Braun, 2002) or the increase of thermal resistance can be represented by a fouling factor (House et al.,1999). In this study, water side fouling fault in the experiment is imitated by reducing the amount of hot or chilled water flow rate to a certain amount of total water flow rate. Therefore the heat transfer coefficient or resistance does not change. In the model it is replicated by increasing water flow pressure resistance of the coil by a user specified value without affecting heat transfer coefficient. There is the same situation for air side fouling; without manipulating air side heat transfer coefficient the air flow pressure resistance is increased by a user specified value.

Filter fault is caused by depositing dirt and dust in it and results in more air pressure drop passing through the filter. To replicate this fault in the model the air flow pressure resistance is increased by a user specified value. Opening blockage of outdoor air damper by debris, leaves etc. is the cause of restricted air flow fault for economizer in equipment fault category which is replicated by increasing the pressure resistance of the damper by a user specified value. Degradation of seating location of mixed air damper caused its leakage and is modeled by adjusting a user specified outdoor air flow rate when the damper is at fully closed position for outdoor air.

2.6.2 Sensor Fault

Offset fault for mixed air temperature and room air temperature sensor is modeled by adding a user specified bias to the simulated sensor output, which is achieved by Eq. (2-34)

$$Y_{output} = Y_{input} + Bi \tag{2-34}$$

Where Y_{output} and Y_{input} are the output and input of sensor and Bi is user specified bias which keeps constant with time.

2.6.3 Controlled Device Fault

Controlled device category includes mixed air damper and heating and cooling valves faults. Two types of faults, namely, stuck fault and leaking fault are modeled for valves and stuck fault is modeled for mixed air damper. Stuck fault which occurs due to the actuator malfunction for both damper and valves is modeled by fixing the simulated controlled device position to be a user specified position. Leaking fault which is caused by wear and tear is modeled by adjusting a user specified flow rate when the controlled device is 100% closed.

2.6.4 Controller Fault

Two types of control faults, namely, unstable control fault and reverse acting control fault, are modeled in this study. Unstable control fault occurs when the PID loops has not been tuned properly and the system is unstably controlled. This fault is modeled by implementing a user specified proportional band for PID controllers. A reverse acting actuator is a typical commissioning fault usually caused by incorrect setting of the directional switch on the actuator. During this fault, the actuator follows the control signal command reversely (i.e., the actuator closes down the heating valve instead of opening it up).

2.6.1 Fault flag system

It is important to design a proper fault flag system that can be used by the users to indicate fault selection and their associated severities. In this study, the fault model implementation has been accomplished by designing a fault flag system in MODSIM

HEAD subroutine (Fortran 90). It is accessible to each TYPE of HVACSIM+ library of components. In the designed fault flag system the category of fault is reflected by the fault variable and the associated fault severity is determined by the fault severity variable. The designed fault flag system for FCU has been summarized in Table 2-6. In Table 2-6, the first column lists the four fault categories, which are equipment, sensor, controlled device and controller faults. The second column lists the device or process that would be affected by a fault. The third column summarizes the potential fault status and fault type for a device or process. The fourth and fifth column list variables used in MODSIM HEAD subroutine to store fault type and severity for each device or process. The last column lists the TYPE in HVACSIM+ library of component that would be affected by the faults associated with each device or process.

Table 2-6. FCU fault flag system summary

Category	Device	Fault type	Fault variable	Fault severity variable	TYPE
Equipment	Fan	0- No fault, 1- Fan motor failure, 2- Fan outlet blockage	fan	Vfan	307
	Heating Coil	0- No fault, 1- Fouling Air-side, 2- Fouling Water-side	coilfault(4)	Vcoilfault(2,3)	314
	Cooling Coil		coilfault(3)	Vcoilfault(2,3)	314
	Filter	0- No fault, 1- Filter restriction	filter	Vfilter	307
	Economizer	0- No fault, 1- Restricted air flow, 2- leaking mixed air damper	economizer	Veconomizer	307
Sensor	Room air temperature sensor	0- No fault; 1- Offset fault	RAtemp	VRAtemp	311
	Mixed air temperature sensor		MAtemp	VMAtemp	311
Controlled Device	Heating Valve	0- No fault, 1- Stuck, 2- leakage	coilfault(2)	Vcoilfault(1)	314
	Cooling Valve	0- No fault, 1- Stuck, 2- leakage	coilfault(1)	Vcoilfault(1)	314
	OA/RA Damper	0- No fault, 1- Stuck	OAdamp	VOAdamp	307
Controller	Heating coil control	0- No fault, 1- Unstable	CONheat	VCONheat	479
	Cooling coil control	0- No fault, 1- Unstable	CONcool	VCONcool	479
	Heating coil reverse action	0- No fault, 1- Reverse	CONheatreverse	-	321
	Cooling coil reverse action	0- No fault, 1- Reverse	CONcoolreverse	-	321

2.7 Fault Model Validation

Given the simulation system model had been validated under fault-free conditions, the only further validations required to ensure realistic representation of faults were those on the altered parameter values. During the validation of fault modeling, it is more important to compare fault symptoms rather than regenerating

the dynamics of each variable. This is due to the complex impacts of faults under real world conditions, and the difficulty of simulating such impacts precisely. Therefore, faulty operation validation does not need a comprehensive process as described for fault free validation. In the following subsections the procedure of fault model validation for FCU is described.

2.7.1 Validation procedure

Both simulation results and experimental data are used to validate the modeling of faults, involving simulation results under both faulty and fault-free conditions (to identify simulated fault symptoms), and similarly for experimental real data (to identify the real fault symptoms). The fault-free and faulty simulation results are generated by adjusting fault flags. In order to ideally validate the system under faulty condition; fault-free experimental data of a similar system running in parallel with the faulty system is necessary. There is a lack of experimental data under fault-free conditions for the same test day and exterior rooms undergoing the faulty test. Thus, a normal test day with close or more severe weather condition (that is, a condition that will cause system variables to change similarly as the tested fault) is picked as a reference day to confirm that the system behavior and the observed symptoms in real data are resulted from the fault and not the weather. As an example, for heating reverse action fault in FCU on Jan 14th a warmer fault-free test day can serve as reference day. Comparison with a warmer test day helps to justify that the observed symptoms are just due to the fault regardless of weather condition. As Figure 2-17 displays, Jan 8th with a warmer weather condition is a candidate to be a reference day for Jan 14th. In Figure 2-17, the normal test day weather conditions are shown by solid lines and the dotted line represents faulty test day weather conditions.

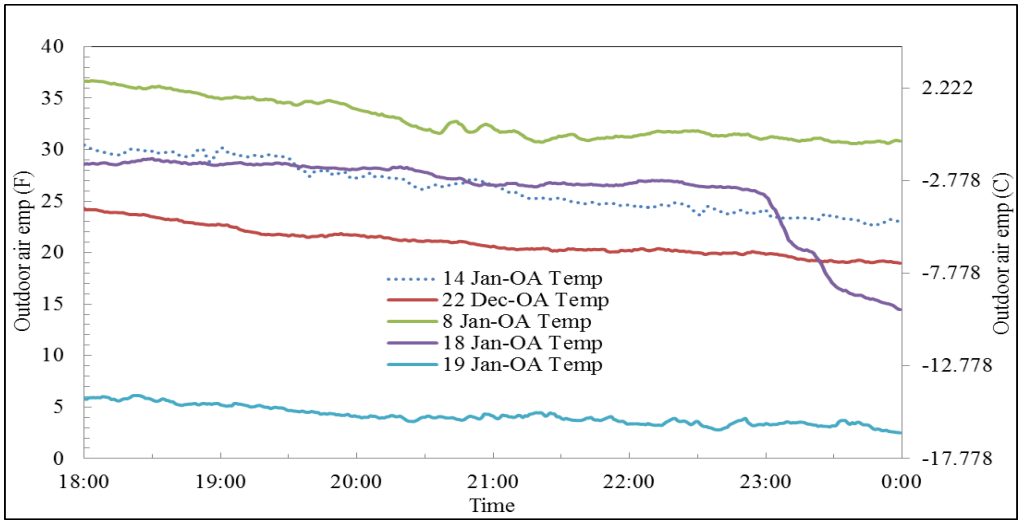

Figure 2-17. Weather comparison to pick a normal test day as reference day for heating control reverse action fault in FCU

To assist validation of FCU fault model, experimental data under faulty conditions (under different faults and severity levels) are collected from east and west facing rooms in the ERS. Like fault-free tests, three test periods are scheduled during summer, fall and winter for collecting faulty experimental data. Different faults are implemented in different seasons because system operational characteristics and control sequence change with weather conditions. Table 2-5 demonstrates the faulty condition which has been tested in different seasons. The season operation has been selected so that a specific fault yields measurable system difference compared with a fault-free system. Since it is impractical to test all levels of severity for a degradation fault only two or three levels of severity has been tested for each degradation fault. Some faults have similar effects on the system during different seasons.

2.7.2 Fault model validation results

Validation of FCU fault model has been done on all faulty test days of three different seasons: fall, winter and summer. For brevity a few fault cases from each category is picked to demonstrate the symptoms associated with a certain fault and

defined severity. The following figures depict the comparison of simulation results under faulty and fault-free conditions with the corresponding experimental operational data. In the presented graphs, red and dashed navy blue lines are representative of experimental data and simulation results, respectively, under the faulty condition. In the same way, purple and dotted green lines are representative of experimental data and simulation results under fault-free condition.

From the equipment category heating coil air-side fouling, cooling coil water-side fouling as well as fan failure faults are picked to show the symptoms associated with these faults. Figure 2-18 (a) demonstrates the fault model simulation results of FCU with heating coil air-side fouling fault on a winter test day (Dec 24th). Air side fouling in the coils happens gradually due to the deposition of indoor dusts and other particles included in indoor or outdoor air on the heat exchanger surfaces in contact with air. Air side fouling of coils leads to increase in system pressure drop and, correspondingly, decrease in heat transfer rate and eventually degrade system performance. In the test site this phenomena is testing just by reducing fan speed mimicking the decrease of supply air flow rate due to increase in pressure drop followed by fouling while under normal condition fan speed is always at high. Thus replicating this fault in the simulation is just by increasing the pressure resistance without manipulating heat transfer coefficient of the coil. In order to emphasis the symptoms associated with heating coil air-side fouling the closest normal test day is selected (Jan 8th). The symptoms associated with this fault are listed as the following:

1) Increase in cooling coil valve position. Heat transfer rate in water-side of cooling coil increases by water flow rate elevation to compensate the decrease of cold air flow rate due to the fouling.

2) Decrease in heating coil valve position and consequently hot water flow rate. Due to this fault, air passages in heating coil are blocked which causes increase in pressure drop and decrease in air flow rate. Air flow rate drops and consequently the proportion of fresh cold air in the supply air decreases which leads to decrease in heat transfer rate on both sides.

Figure 2-18 (b) demonstrates the fault model simulation results of FCU with cooling coil water-side fouling fault on a summer test day (July 24th). The water side fouling is caused by deposition of mineral material of circulating water on the surfaces of heat exchanger in contact with water. This phenomenon results in heat exchanger performance degradation by reducing the overall heat transfer coefficients and increasing the resistance to the fluid flow. In the experiment, water side fouling faulty test is employed by restricting the maximum water flow rate through the coil by 50% and 25% to mimic the increase of resistance to water flow rate. Thus, heat transfer coefficient of the coil does not change during the experiment. Replicating this fault to the model is accomplished just by increasing water side pressure resistance without manipulating heat transfer coefficient of the cooling coil. The closest normal test day to serve as reference day is July 16th. The symptoms associated with this fault are listed as the following:

1 Increase in cooling coil valve position. Cooling water flow is restricted due to this fault therefore its lack during the cooling mode operation of FCU is compensated by increase in valve position.

2 Increase in room air temperature. Increase in cooling coil valve position in the morning result in more chilled water flow rate which is adequate to keep room temperature set point. But restricted chilled water flow rate shows its obvious

effect in the afternoon. Even fully opening of cooling coil valve does not result in adequate water flow rate to keep room cooling temperature set point.

Figure 2-18 (c) depicts the fault model simulation results of FCU with fan failure fault on a fall test day (Oct 21st). A cooler normal test day is selected to serve as reference day (Oct 20th). The symptoms associated with this fault are as the following:

1) Increase in cooling coil valve position. Cooling valve position elevation is the results of decrease in forced convection heat transfer rate due to the fan failure.
2) Room temperature floating. Even fully opening of the cooling coil valve is unable to meet room cooling demand. Because the equipment in charge of blowing the air through the coils is broken.

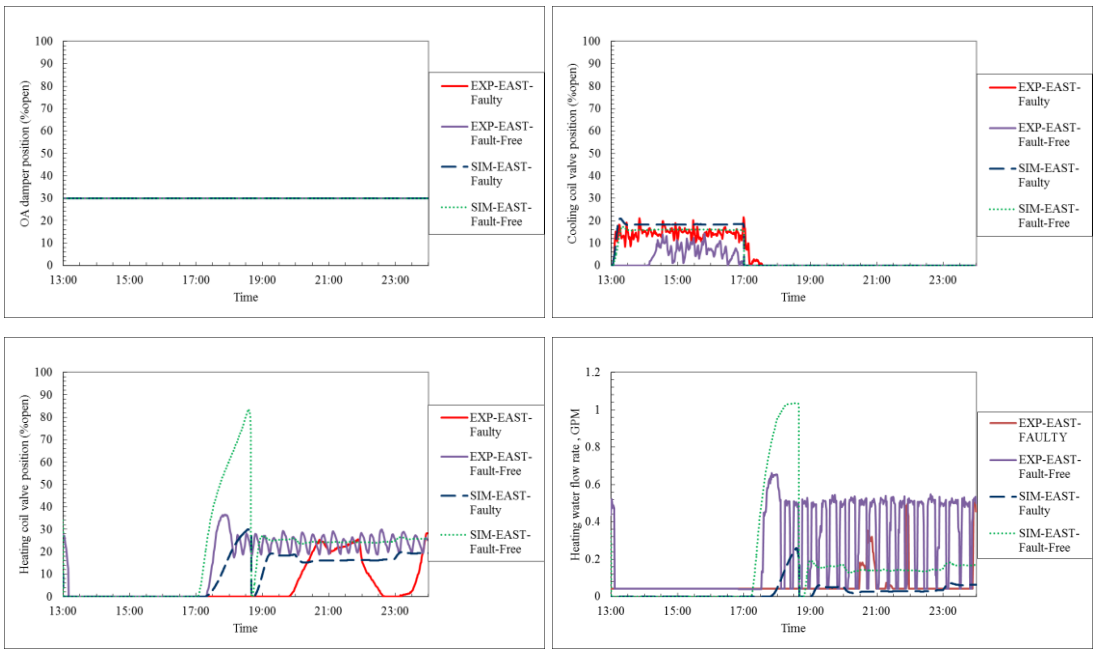

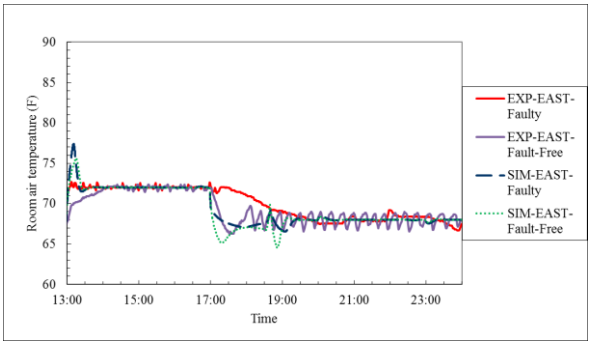

(a) West-facing room results for FCU heating coil air-side fouling (12.24.2011)

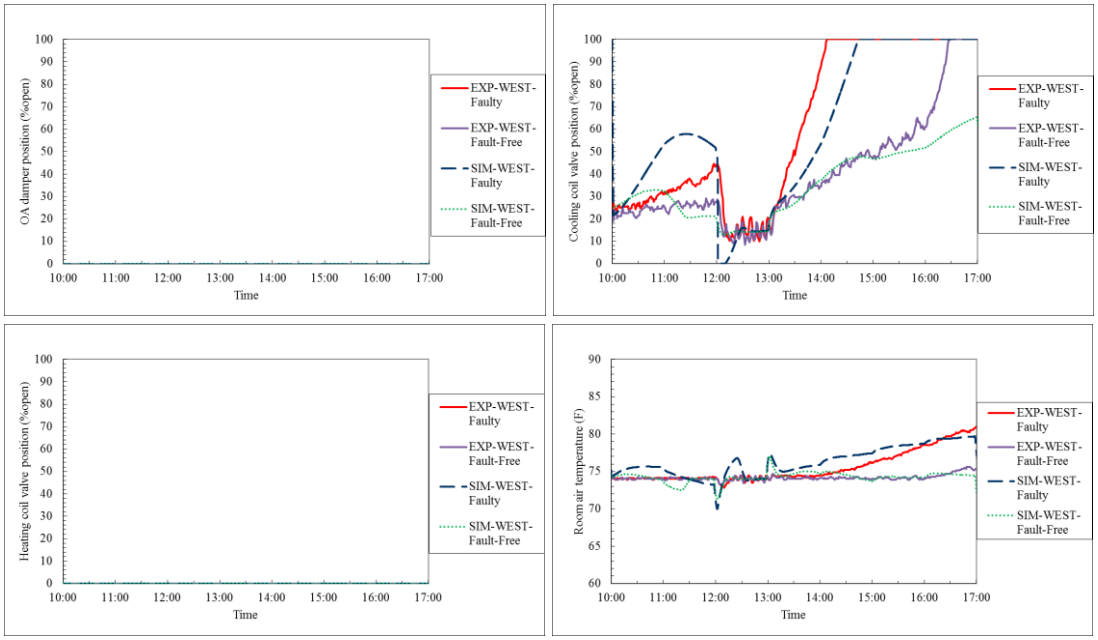

(b) West-facing room results for FCU cooling coil water-side fouling (07.24.2012)

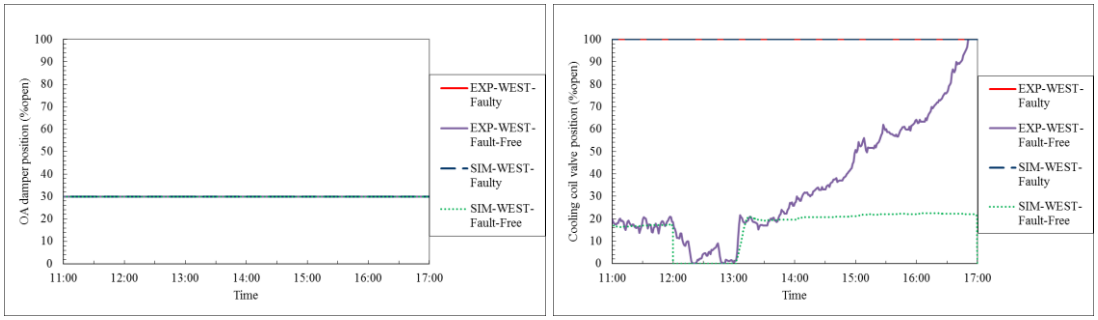

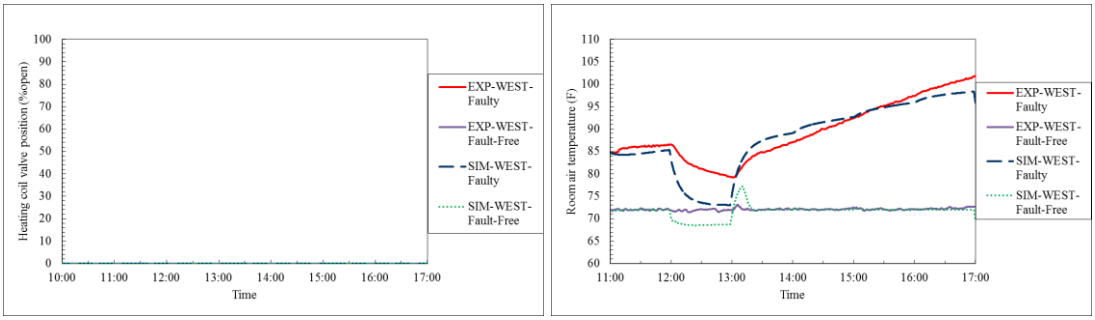

(c) West-facing room results for FCU fan failure (10.21.2011)

Figure 2-18. Some examples of FCU equipment category fault

From sensor category the room temperature sensor bias fault is picked to show. Figure 2-19 depicts the fault model simulation results of FCU with a +2°F bias in room temperature sensor reading on a winter test day (Jan 4th). The closest normal test day is selected to serve as reference day (Jan 8th). The symptoms associated with this fault are as the following:

- Decrease in heating coil valve position and hot water flow rate. Room temperature sensor reading is passed to the controller to keep room temperature by adjusting heating and cooling coil valve positions. Room temperature sensor bias causes artificial decrease in the room heating load and heating coil load decreases accordingly.
- Decrease in the room temperature by 2°F. The dashed navy blue line is representing the room temperature (result of thermal superblock) while the light blue one is representing sensor reading (result of sensor superblock) under faulty condition. The simulated room temperature under the faulty condition is 2°F less than the temperature sensor reading.

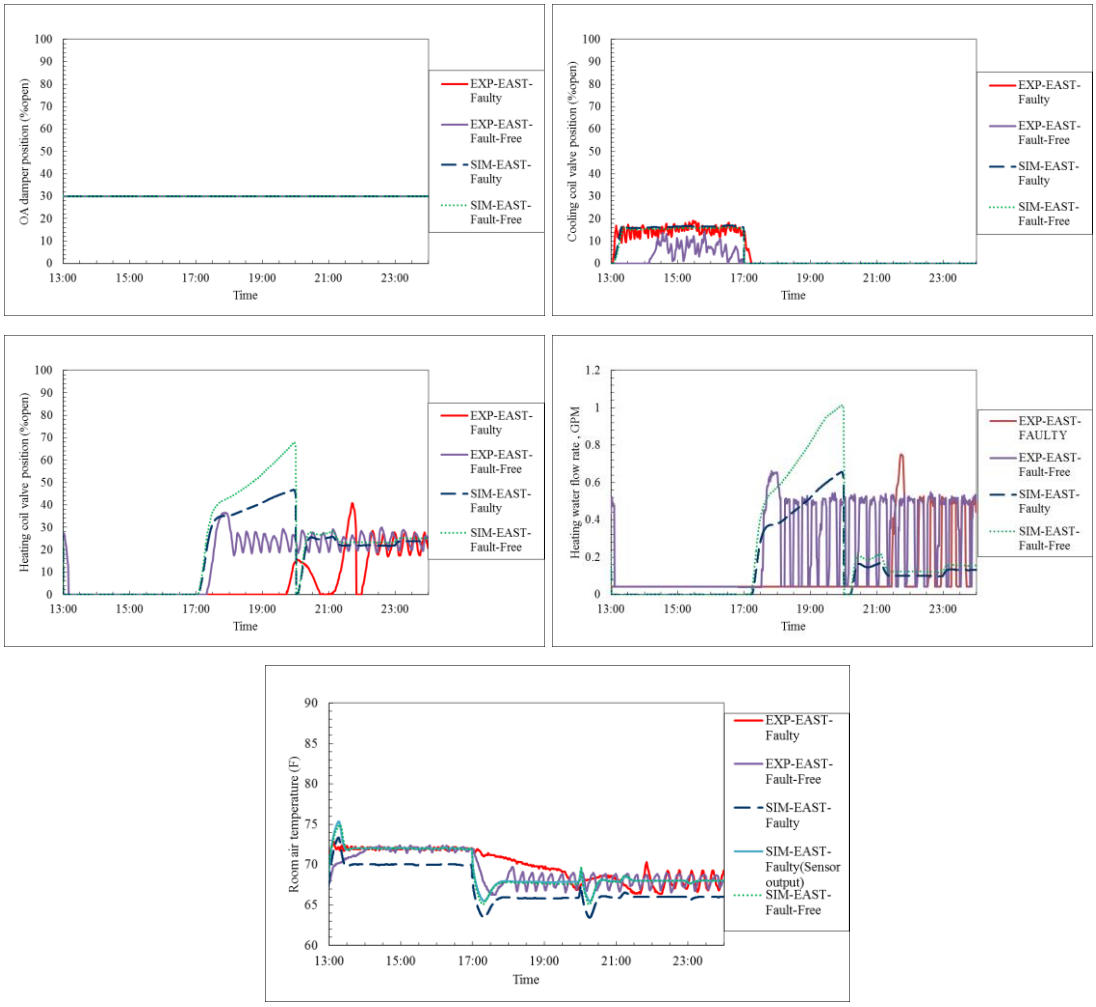

Figure 2-19. East-facing room results for FCU room temperature sensor bias (+2˚F) (01.04.2012)

Form the controlled device category fault, heating coil valve stuck at fully open position and leakage as well as cooling coil valve stuck at partially open position are picked to show the symptoms associated with each fault. Those fault occurs as the result of actuator malfunctioning. Figure 2-20 (a) demonstrates the fault model simulation results of FCU with heating coil valve stuck at fully open position on a winter test day (Jan 10th). The closest normal test day is selected to serve as reference day (Jan 8th). Figure 2-20 (b) displays the fault model simulation results of FCU with heating coil valve leakage fault on a winter test day (Jan 12th). This fault occurs when

the valve signal is totally closed but due to its wear and tear, valve is unable to block water flow rate through the coil. A warmer normal test day is selected to serve as reference day (Dec 22nd).The symptoms of these two faults can be readily distinguished by noticing:

1) The contradiction of heating coil valve position and heating water flow rate. While the controller is sending a signal for the heating coil valve to be closed, the heating water flow rate is at the maximum level for the fully open stuck valve and at 0.5 GPM for leaking valve fault.

2) The heating coil valve position at 0% open on a cold winter evening. According to the fault-free experimental data, the west-facing room calls for heating. The same behavior is displayed in the simulation result for a fault-free condition.

3) The cooling coil valve position on a cold winter evening. Under the faulty condition on a winter night, the zone calls for cooling in both the experiment and simulation cases due to the hot supply air, which is caused by excess hot water flow rate through the heating coil.

4) The room temperature maintained at cooling setpoint. For the faulty situation the FCU is operating in cooling mode, so room temperature is kept near the cooling setpoint, while for the fault-free condition it is fluctuating around the heating setpoint.

Figure 2-20 (c) demonstrates the fault model simulation results of FCU with cooling coil valve stuck at partially open position on a summer test day (July 28th). The closest normal test day to serve as reference day is Aug 9th. The symptoms associated with this fault can be readily distinguished by noticing:

1) The cooling coil valve position at 0% open on a hot summer day. According to the fault-free experimental data, the west-facing room calls for cooling.

The same behavior is displayed in the simulation result for a fault-free condition.

2) The heating coil valve position on a hot summer day. Under the faulty condition, the zone calls for heating in both the experiment and simulation cases due to the extremely cold supply air, which is caused by excess chilled water flow rate through the cooling coil.

3) The room temperature maintained at heating setpoint. For the faulty situation the FCU is operating in heating mode, so room temperature is kept near the heating setpoint, while for the fault-free condition it is fluctuating around the cooling setpoint.

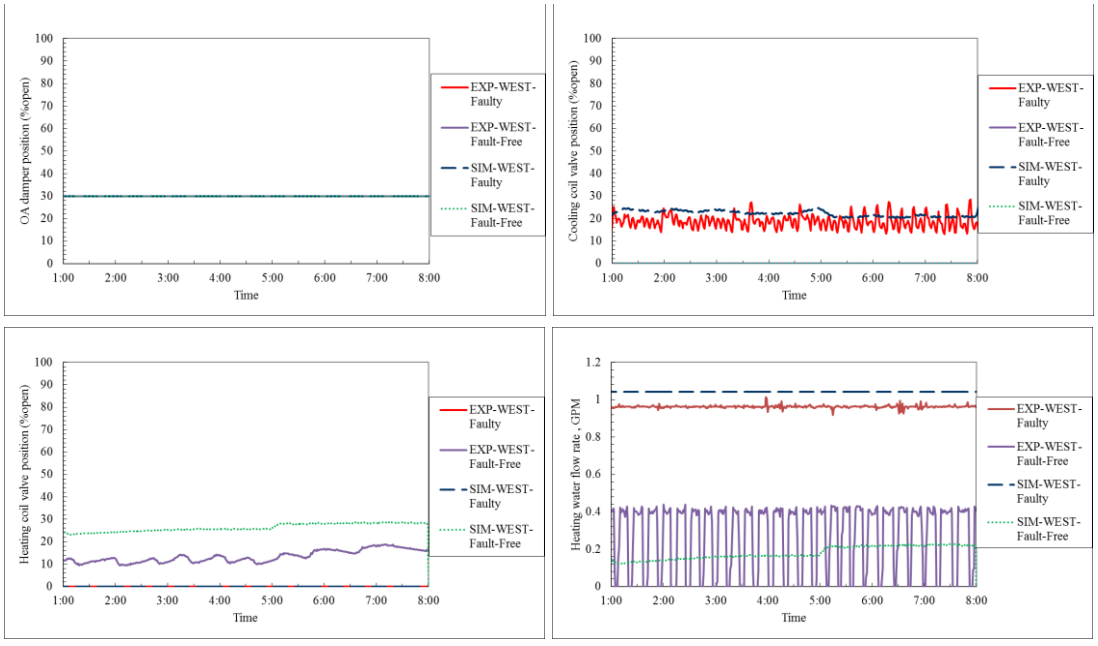

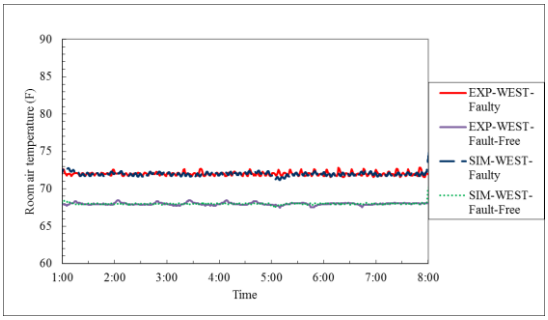

(a) West-facing room results for FCU heating coil valve stuck at fully open position (01.10.2012)

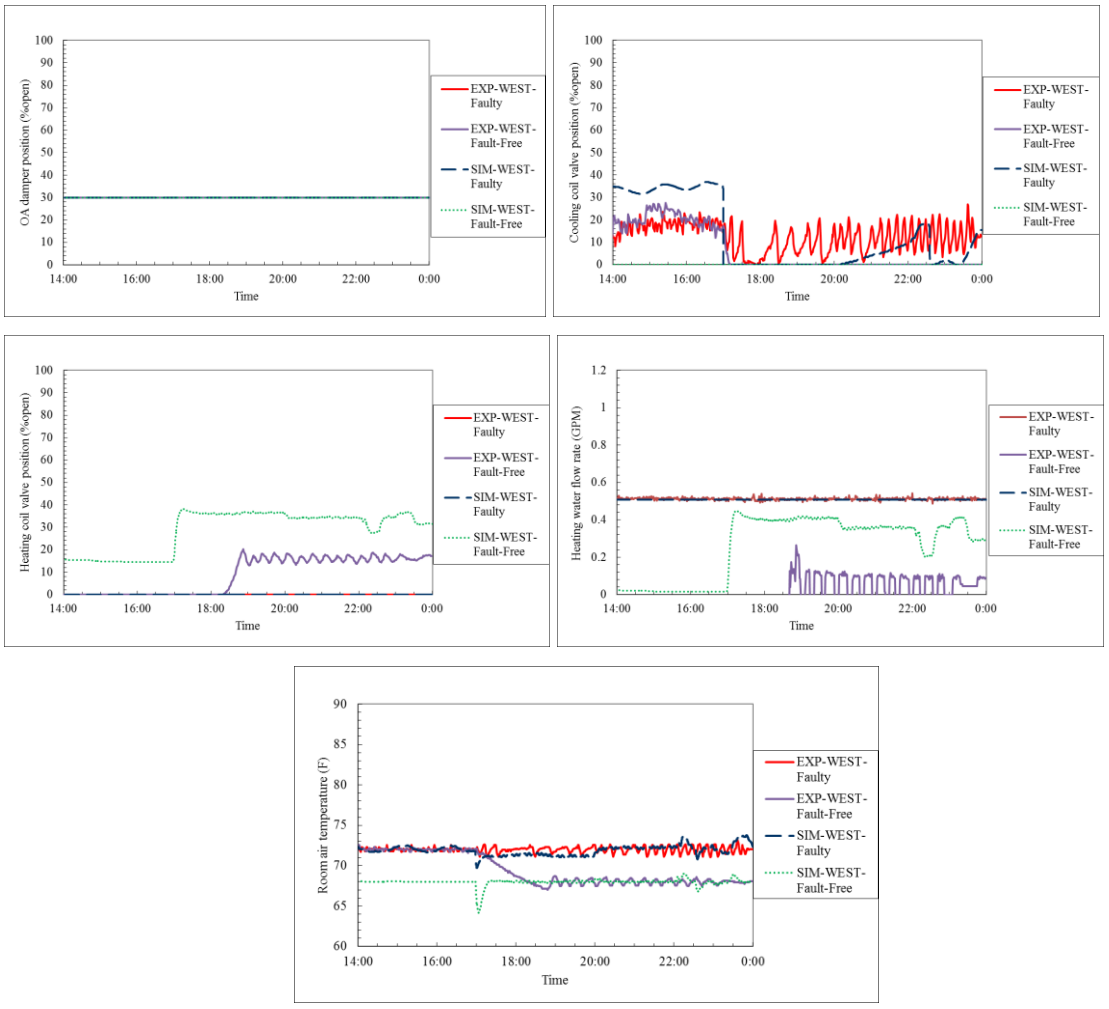

(b) West-facing room results for FCU heating coil valve leakage (01.12.2012)

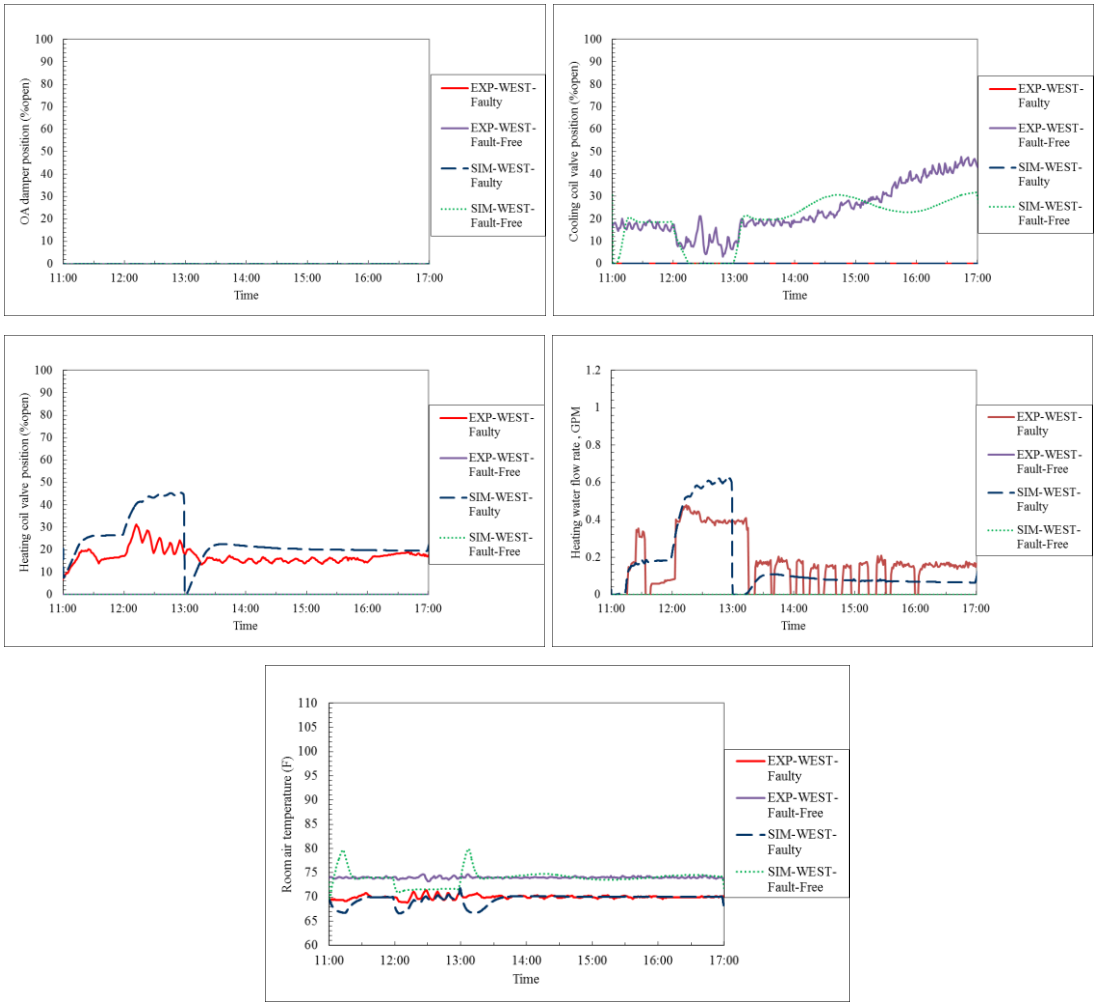

(b) West-facing room results for FCU cooling coil valve stuck at partially open position (07.28.2011)

Figure 2-20. Some examples of FCU equipment category fault

To illustrate a fault case for control category, reversed action of heating coil in an east-facing zone on a winter evening (Jan 14th) is selected. A reverse-acting actuator is a typical commissioning fault usually caused by incorrect setting of the directional switch on the actuator. During this fault, the actuator follows the control signal command reversely (i.e., the actuator closes down the heating valve instead of opening it up). A warmer normal test day would cause the system variables to behave

similarly to the fault, so this is chosen as a reference day (Jan 8th). The symptoms of the heating coil reverse acting fault can be readily distinguished by noticing:

1) The contradiction of heating coil valve position and heating water flow rate. While the controller is sending a signal for the heating coil valve to be closed, the heating water flow rate is at the maximum level.

2) The heating coil valve position at 0% open on a cold winter evening (below 30F). According to the fault-free experimental data, the east-facing room on a warmer normal day calls for heating. The same behavior is displayed in the simulation result for a fault-free condition.

3) The cooling coil valve position on a cold winter evening (below 30F). Under the faulty condition on a winter evening, the zone calls for cooling in both the experiment and simulation cases due to the extremely hot supply air, which is caused by excess hot water flow rate through the heating coil.

4) The room temperature maintained at cooling setpoint. For the faulty situation the FCU is operating in cooling mode, so room temperature is kept near the cooling setpoint, while for the fault-free condition it is fluctuating around the heating setpoint.

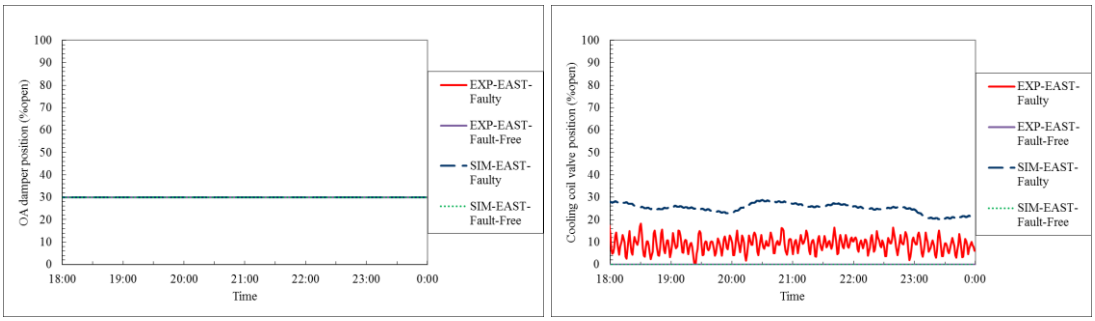

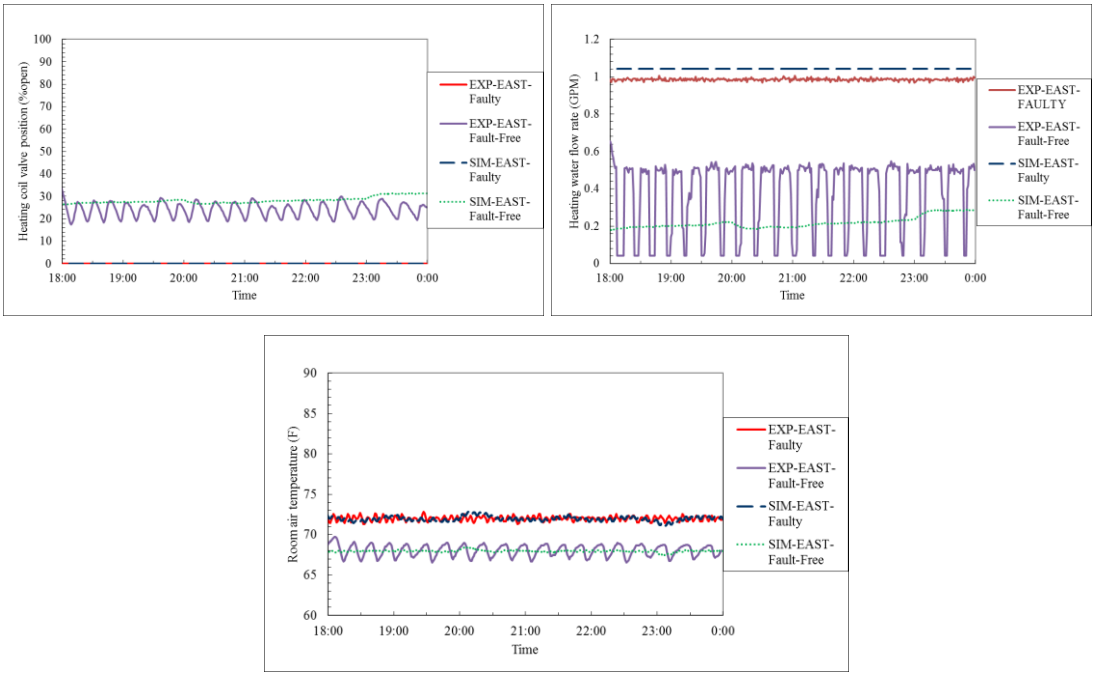

Figure 2-21 .East-facing room results for FCU heating control reverse action (01.14.2012)

2.8 Conclusion and Summary

A validated, dynamic numerical model of a FCU has been developed as a single integrated component for inclusion in the component library of the HVACSIM+ simulation package by adding three new TYPEs to that library. The structure of the FCU model and the justification for using the HVACSIM+ package in particular have been discussed. Validation of the FCU model started with component level validation, followed by validation of the model "installed" within an overall system. Experiments were conducted to investigate and determine key model parameters. Real operational data provided by ERS served as a reference to which simulation results were compared. Under fault-free conditions, the FCU model agreed well with reference data for several days in different seasons (summer, fall and winter). A fault flag system gives the model the flexibility to simulate various faults modes with differing

severities without the need to develop additional TYPEs. That the model underwent a comprehensive fault matrix and validated well against experimental data establishes its validity to serve as a tool for evaluating FCU fault detection and diagnostic methods.

3. CHAPTER THREE: DUAL DUCT DOUBLE FAN SYSTEM DYNAMIC MODEL DEVELOPMENT IN HVACSIM+ AND VALIDATION- FAULTY AND FAULT FREE

3.1 Introduction

In a dual duct system, hot and cold air flows are separately carried by two parallel duct systems. The hot deck is equipped with a heating coil and the cold deck is equipped with a cooling coil. The two decks run in a parallel configuration throughout the building. In a terminal unit, the proper proportions of hot and cold air streams are modulated by cold air and hot air dampers before proceeding downstream to the space. The simultaneous availability of hot and cold air enriches the flexibility of this system to handle zones with widely varying loads. Meanwhile, energy could be saved by utilizing outside air directly as hot air or cold air in different seasons. The dual duct systems may be designed as constant air volume (CAV) or variable air volume (VAV). In a CAV dual duct system, the supply air flow rate through the supply fan and to each zone is constant. However, the flow rates through the cold and hot decks vary depending on the requirements to satisfy the individual zone load. In a VAV dual duct system, the supply air flow rate through the supply fan is not constant and is dependent on the zone temperature control and ventilation needs. Similar to single duct VAV terminal units, VAV dual duct terminal units can also be categorized as pressure-dependent or pressure-independent units. A pressure-dependent VAV control scheme uses the space temperature sensor to directly control the position of the modulating devices. The actual airflow delivered to the space is a by-product of this position and depends on the duct system static pressure at the inlet of the terminal unit. Although the space temperature sensor will continually correct the position of the modulating device, the response can be sluggish and cause unacceptable temperature variations within the space. In contrast, a pressure-independent VAV

control scheme directly controls the actual volume of primary air that flows to the space (Kreider et al. 2002). An airflow-measuring device on the terminal unit makes this possible. The position of the modulation device is not directly controlled and is basically a by-product of regulating the airflow through the unit. Because the airflow delivered to the space is directly controlled, it is independent of inlet static pressure. Pressure-independent control increases the stability of airflow control, and allows minimum and maximum airflow settings to become actual airflows rather than physical positions of the modulation device. It is clearly the most popular form of VAV terminal unit control. More details about how dual duct systems are controlled can be found in (Kreider et al. 2002).

Over the past three decades, various computer software applications have been developed to simulate dynamic interactions between a building's envelope, its internal loads, its ambient conditions, and its HVAC systems, but very little attention has been devoted to dual duct systems. Salsbury et al. (2000) discussed the potential of simulation as a performance validation tool to evaluate a dual duct single fan system installed in an office in San Francisco. But there has been no prior work specifically about dynamic simulation and model validation for dual duct systems. The development of advanced control, operation, and automated fault detection and diagnosis techniques requires reliable simulation tools, therefore there is a need to develop a simulation tool that is capable of simulating realistic fault free and faulty operational data for dual duct systems.

The work documented here models a pressure-independent VAV dual duct double fan system serving four zones -vary in orientation- to be run within the HVACSIM+ dynamic simulation software package. Dynamic simulation of dual duct system presents unique challenges whish are addressed in this chapter. The developed

model not only opens ways to synthesize operational data under fault-free conditions, but also makes it possible to predict the symptoms associated with various faulty conditions and their effects on the system performance and occupant comfort. A comprehensive and systematic validation procedure, using data collected experimentally from real dual duct system at ERS laboratory, is used to validate the tool under both faulty and fault-free operating conditions in three different seasons. The validated tool not only predicts real-world dual duct system behavior under different control strategies, but it also predicts symptoms associated with various faults, as well as the effects those faults have on system performance at various severities. This chapter describes the challenges during the air flow network development and the way to tackle them. It also express the procedure of model development from the new added TYPEs to HVACSIM+ library of components to validation of the model at both component and system levels. It also spends on fault modeling by designing fault flag and validation of fault model.

3.2 Test Facility and Experimental Set up

Experiments have been conducted at Iowa Energy Center Energy Resource Station (ERS) on a full scale dual duct system in three different seasons to generate operational data used in validation of the developed model for this study. The ERS has been described in at least three earlier studies (Norford et al. 2000, Castro et al. 2003, Li et al. 2010). The major feature of this test facility is two identical HVAC systems (A and B systems). However, significant modifications have been made to the two identical single duct AHU systems (AHU-A and B) to convert them from two

single duct systems as previously described to one dual duct double fan system with one return duct.

More specifically, the following major changes have been made: 1) The two existing and identical single duct AHUs (AHU-A and B) were connected by a duct (bridge), so that the mixing box and return duct of the AHU-B were used as the dual duct mixing box and return duct; 2) In AHU-A, the duct work before the bridge connection was completely blocked. The downstream (after the connecting bridge) components of AHU-A, including a heating coil, a cooling coil (not used), and a supply fan, were used in the dual duct system; 3) In the four test rooms that were used in this study, pressure independent dual duct terminal units were installed. After these changes, AHU-A and B were respectively serving as the hot deck and cold deck of the new dual duct system. Instrumentation used in this study consisted of humidity, pressure, temperature and air flow sensors as well as electric power meters to monitor the system. Figure 3-1 demonstrates the new dual duct double fan system and the four test rooms including: west A, south A & B and east B.

ERS has provided operational data under a wide variety of fault-free and faulty operational conditions in three different seasons: summer, fall and winter. To generate dual duct system operational data under normal conditions all rooms were operated without imposed faults. To establish data under faulty conditions, the east B, south A and west A-facing rooms were operated with deliberately imposed faults while the

south B room ran normally. The zones have identical construction and details about the zone envelop structure are provided by Price and Smith (2003).

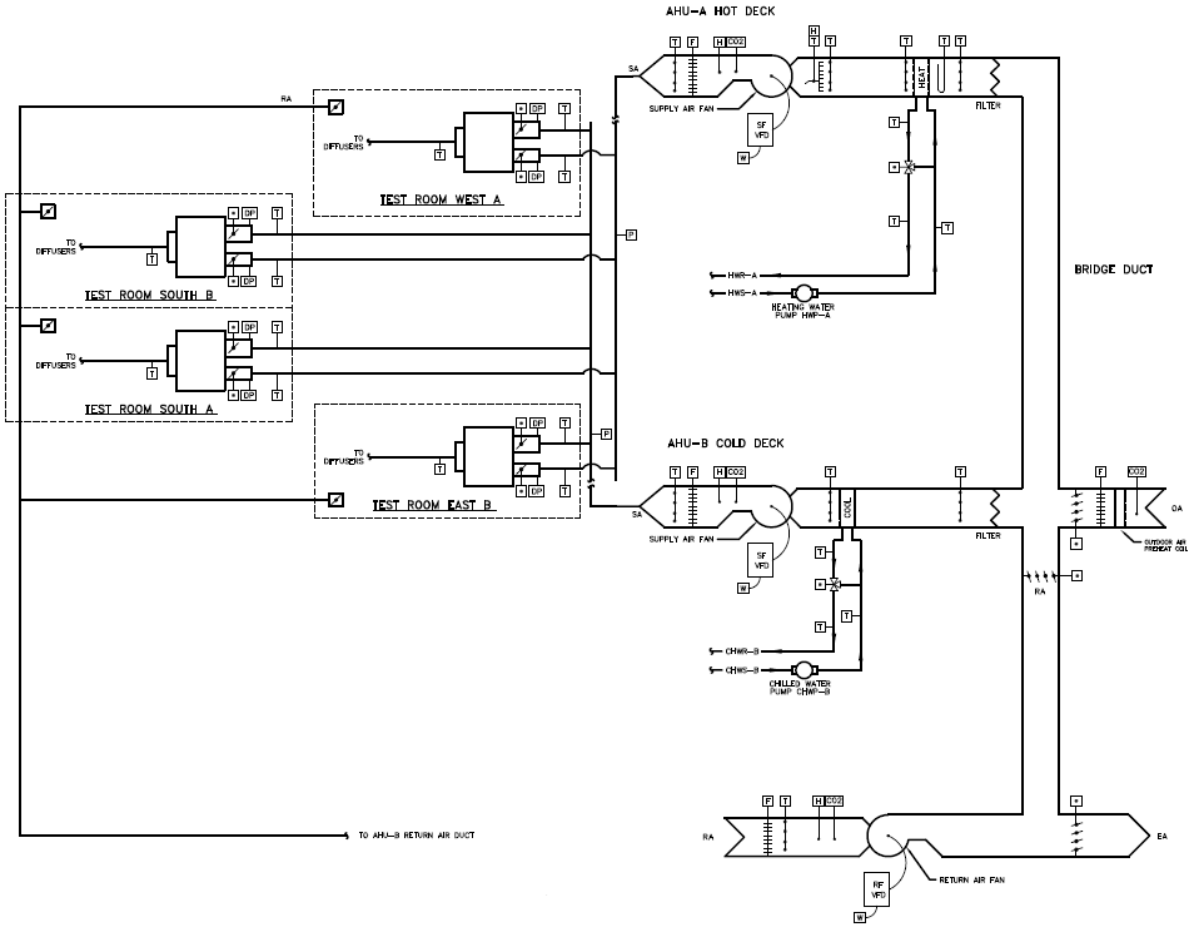

Figure 3-1. Schematic of dual duct double fan system at ERS serving four perimeter zones

The speed of supply fans are modulated to maintain each deck static pressure at the static pressure setpoint, which is generally at 1.6 in. W.G. Two PI control algorithms are used to control the speed of cold and hot deck supply fans. The control sequence used to control the return fan is air flow rate matching, the summation of airflow rate from hot and cold decks. In the summer the economizer mode is disabled and the minimum requirement for outdoor air damper opening is 0% while in the winter and fall economizer is enabled and the minimum requirement for outdoor air

damper opening is 45%. Therefore, in the summer cold deck supply air temperature is maintained at the set point just by mechanical cooling or control of cooling coil valve. But in the winter and fall the control sequence used to maintain cold deck supply air temperature at the setpoint is divided into three control regions, namely, mechanical cooling, mechanical and economizer cooling and economizer cooling as shown in Figure 3-2. Each region depends on whether or not outdoor air temperature is greater or less than a reference temperature known as the economizer temperature setpoint (60°F), and whether the cold deck supply air temperature is above or below setpoint.

The regions correspond to the output from a single PI control algorithm that is split into the control of outdoor air damper and cooling coil valve. The PI control algorithm has an output that ranges from 0 to 200. During the mechanical and mechanical and economizer cooling modes, the output from the PI control algorithm ranges from 100 to 200, corresponding to a cooling coil position from 0 to 100 % open. The outdoor air damper is held in the minimum position (mechanical cooling only) when outdoor air temperature is above economizer setpoint. The outdoor air damper is fully open (mechanical and economizer cooling) when outdoor air temperature is less than economizer setpoint and when the output of PI is larger than 100. As outdoor air temperature drops, the need for mechanical cooling is eliminated (output from the PI control algorithm drops below 100) thereby switching the control sequence to the economizer cooling mode. In this mode, cold deck supply air temperature is maintained by modulating the outdoor air damper. The output from the PI control algorithm ranges from 0 to 100, corresponding to the outdoor air damper position ranges from the minimum requirement to 100 % open.

During this project, AHU-A provides 90°F supply air as the hot deck, and AHU-B provides 55°F as the cold deck to the four dual duct mixing boxes. All four test

rooms (EB, SA, SB, and WA) are equipped with the identical model dual-duct mixing box. The room temperature setpoint for the four test rooms is constant during the test and is 68°F for heating setpoint and 72°F for cooling setpoint.

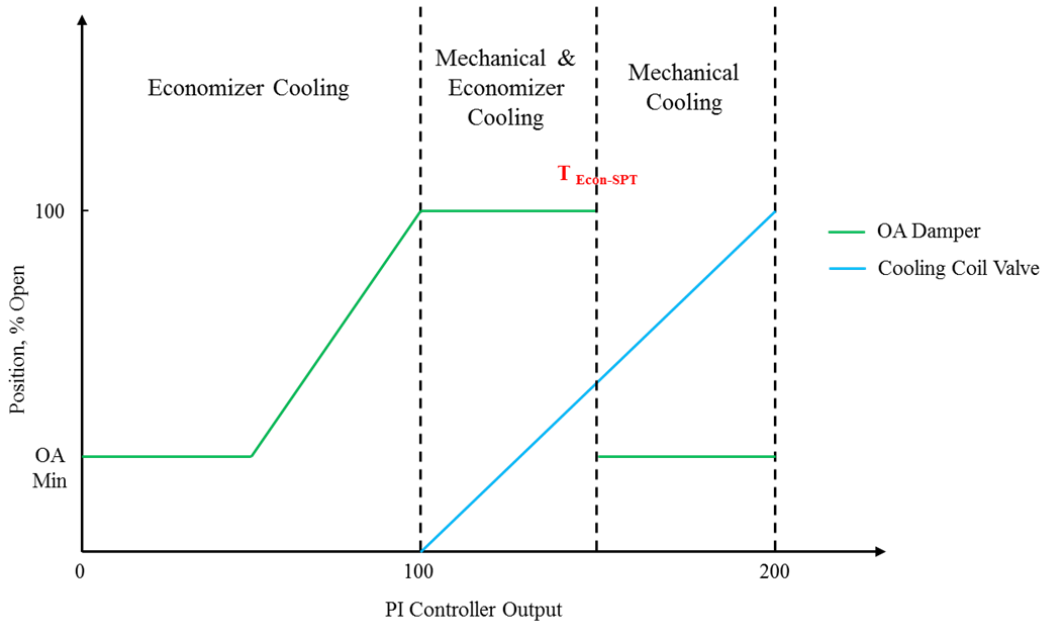

Figure 3-2. Cold deck supply air temperature control sequence

The dual-duct terminal unit mixes air from the hot and cold deck supply inlets in order to maintain the space temperature in the test room. The dampers modulate from a minimum CFM setpoint of 100 CFM for both the cold and hot decks, to a maximum CFM setpoint of 1000 and 400 CFM for the cold and hot deck respectively. Each dual duct box terminal unit is controlled by a Johnson Controls VMA-1420 controller to implement the control sequence. The VMA controller determines the flow setpoint for each deck, which is compared to the actual flow rate that is measured via a differential pressure sensor for each deck. The controller modulates the damper open and close in order to achieve the setpoint. Figure 3-3 shows the dual duct terminal unit control

diagram. Since the implemented control sequence by Johnson Control is a patented one, a similar control sequence from Carrier is selected as a substitute.

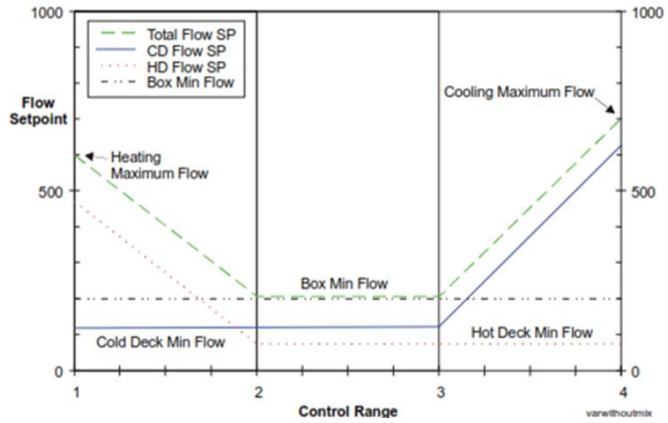

Figure 3-3. Dual duct terminal unit control diagram

On a call for cooling, the hot deck damper will remain at its minimum position (for 100 CFM) and the cold deck damper will modulate open in order to satisfy the space temperature setpoint. As the space load decreases the cold deck damper will gradually close until it reaches its minimum position (for 100 CFM). On a call for heating, the cold deck damper will remain at its minimum position and the hot deck damper will modulate open to satisfy the room temperature setpoint.

3.3 Fault-Free Dynamic Model Development

In order to model dual duct system properly in HVACSIM+, all of the constitutive processes represented by the model are divided among different superblocks. Each superblock represents one category of process states associated with the system that is both physically and numerically independent from- or at most, coupled only weakly to- any other category of the process states in the system. In the case of the dual duct system, five distinct categories of states—(1) sensors, (2) actuators, (3) control logic, (4) fluid (i.e., mass flow and pressure), and (5) thermal

(temperature and humidity)—are each modeled by a dedicated superblock/network. Especially for a large system like dual duct containing various components; breaking the system down into the constituent independent subsystems helps to reduce time intensity of the simulation. This section presents the subsystem structures of a dual duct system in HVACSIM+, the constituent TYPEs of each superblock and the required TYPEs which should be added to the HVACSIM+ library of components to model dual duct system. Furthermore, the special challenges to model air flow network of dual duct system are described. In addition, the process of determining the parameters of key/new components in the air flow and thermal networks are described.

3.3.1 Dual duct double fan system structure in HVACSIM+

The representative components (TYPEs) of each state category in dual duct system are grouped as a network to create a single superblock/network. Each superblock is an independent subsystem within which the system of governing equations of one state category is solved simultaneously. In the air flow superblock mass-pressure equations are solved simultaneously independent from other process states constituent of dual duct system. Figure 3-4 shows air flow network configuration of ERS dual duct system with double fans.

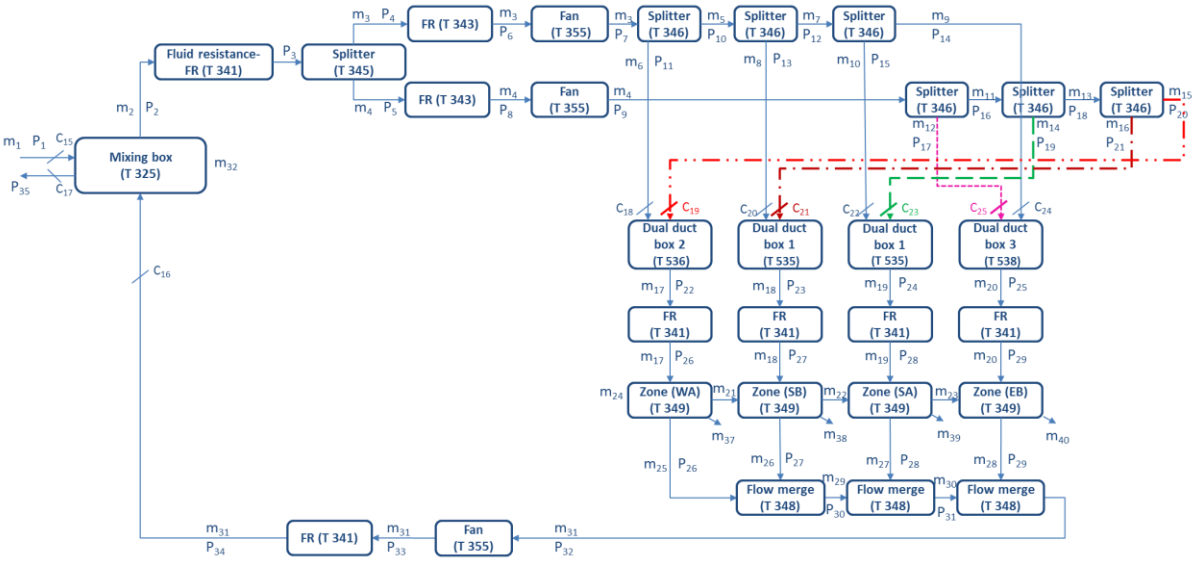

Figure 3-4. Dual duct system air flow network configuration

In this Figure, each box represents an UNIT to which a TYPE has been assigned. The description and the TYPE that each UNIT uses have been provided within the UNIT box. The inputs and outputs of each UNIT have also been specified. In Figure 3-4, mass flow rates, pressures, and control signals are respectively presented by m, p and C.

Similarly the constitutive components of dual duct system thermal state are grouped to create thermal network as an independent superblock/ network. Figure 3-5 demonstrates the thermal network configuration of ERS dual duct system with double fans. Like air flow superblock, each unit is representative of a component described by a TYPE containing the governing equations of each component thermal state. In Figure 3-5, temperature, humilities, and heat transfer rates are respectively presented by T, H and Q.

All of the control signal inputs are provided by control superblock. Figure 3-6 shows the control network of dual duct system comprising the control signals passed to different superblocks.

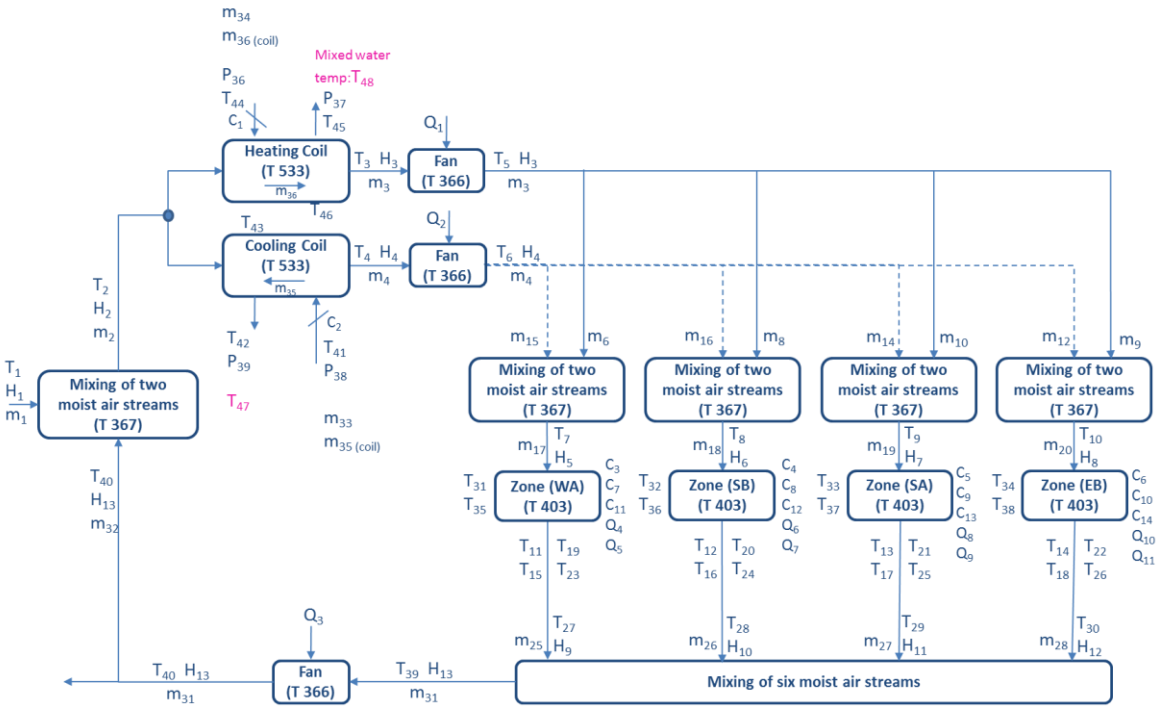

Figure 3-5. Dual duct system thermal network configuration

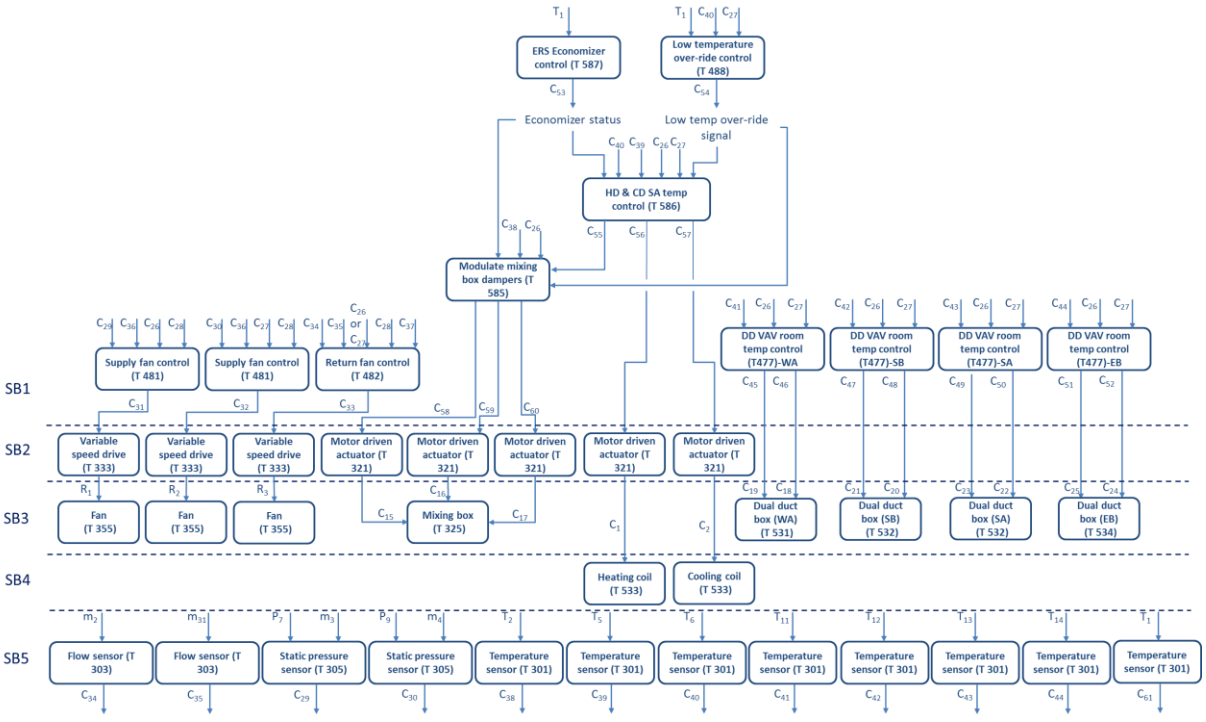

Figure 3-6. Dual duct system control network configuration

3.3.1.1 New TYPEs added to HVACSIM+ to model dual duct double fan system

Most of the TYPEs that have been used in this dual duct air flow network (Figure 3-4) are the existing TYPEs provided by the HVACSIM+ component library and have been used in previous studies. Three new TYPEs, i.e., TYPEs 535, 536 and 538 have been developed to simulate the air flow rate and pressure in dual duct terminal units. TYPE 535 determines hot, cold, and total air flow rates at the two inlets and one outlet, when pressures at these inlets and outlet are given. TYPE 536 determines air flow rate for hot deck inlet, total air flow rate for outlet, and cold deck inlet pressure, when hot deck inlet pressure, outlet pressure, and cold deck inlet air flow rate are given. Similarly, TYPE 538 determines air flow rate for cold deck inlet, total air flow rate for outlet, and hot deck inlet pressure, when cold deck inlet pressure, outlet pressure, and hot deck inlet air flow rate are given. These different TYPEs are used for different test room configurations. Dominant equations of TYPE 535, which is used as dual duct terminal unit for south B room (refer to Figure 3-4), are presented in Eqs. (3-1) to (3-3).

$$m_8 = \sqrt{\frac{P_{13} - P_{23}}{R_{hot\ damper}}} \tag{3-1}$$

$$m_{16} = \sqrt{\frac{P_{21} - P_{23}}{R_{cold\ damper}}} \tag{3-2}$$

$$m_{18} = m_8 + m_{16} \tag{3-3}$$

m_8, m_{16} and m_{18} as well as P_{13}, P_{21} and P_{23} have been illustrated in Figure 3-4. Furthermore, $R_{hot\ damper}$ and $R_{cold\ damper}$ are the pressure resistances of hot and cold dampers, respectively. The required parameters including the duct and damper pressure resistance determination is described in section 3.3.2. The governing equations of TYPE 536 and 538 are similar. For example, the dominant equations for

TYPE 536, which is used as terminal unit for West-A room, are presented in Eqs. (3-4) to (3-6).

$$m_6 = \sqrt{\frac{P_{11} - P_{22}}{R_{hot\ damper}}} \tag{3-4}$$

$$P_{20} = P_{22} + R_{cold\ damper} m_{15}^2 \tag{3-5}$$

$$m_{17} = m_6 + m_{15} \tag{3-6}$$

m_6, m_{15} and m_{17} as well as P_{11}, P_{20} and P_{22} have been illustrated in Figure 3-4. Equations for TYPE 538 are not presented here for brevity.

all of the TYPEs that have been used in dual duct thermal network (Figure 3-5) are the existing TYPEs provided by the HVACSIM+ component library and have been used in previous studies. In order to control the dual duct terminal units, a new TYPE has also been added to HVACSIM+ library (Figure 3-6). TYPE 477 is representing the Carrier dual duct terminal units with control strategy close to ERS dual duct terminal units. Carrier control sequence for dual duct terminal units can be found in APPENDIX C.

3.3.1.2 Special Challenges in the simulation of dual duct systems

In comparison with single duct systems, dual duct systems present unique challenges, especially regarding air flow simulations. Because the dual duct air flow network has two separate air flow paths (hot and cold) that are strongly coupled, it is subject to convergence issues. Therefore, how to simulate them simultaneously and robustly is a key obstacle. Here, the focus is to model the constituent components of a dual duct system in terms of their governing equations, as well as the arrangement of these equations to achieve a stable and efficient simulation. The arrangement of UNITs as well as the equation formats within a UNIT need to be carefully considered

to avoid convergence problems. Different UNIT arrangements and equations formats were tried and discarded before those shown in Figure 3-4 were found effective. One unique TYPE specifically used for the dual duct air flow network is the main duct splitter unit TYPE 345. The equations used in this TYPE are summarized here:

$$m_4 = \frac{R_{HD} m_2 \mp \sqrt{R_{HD}\, R_{CD}\, m_2^2 - (R_{HD} - R_{CD})(P_4 - P_5)}}{(R_{HD} - R_{CD})} \tag{3-7}$$

$$m_3 = m_2 - m_4 \tag{3-8}$$

$$P_3 = P_4 + R_{HD}\mathrm{m}_3^2 - R_{inlet}\mathrm{m}_2^2 \tag{3-9}$$

m_2, m_3 and m_4 as well as P_3, P_4 and P_5 have been illustrated in Figure 3-4. Furthermore, R_{HD}, R_{CD} and $\mathrm{R}_{\mathrm{inlet}}$ are the pressure resistances of the junction dividing the flow between hot and cold decks.

The TYPE 345 splitter equations are different from those of TYPE 346, commonly used in single duct simulations. For comparison, the equations for TYPE 346 are provided as Eqs. (3-10) to (3-12).

$$\mathrm{m}_{\mathrm{main\ outlet}} = \mathrm{m}_{\mathrm{inlet}} - \mathrm{m}_{\mathrm{branch}} \tag{3-10}$$

$$P_{inlet} = P_{main\ outlet} + R_{main\ outlet}\mathrm{m}_{main\ outlet}^2 + R_{inlet}\mathrm{m}_{\mathrm{inlet}}^2 \tag{3-11}$$

$$P_{\mathrm{branch}} = P_{main\ outlet} + R_{main\ outlet}\mathrm{m}_{main\ outlet}^2 - R_{branch}\mathrm{m}_{\mathrm{branch}}^2 \tag{3-12}$$

Considering the first splitter after the supply fan in the hot deck (the top deck) $\mathrm{m}_{\mathrm{inlet}}$ and $\mathrm{P}_{\mathrm{inlet}}$ are m_3 and P_7, $\mathrm{m}_{\mathrm{main\ outlet}}$ and $\mathrm{P}_{\mathrm{main\ outlet}}$ are m_5 and P_{10} and $\mathrm{m}_{\mathrm{branch}}$ and $\mathrm{P}_{\mathrm{branch}}$ are m_6 and P_{11}. Parameters $\mathrm{R}_{\mathrm{inlet}}$, $\mathrm{R}_{\mathrm{main\ outlet}}$ and $\mathrm{R}_{\mathrm{branch}}$ are the respective pressure resistances. The use of TYPE 345 as the main duct splitter was found to be critical to receive robust and converging performance of dual duct air flow network simulations.

3.3.2 Model parameters

For each UNIT of every superblock, the values for the parameters need to be determined. Therefore, there are too many parameters need to be determined for simulation to represent the dual duct double fan system at the test facility. Many of the components in this dual duct system, such as the mixing box, heating/cooling coils, hot and cold deck supply fans and the return fan are the same components used in the ASHRAE 1312 research project (Li, et al., 2010). Therefore, some parameters obtained from ASHRAE 1312 project are kept the same for these components. Some other parameters are determined through a designed experiment especially for the critical and new components like hot and cold deck dampers in the terminal units and heating and cooling coil valves. Therefore, at this point component level validation is accomplished for those key components to determine their representative parameters. In the following the parameter determination procedure for different components in the air flow and thermal network are discussed in detail.

3.3.2.1 Air flow network parameters determination

In the modelling of air flow network, duct work pressure resistances and fan performance curve are of significance and need to undergo component validation. As mentioned earlier, other than the modifications to the duct work of AHU-A & B, to convert them to a dual duct double fan system, VAV boxes are replaced by four new terminal units. Therefore, duct work pressure resistances especially in the modified junctions and also dual duct terminal unit dampers model parameters need to be determined. ERS run component test for hot and cold dampers in the terminal unit of south B room to provide data to determine their required parameters. The procedure of determining parameters for the modified junctions and terminal unit dampers are described in sections 3.3.2.1.1 and 3.3.2.1.2 respectively. Furthermore, significant

differences were found between the fan data generated from the ASHRAE 1312 project and this study. Therefore, new parameters are generated for supply fans and return fan which are discussed in section 3.3.2.1.3. APPENDIX D provides a detailed table that summarizes all parameters needed for the dual duct simulation and their values based on the ERS system.

3.3.2.1.1 Pressure resistance of modified junctions in supply and return ducts

In this project, which uses explicit method, the relationship between mass flow rate and corresponding pressure drop for a straight duct (TYPE 341), a flow split junction (TYPE 345 & 346), and a flow merge junction (TYPE 348) is modeled using the flow resistance model as expressed in Eq. (3-13):

$$\Delta P = R_T w^2 \tag{3-13}$$

where ΔP is the pressure drop, w is the mass flow rate, and R_T is the air flow resistance. One parameter, namely, the flow resistance for the straight duct R_T, needs to be determined for each straight duct. One flow split model (TYPE 345) for main duct and three flow split models (Type 346) before the first three zones are used to model the flow split junctions. Each flow split junction is characterized by three pressure resistances. The flow split model incorporates pressure resistances for the fitting and the straight ducts connecting with it. Three flow merge models (Type 348) are used in the return duct to model the flow merge junctions for the zones. Similar to the flow split model, flow merge model also includes three flow resistances which incorporate the pressure resistances for both fitting and straight ducts connected to the fitting.

To determine the flow resistance parameter needed in a straight duct model, the friction loss for a typical galvanized steel duct is determined first based on the duct

size and design air flow rate (ASHRAEb, 2001). Eq. (3-13) is then used to calculate the flow resistance R_T based on the design air flow rate (w) and corresponding friction loss (ΔP).

For a flow split or flow merge model, the friction loss coefficient for the junction is firstly determined based on the junction size and its design air flow rate (Pita, 2002). The pressure drop for a flow split or merge junction at the design air flow rate is then calculated based on the friction loss coefficient (Pita, 2002):

$$\Delta P = C * (\frac{V}{4000})^2 \quad (3\text{-}14)$$

where C is the loss coefficient, and V is the design air velocity (ft/min). Based on the design air flow rate and pressure drop, the flow resistance for the converging or diverging junctions in supply and return ducts are calculated using Eq. (3-13). Notice that the three flow resistances used in the flow split or merge models also include the straight ducts connected to the fitting. Detailed calculation information is summarized in APPENDIX E.

3.3.2.1.2 Pressure resistance of hot and cold dampers in dual duct terminal units

Since dual duct terminal units are new components in the modified AHUs at ERS, a new component test was performed in south B room for its hot and cold dampers. During damper component testing, damper positions were systematically adjusted from 0% to 100% open with 10% increments for cold and hot dampers in the south B room dual duct terminal unit. The pressure drop across the dampers and resulting discharge air flow rate were measured after the system reached steady state. Experimental data generated from this component test are then used to determine hot and cold dampers' loss coefficient (K_θ) and then pressure resistances at various damper positions. The pressure drop across the dampers is calculated by Eq. (2-5).

As Eq. (2-5) shows $log_e K_\theta$ is a function of damper position. Various models considering linear region covering various ranges of θ (damper opening) were fitted to the experimental data points using the three region model approach for $log_e K_\theta$ versus damper position (refer to Eqs.(2-6)- (2-8)). The changes between different models (in Figure 3-7) included starting and ending damper positions for each region and/or model parameters. The goal was to develop a model with good overall R^2 and also small modeling error between 50 and 60% damper positions. As Figure 3-7 demonstrates that approach was unable to fit a model with proper coverage for all data points especially for damper opening between 50 and 60 % which is very commonly used damper position range (according to the experimental data examination). Therefore different approach, least square method, is used to fit a polynomial model which is the best model to the experimental data points. As Figure 3-8 depicts the polynomial model represents component test data point with close agreement covering for the whole range of damper opening.

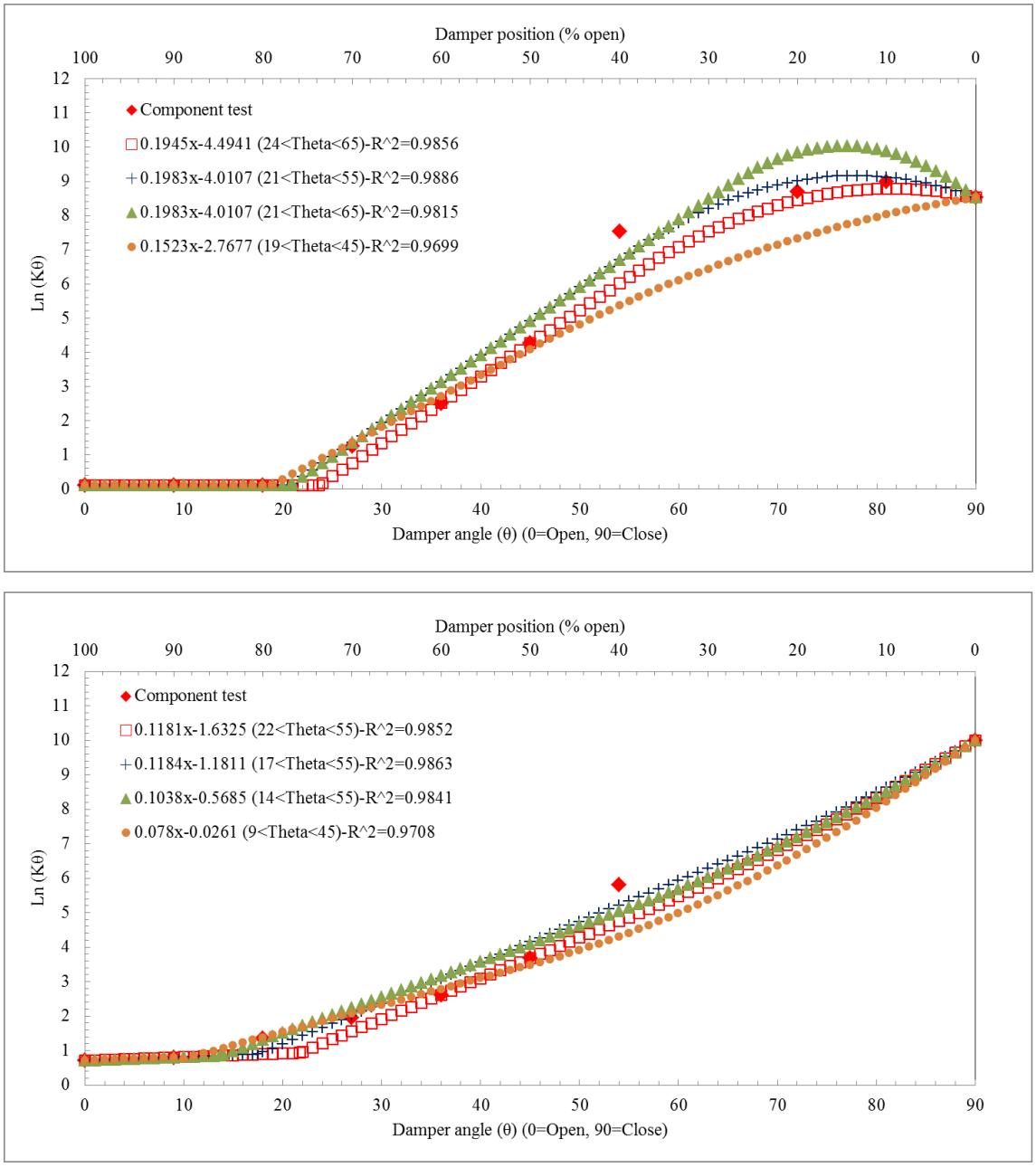

Figure 3-7. Hot (top) and cold (bottom) damper models (using three region approach) in dual duct terminal unit

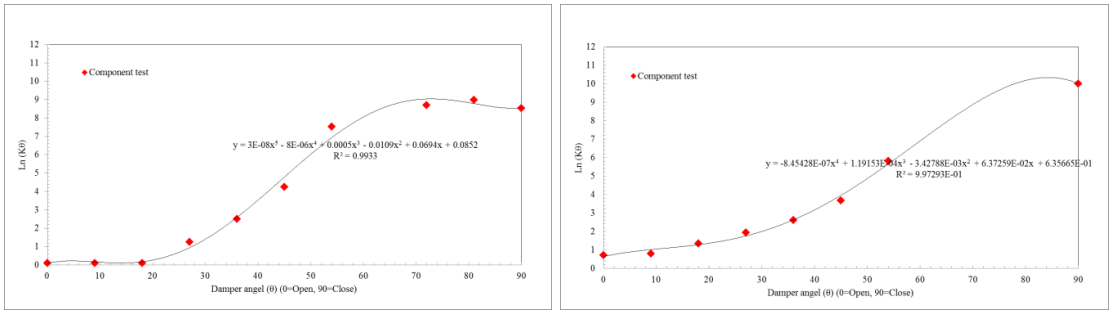

Figure 3-8. Hot (left) and cold (right) damper models (using least square method) in dual duct terminal unit

3.3.2.1.3 Coefficient of fans (hot and cold deck supply fan and return fan)

Although the supply fans used in this dual duct system are the same as the ones (AHU-A and -B) used in the ASHRAE 1312 project, significant differences were found between the fan data generated from the ASHRAE 1312 project and this study, mostly due to the duct work modifications and different operating conditions. Therefore, new parameters are generated from experimental data collected under normal operation for the two supply fans. The procedures used in determining the new fan parameters are similar to those described in the previous chapter and ASHRAE RP1312 project and not repeated here.

Therefore, new parameters are generated from experimental data (June 9th 2013 and Oct 3rd 2013 for cold deck and Nov 12th 2013 for hot deck) for the two supply fans. The experimental data has picked to cover the widest range of supply fan operations for both cold and hot decks. According to Figure 3-9, the fitted model in ASHRAE 1312 project for hot and cold deck supply fans shows large deviation from experimental data. It was found out that shifting the intercept of the fitted model in 1312 project for dimensional pressure curve of both supply fans result in a good fit for the new fans with acceptable R^2. The navy blue line in these figures is representing the updated model for both supply fans.

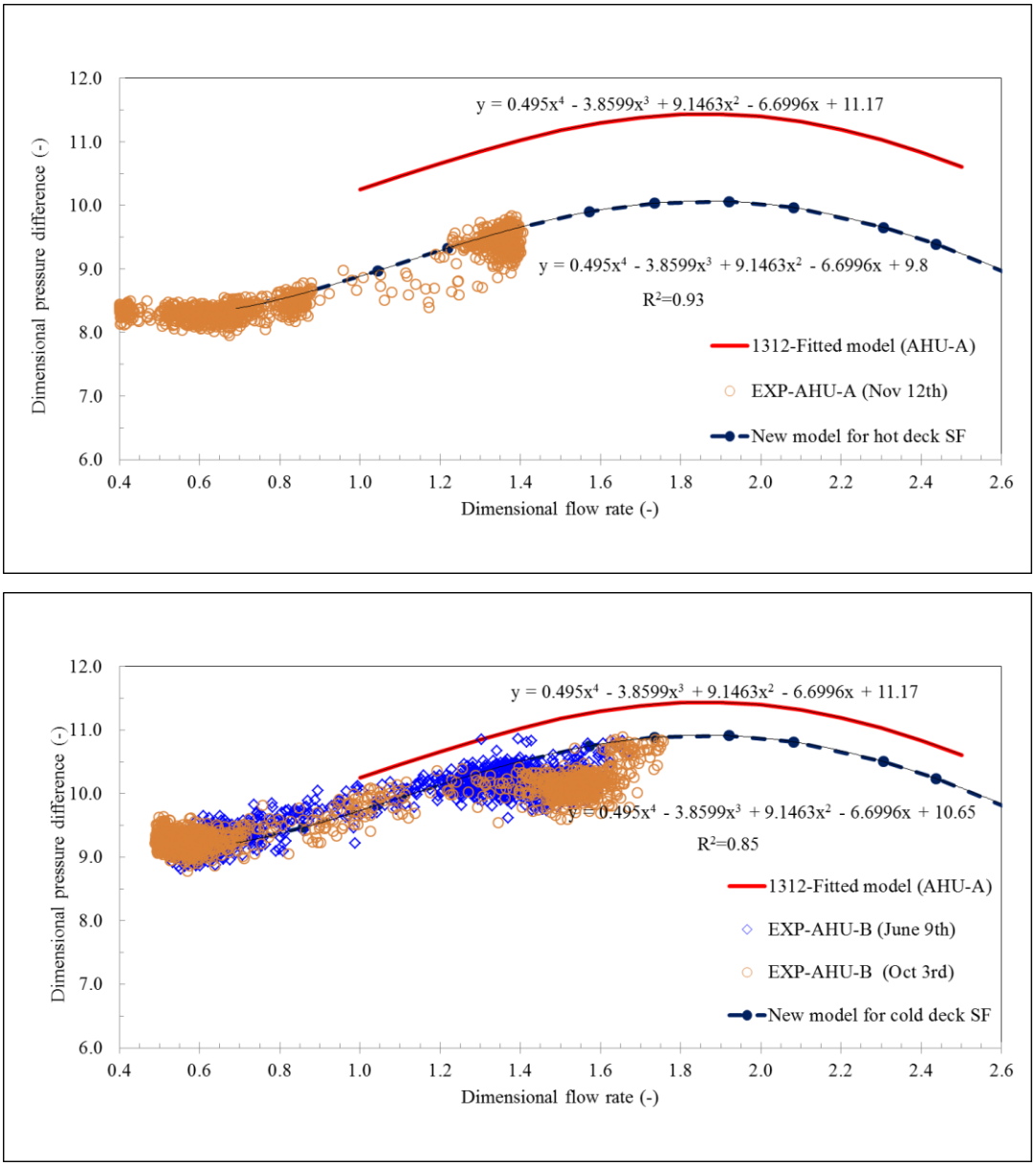

Figure 3-9. Hot deck (top) and cold deck (bottom) supply fan dimensional performance curve

Unlike performance curve, shifting the fitted model in 1312 project for efficiency curves does not result in a good fit for experimental data. Therefore a new model is generated for efficiency curve of each supply fan. Figure 3-10 demonstrates the new model for efficiency curve with navy blue line which predicts the efficiency of hot and cold deck

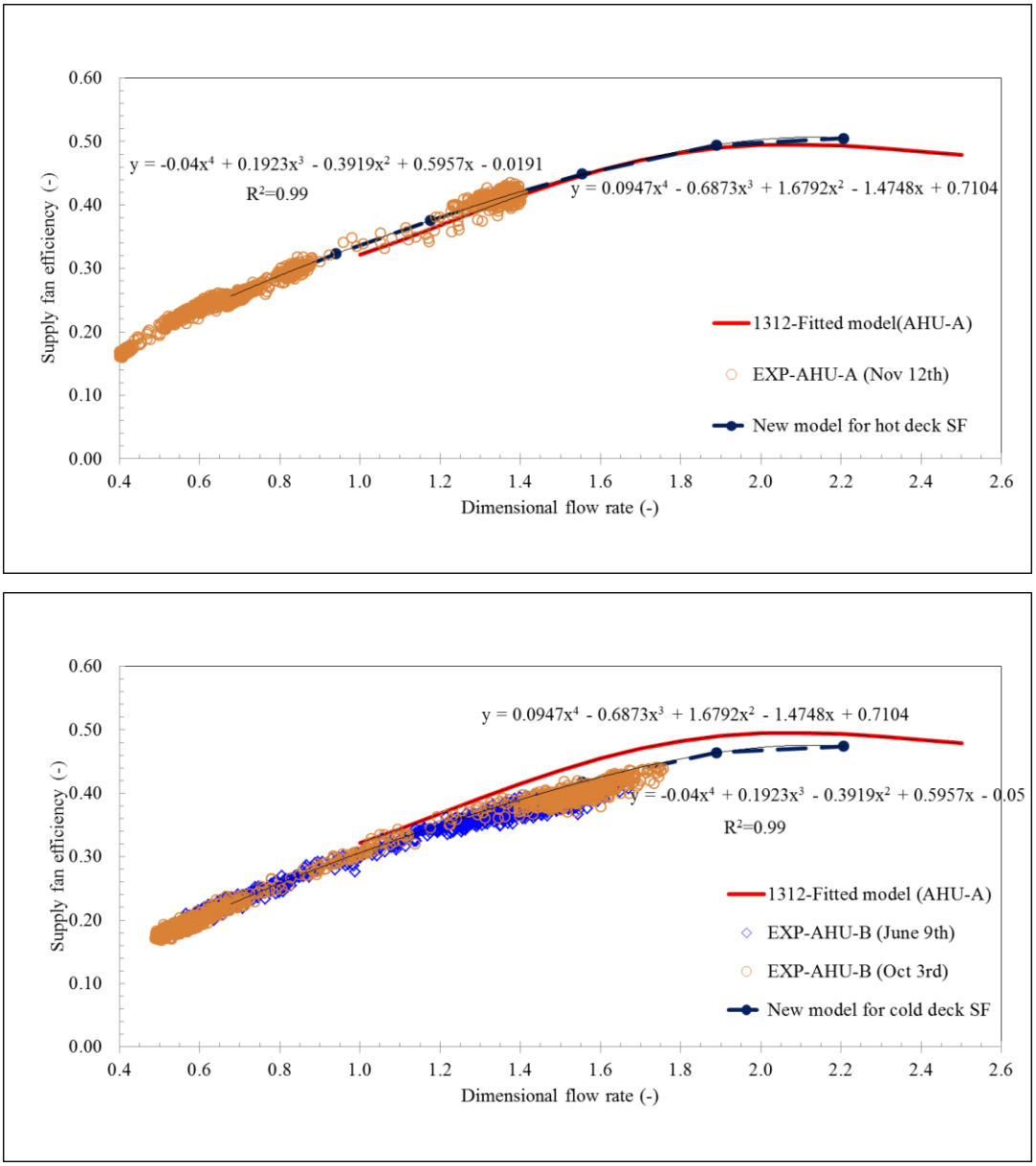

Figure 3-10. Hot deck (top) and cold deck (bottom) supply fan dimensional efficiency curve

A similar analysis has been done for return fan by collecting experimental data of several normal test days. As experienced in ASHRAE 1312 project, return fan data are so scattered to be able to fit a model properly representing the return fan behavior. As Figure 3-11 illustrates neither 1312 project polynomial model nor the fitted model are the best fits for predicting the return fan function. Therefore, comparison of

simulation results and experimental data for return fan cannot be reliable in system level validation.

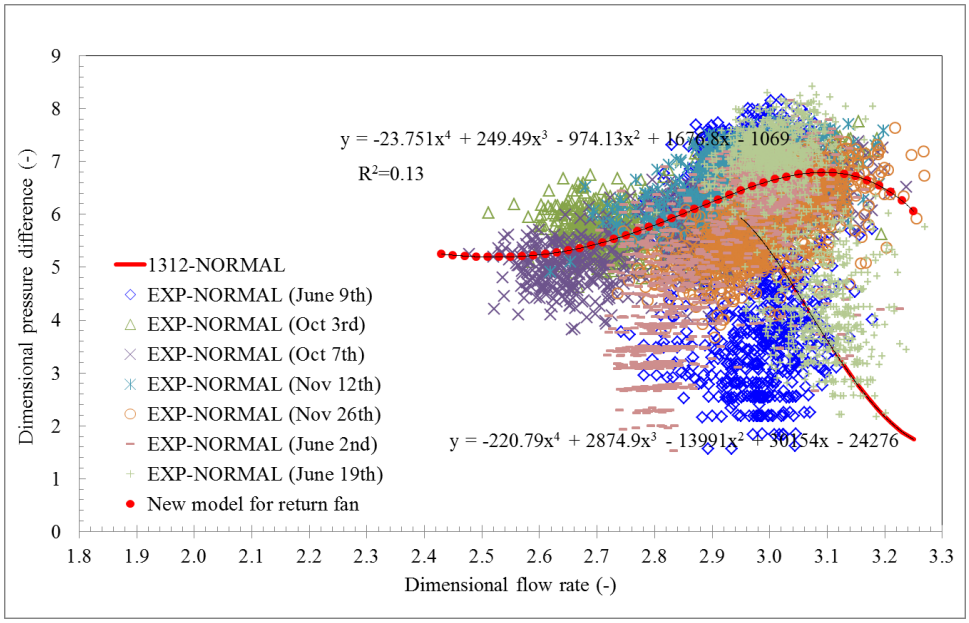

Figure 3-11. Return fan dimensional performance curve

3.3.2.2 Thermal network parameters determination

All of the components used in the dual duct double fan system thermal network are the same components used in the ASHRAE 1312 research project. Therefore, the thermal network parameters obtained from ASHRAE 1312 project are kept the same for these components. Due to the changes in operational condition of pumps and in the head pressure of heating and cooling water loops, the heating and cooling coil valves underwent a component level validation using the experimental data provided by ERS.

3.3.2.2.1 Heating and cooling coil valves model

Heating coil in AHU-A and cooling coil in AHU-B have three way valve to control water flow rate through the coil. HVACSIM+ provides a three port valve

model (used in TYPE 524) which is illustrated in Figure 3-12. When valve position varies, valve resistance changes which results in the change of water flow rates through the coil and bypass pipes. As demonstrated in Figure 3-12, four water flow resistances are used: coil flow resistance (R_{coil}), bypass pipe flow resistance (R_{bypass}), valve resistance that controls the coil water flow (R_{v1}), and valve resistance that controls bypass water flow (R_{v2}). The valve resistances (R_{v1} and R_{v2}) are calculated based on the valve position and characteristics according to Eq. (2-25).

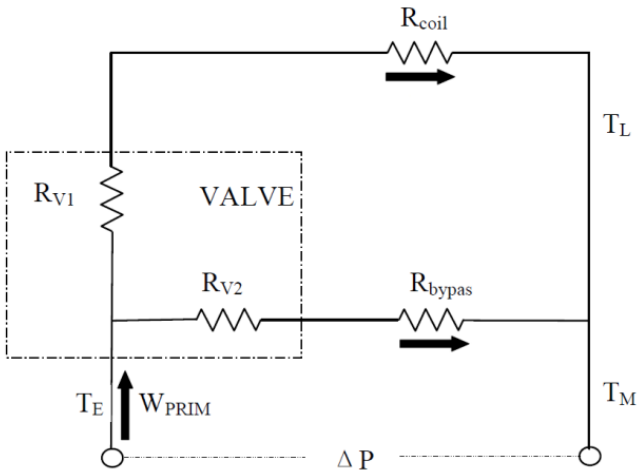

Figure 3-12. Diagram of a three port valve model (W_{prim} refers to the total water flow rate)

As discussed in 1312 research project, the valve model used in TYPE 524 is unable to precisely predict the cooling and heating coil three way valves behavior. Therefore, a new three way valve model was developed which is used here too. But the calculated parameters in 1312 project cannot be used here due to the difference in the loops head pressure. No specific component tests were performed for heating and cooling coil valves validation. But using experimental data provide enough information to validate these components. At the test facility the total water flow rate (W_{prim}) through the heating and cooling loops, mixed water temperature (T_M) as well

as entering and leaving water temperatures (T_E & T_L) are recorded which give the ability of calculating water flow rate through the coil using Eq. (3-15).

$$W_{prim}\frac{(T_M-T_E)}{(T_L-T_E)} = W_{coil} \quad (3\text{-}15)$$

The experimental data are picked from normal test days covering a wide range of valve openings. Therefore, heating and cooling coil three way valves can undergo component validation to obtain the new parameters.

Water flow rate through the coil or bypass path is calculated based on Eq. (2-26). For coil and bypass water flow rate calculations R is respectively calculated by Eq. (3-16) and (3-17):

$$R = R_{coil} + R_{v1} \quad (3\text{-}16)$$

$$R = R_{by-pass} + R_{v2} \quad (3\text{-}17)$$

In the developed valve model, three regions represent fractional flow (Eq. (2-28)) of the cooling and heating coil valves including cut-off region ($0 < x < x_l$=0.2); linear region ($x_l < x < x_h$); and high-end region (0.8= $x_h < x < 1$). Fractional flow is calculated using the following equations which calculate a and b in different regions:

For cut-off region ($0 < x < x_l$):

$$a = \frac{C_L}{x_l} \; and \; b = 0 \quad (3\text{-}18)$$

For linear region ($x_l < x < x_h$):

$$a = \frac{C_H-C_L}{x_h-x_l} \; and \; b = \frac{x_h C_L - x_l C_H}{x_h-x_l} \quad (3\text{-}19)$$

For high end region ($x_h < x < 1$):

$$a = \frac{1-C_H}{1-x_h} \; and \; b = \frac{C_H-x_h}{1-x_h} \quad (3\text{-}20)$$

The parameters of heating and cooling coil valves are calculated using Eqs. (2-32) & (2-33).

Table 3-1 summarizes the parameters for heating and cooling coil valves and bypass paths. Figure 3-13 & Figure 3-14 demonstrate the comparison between simulated heating and cooling water flow rate through the coil and bypass at different valve positions and corresponding experimental data. Although, predicted flow rates by model does not exactly match with experimental values but it is representing the best fit model and yields to satisfactory results. The R^2 for the predicted water flow rate through the heating coil and cooling coil valve by the regressed model is 0.87 and 0.56 respectively.

Table 3-1. Cooling and heating coil valves parameters estimated from experimental data

Parameters	Explanation	Value
$R_{cooling\ coil}$	Cooling coil water flow resistance, 0.001 kg-m	0.001
$K_{V\text{-}cooling\ coil}$	Cooling coil valve capacity, m^3/hr	3.65
$C_{L\text{-}cooling\ coil}$	Cooling coil valve leakage (fractional flow), %	0.0123
$C_{H\text{-}cooling\ coil}$	Cooling coil high-end fractional flow, %	0.9701
$R_{cooling\ coil\text{-}bypass}$	Cooling coil water flow resistance, 0.001 kg-m	0.001
$K_{V\text{-}cooling\ coil\text{-}bypass}$	Cooling coil valve capacity, m^3/hr	4
$C_{L\text{-}cooling\ coil\text{-}bypass}$	Cooling coil valve leakage (fractional flow), %	0.95
$C_{H\text{-}cooling\ coil\text{-}bypass}$	Cooling coil high-end fractional flow, %	0.0123
$R_{heating\ coil}$	Heating coil water flow resistance, 0.001 kg-m	10
$K_{V\text{-}heating\ coil}$	Heating coil valve capacity, m^3/hr	1.28
$C_{L\text{-}heating\ coil}$	Heating coil valve leakage (fractional flow), %	0.01
$C_{H\text{-}heating\ coil}$	Heating coil high-end fractional flow, %	0.971
$R_{heating\ coil\text{-}bypass}$	Heating coil water flow resistance, 0.001 kg-m	10
$K_{V\text{-}heating\ coil\text{-}bypass}$	Heating coil valve capacity, m^3/hr	1.335
$C_{L\text{-}heating\ coil\text{-}bypass}$	Heating coil valve leakage (fractional flow), %	0.99
$C_{H\text{-}heating\ coil\text{-}bypass}$	Heating coil high-end fractional flow, %	0.12

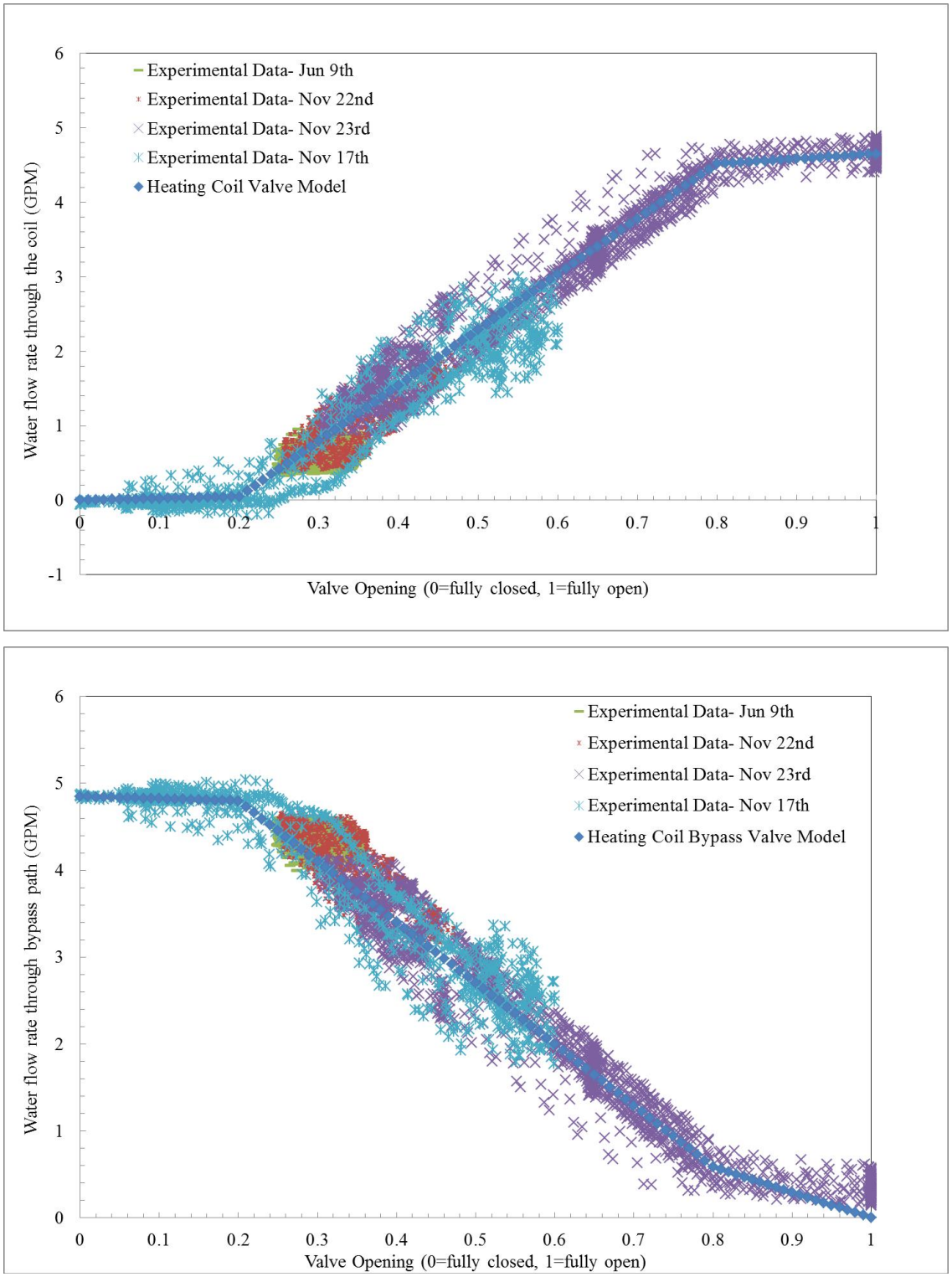

Figure 3-13. Experimental and simulated water flow rates through the coil and bypass path vs. valve opening for heating coil

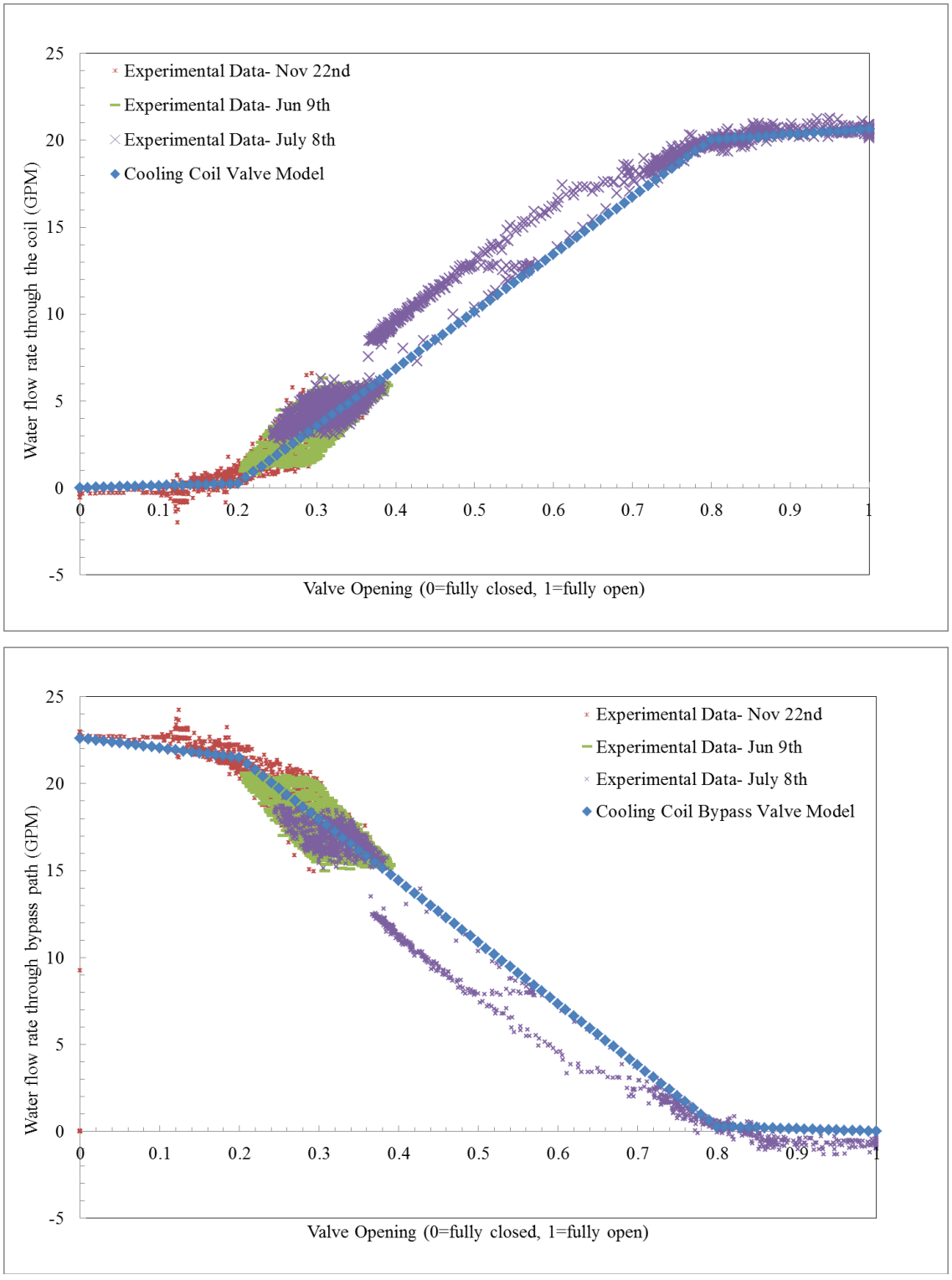

Figure 3-14. Experimental and simulated water flow rates through the coil and bypass path vs. valve opening for cooling coil

In order to solve the system of governing equations in dual duct system; MODSIM calls model definition file and boundary data files. Model definition file contains structure of the model, physical and geometric characteristics of each component, state variables initial value and state variables comprising time dependent boundary variables. Therefore, the dual duct system model is influenced directly or indirectly by both steady and time dependent factors that are included in the overall system simulation: device performance parameters, zone interior loads, outdoor air temperature and humidity, room and plenum sol- air temperatures, and inlet cooling and heating water temperatures. The only type of controllable internal load applied in each test room served by dual duct system is lighting loads. Figure 3-15 is representing the actual schedule of the internal gain profile. The ambient air physical properties and solar radiation effective on room heating and cooling loads as well as internal heat gain are defined as time variant boundary conditions.

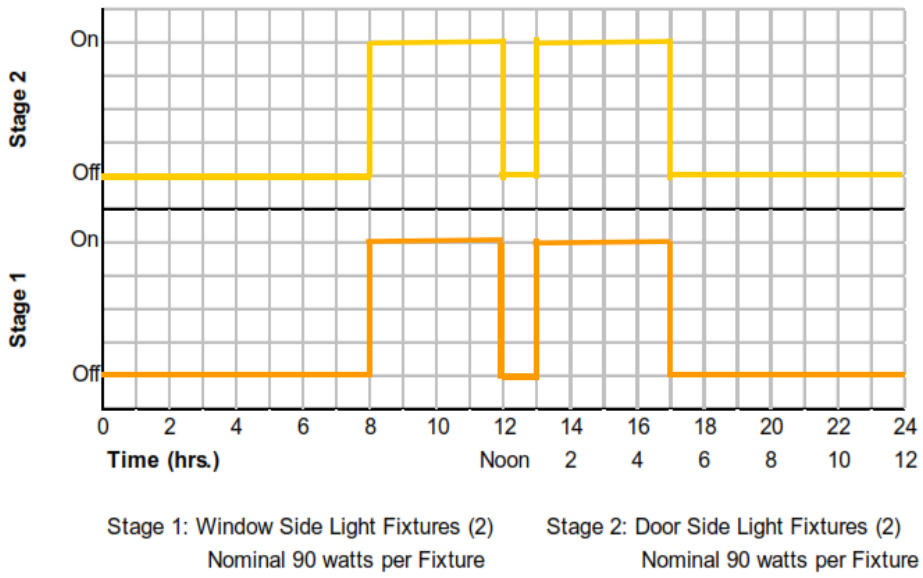

Figure 3-15. Lighting schedule as time dependent boundary conditions

3.4 Fault-free Model Validation

Validation of a large system model, such as the one developed here, is a complicated process. Although component models used in HVACSIM+ have mostly been experimentally validated, a system level model validation has not been reported in the literature. Validation of the dual duct system model has been accomplished by a two level approach: at the component level model, and at the system level model. At each level of validation, the model parameters or structures are adjusted to achieve good agreement between simulated and experimental data. Many of the components in this dual duct system are the same components used in the ASHRAE RP1312 research project (Li, et al., 2010). Therefore, parameters obtained from that project have been kept the same for these components.

In the component level validation for each UNIT, the values for the parameters need to be determined. These parameter values are determined either through manufacturer's catalog data or a component test (especially for critical/new components) or experimental data. However, for the duct work, the pressure resistances of the converging and diverging junctions in supply and return ducts are calculated based on a loss coefficient method (Pita 2002).

Even if all component models perform satisfactorily, the system performance may still not be satisfactory due to error propagation and problems with numerical stability in the calculations. In this section the general strategy used for system level validation of fault-free model is discussed.

3.4.1 Validation procedure

In order to simplify the validation of large systems at the system level validation, a hierarchical approach is taken. The system has already broken down into the constituent state categories at the model development stage. It is not only helpful in

reducing computational time but also grants the possibility of hierarchical validation at the system level validation. Validation of the developed model is accomplished in three consequent steps:

1) Air flow network validation:

   This step of system level validation is dedicated to validate the air flow state category of the system providing the necessary boundary conditions from experimental data. At this step, the pressure resistances of duct work and dampers defining the system performance curve interacting with fan performance curves are examined using the real system control signals. Generally, variables examined for this step of system level validation include total supply air flow rate and return air flow rate as well as their values for each zone.

2) Air flow and thermal network validation:

   The first step of validation guarantee the proper performance of air flow network model which can be coupled to thermal network model for the next step of validation. The model is fed by control signal from experimental data and time dependent boundary conditions including environment temperature and humidity, rooms and plenums sol-air temperatures, internal loads and inlet heating and cooling water temperatures. A close examination of heating and cooling coil performance fed by the real system valve positions as well as zones thermal dynamic are of significance at this step of validation.

3) The entire system validation:

   In reality, this step is the final goal of dynamic model validation. The control network, sensor and actuator networks are coupled to the validated air flow and thermal networks to construct the entire simulation model. The entire

system validation fed by time dependent boundary condition is the final achievement of this step. All variable examined in the previous steps besides the control signals are compared against experimental data to validate the entire system model.

This approach is really helpful to narrow down the problems and contradictions between the simulation results and experimental data associated with modeling of constitutive state processes of the system.

3.4.1.1 Air flow network validation results

In order to validate the air flow network model independently from other networks, control signals (mixing box dampers, terminal units hot and cold dampers, supply and return fan speeds) are provided directly from experimental data as boundary conditions. The system level validation of dual duct system air flow network is further designed to include two steps. The first step is to validate a subsystem starting from the hot and cold supply deck splitters all the way down to the rooms (before any flow merging). As Figure 3-16 demonstrates this step validates the hot and cold air supply decks, including the majority of modifications of the duct work. Satisfactory results from this first step ensure the accuracy of new parameters and new TYPEs. Subsequently, the entire air flow network validation is performed.

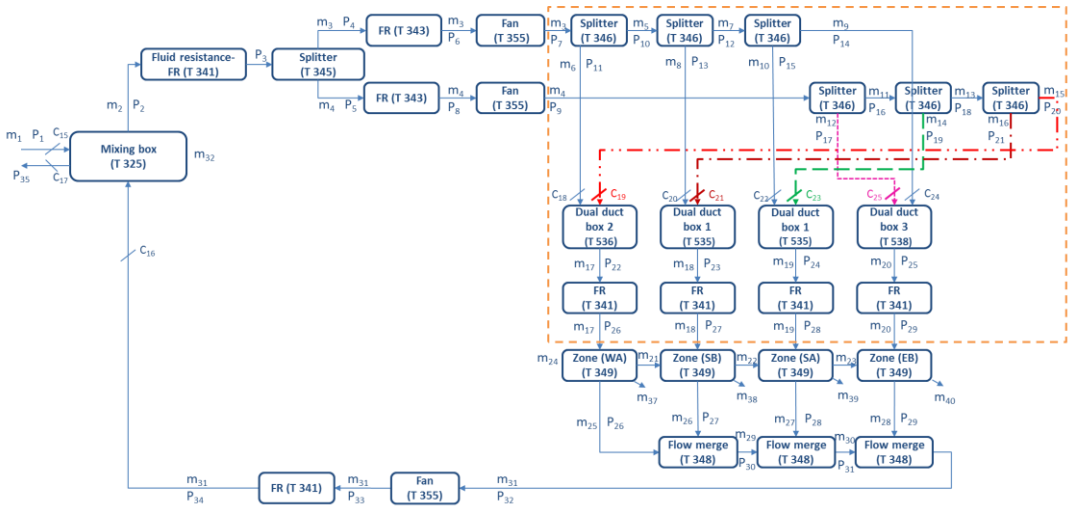

Figure 3-16. Dual duct system air flow network sub-system

In order to perform the first step of validation, hot and cold deck air flow rates (m_3 and m_4 in Figure 3-16) along with corresponding damper positions for each zone, are obtained from experimental data to be boundary conditions. Experimental data from a normal test day in cooling season (June 9th, 2013) are used for sub-system level validation. Figure 3-17 displays the simulation results for the defined sub-system in the cooling season test case (June 9th 2013 data). In this Figure, navy blue and red lines respectively represent experimental data and model predicted results and green lines represent the control signal that is provided to the model from experimental data. As Figure 3-17 displays each pair of the graphs respectively display hot and cold air flow rate to the West-A, South-B, South-A and East-B rooms. According to this figure, the comparison of experimental data and simulation results demonstrates that the pressure resistances calculated for the new splitters and the fitted model for hot and cold dampers in VAV terminal units simulates the distribution of air flow among various rooms satisfactorily.

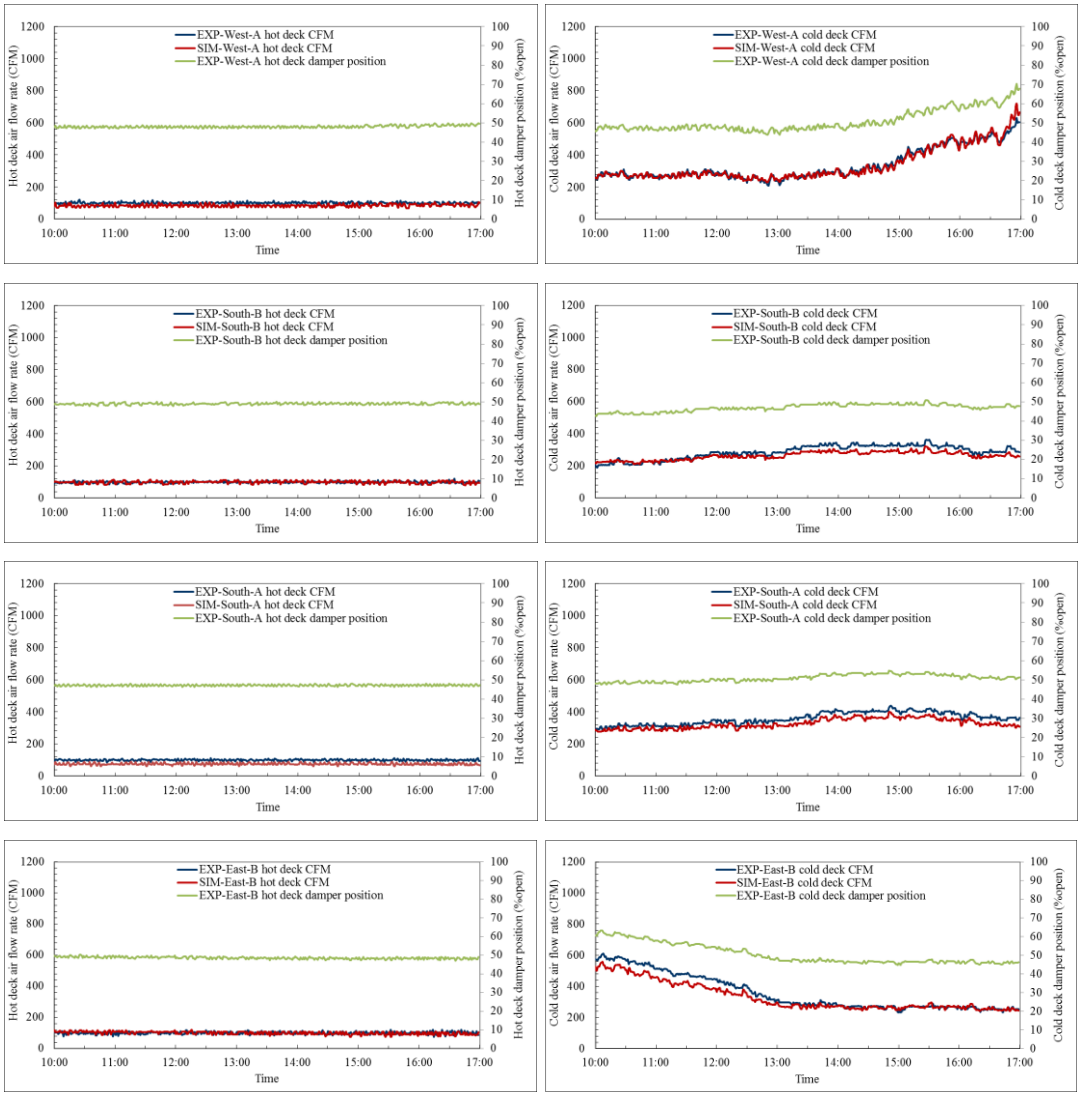

Figure 3-17. Dual duct system air flow network sub-system simulation result comparison with the real operational data (June 9th 2013)

There are slight discrepancies between the simulated hot and cold air flow rates and the real data due to the fact that component tests for damper model validation were only performed in the south-B room.

Lastly, the entire air flow model is validated using data from June 9th 2013, Oct 1st 2013, Oct 3rd 2013, Oct 7th 2013, November 12th 2013 and November 25th 2013. For the cooling season test days, the outdoor air damper is fully closed and the system is in 100% recirculation mode. For the heating and swing seasons, the outdoor air

damper position is mostly maintained at a minimum position (45%). But when outdoor air temperature is below 15.56 °C (60 °F), the outdoor air damper is controlled by an economizer mode. Satisfactory results from this step ensure the accuracy of new parameters for the existing and revised components (mixing box, hot and cold deck supply and return fans, pressure resistances of different components, converging and diverging junctions) and new TYPEs (dual duct terminal units).

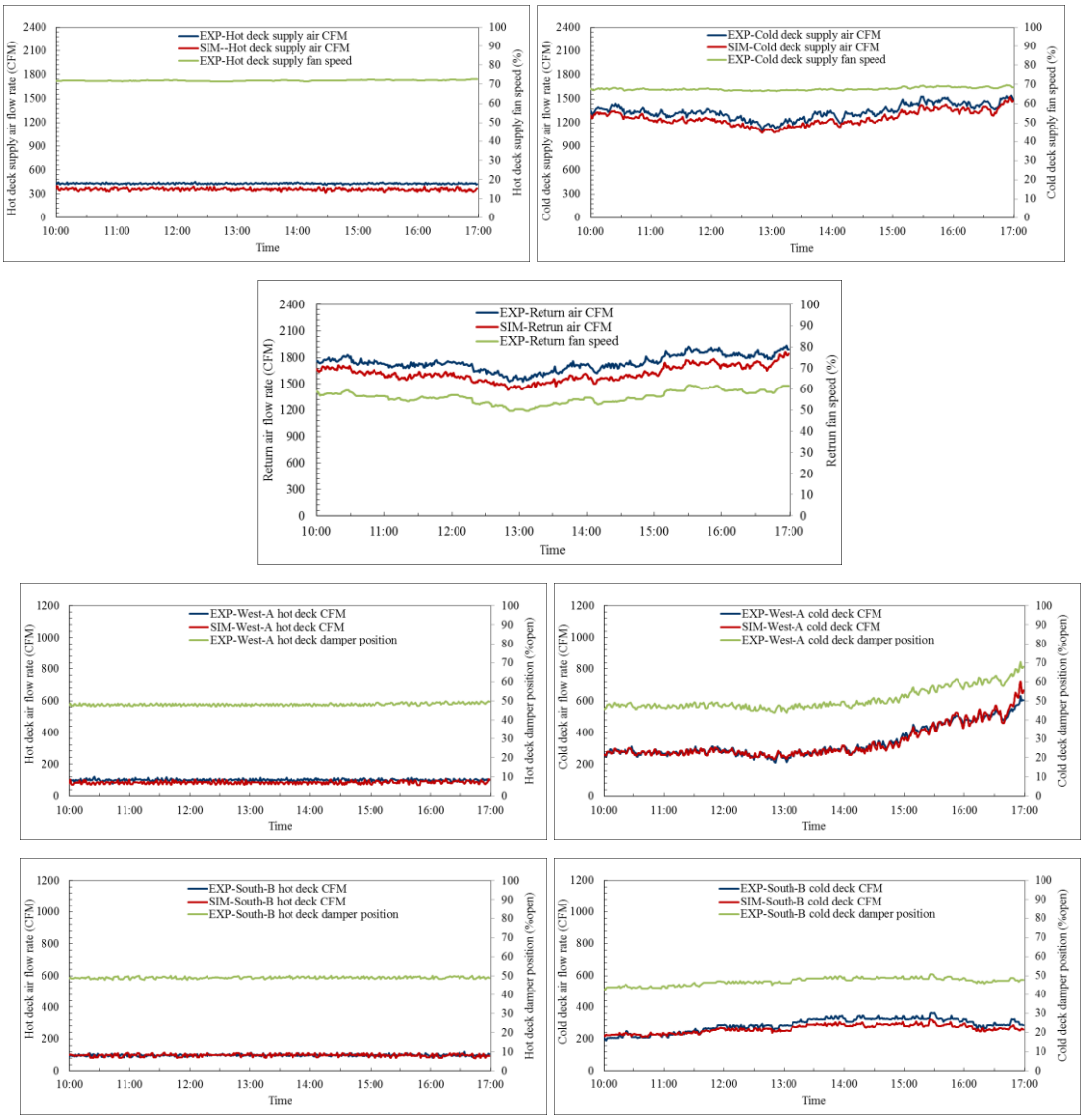

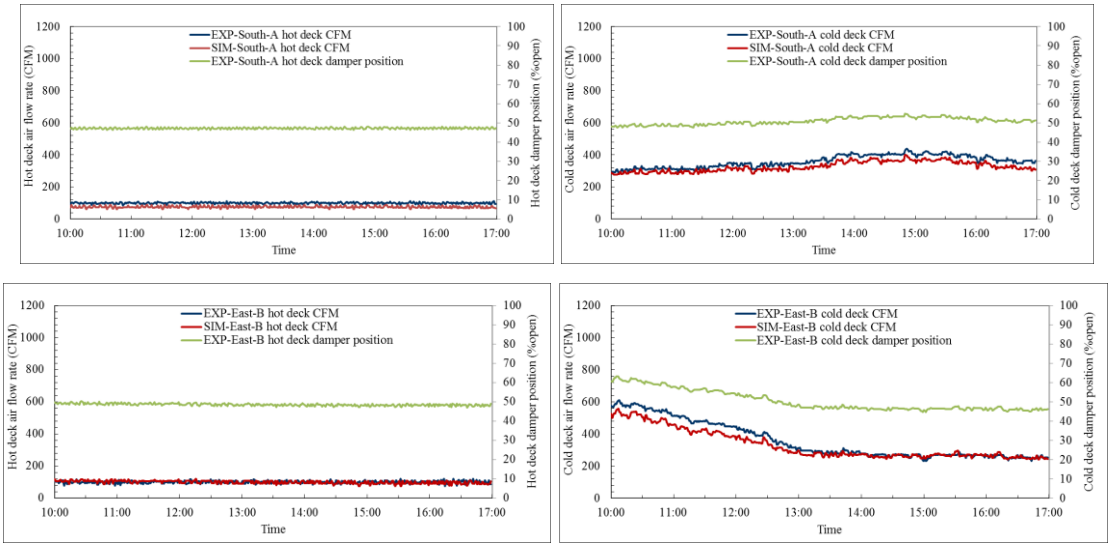

Figure 3-18. Dual duct system air flow network simulation result comparison with the real operational data (June 9th 2013)

Figure 3-18 displays the simulation results for the entire air flow network simulation in the cooling season test case (June 9th 2013 data). The first three graphs illustrate hot and cold deck supply air and total return air flow rates. Each pair of the following graphs respectively display hot and cold air flow rate to the West-A, South-B, South-A and East-B rooms. In general, model predicted results are in close agreement with operational data. The difference between experimental and model predicted hot air supply flow rate is on average within 0.0368 m^3/s (78 CFM) and this difference for cold air supply flow rate is on average within 0.0269 m^3/s (57 CFM). The biggest discrepancy between the model predicted results and experimental data is the 0.094 m^3/s (200 CFM) for cold air and 0.055 m^3/s (117 CFM) for hot air supply flow rates. As Figure 3-18 displays, the East-B room cold air flow rate simulation shows the highest discrepancy when damper positions are greater than 60%. Results from other seasons have very similar trends to those shown in Figure 3-18 and, for brevity are not presented here. For other seasons, the difference between experimental and model predicted hot air supply flow rate is on average within 0.07 m^3/s (150

CFM) and this difference for cold air supply flow rate is on average within 0.12 m^3/s (250 CFM). The amount of discrepancy between the model and experiment for outdoor air is around 0.094 m^3/s (200 CFM), which is about 14 percent of the outdoor air flow rate.

Since the mixing box used in this dual duct system is the same as the one (AHU-B mixing box) used in the ASHRAE RP1312 project, the parameters obtained in that project are used here. But it seems that the mixing box parameters are not properly tuned for this project reflecting it's dynamic. Unfortunately, the experimental data are not enough to retune the mixing box parameters and no component test has been performed for it.

3.4.1.2 Airflow and thermal network validation results

In order to validate the air flow and thermal network model independently from control network, control signals (mixing box dampers, terminal units hot and cold dampers, supply and return fan speeds, heating and cooling coil valves) are provided directly from experimental data as boundary conditions. In addition to control signals time dependent boundary conditions (outdoor air temperature and humidity, sol-air temperature of rooms and plenums with various orientations) are also provided to the model composed of air flow and thermal networks. The system level validation of dual duct system air flow and thermal network is designed to validate the thermal performance of dual duct system while the numerically calculated air flow rates are provided by air flow network. This level of validation is also done for different test cases like air flow network validation. Here a test case in fall season (Oct 7^{th} 2013) is presented as illustration.

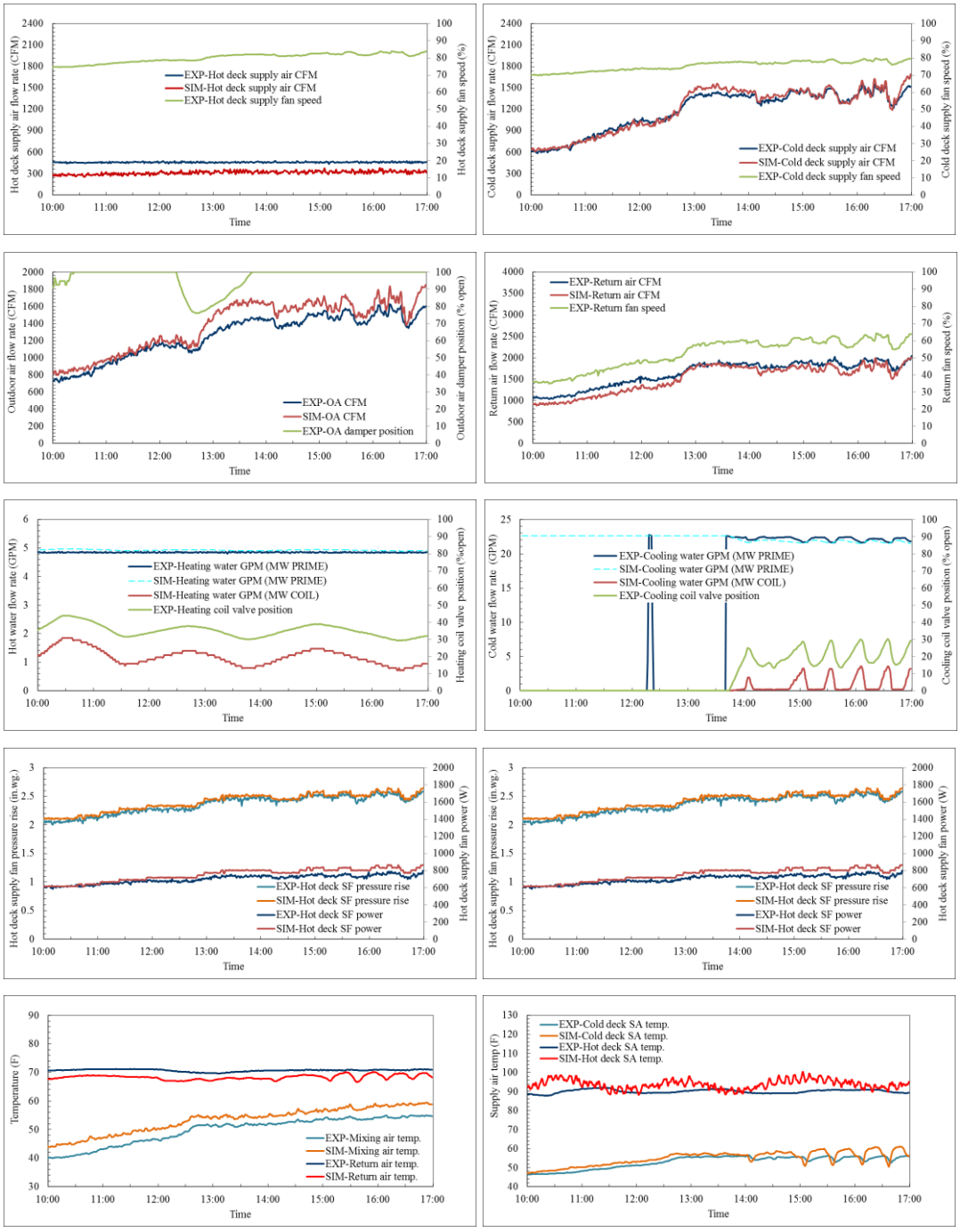

(a) Air handling unit result of dual duct system air flow and thermal network validation

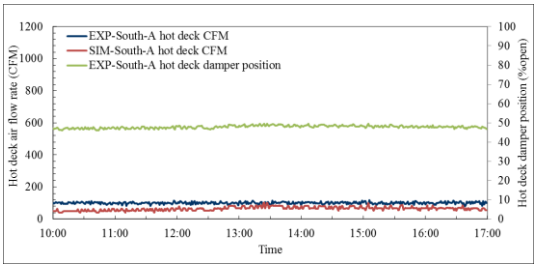
EXP-South-A hot deck CFM
SIM-South-A hot deck CFM
EXP-South-A hot deck damper position
Hot deck air flow rate (CFM)
Hot deck damper position (%open)
Time

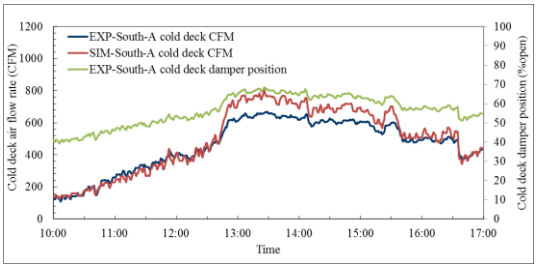
EXP-South-A cold deck CFM
SIM-South-A cold deck CFM
EXP-South-A cold deck damper position
Cold deck air flow rate (CFM)
Cold deck damper position (%open)
Time

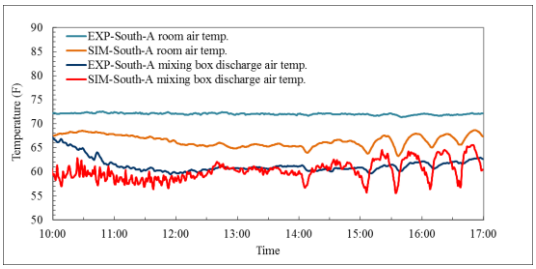
EXP-South-A room air temp.
SIM-South-A room air temp.
EXP-South-A mixing box discharge air temp.
SIM-South-A mixing box discharge air temp.
Temperature (F)
Time

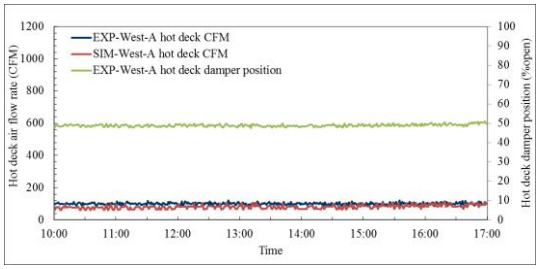
EXP-West-A hot deck CFM
SIM-West-A hot deck CFM
EXP-West-A hot deck damper position
Hot deck air flow rate (CFM)
Hot deck damper position (%open)
Time

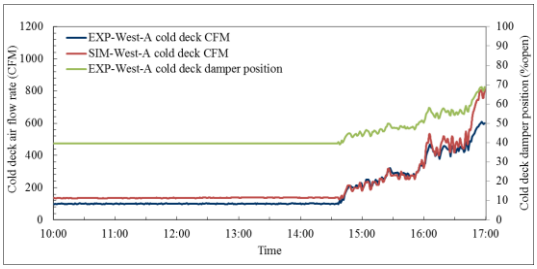
EXP-West-A cold deck CFM
SIM-West-A cold deck CFM
EXP-West-A cold deck damper position
Cold deck air flow rate (CFM)
Cold deck damper position (%open)
Time

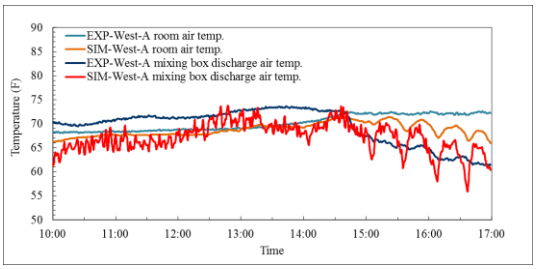
EXP-West-A room air temp.
SIM-West-A room air temp.
EXP-West-A mixing box discharge air temp.
SIM-West-A mixing box discharge air temp.
Temperature (F)
Time

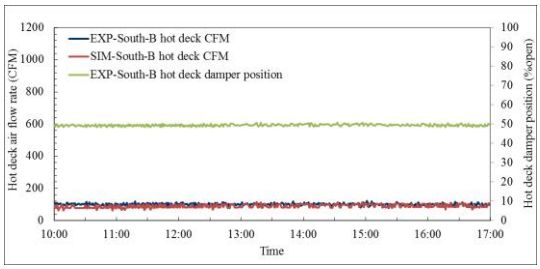
EXP-South-B hot deck CFM
SIM-South-B hot deck CFM
EXP-South-B hot deck damper position
Hot deck air flow rate (CFM)
Hot deck damper position (%open)
Time

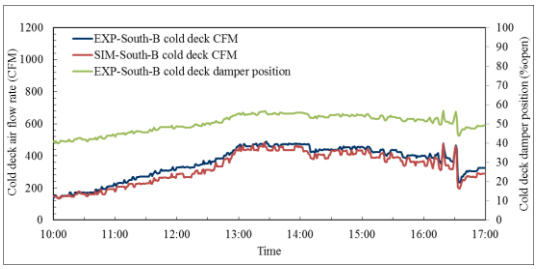
EXP-South-B cold deck CFM
SIM-South-B cold deck CFM
EXP-South-B cold deck damper position
Cold deck air flow rate (CFM)
Cold deck damper position (%open)
Time

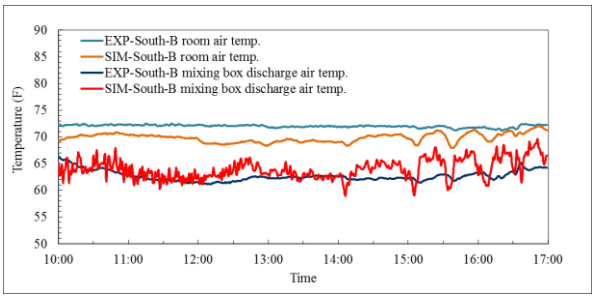
EXP-South-B room air temp.
SIM-South-B room air temp.
EXP-South-B mixing box discharge air temp.
SIM-South-B mixing box discharge air temp.
Temperature (F)
Time

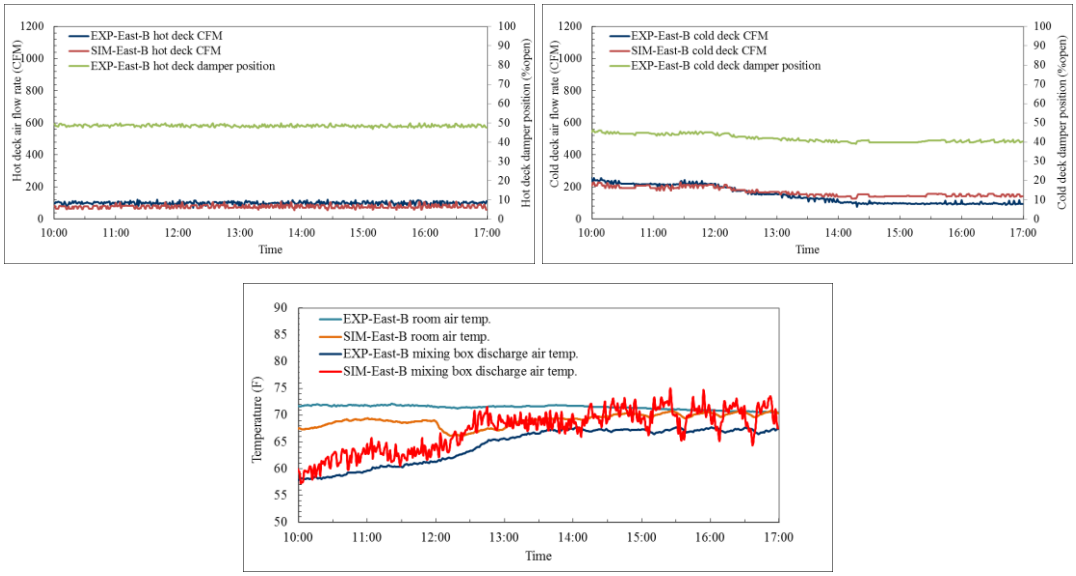

(b) Zones result of dual duct system air flow and thermal network validation

Figure 3-19. Dual duct system air flow & thermal network simulation result comparison with the real operational data (Oct 7th 2013)

Figure 3-19 (a) demonstrates the simulation results of air flow and thermal networks for AHU and air flow and thermal states of the serving zones. In the first three pairs of graphs in this Figure, navy blue and red lines respectively represent experimental data and model predicted results and green lines represent the control signal that is provided to the model from experimental data. The first four graphs illustrate hot and cold deck supply air; fresh air and total return air flow rates. The model predicted hot deck air flow rate deviation from experimental data is around 0.07 m^3/s (150 CFM). There is good agreement between simulation result and experimental data for cold deck supply air flow rate. The deviation of model predicted hot deck supply air flow rate from experimental data affect the comparison of return air flow rate too. As mentioned earlier, due to the lack of information retuning the mixing box parameters for this project was not possible and we can see some deviation in the function of mixing box dampers here.

The deviation of model predicted hot deck supply air flow rate from experimental data can be explained from two perspectives: flow meter uncertainty in low flow rates and the uncertainty associated with the component models particularly fans and dampers here. A close look at the experimental data for hot air flow distribution between zones indicate that the summation of individual flow meter readings in each zone does not match with the total amount of experimentally recorded hot deck supply air flow rate. In addition, as discussed earlier there are uncertainty associated with the fitted model for fan and dampers which both mutually affect the head and system curve and finally the operation point of the system. Furthermore, according to the damper models, they impose a large resistance to the air flow network and even one degree difference in their position cause a different air flow rate to the zones. A comparison of the hot deck damper position in each room dual duct terminal unit indicates that they are not exactly the same.

In the third pair of graphs in Figure 3-19 (a) the hot and cold water flow rate through the coil predicted by the model is displayed. At the ERS test facility just the primary water flow rates in heating and cooling loops are measured and the water flow rate through the coil is not recorded. The forth pair of graphs show the hot and cold deck supply fans pressure rise and power consumption. The model predicted pressure rise and power consumption for both supply fans follow the trend and value of experimental data in close agreement. The last pair of graphs in this figure illustrates the comparison of simulation results and experimental data for mixing and return air temperature as well as hot and cold deck supply air temperatures.

The model predicted return air temperature deviation form experimental data is the result of different dynamic behavior of the modeled room from the real one as discussed before. Figure 3-19 (b) illustrates the room air temperature of different

zones. The mixing air temperature is the result of mixing fresh air and return air. The deviation of model predicted mixing air temperature form the experimental data is the consequence of return and fresh air flow rates and also return air temperature from experimental data.

The model predicted supply air temperature deviation from experimental data emanates from the uncertainty associated with the water flow rate through the coil. This is especially more obvious for hot deck supply air temperature. Different analyses have been done on the model of coil (TYPE 533) to investigate the reason of this deviation. As mentioned earlier, in valve models development the water flow rates through the coils are calculated based on entering, leaving and mixing water temperatures as well as primary water flow rate. Any inaccuracy in temperature sensor readings can affect water flow rate calculation and consequently coil leaving air temperature calculation. As Figure 3-13 shows for heating coil valve opening ranging from 0.2 to 0.6 the calculated lower and higher limit of water flow rate through the coil differs 1 GPM. Therefore, the deviation of supply air temperature can be explained by the uncertainty associated with water flow rate calculation.

Hot and cold decks air flow distribution between different rooms as well as mixed air temperature in terminal units and room air temperature are illustrated in Figure 3-19 (b). The deviation of room air temperatures is within a range of 2 to 6 ^{o}F which obviously certifies the difference in dynamic behavior of the modeled room and real one.

3.4.1.3 Entire system validation results

The last step of dual duct system validation is to couple the entire system constituent superblocks including control, actuator, air flow, thermal and sensor networks. As mentioned earlier, the control strategy used in this project differs from

the one used at ERS. Because, Johnson Control has implemented a pattern recognition method to control the dual duct terminal units which is a patented control strategy. The previous steps of validation ensure the validity of the air flow and thermal networks while they are fed by real experimental inputs specially control signals. The goal of this project is to provide a testbed for research and development of improved methods for automatic control and AFDD of HVAC systems. Therefore, we suffice to apply a similar control strategy to dual duct terminal units to study the capabilities of the developed testbed for dual duct system in the directions of project objectives. Therefore, the performance of the model is just evaluated by RMSE as is shown in Table 3-2 to have a sense of the model deviation from the real operational data.

A test case in summer (June 9th 2013) is picked to illustrate the final simulation results of dual duct double fan system. Figure 3-20 demonstrates the simulation result comparison against experimental data for the entire model simulation of dual duct double fan system. In this Figure AHU (Figure 3-20 (a-c)) as well as east-B and south-B rooms (Figure 3-20 (d,e)) results are illustrated.

In Figure 3-20 (a) the model predicted control signals are compared against experimental data. Deviation of the model predicted cold deck and return fan speeds from experimental data can be explained by the cold deck supply and return air flow rates graphs in Figure 3-20 (b). This contradiction is also originated from the deviations illustrated in cold deck air flow rate graphs in Figure 3-20 (d,e). Not only the dynamic of the modeled rooms are different form the real one but also the applied control strategy for the modeled dual duct terminal units does not match with the real one. These variations lead to different zone damper responses and consequently the cold and hot air flow rates to the rooms. Here, the consequence of deviation in cold deck air flow rate affect the cold deck supply fan in charge of maintaining the static

pressure of the cold deck. As Figure 3-20 (d,e) shows the rooms are in cooling mode and dual duct terminal units modulate the hot deck damper to maintain the minimum requirement of hot air flow rate (100 CFM) while cold deck damper modulates the cold air flow rate to meet room air set point. According to Figure 3-20 (c) return air temperature and mixing air temperature are reflecting the same temperature due to no presence of fresh air.

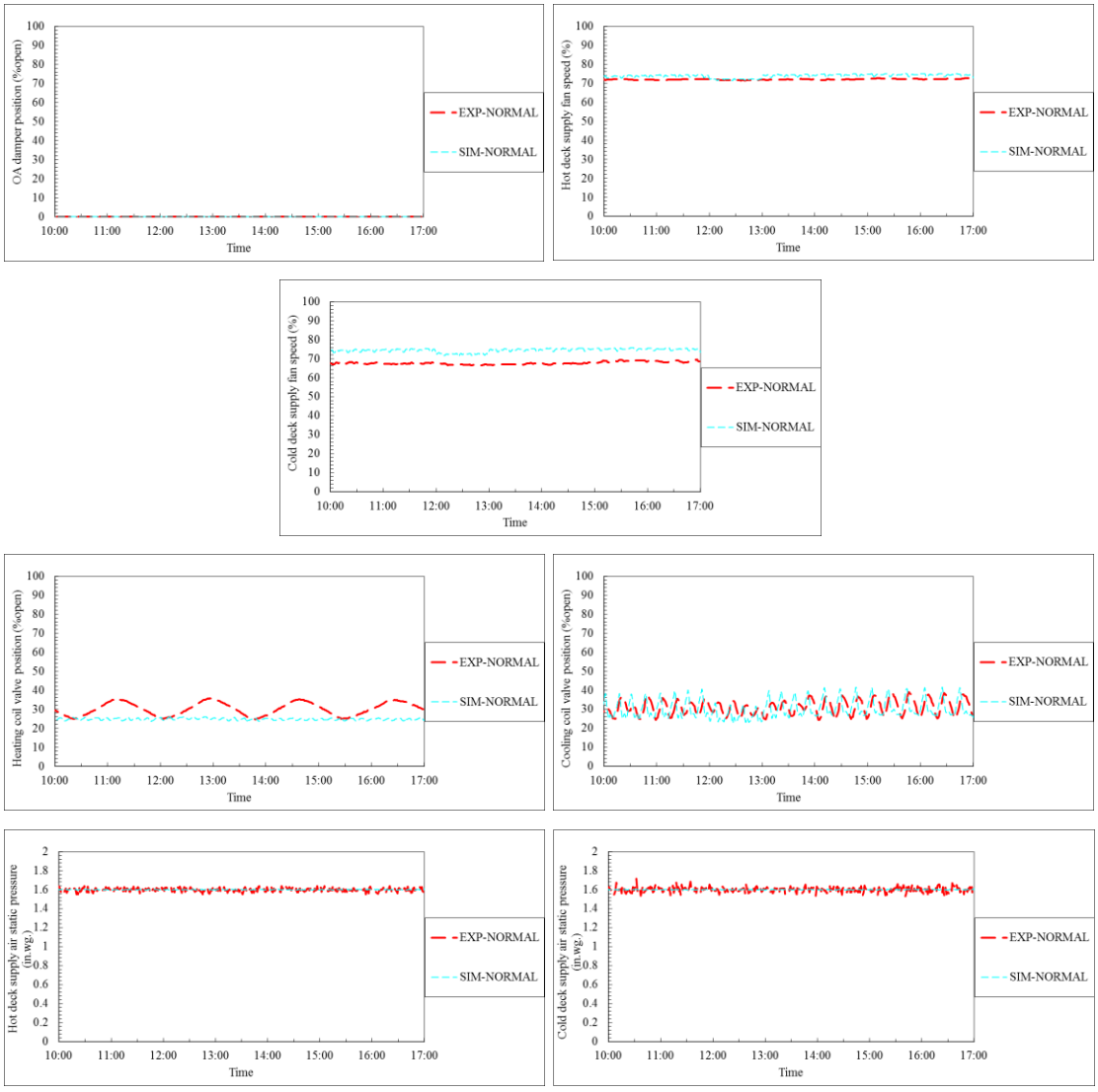

(a) Control signals of dual duct system AHU

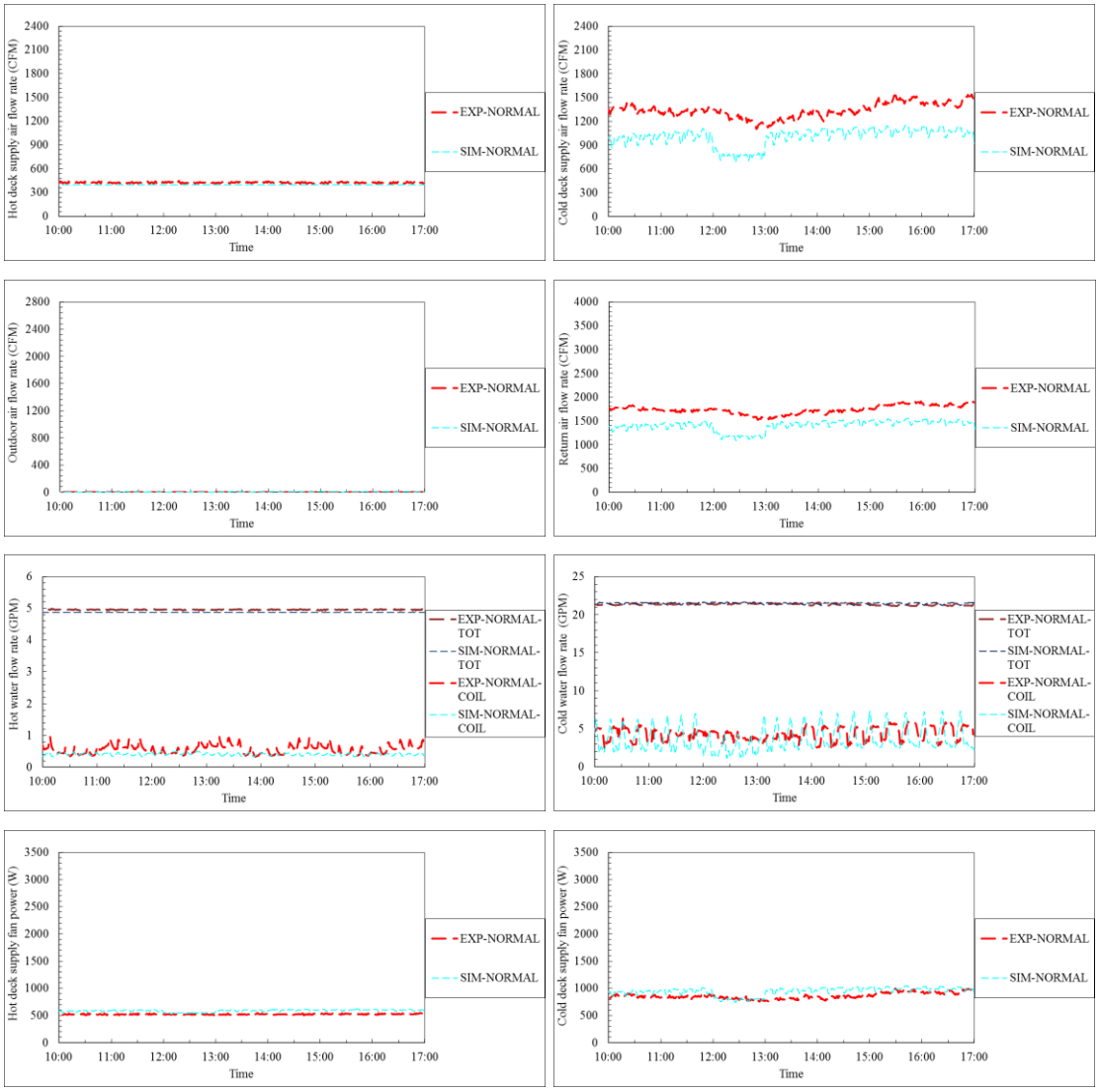

(b) Air and water flow rates and power consumption of supply fans in dual duct system AHU

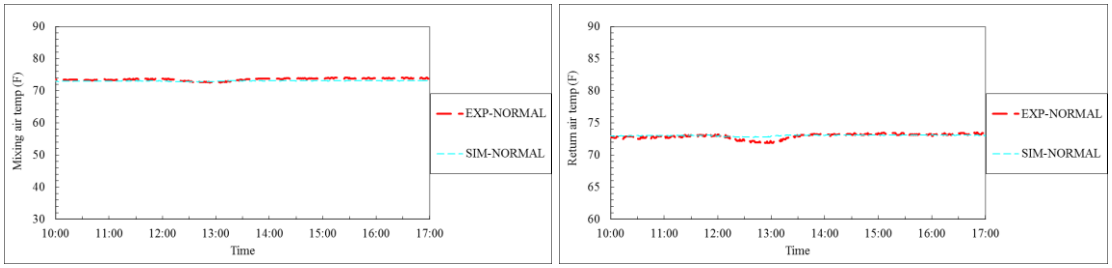

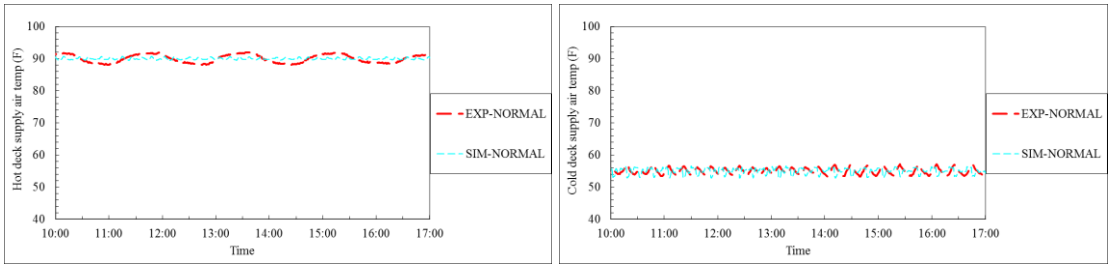

(c) Temperatures of dual duct system AHU

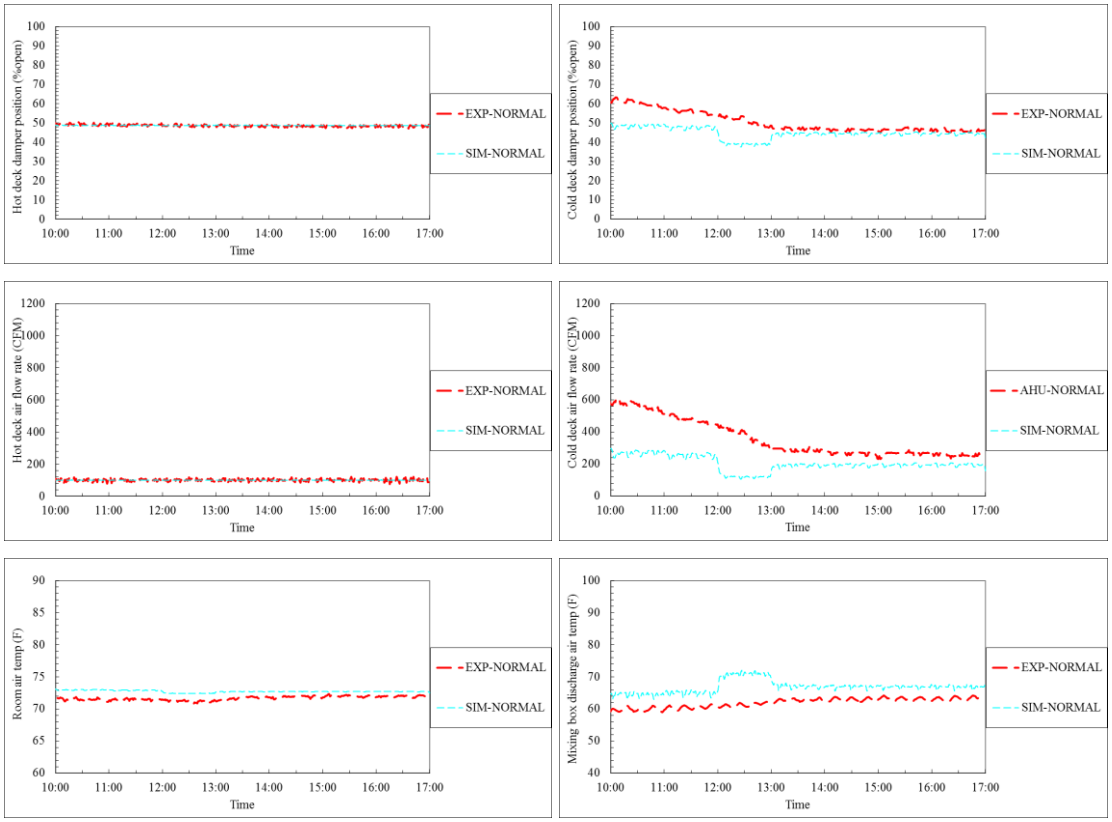

(d) East-B room

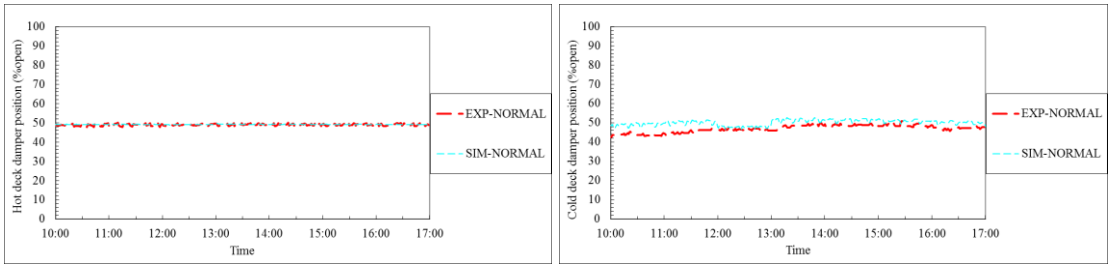

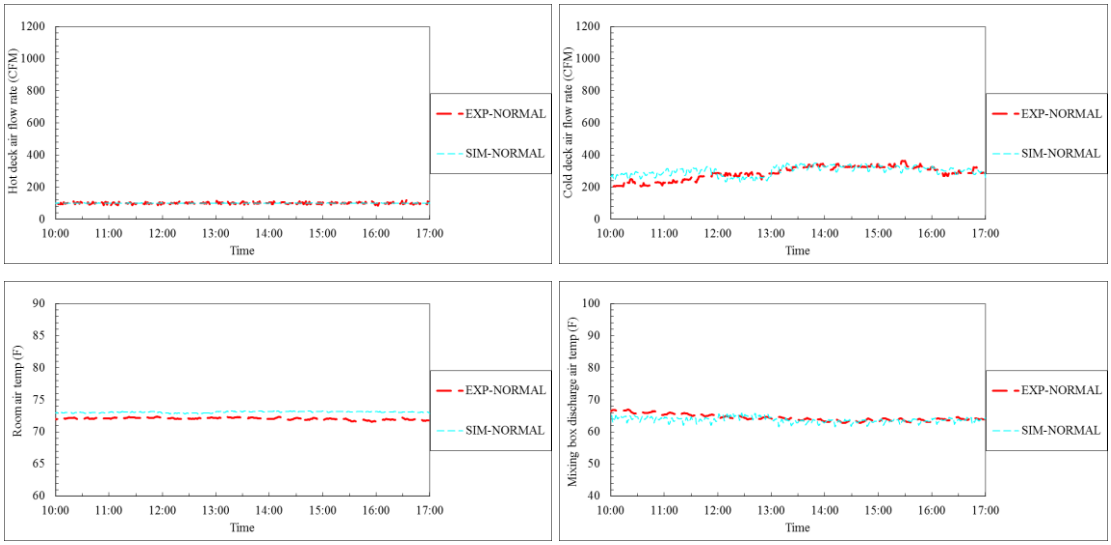

(e) South-B room

Figure 3-20. Dual duct system simulation result comparison with the real operational data (June 9th 2013)

The performance of the developed model in predicting the dynamic of each variable representing dual duct system function is evaluated using the R^2 and RMSE defined in Eqs. (1-1) & (1-2)) and is tabulated in Table 3-2. As the control strategy for the modeled dual duct system is not exactly the same as the real system RMSE for some variables, especially for control signals including valves, dampers and supply fan speeds, is significant. The error in predicting the control signals also propagates to other variable predictions.

Table 3-2. Dual duct system model performance

Variable			RMSE
AHU	Supply fan speed	Hot deck	1.46
		Cold deck	6.72
	Supply fan power	Hot deck	62.947
		Cold deck	94.90
	Valve position	Heating coil	6.278
		Cooling coil	5.021
	Water flow rate	Heating coil	0.205
		Cooling coil	1.846
	Supply air flow rate	Hot deck	29.18
		Cold deck	364.62
	Temperature	Mixing air	0.567
		Return air	0.336
		Hot deck supply air	1.27
		Cold deck supply air	1.44
East-B Room	Damper position	Hot deck	0.682
		Cold deck	10.003
	Air flow rate	Hot deck	8.221
		Cold deck	229.56
	Temperature	Mixing box discharge air	5.276
		Room air	1.084
South-B Room	Damper position	Hot deck	0.521
		Cold deck	3.63
	Air flow rate	Hot deck	5.375
		Cold deck	38.334
	Temperature	Mixing box discharge air	1.31
		Room air	0.978

3.5 Fault Model Development

The designed fault flag system for FCU is extended to include the faulty conditions associated with dual duct double fan systems. The category of faults which may occur in dual duct double fan systems and the devices affected by these faults are listed in Table 3-3. The dual duct system model simulates those faults with varying severity, which projects proportionally to the fault symptoms observable in data. As Table 3-3 demonstrates, various fault categories associated with dual duct system are listed in four different categories: AHU equipment, sensor, actuator and controllers. In AHU equipment category the fan motor failure for hot and cold deck supply fans as well as return fan is modeled. Furthermore, the fouling fault for air side and water

side of both heating and cooling coils are simulated. In the sensor category, hot and cold deck temperature sensors as well as static monometers undergo offset fault modeling. Under actuator category, the stuck fault with different severities is simulated for heating and cooling coil valves and outdoor air damper in mixing box. In control category, two types of fault, namely, unstable control fault for heating and cooling loop and outdoor air damper as well as improper temperature fault for hot and chilled water are modeled. A brief review of various fault categories and their implementation to different devices of the real system can be found in Chapter two Section 2.6.

Table 3-3. Dual duct double fan system fault summary

Category	Device	Fault Name	Fault Type	Summer Test Days	Fall Test Days	Winter Test days
Equipment	Cooling Supply Fan	Failure	Abrupt	1		
	Heating Supply Fan	Failure	Abrupt		1	
	Return Fan	Failure	Abrupt			1
	Heating Coil	Inadequate Capacity	Restricted HW flow		1	1
		Fouling-Airside	Gradual to 50% flow		1	
	Cooling Coil	Inadequate Capacity	Restricted CHW flow	1		1
		Fouling-Airside	Gradual to 50% flow	1		
Sensor	Cold Deck SA Temp	Offset	Degradation	1	1	1
	Hot Deck SA Temp	Offset	Degradation	1	1	1
	Cold Duct SA Pressure	Inadequate Pressure	Degradation	1		1
	Hot Duct SA Pressure	Inadequate Pressure	Degradation		1	1
Actuator	Cooling Damper	Stuck	Full Open	1	1	
			Full Closed	1	1	
			Partial Open (50%)	1	1	
	Heating Damper	Stuck	Full Open	1	1	
			Full Closed	1	1	
			Partial Open (50%)	1	1	
	AHU OA Damper	Stuck	Full Open	1		1
			Full Closed (20%)		1	1
			Partial Open (50%)			1
Control	Heating Sequence	Unstable Control	Degradation		2	2
	Cooling Sequence	Unstable Control	Degradation	2		2
	OA Damper Sequence	Unstable Control	Degradation			2
	Heating Water	Supply Temp Too Low	Implementation		1	
	Chilled Water	Supply Temp Too High	Implementation	1		

3.5.1 Fault flag system

The designed fault flag system for dual duct double fan system has been summarized in Table 3-4. In Table 3-4, the first column lists the four fault categories; the second column lists the device or process that would be affected by a fault. The third column summarizes the potential fault status and fault type for a device or process. The fourth and fifth column list variables used in MODSIM HEAD subroutine to store fault type and severity for each device or process. The last column lists the TYPE in HVACSIM+ library of component that would be affected by the faults associated with each device or process.

Table 3-4. Dual duct double fan system fault flag system summary

Category	Device	Fault type	Fault variable	Fault severity variable	TYPE
Equipment	Cooling Supply Fan	0- No fault, 1- Fan motor failure, 2- Fan outlet blockage	sfancold	vsfan	355
	Heating Supply Fan	0- No fault, 1- Fan motor failure, 2- Fan outlet blockage	sfanhot	vsfan	355
	Return Fan	0- No fault, 1- Fan motor failure, 2- Fan outlet blockage	rfan	vrfan	355
	Heating Coil	0- No fault, 1- Fouling Air-side, 2- Fouling Water-side	coilfault(4)	Vcoilfault(2,3)	533
	Cooling Coil		coilfault(3)	Vcoilfault(2,3)	533
Sensor	Cold Deck SA Temp	0- No fault; 1- Offset fault	SAcoldtemp	VSAcoldtemp	311
	Hot Deck SA Temp		SAhottemp	VSAhottemp	
	Cold Duct SA Pressure	0- No fault; 1- Offset fault	pscoldset	Vpscoldset	481
	Hot Duct SA Pressure		pshotset	Vpshotset	
Actuator	Cooling Damper	0- No fault, 1- Stuck	CLGdamp	VCLGdamp	531, 532, 534
	Heating Damper	0- No fault, 1- Stuck	HTGdamp	VHTGdamp	531, 532, 534
	AHU OA Damper	0- No fault, 1- Stuck, 2- leakage	OAdamp	VOAdamp	325
Control	Heating Sequence	Unstable Control	Degradation		
	Cooling Sequence	Unstable Control	Degradation		
	OA Damper Sequence	Unstable Control	Degradation		
	Heating Water	Supply Temp Too Low	Implementation		
	Chilled Water	Supply Temp Too High	Implementation		

3.6 Fault Model Validation

Given the simulation system model had been validated under fault-free conditions, the only further validations required to ensure realistic representation of faults are those on the altered parameter values. During the validation of fault modeling, it is more important to compare fault symptoms rather than regenerating the dynamics of each variable. This is due to the complex impacts of faults under real world conditions, and the difficulty of simulating such impacts precisely. Therefore, faulty operation validation does not need a comprehensive process as described for fault free validation. The overall procedure of fault model validation for the secondary systems in this project has been described in Chapter one. It is worth mentioning that false implementation of faults is applied to all rooms except for south-B room. Therefore, when dual duct terminal units undergo faulty operation comparison of south-A room (under faulty condition) with south-B room (under fault-free condition, reference model) simulation results is helpful in fault symptoms identification.

To assist validation of dual duct double fan system fault model, experimental data under faulty conditions (under different faults and severity levels) are collected from AHU and east-B and west-A and south-A facing rooms in the ERS. Like fault-free tests, three test periods are scheduled during summer, fall and winter for collecting faulty experimental data. Different faults are implemented in different seasons because system operational characteristics and control sequence change with weather conditions. Table 3-3 demonstrates the faulty condition which has been tested in different seasons. The season operation has been selected so that a specific fault yields measurable system difference compared with a fault-free system.

3.6.1 Fault model validation results

Validation of dual duct double fan system fault model has been done on all faulty test days of three different seasons: summer, fall and winter. The symptoms associated with each fault at every season for AHU and zones are listed in Table 3-5. Furthermore, the picked reference normal test days which can help to show the symptom caused by the faults to the system have also been summarized.

Table 3-5. Summary of symptoms associated with each fault in dual duct double fan system

Category	Device	Fault Name	Fault severity	Case #	Summer Test	Test date	Reference normal test day	Fall Test	Test date	Reference normal test day	Winter Test	Test date	Reference normal test day	Observed AHU symptoms	Observed Zone symptoms	Note
AHU Equipment	Cooling Supply Fan	Failure	Failure	**1**	1	June 4th & 25th	Hotter (June 9th) (June 19th)							cold deck SF speed ↑/ cold deck SF power=0 ↓/ cooling coil VLV=0% ↓ -> chilled water flow rate ↓/ heating coil VLV ↓ -> hot water flow rate ↓/ cold deck static pressure=0 ↓/ cold deck SA CFM ↓-> return air CFM ↓/ mixing air & return air temp↑	discharge air temp ↑/ room temp ↑/ cold deck damper ↑ but cold deck CFM=0	
	Heating Supply Fan	Failure	Failure	**2**							1	Nov 5th	cooler (Nov 25th)	hot deck SF speed ↑/ hot deck SF power=0 ↓/ heating coil VLV=0% ↓ -> hot water flow rate ↓/ hot deck static pressure=0 ↓/ hot deck SA CFM ↓-> return air CFM ↓/ return air temp↓	discharge air temp ↓ / room temp ↓/ hot deck damp ↑ but hot deck CFM =0	
	Return Fan	Failure	Failure	**3**				1	Sep 12th	Hotter (Sep 11th)				return fan speed ↑=100% but power=0	-	
	Heating Coil	Inadequate Capacity	Restrict HW flow	**4**				1	Sep 13th	Cooler (Sep 23rd)	1	Nov 6th	Cooler (Nov 25th)	heating coil VLV ↑ but hot water GPM doesn't change/ total hot water flow rate ↓		

		Fouling - Airside	gradual to 50% flow	**5**						1	Nov 7th	Cooler (Nov 25th)	hot deck SF speed ↑-> hot deck SF power ↑/ heating coil VLV ↓ -> hot water flow rate ↓		
	Cooling Coil	Inadequate Capacity	restrict CHW Flow	**6**	1	July 2nd	Hotter (June 19th)	1	Sep 14th	Hotter (Sep 11th)				cooling coil VLV ↑/ cold water GPM ↑(summer) & cold water flow rate does not change (fall) / total cold water flow rate ↓	-	
		Fouling - Airside	gradual to 50% flow	**7**	1	July 3rd	Hotter (June 19th)							cold deck SF speed ↑-> cold deck SF power ↑/ cooling coil VLV ↑ -> cold water flow rate ↑ / cold deck static pressure ↑	cold deck damper ↓ but cold deck CFM no change	
Sensor	Cold Deck SA Temp	Drift	+ 5 degF	**8**	1	June 5th & 29th	Hotter (June 14th) (June 19th)	1	Sep 17th	Hotter (Sep 11th)	1	Nov 9th	Hotter (No hotter test day) the best choice is Nov 22nd	cold deck SF speed ↓ -> cold deck SF power ↓/cooling coil VLV ↑-> cold water flow rate ↑/ cold deck SA flow arte ↓-> return air flow rate ↓ / cooling coil outlet air temp ↓	mixing box cold deck entering air temp ↓/ cold deck damper ↓ -> cold deck CFM ↓	
	Hot Deck SA Temp	Drift	- 5 degF	**9**	1	June 20th	cooler (May 30th)	1	Sep 18th	Cooler (Sep 23rd)	1	Nov 11th	Cooler (Nov 25th)	heating coil VLV ↑-> hot water flow rate ↑/ cooling coil VLV ↑-> cold water flow rate ↑/ cold deck SA flow rate ↑-> return air flow rate↑/ heating coil outlet air temp↑	mixing box hot deck entering air temp ↑/ cold deck damp ↑-> cold deck flow rate↑	

	Common RA Temp	Drift	+5 degF	**10**	1	June 7th & 21st	Hotter (June 19th)	1	Sep 19th	Hotter (Sep 11th)	1	Nov 10th	Hotter (No hotter test day) the best choice is Nov 22nd			There is no reason for this faulty test
	Cold Duct SA Pressure	Inadequate Pressure	1.6" -> 0.6"	**11**	1	June 11th	Hotter (June 9th)	1	Sep 15th	Hotter (Sep 11th)				cold deck SF speed ↓ -> cold deck SF power ↓ / cooling coil VLV ↓-> cold water flow rate ↓/ cold deck static pressure ↓	cold deck damper ↑ but cold air flow rate no change	
	Hot Duct SA Pressure	Inadequate Pressure	1.6" -> 0.6"	**12**	1	June 12th	Cooler (June 2nd)	1	Sep 16th	Cooler (Oct 8th)	1	Nov 4th	Cooler (Nov 25th)	hot deck SF speed ↓ -> hot deck SF power ↓/ heating coil VLV ↑-> hot water flow rate ↑/ hot deck static pressure ↓	hot deck damper ↑ but hot air flow rate no change	
Actuator	Cooling Damper	Stuck	100%	**13**	1	July 8th	Cooler (No cooler test day) the best choice is May 30th				1	Nov 13th	Cooler (Nov 27th)	hot & cold deck SF speed ↑-> hot & cold deck SF power ↑/heating & cooling coil VLV ↑-> hot & cold water flow rate ↑/ hot & cold deck SA CFM ↑-> return air flow rate ↑/ hot & cold deck static pressure ↓/ Mixing & return air temp ↓	room air temp ↓/ mixing box discharge air temp ↓/ hot deck damper ↑ -> hot deck flow rate ↑/ cold deck damp =0 but cold deck flow rate ↑	
			100%	**14**	1	July 6th	Hotter (No hotter test day) the best choice is June 19th				1	Nov 14th	Hotter (Nov 1st)	hot & cold deck SF speed ↓-> hot & cold deck SF power ↓/ heating & cooling coil VLV ↓-> hot & cold water flow rate ↓/ cold deck SA CFM ↓-> return air flow rate ↓/ Mixing & return air temp ↑	room air temp ↑/ cold deck damper =100 but no cold air flow rate/ mixing box discharge air temp ↑	

			50%	**15**	1	July 7th	Hotter (No hotter test day) the best choice is June 19th				1	Nov 15th	Cooler (Nov 3rd)	Hot deck Sa flow rate ↑&↓/ cold deck SA CFM ↑ -> return air flow rate ↑/ hot & cold deck SF speed ↑-> hot &cold deck SF power ↑/ mixing and return air temp ↓	room temp ↓/ mixing box discharge air temp ↓/ hot deck damper ↑ & ↓-> hot deck air flow rate ↑ & ↓/ cold deck damper=50% ↑ and cold deck flow rate =cons ↑	dependi ng on the season and the room heating require ment is different
	Heating Damper	Stuck	100%	**16**	1	July 9th	Cooler (June 2nd)				1	Nov 16th	Hotter (Nov 1st)	hot & cold deck SF speed ↑-> hot & cold deck SF power↑/ heating & cooling coil VLV ↑- hot & cold water flow rate ↑/ hot &cold deck SA flow rate ↑-> retrun air flow rate ↑/ return air temp↑	room air temp ↑/ mixing bix discharch air temp↑/ cold deck damper ↑-> cold deck flow rate room air temp ↑/ hot deck damper=0% ↓ but hot deck flow rate ↑	
			100%	**17**	1	July 10th	cooler (June 2nd)				1	Nov 17th	Cooler (Nov 25th)	hot & cold deck SF speed ↓-> hot & cold deck SF power↓/ heating & cooling coil VLV ↓-> hot & cold water flow rate ↓/ hot &cold deck SA flow rate ↓-> retrun air flow rate ↓/ return air temp ↓	room air temp ↓/ mixing box discharge air temp ↓/ hot deck damper= 100% but no hot deck flow rate/ cold deck damper ↓ -> cold deck flow rate ↓	
			50%	**18**	1	July 11th	Hotter (June 19th)				1	Nov 18th	Hotter (No hotter test day)	heating coil VLV ↑-> hot watre flow rate ↑	cold deck damper ↑ -> cold deck CFM ↑	since all rooms are in cooling mode with the minimu m require ment of hot air=100 CFM which is equivale nt to 50% open hot deck damper, no

															obvious symptom is observed
	AHU OA Damper	Stuck	100%	**19**	1	July 4th	Hotter (June 19th)	1	Sep 20th	Hotter (Sep 11th)				hot & cold deck SF speed ↓-> hot & cold deck SF power ↓/ cooling coil VLV ↑-> cold watre flow rate ↑/ outdoor air flow rate ↑	-	because the outdoor air flow rate even in 100% opening of outdoor air damper is small, no obvious symptom is observable
			20%	**20**				1	Sep 21st	similar a little cooler (Oct 2nd)	1	Nov 8th	Hotter (No hotter test day) the best choice is Nov 1st	OA CFM ↓/ heating coil VLV ↓ -> hot water flow rate ↓/ mixing air temp ↓	-	no obvious symptoms were observed specially for fall

			50%	**21**				1	Sep 22nd	similar a little warmer (Sep 23rd)			OA CFM ↓/ heating coil VLV ↓ -> hot water flow rate ↓/ cooling coil VLV ↑ -> cold water flow rate ↑/ mixing air temp ↑	-	The symptoms are especially observable when the economizer cooling is active. When outdoor air damper is at the minimum requirement (45% open) no obvious symptoms can be detected.
Control	Heating Sequence	Unstable Control	two stages	**22**				2	Sep 26th	Sep 11th	2	Nov 21st	Nov 25th	fluctuation in heating coil VLV, hot water flow rate and hot deck SA temp	-	
	Cooling Sequence	Unstable Control	two stages	**23**	2	June 30th & July 1st	June 11th	2	Sep 24th	Sep 11th				fluctuation in cooling coil VLV, cold water flow rate and cold deck SA temp	-	

	OA Damper Sequence	Unstable Control	two stages	**24**			2	Oct 5& 6th				-	-	No symptom observed in experimental data because outdoor air temperature is so that AHU-B controls SA temp in mechanical and economizer mode and damper position is totally open. No fluctuation is observed in outdoor air damper control
	Heating Water	Supply Temp Too Low	Operational	**25**						1	Nov 19th	Cooler (Nov 26th)	heating coil VLV ↑-> hot water flow rate ↑/ hot deck SA temp ↓/ cold deck SA flow rate ↓-> return air flow rate ↓/ cold deck SF speed ↓-> cold deck SF power ↓	mixing box discharge air temp ↓/ cold deck damper ↓-> cold deck flow rate ↓	

	Chilled Water	Supply Temp Too High	Operational	**26**	1	June 13th	(June 9th)						hot & cold deck SF speed ↑ -> hot & cold deck SF power ↑/ cooling coil VLV ↑-> cold water flow rate ↑/ heating coil VLV ↓-> hot water flow rate ↓/ cold deck SA flow rate ↑-> return air flow rate ↑/ mixing & return air temp ↑/ hot & cold deck SA temp ↑/ cold deck static pressure ↓	room air temp ↑/ mixing box discharge air temp ↑/ cold deck damper ↑ -> cold deck flow rate ↑	

For brevity a few fault cases from each category is picked to demonstrate the symptoms associated with a certain fault and defined severity. The following figures depict the comparison of simulation results under faulty and fault-free conditions with the corresponding experimental operational data. In the presented graphs, navy blue and dark red lines are representative of experimental data and simulation results, respectively, under the faulty condition. In the same way, dashed red and dashed light blue lines are representative of experimental data and simulation results under fault-free condition. The graphs included in Figures (a) to (c) compare simulation result under faulty and fault-free conditions with the corresponding experimental data for AHU. While the graphs in Figures (d) and (e) represents comparison of simulation results and experimental operational data for zones under both conditions.

From the equipment category cold deck supply fan failure and inadequate capacity for the hot deck heating coil on water side faults are picked to show the symptoms associated with these faults. Figure 3-21 demonstrates the failure of cold deck supply fan fault simulation results of dual duct double fan system on a summer test day (June 25th). The fault is implemented at the test facility by shutting off the power to the cold deck supply fan. A hotter normal test day (June 19th) can serve as the reference day to emphasis that the observed symptoms are due to the fault not the weather condition. The symptoms associated with this fault are listed as the following:

Fault symptoms observable in AHU:

1) Increase in cold deck supply fan speed. Although this symptom is not observable from the experimental data because it just demonstrates the fan rotational speed when it is off. This contradiction is due to the false implementation of fault to the test system. While the simulation result is

reflecting the control signal passed to the cold deck supply fan assuming that it should provide the set point static pressure. Since the cold deck pressure set point cannot be maintained due to the occurrence of this fault, the control superblock commands for more speed.

2) Decrease in cold deck supply fan power. Due to the cold deck supply fan motor failure no power is drained.
3) Decrease in heating coil valve position and consequently hot water flow rate. This symptom is due to the heating coil load drop which is caused by elevation in return air temperature.
4) Decrease in cooling coil valve position. Cooling coil valve is totally closed because there is no air flow in the cold deck and so no call for cooling.
5) Decrease in static pressure of cold deck. Static pressure of cold deck decreases to zero because there is no flow rate in this deck.
6) Decrease in cold deck supply air flow rate and consequently return air flow rate. No flow rate in the cold deck due to this fault and return air flow rate reduction.
7) Increase in mixing air, return air and cold deck supply air temperatures. No cold air is provided by the cold deck which results in the elevation of those temperatures.

Fault symptoms observable in zones:

1) Increase in discharge air temperature from dual duct terminal unit.
2) Increase in room air temperature.
3) Increase in cold deck damper position. Room air temperature elevation triggers the dual duct terminal unit controller to provide more cold air by opening the cold deck damper to 100% open.

4) Decrease in cold deck air flow rate. No cold air flow rate is provided to the room while cold deck damper is totally open.

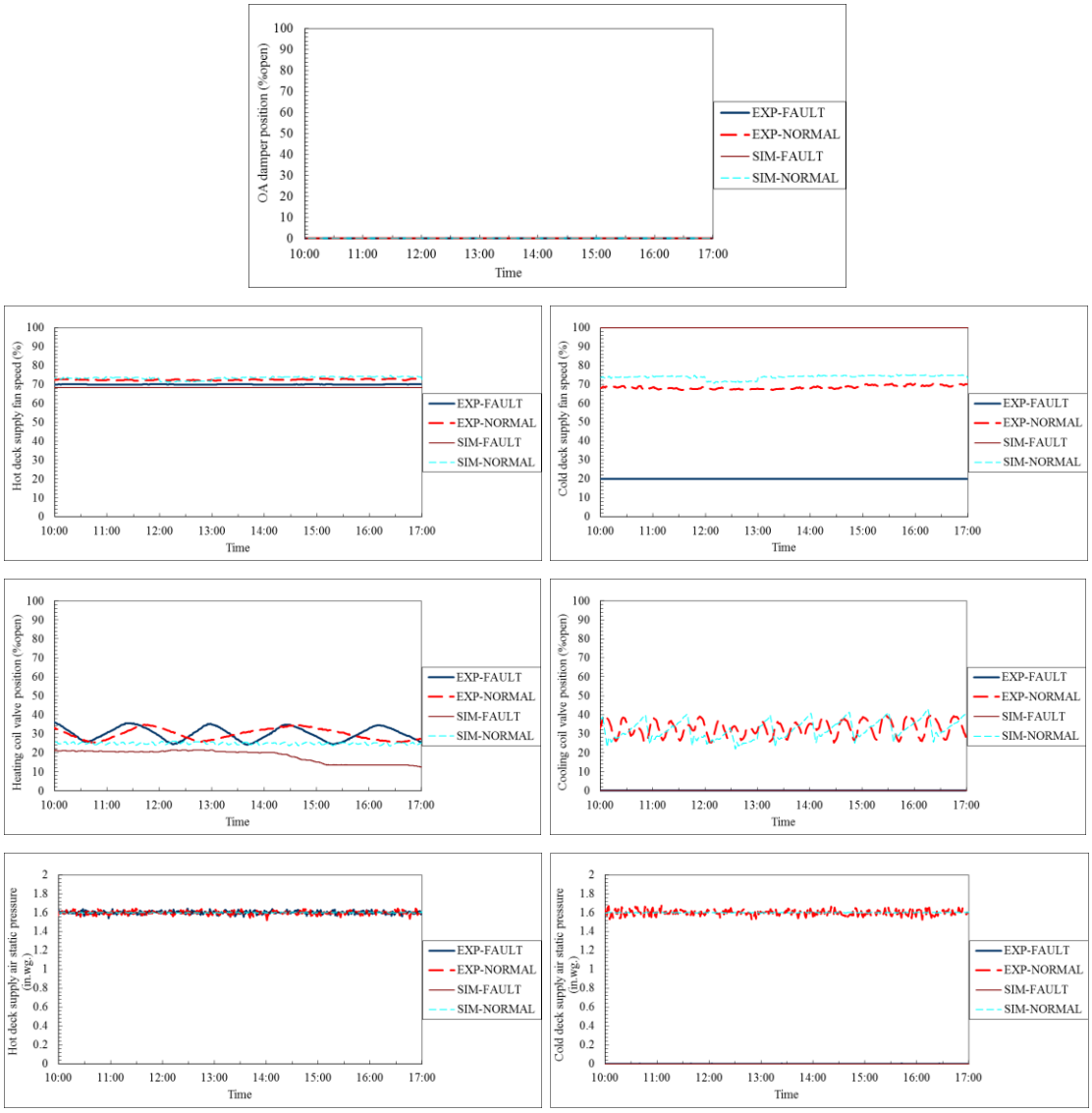

(a) Dual duct system AHU control signals

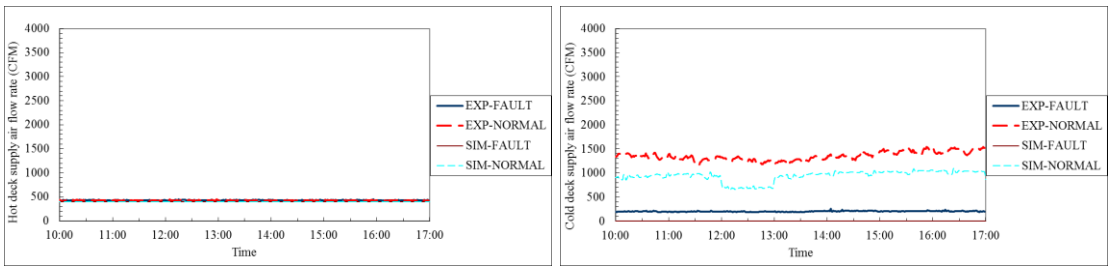

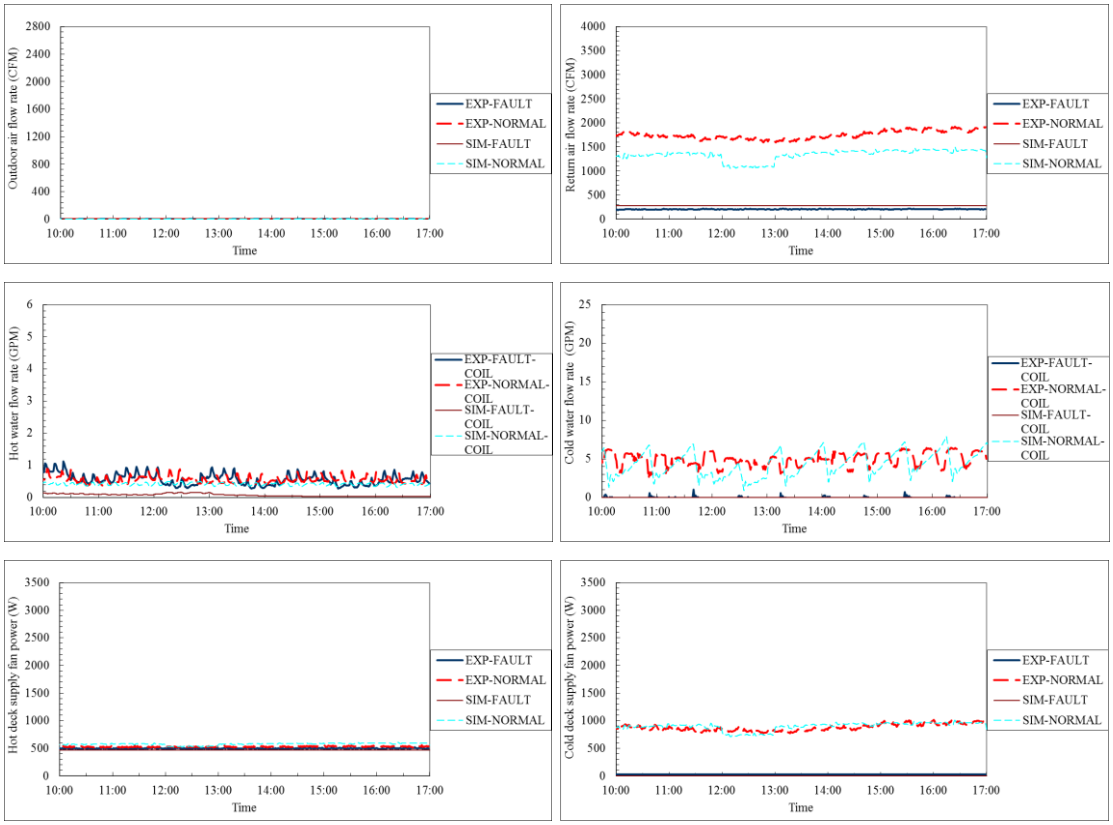

(b) Air & water flow rates and supply fan power consumptions in dual duct system AHU

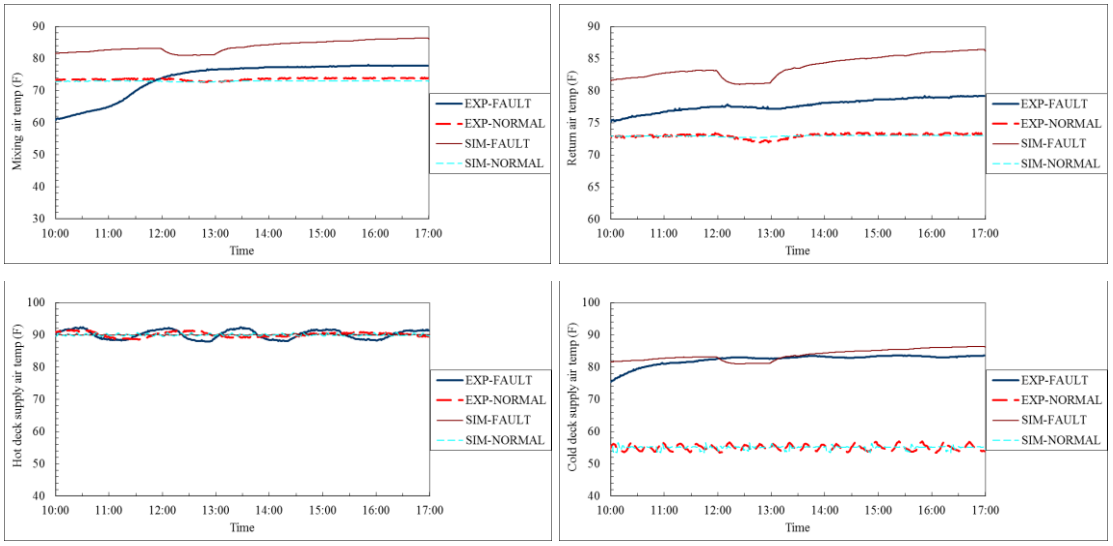

(c) Temperatures of dual duct system AHU

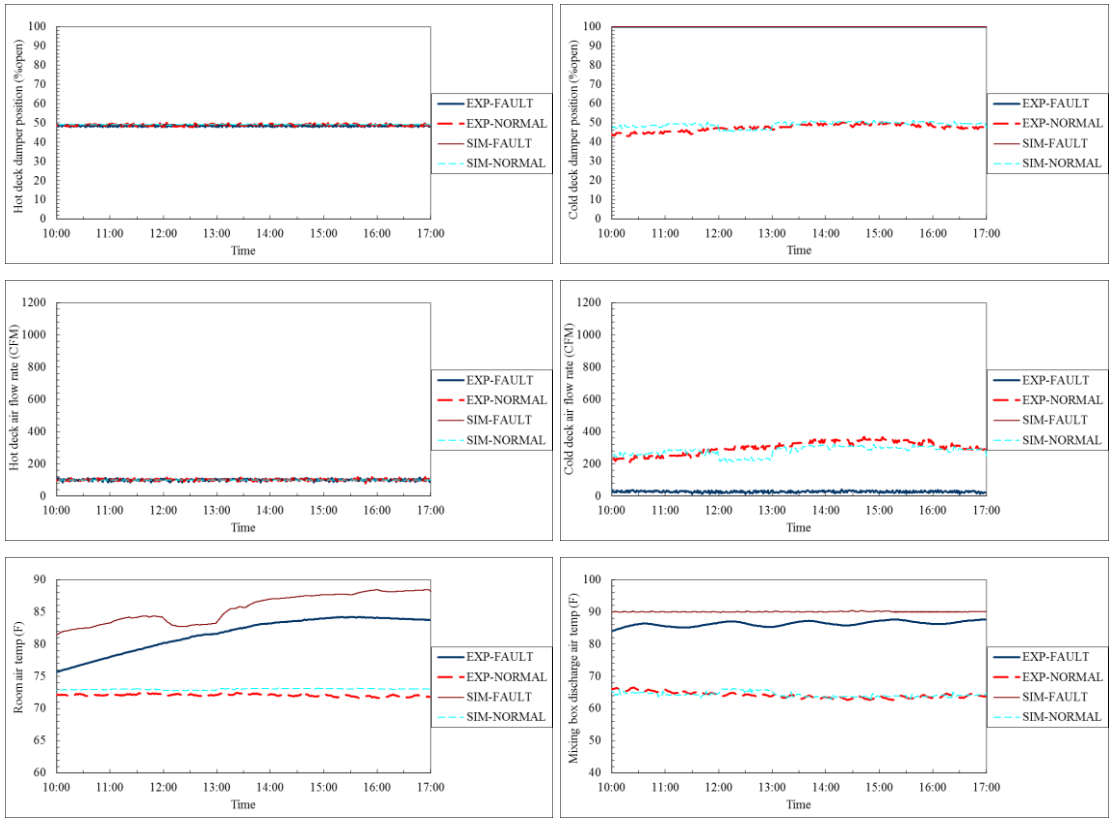

(d) South-B room results

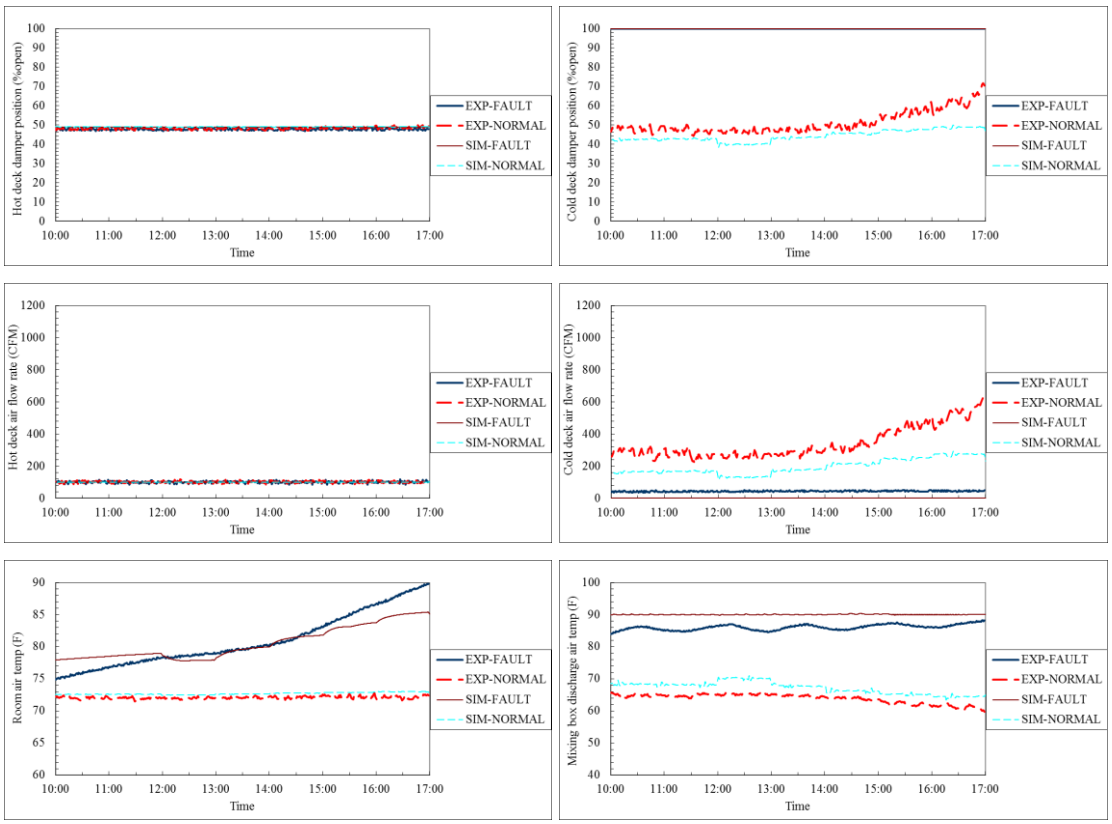

(e) West-A room results

Figure 3-21. Validation of cold deck supply fan failure fault in dual duct double fan system (June 25th)

Figure 3-22 demonstrates the fault model simulation results of dual duct double fan system with heating coil water-side inadequate capacity fault on a winter test day (Nov 6th). This fault is caused by the water-side fouling due to deposition of mineral material of circulating water on the surfaces of heat exchanger in contact with water. In the experiment, this faulty test is employed by throttling the isolation ball valve on the outlet of heating coil to restrict water flow rate from 5 GPM to 1.5 GPM. A cooler normal test day like Nov 25th can be picked to serve as the reference day. The symptoms associated with this fault are listed as the following:

Fault symptoms observable in AHU:

1) Increase in heating coil valve position but no increase in hot water flow rate through the coil. In order to maintain the hot deck supply air temperature set point, the controller calls for more heating which leads to elevation of heating coil valve position. But due to the fouling on water-side and increase in pressure resistance of the coil even more valve opening doesn't result in more hot water flow rate through the coil.
2) Decrease in the total water flow rate of heating loop. Due to the pressure resistance increase in the hot water loop, a reduction from 5 GPM to 1.5 GPM is observed in the total hot water flowrate.

No symptoms are observed in the zones due to this fault.

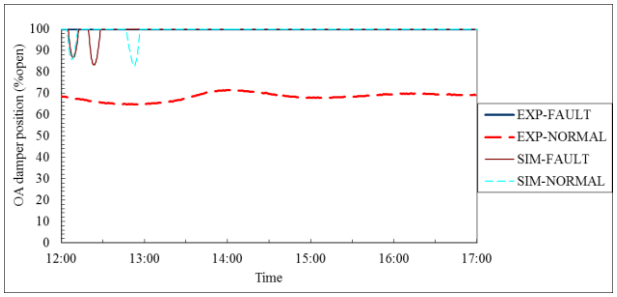

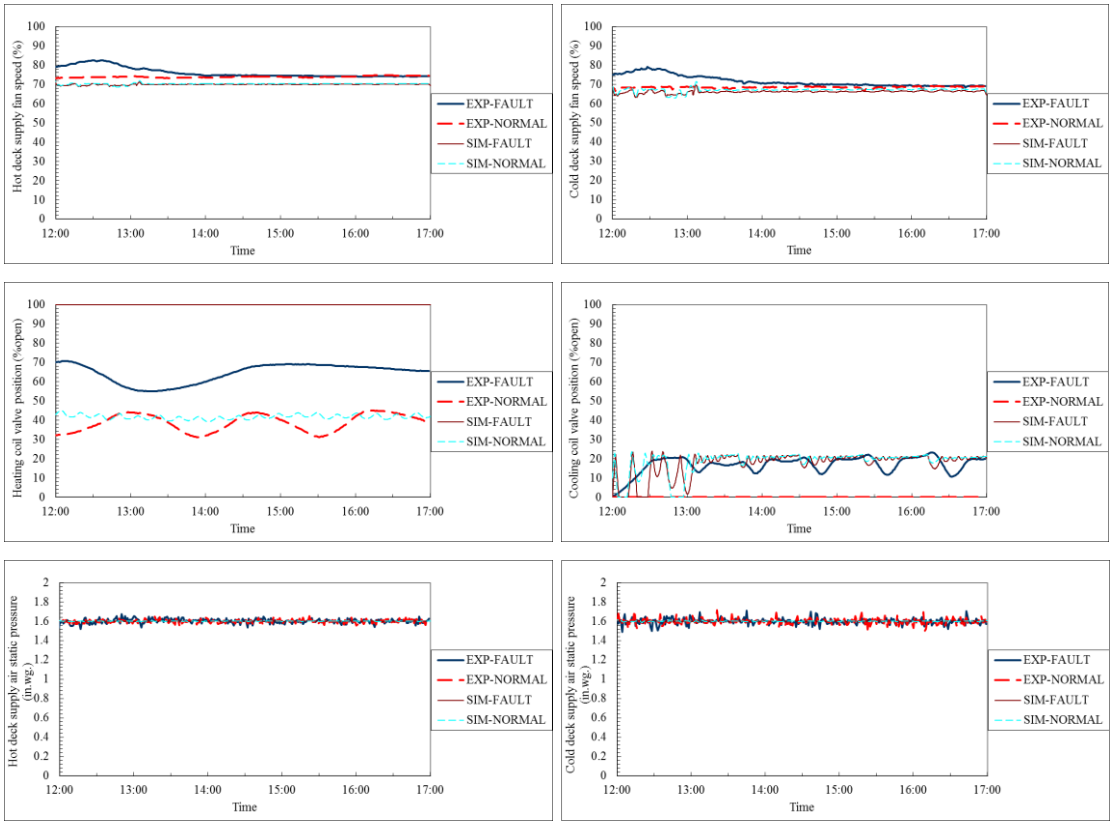

(a) Dual duct system AHU control signals

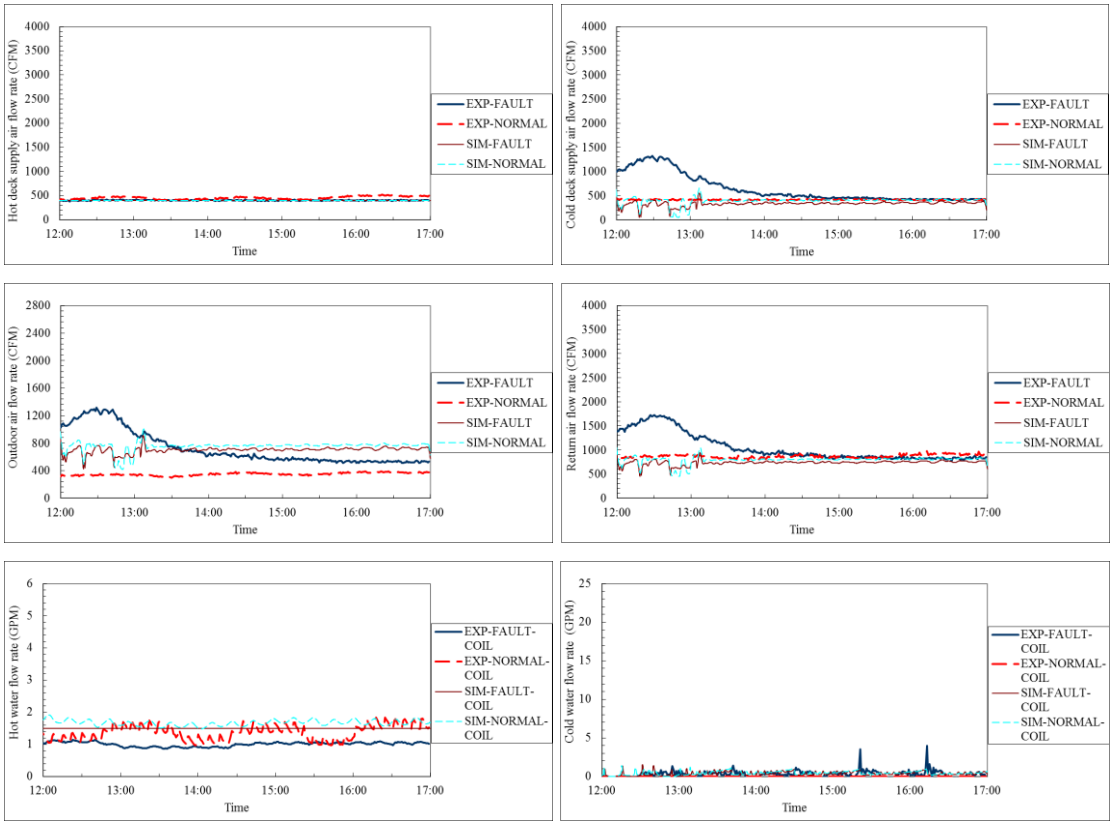

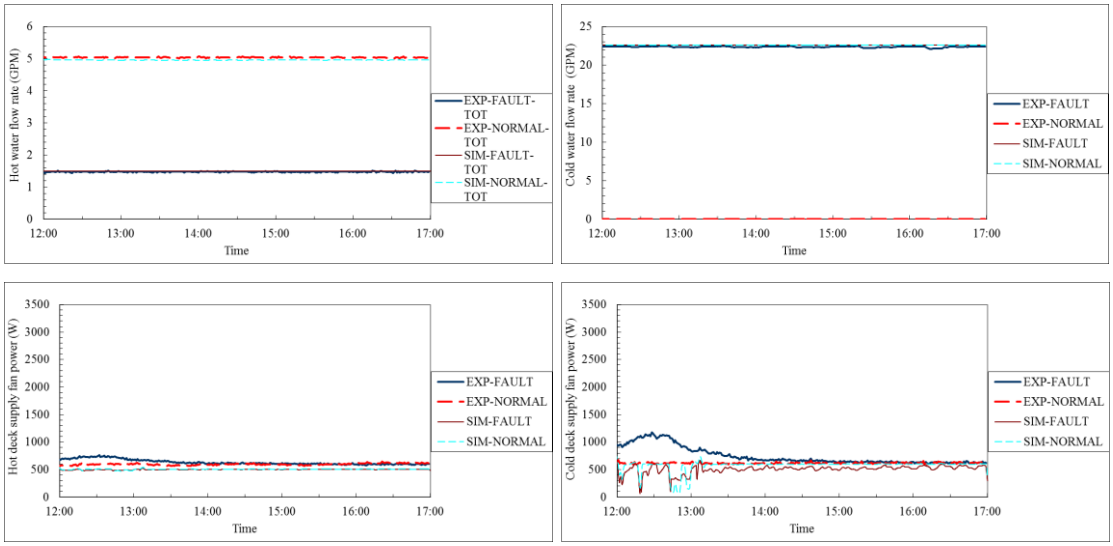

(b) Air & water flow rates and supply fan power consumptions in dual duct system AHU

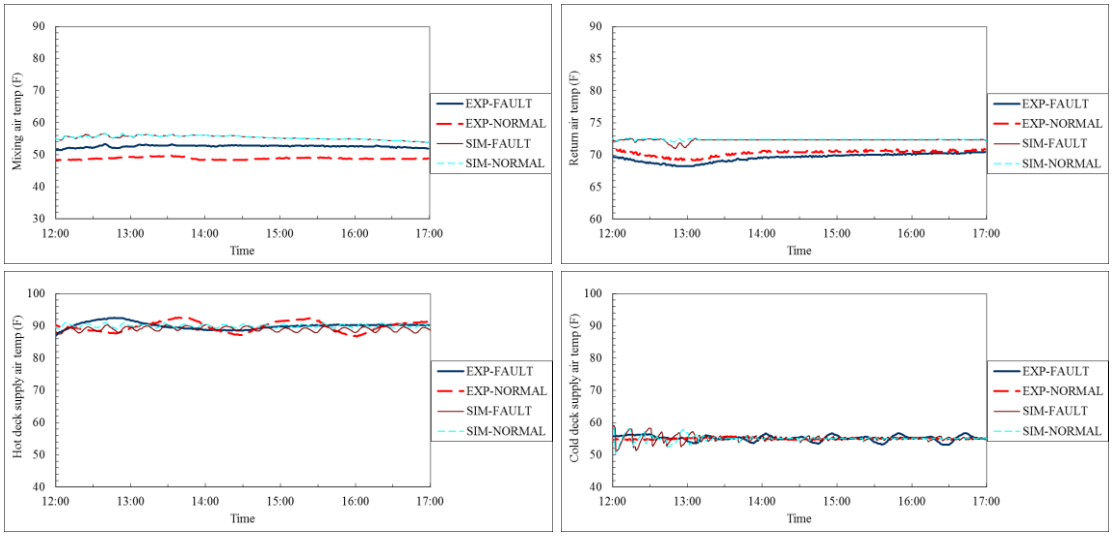

(c) Temperatures of dual duct system AHU

Figure 3-22. Validation of cooling coil inadequate capacity on water side fault in dual duct double fan system (Nov 6th)

From sensor category the cold deck supply air temperature sensor bias and hot deck supply air static pressure sensor bias faults are picked as illustration. Figure 3-23 depicts the fault model simulation results of dual duct double fan system with a +5˚F bias in cold deck supply air temperature sensor reading on a fall test day (Sep 17th). A

hotter normal test day (Sep 11th) is selected to serve as the reference day. The symptoms associated with this fault are as the following:

Fault symptoms observable in AHU:

1) Increase in cooling coil valve position and consequently chilled water flow rate. This fault causes artificial increase in cooling load of cold deck cooling coil which is in charge of maintaining the cold deck supply air temperature set point.
2) Decrease in cold deck supply air flow rate. Due to this fault, the real cold deck supply air temperature is colder than the defined set point. Therefore, to keep the room air temperature set point the controller calls for less cold air which affects the total cold deck supply air flow rate.
3) Decrease in return air flow rate. This symptom is cause by reduction in cold deck supply air flow rate.
4) Decrease in cold deck supply fan power consumption. This symptom is the result of cold deck supply air flow rate drop.

Fault symptoms observable in zones:

1) Decrease in cold deck damper position in dual duct terminal units.
2) Decrease in cold deck air flow rates to the rooms.

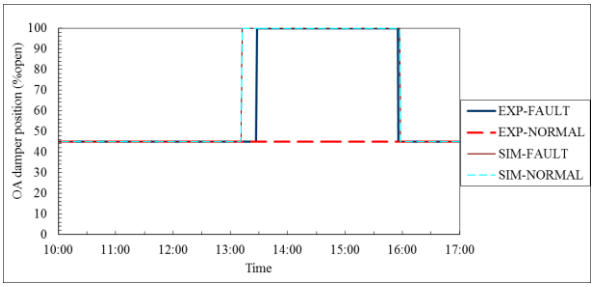

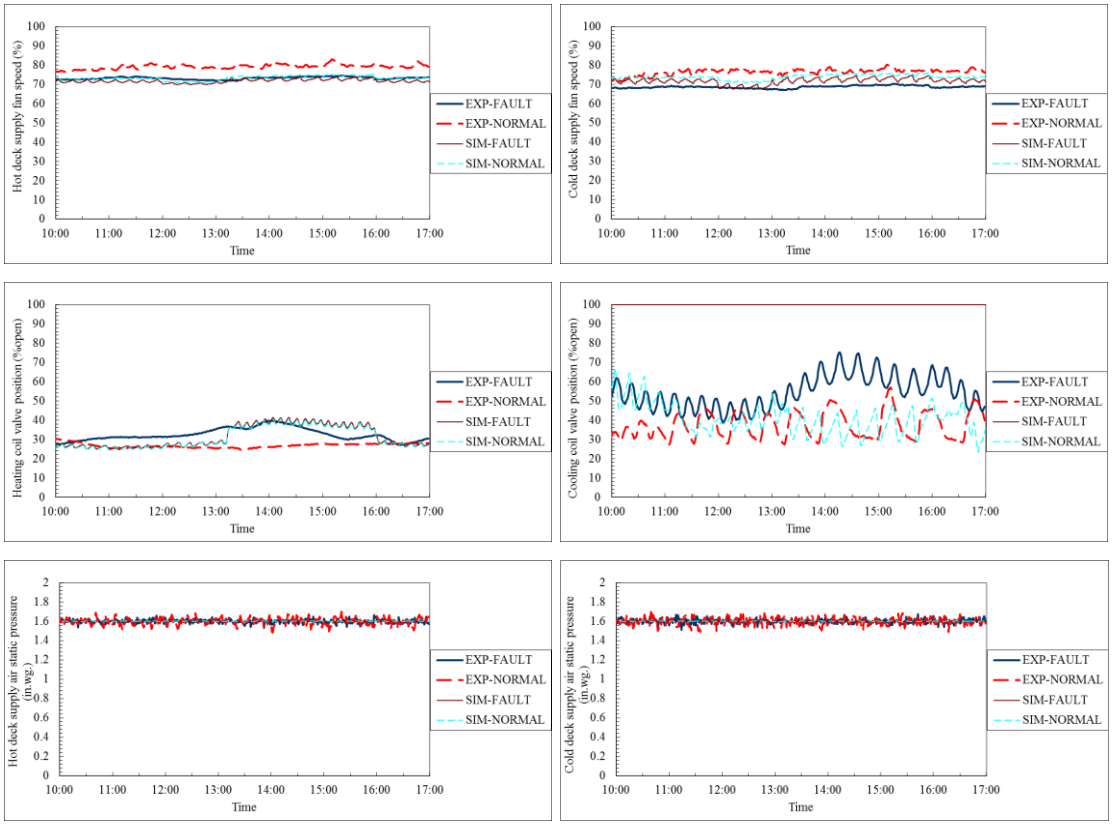

(a) Dual duct system AHU control signals

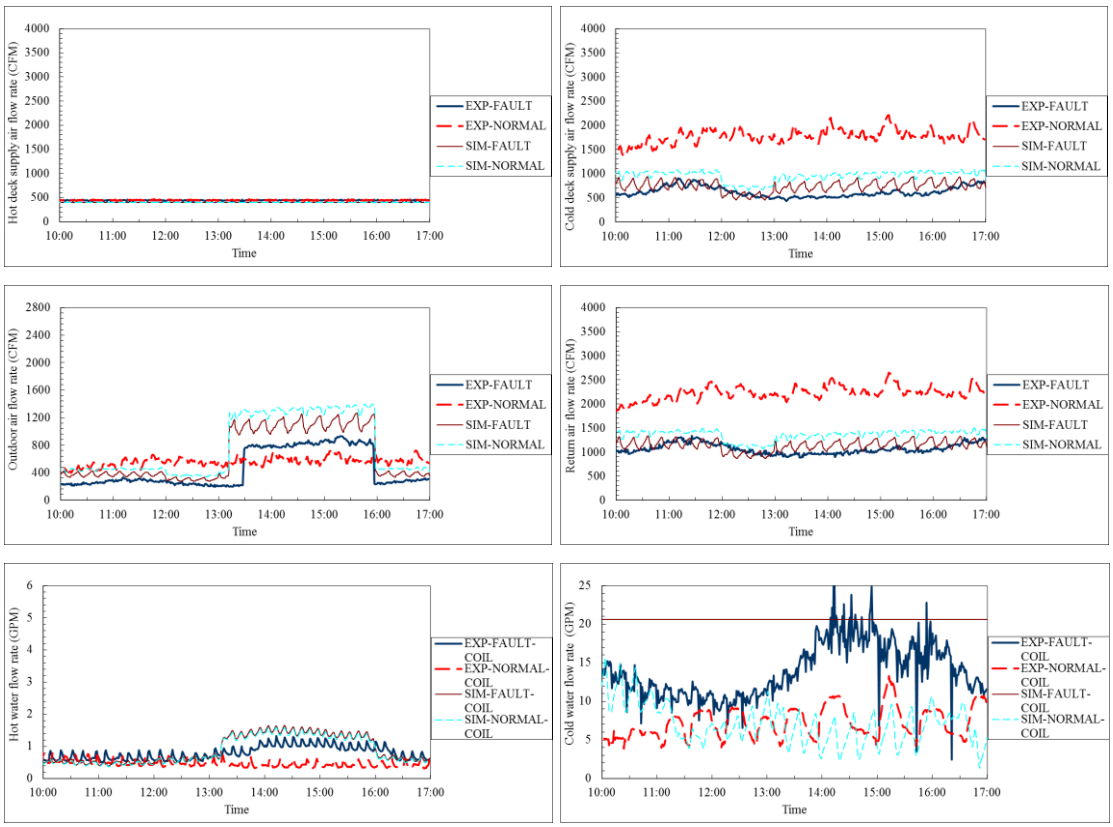

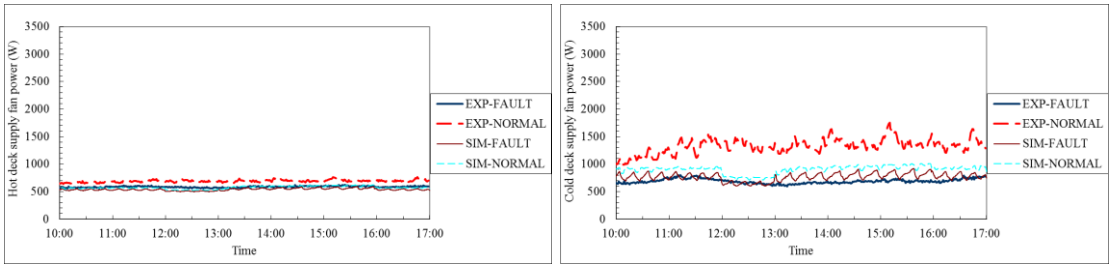

(b) Air & water flow rates and supply fan power consumptions in dual duct system AHU

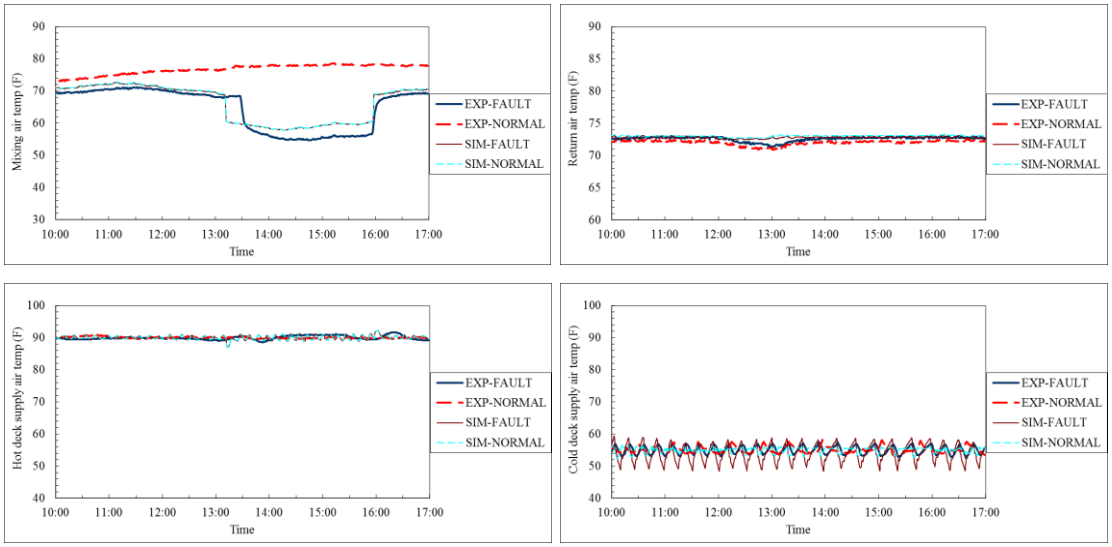

(c) Temperatures of dual duct system AHU

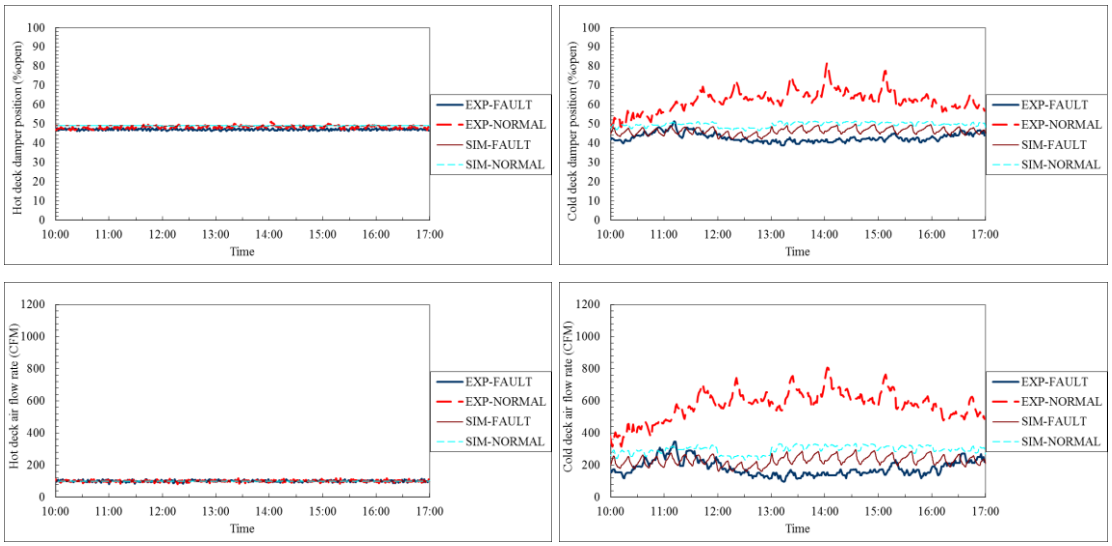

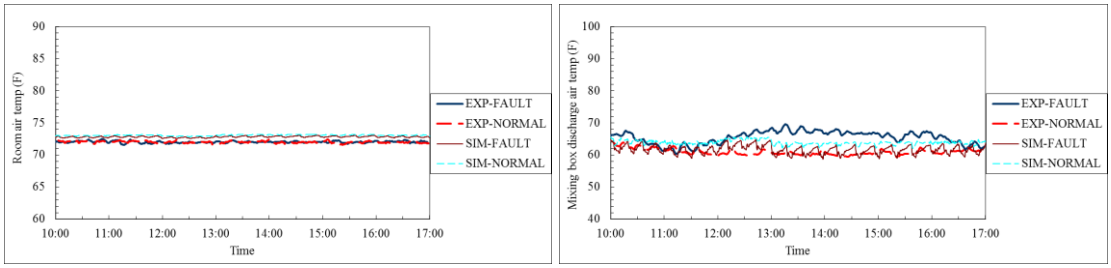

(d) South-A room results

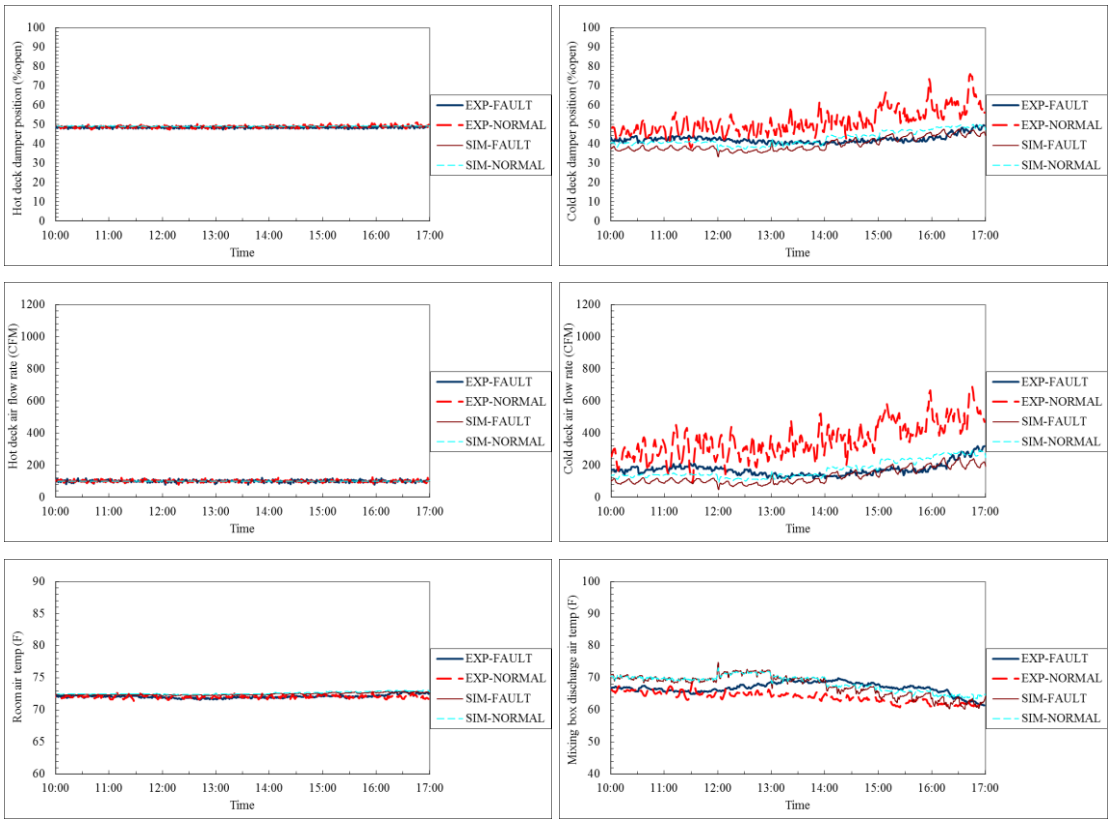

(e) West-A room results

Figure 3-23. Validation of cold deck supply air temperature sensor bias fault (+5 °F) in dual duct double fan system (Sep 17th)

Figure 3-24 depicts hot deck supply air inadequate static pressure on a summer test day (June 12th). At the test facility and simulation model, this fault is implemented by changing the hot deck supply air pressure set point from 1.6 to 0.6 in W.G. A cooler normal test day (June 2nd) is selected to serve as the reference day. The symptoms associated with this fault are as the following:

Fault symptoms observable in AHU:

1) Decrease in the hot deck supply fan speed. Due to the reduction in the hot deck static pressure the operating point of the system (the intersection of fan performance curve and system curve) descend from a higher speed to a lower one.
2) Decrease in the hot deck supply air static pressure. The controller adjusts hot deck fan speed to maintain the new hot deck static pressure (0.6 in W.G.).
3) Decrease in the hot deck supply fan power. Reduction in hot deck supply fan speed is the reason of this symptom.

Fault symptoms observable in AHU:

1) Increase in the hot deck damper position at dual duct terminal units. The operating point of the system has a descending trend due to the fault which means a milder slop for the system curve. In order to provide a certain amount of hot air to the rooms, a higher damper position is needed under this faulty condition.

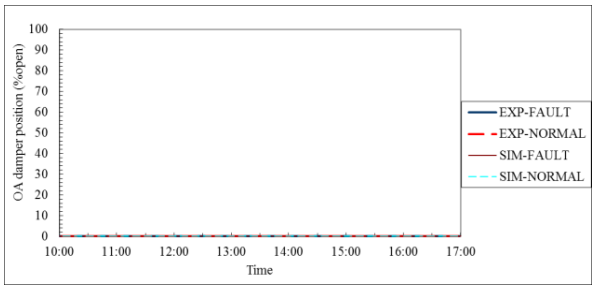

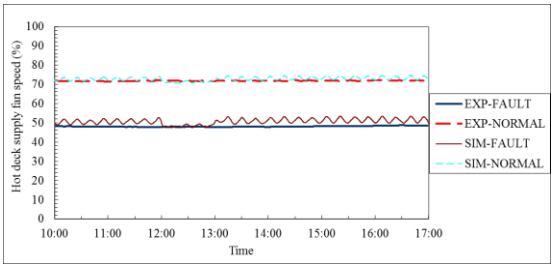

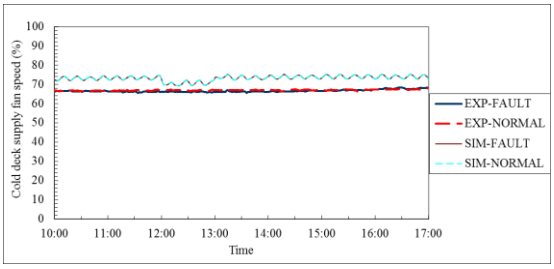

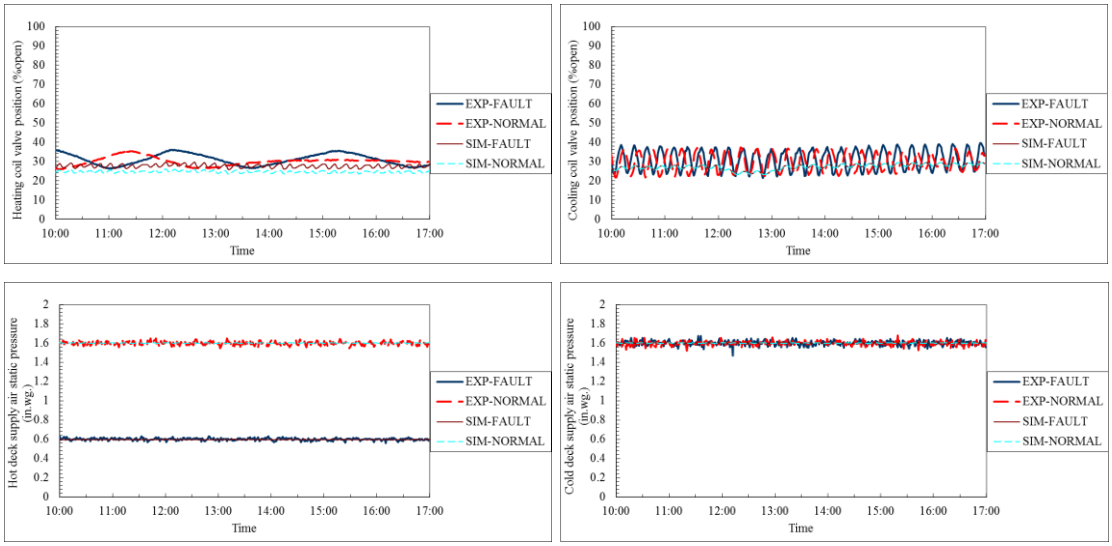

(a) Dual duct system AHU control signals

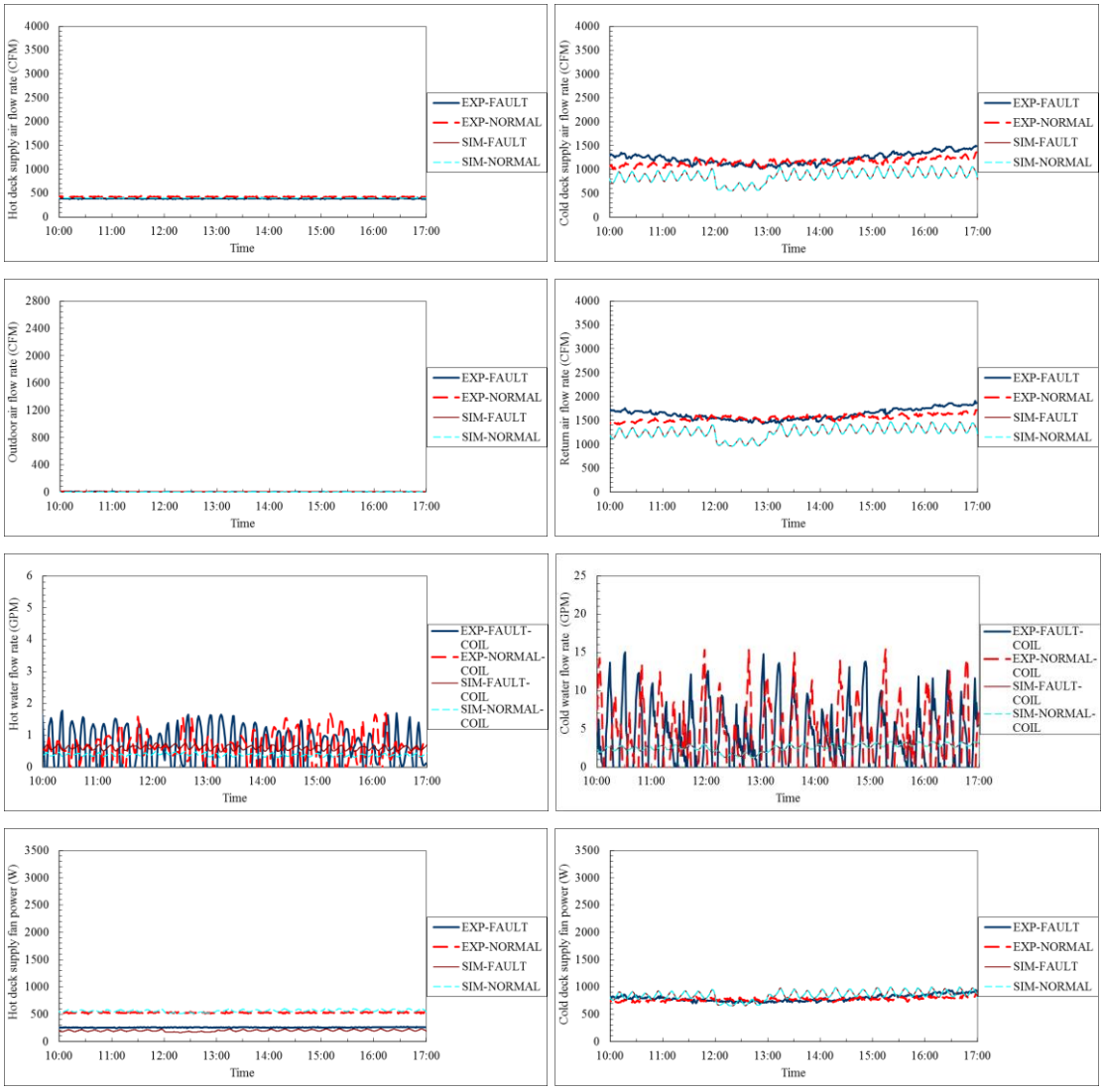

(b) Air & water flow rates and supply fan power consumptions in dual duct system AHU

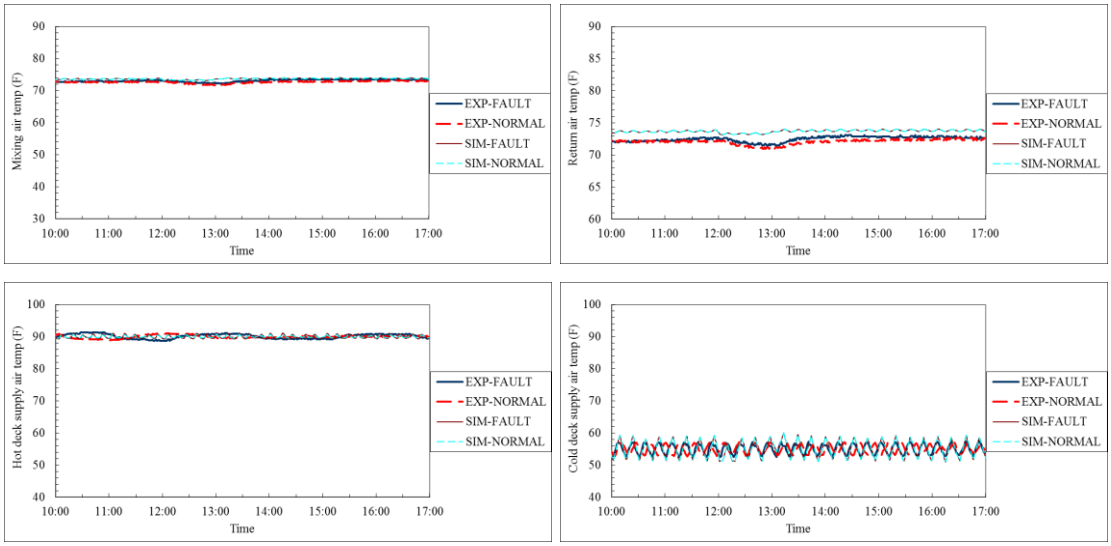

(c) Temperatures of dual duct system AHU

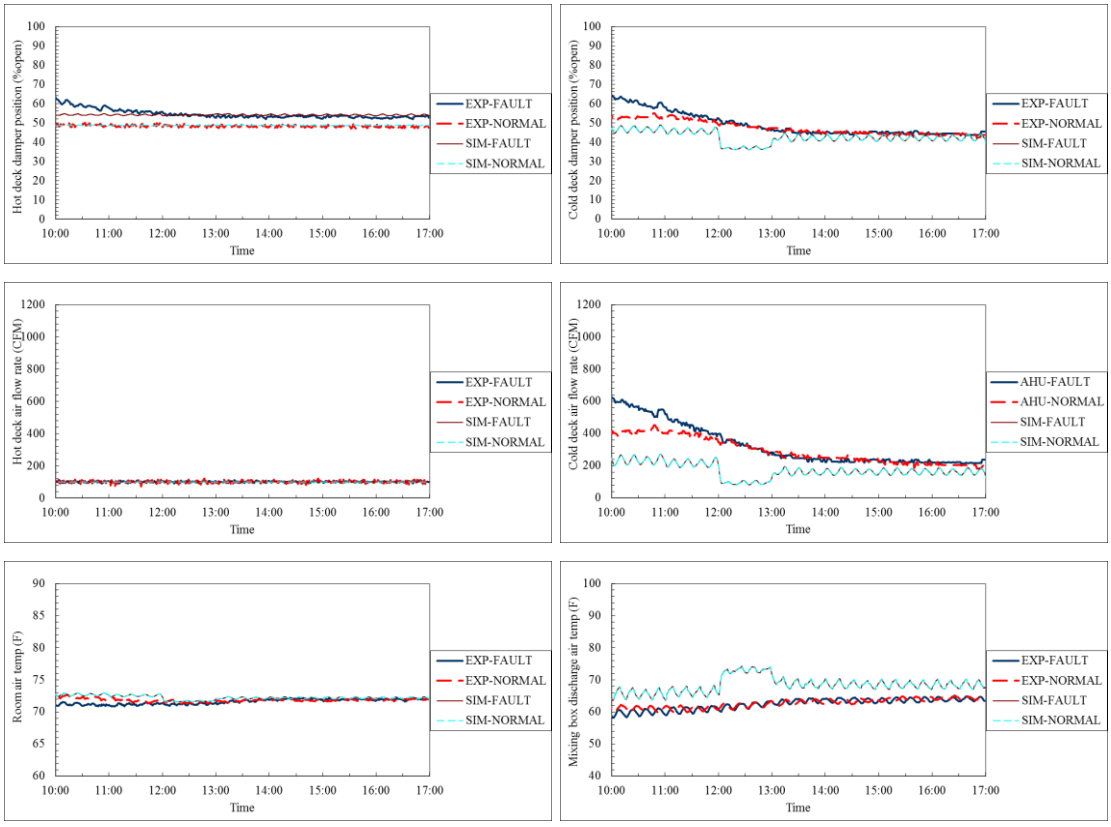

(d) East-B room results

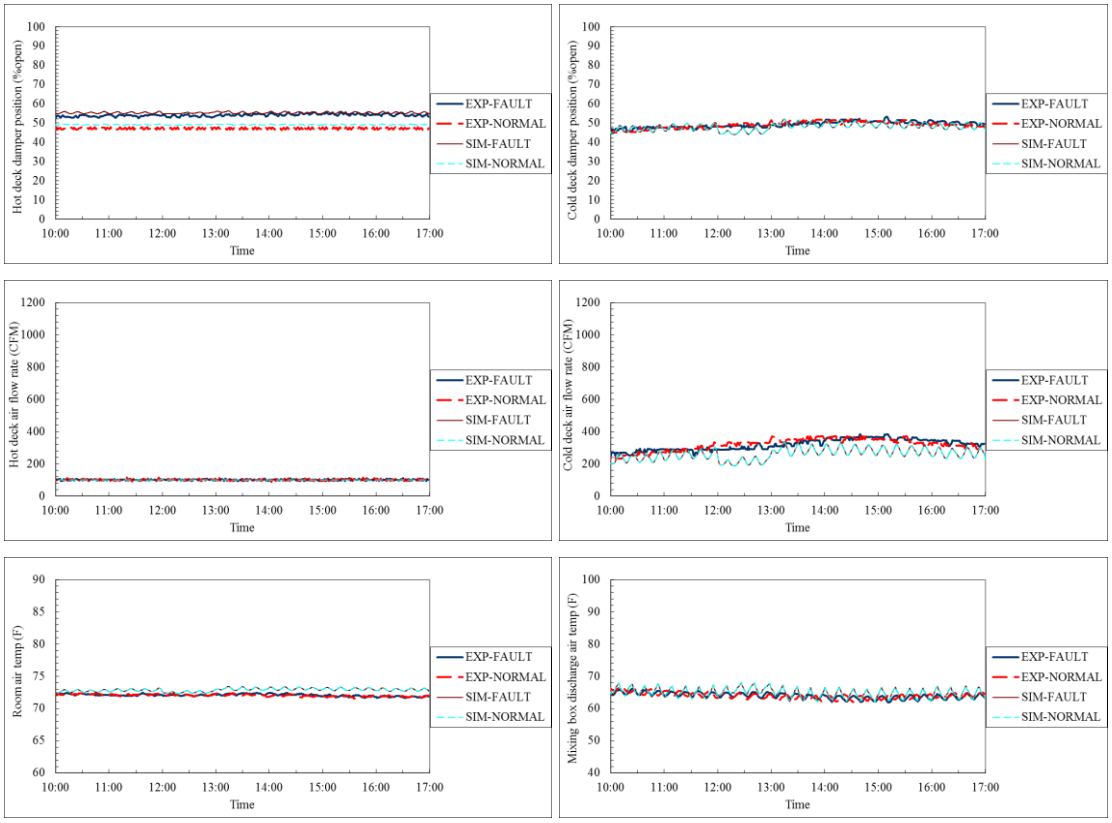

(e) East-B room results

Figure 3-24. Validation of hot deck supply air static pressure sensor bias fault (0.6 in W.G.) in dual duct double fan system (June 12th)

From actuator category the cold deck damper stuck at fully open position and the hot deck damper stuck at fully closed positions are selected to show the validation of the developed model under faulty condition. Figure 3-25 depicts the fault model simulation results of dual duct double fan system with cold deck damper in the dual duct terminal unit stuck at fully open position on a summer test day (July 8th). The closest normal test day (May 30th) is selected to serve as the reference day. The symptoms associated with this fault are as the following:

Fault symptoms observable in AHU:

1) Increase in the cold and hot deck supply air flow rates. Increase in the cold deck supply air flow rate is the consequence of this fault which

results in the elevation of hot air flow requirement of the rooms to keep temperature set point.

2) Increase in the return air flow rate. Escalation of supply air flow rates in both hot and cold decks ends up to this symptom.
3) Increase in the hot and cold deck supply fan speeds. The elevated hot and cold deck air flow rates result in the elevation of corresponding supply fan speeds.
4) Increase in the hot and cold deck supply fan power consumption. Fan power consumption is a direct function of air flow rate and speed. Obviously increase in both flow rate and speed cause power consumption growth.
5) Increase in heating and cooling coil valve positions and consequently hot and cold water flow rates through the coils. The heating and cooling coil loads has increased due to the both decks supply air flow rate rise.
6) Decrease in the return air temperature and consequently mixed air temperature. Due to the excessive amount of cold air to the rooms, their dual duct terminal units operate in the heating mode to maintain the heating temperature set point (68 $^{\circ}$F).

Fault symptoms observable in zones:

1) Decrease in the cold deck damper position. Dual duct terminal unit controller reacts to the excessive amount of the cold air provided to the room. While controller command is to close down the cold deck damper but actuator does not follow it due to its malfunction.
2) Increase in the cold deck air flow rate to the room.

3) Increase in hot deck damper position and consequently hot deck air flow rate. Room calls for heating due to the excessive amount of cold air to keep room temperature set point.

4) Decrease in room air temperature. This fault causes the shift of dual duct terminal unit controller operation from cooling mode to heating mode. Room air temperature is maintained at heating temperature set point.

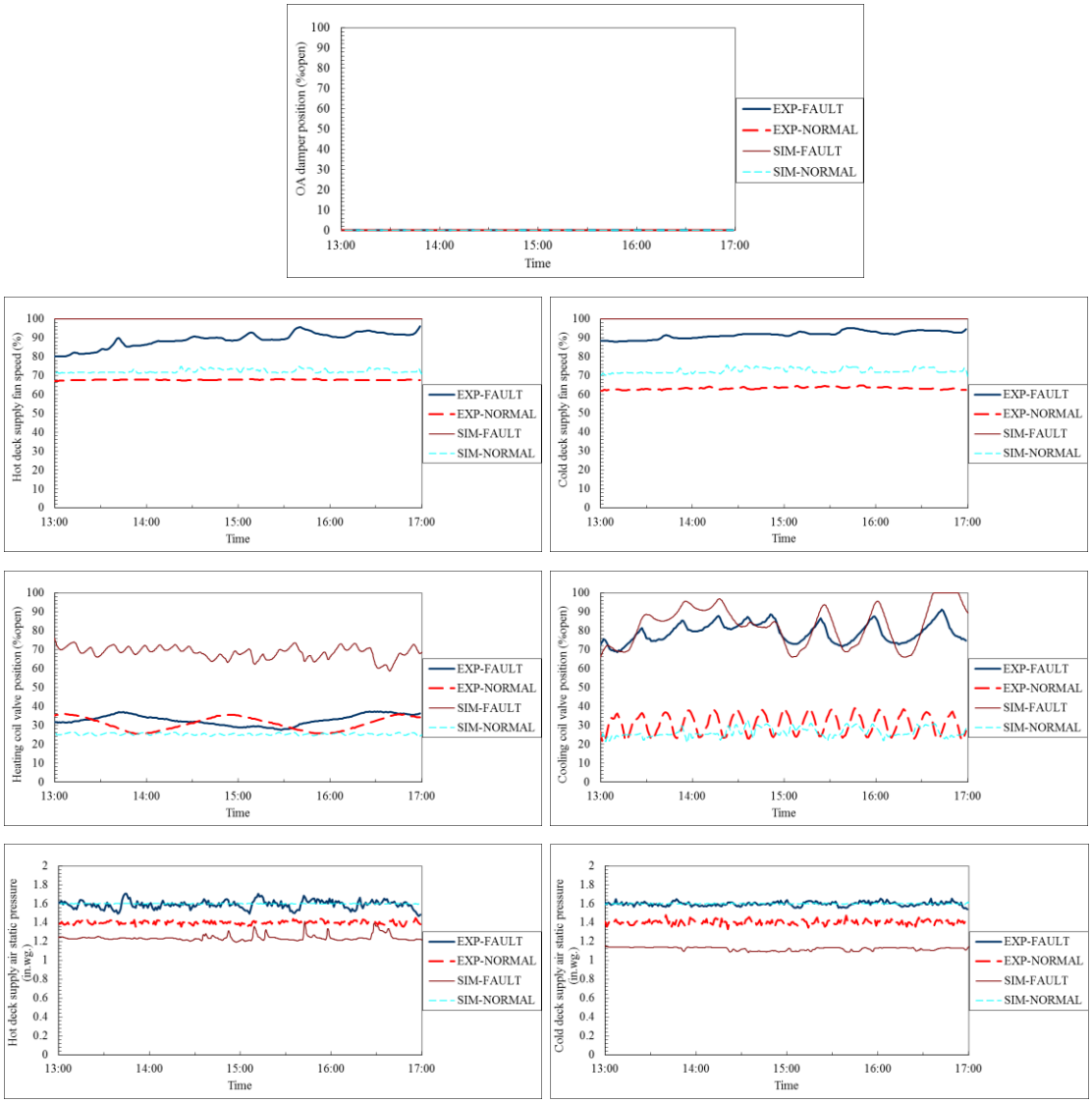

(a) Dual duct system AHU control signals

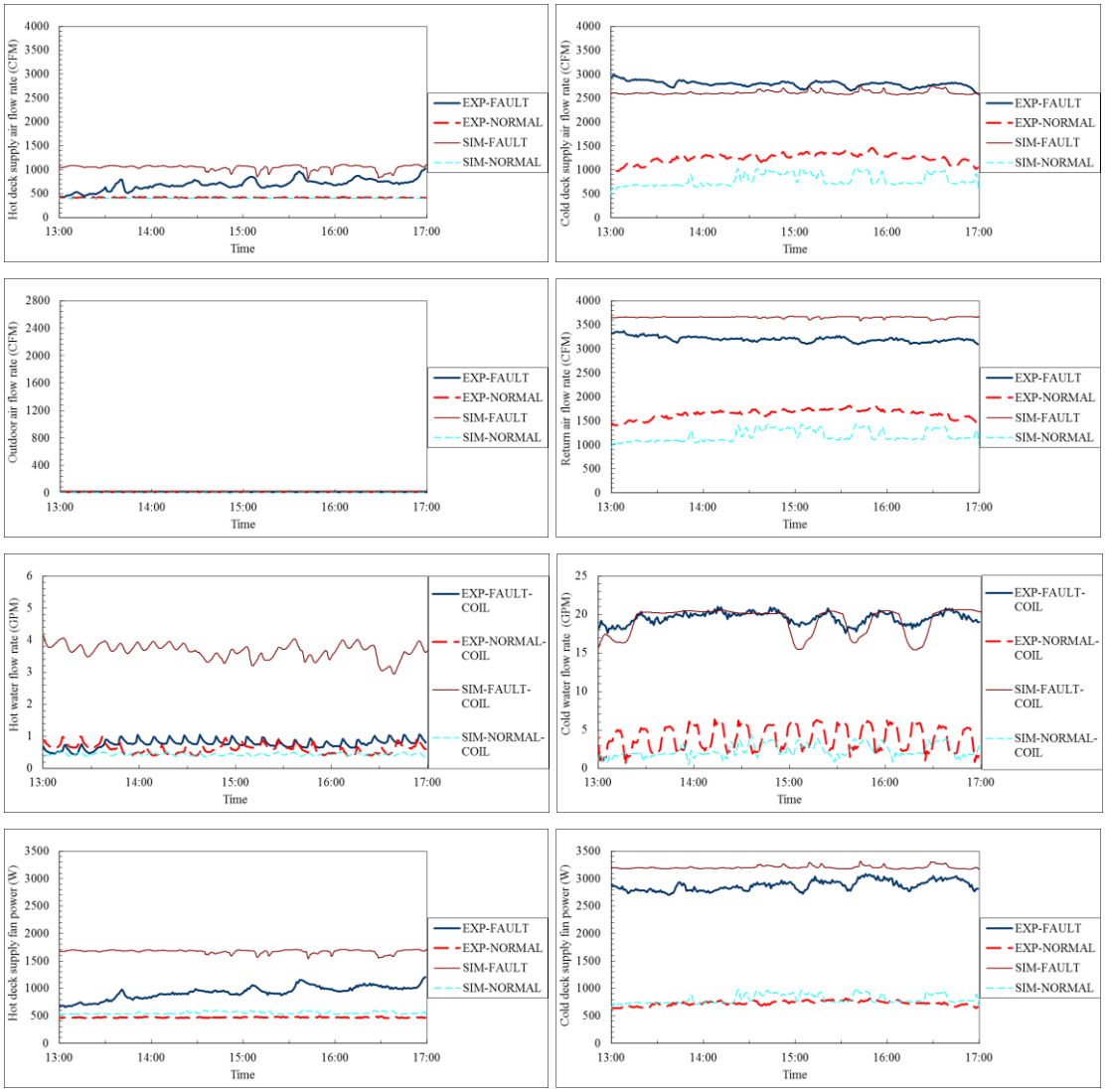

(b) Air & water flow rates and supply fan power consumptions in dual duct system AHU

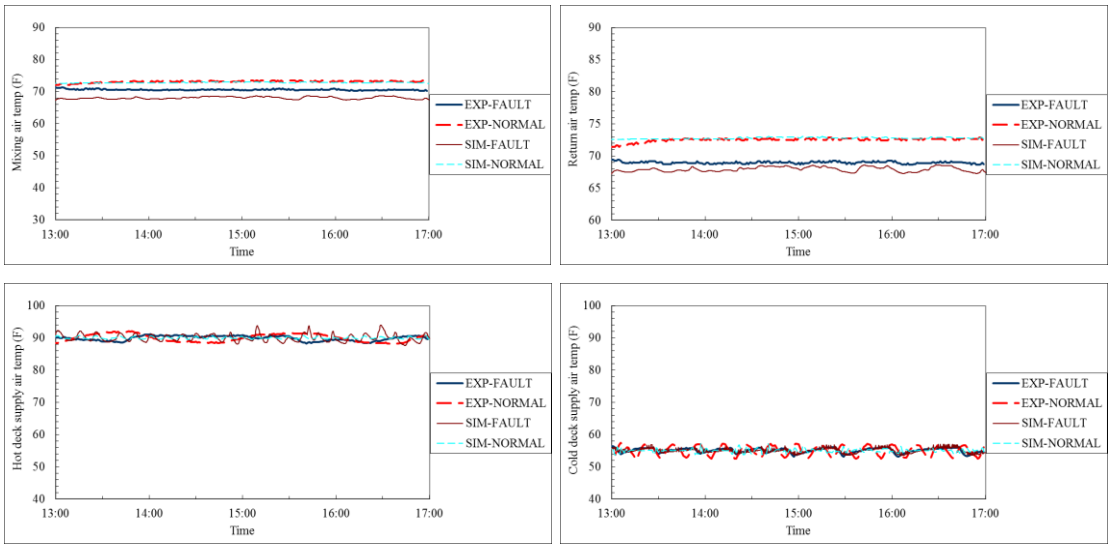

(c) Temperatures of dual duct system AHU

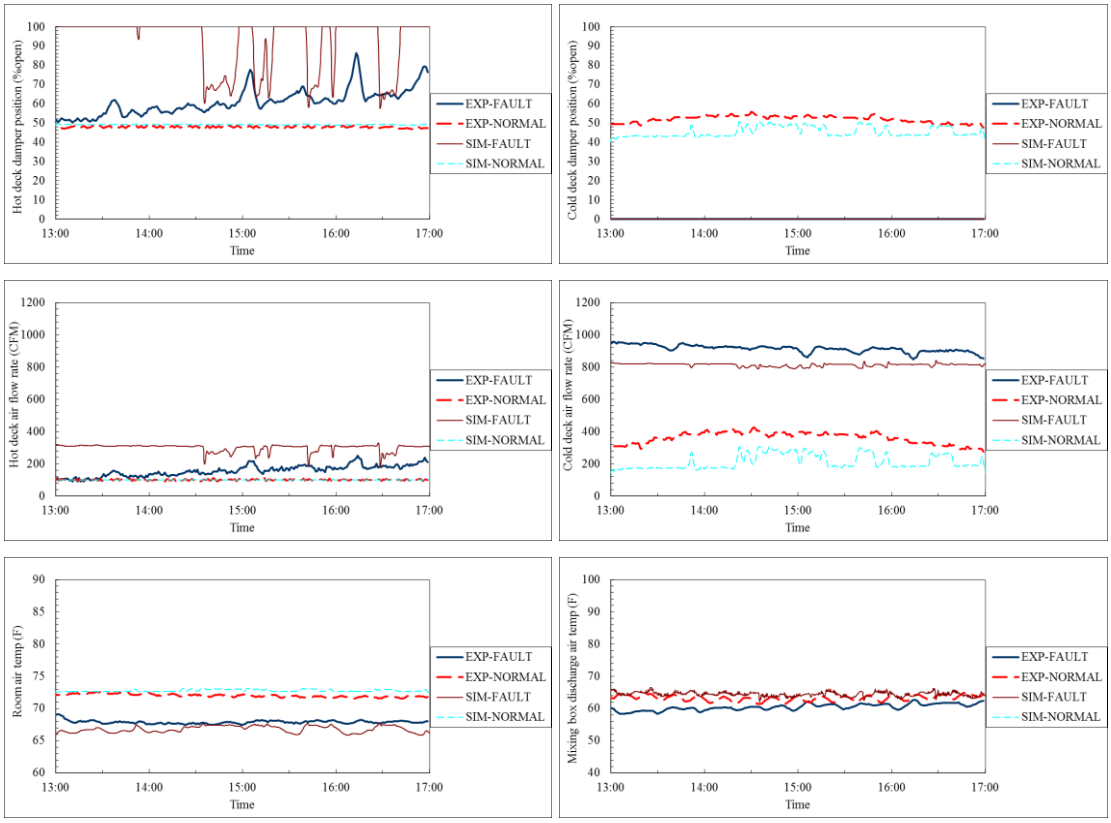

(d) South-A room results

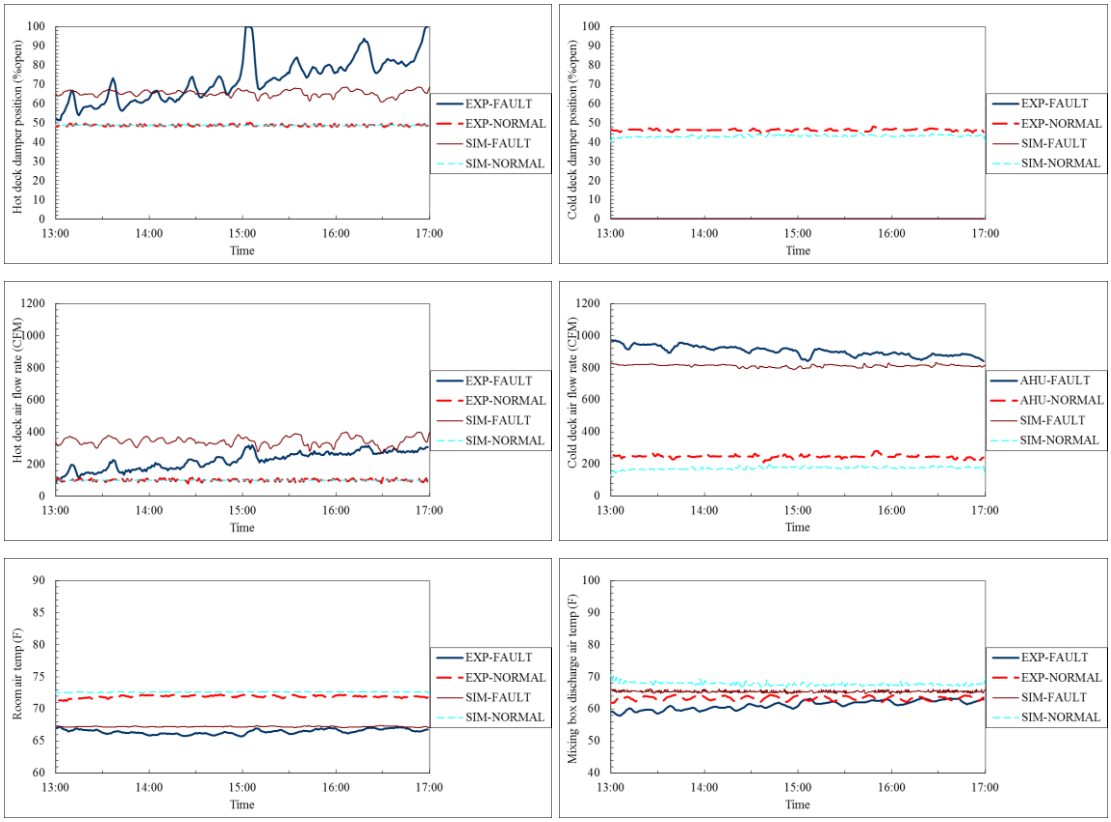

(e) East-B room results

Figure 3-25. Validation of dual duct terminal unit cold deck damper stuck at fully open position fault in dual duct double fan system (July 8th)

Figure 3-25 depicts the fault model simulation results of dual duct double fan system with hot deck damper in the dual duct terminal unit stuck at fully closed position on a winter test day (Nov 17th). A colder normal test day (Nov 25th) is selected to serve as the reference day. The symptoms associated with this fault are as the following:

Fault symptoms observable in AHU:

1) Decrease in the cold and hot deck supply air flow rates. Decrease in the hot deck supply air flow rate is the consequence of this fault which results in the reduction of cold air flow requirement of the rooms to keep temperature set point.
2) Decrease in the return air flow rate. Reduction of supply air flow rates in both hot and cold decks ends up to this symptom.
3) Decrease in the hot and cold deck supply fan speeds. The reduced hot and cold deck air flow rates result in the drop of corresponding supply fan speeds.
4) Decrease in the hot and cold deck supply fan power consumption. Fan power consumption is a direct function of air flow rate and speed. Obviously decrease in both flow rate and speed cause power consumption drop.
5) Decrease in heating coil valve position and consequently hot water flow rate through the coil. The heating coil load has decreased due to the hot deck supply air flow rate reduction.
6) Decrease in the return air temperature and consequently mixed air temperature. This symptom is caused by the reduction in the amount of hot air flow rates to the rooms.

Fault symptoms observable in zones:

1) Increase in the hot deck damper position. While controller in dual duct terminal unit commands to open up the hot deck damper but actuator does not follow it due to its malfunction.
2) Decrease in the hot deck air flow rate to the room.
3) Decrease in the cold deck damper position and consequently cold deck air flow rate to the rooms.
4) Decrease in the room air temperature. This fault causes the shift of dual duct terminal unit controller operation from cooling mode to heating or neutral mode.

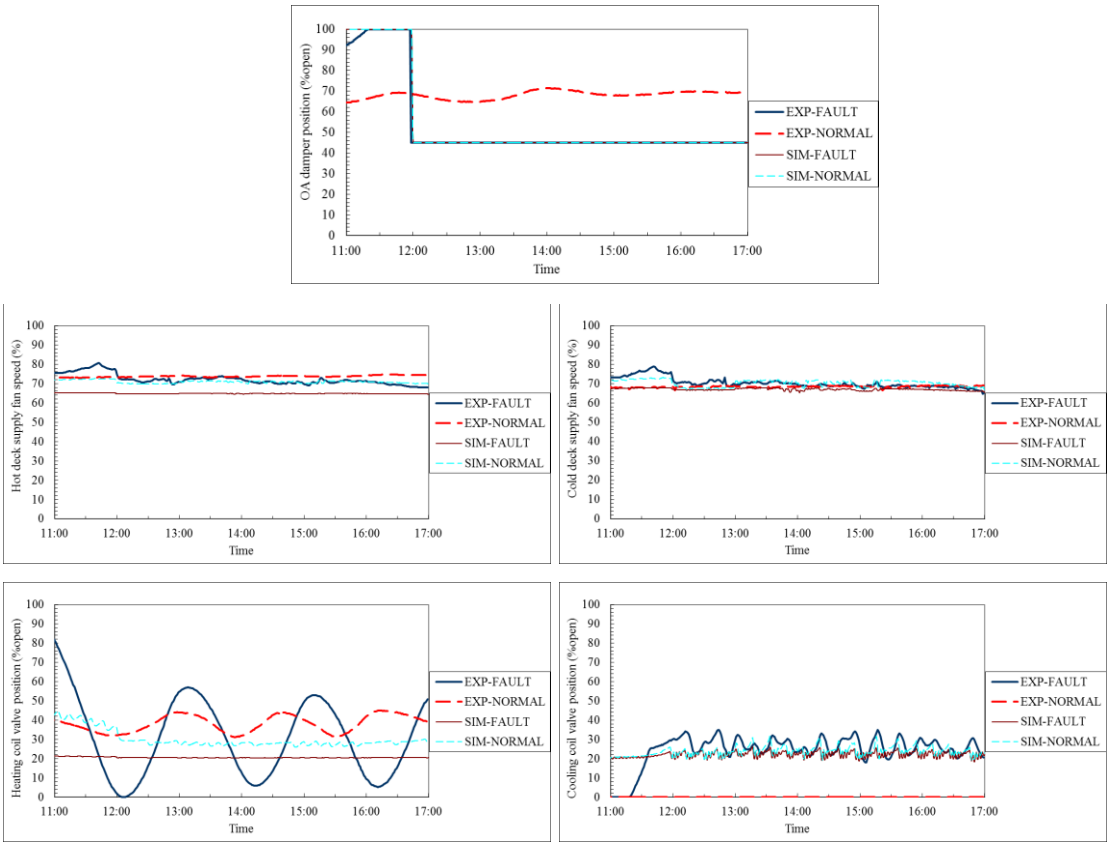

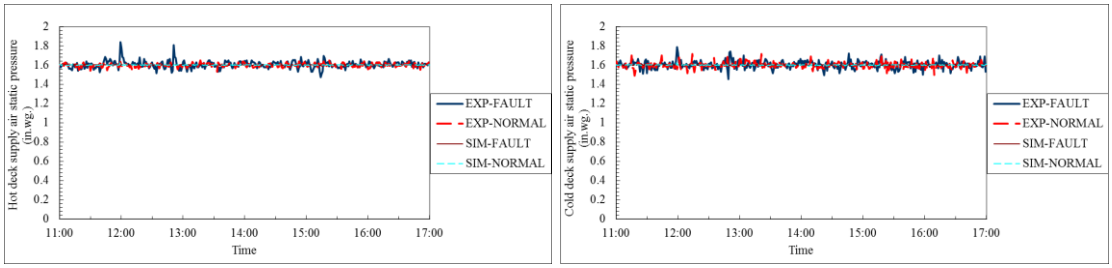

(a) Dual duct system AHU control signals

(b) Air & water flow rates and supply fan power consumptions in dual duct system AHU

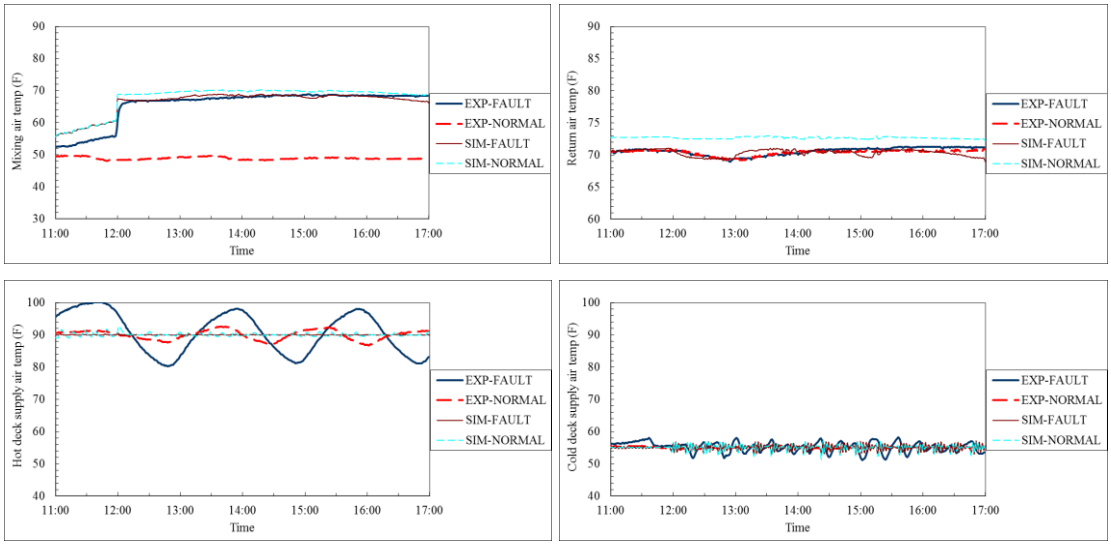

(c) Temperatures of dual duct system AHU

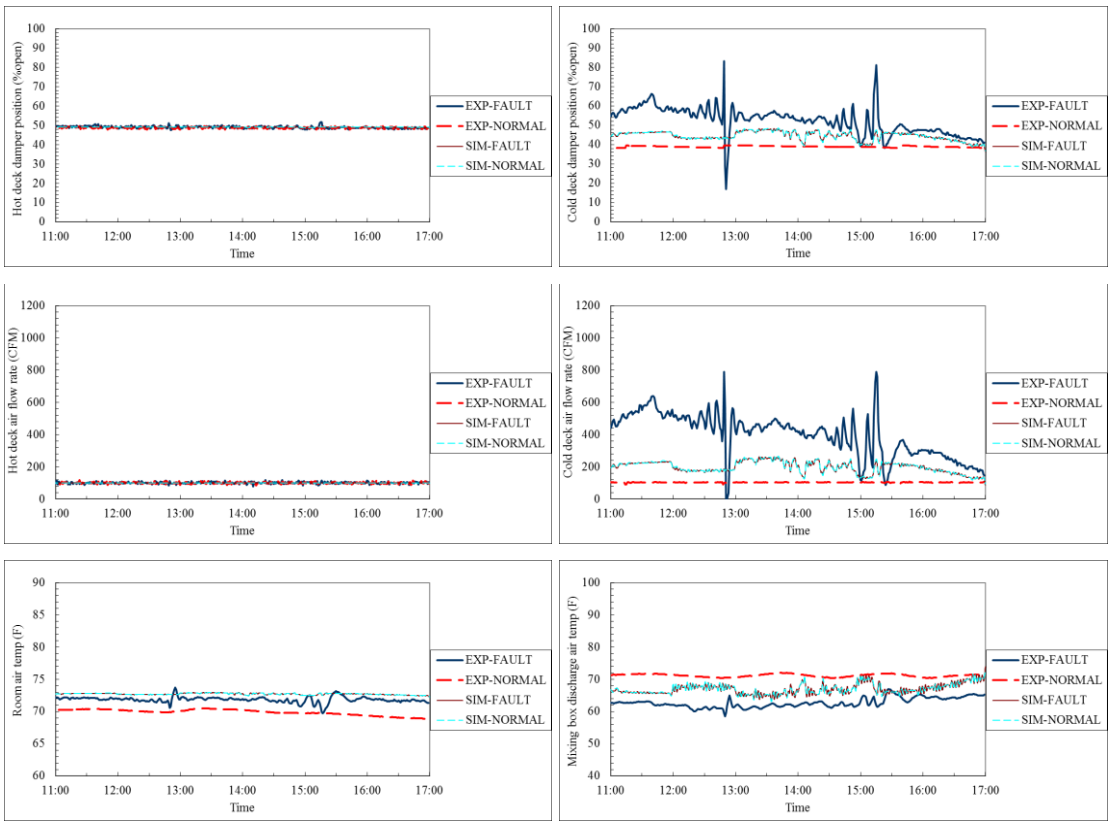

(d) South-B room results

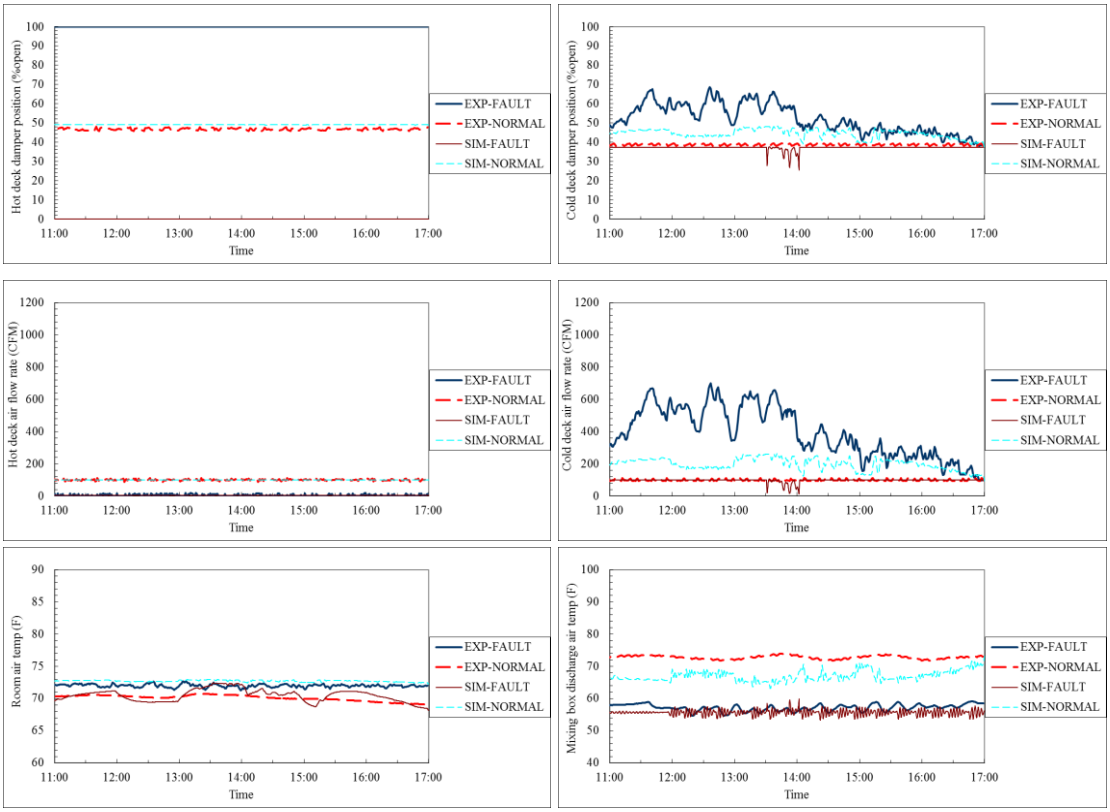

(e) South-A room results

Figure 3-26. Validation of dual duct terminal unit hot deck damper stuck at fully closed position fault in dual duct double fan system (Nov 17th)

To illustrate a fault case for control category, chiller fault on a summer test day (Jun 13th) is selected. Due to this fault the chilled water supply temperature is too high. At the test facility this fault is simply implemented by disabling the chiller which provides chilled water to the cooling coil in AHU-B. In the model this fault is reflected in the inlet chilled water temperature which is a time dependent boundary variable. A close normal test day (June 9th) is chosen to be served as reference day. Figure 3-27 demonstrates the validation of the developed model for dual duct double fan system under this faulty condition. The symptoms of this fault can be readily distinguished by noticing:

Fault symptoms observable in AHU:

1) Decrease in the heating coil valve position and heating water flow rate. The load of heating coil in hot deck drops due to the increase in the inlet air temperature (mixed air temperature).
2) Increase in the cooling coil valve position and chilled water flow rate. Cold deck supply air temperature controller commands to open up cooling coil valve to maintain temperature set point but it is unable to do so. Because the chilled water inlet temperature is too high.
3) Increase in the cold deck supply air flow rate. Since the supplied cold air to the rooms is not cold enough; the dual duct terminal unit controller calls for more cooling by opening up the cold deck damper to 100% open.
4) Decrease in the cold deck supply air static pressure. The operating point of cold deck drops to a lower point due to the increase in supply air flow rate. This deck supply fan is not able to keep the pressure set point even by operating in full speed.
5) Increase in the hot and cold deck supply fan speeds. The pressure drop in the cold deck has a similar effect on the hot deck which causes hot deck supply fan operation at a higher speed to compensate the pressure drop and maintain the static pressure set point.
6) Increase in the hot and cold deck supply fan power. Both supply fans work harder to maintain the supply decks pressure set point and draw more power.
7) Increase in the return air flow rate. This symptom is caused by the cold deck supply air flow rate increase.

8) Increase in the return air temperature and consequently mixing air temperature. The cold deck supply air temperature to the rooms is too high to keep room temperature set point. Therefore, the returned air temperature from the rooms is too high and the mixture of this air with the fresh air would be also high.
9) Increase in the hot and cold deck supply air temperatures. Supply air temperature of both decks float because the mixed air temperature (the inlet temperature to both hot and old deck) is too high. Even totally closing down the heating coil valve and totally opening up the cooling coil valve is unable to maintain supply air temperature set point.

Fault symptoms observable in zones:

1) Increase in the cold deck damper position.
2) Increase in the cold deck air flow rate.
3) Increase in the terminal unit discharge air and room air temperature. The discharged air from dual duct terminal unit is the mixture of both hot and cold decks air streams. Both decks supplied air temperatures are too high to maintain room temperature set point.

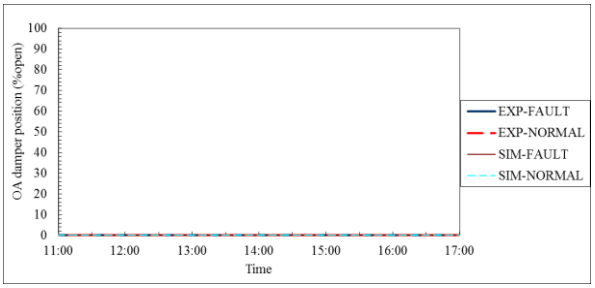

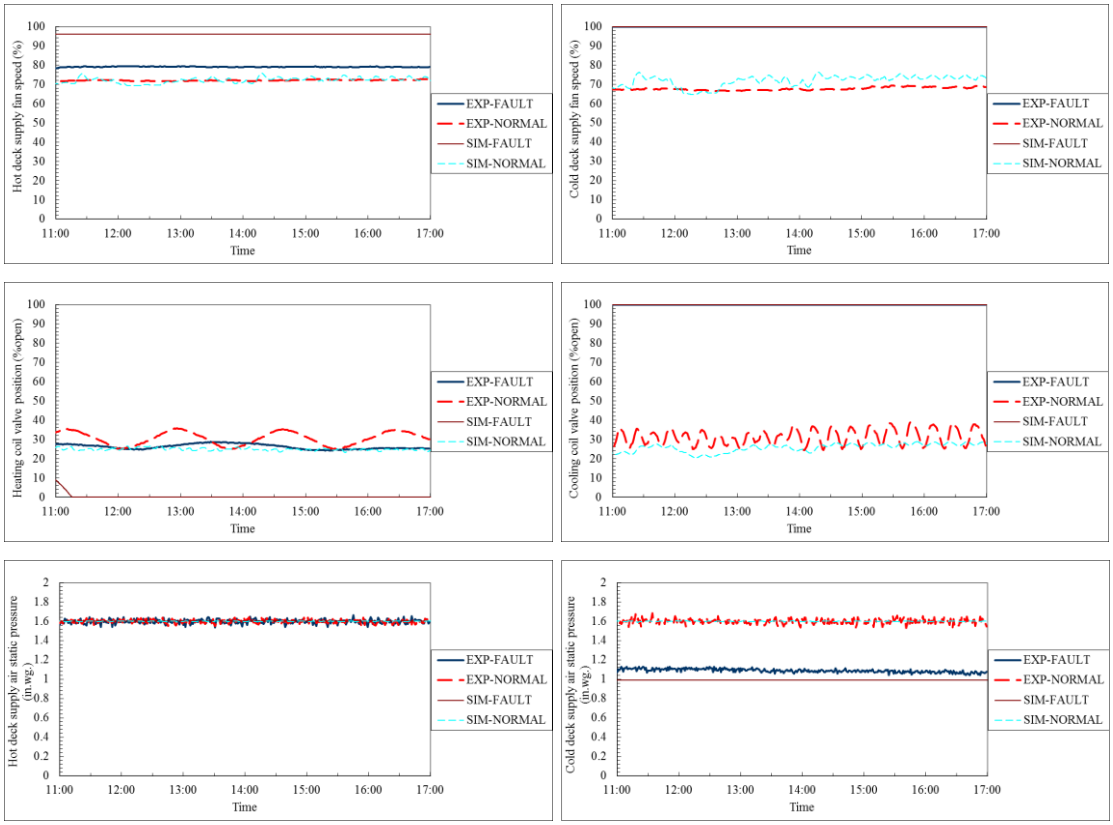

(a) Dual duct system AHU control signals

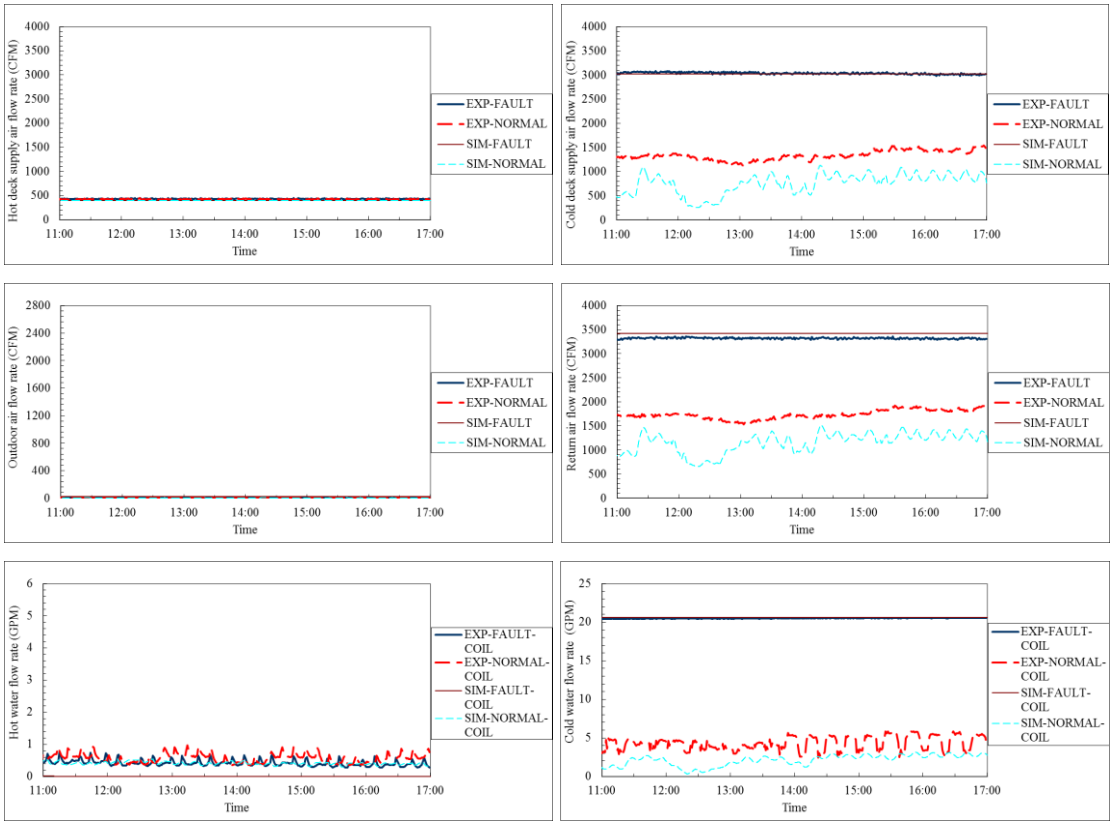

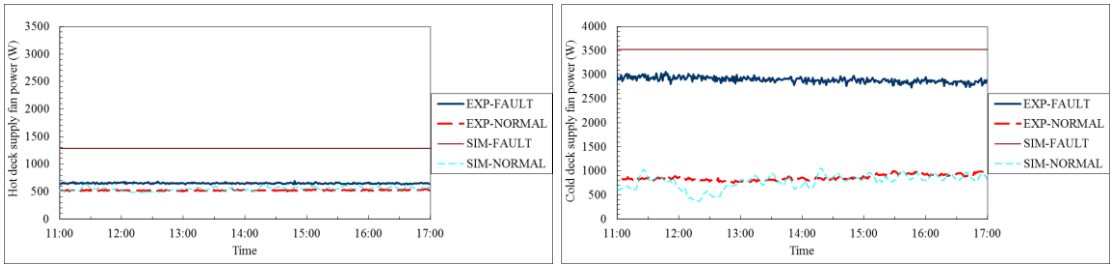

(b) Air & water flow rates and supply fan power consumptions in dual duct system AHU

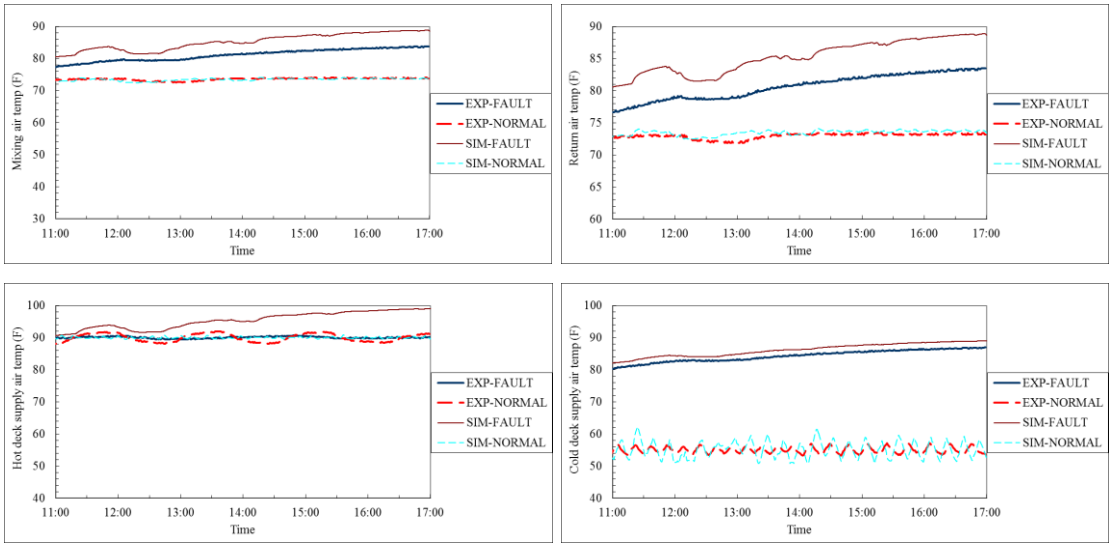

(c) Temperatures of dual duct system AHU

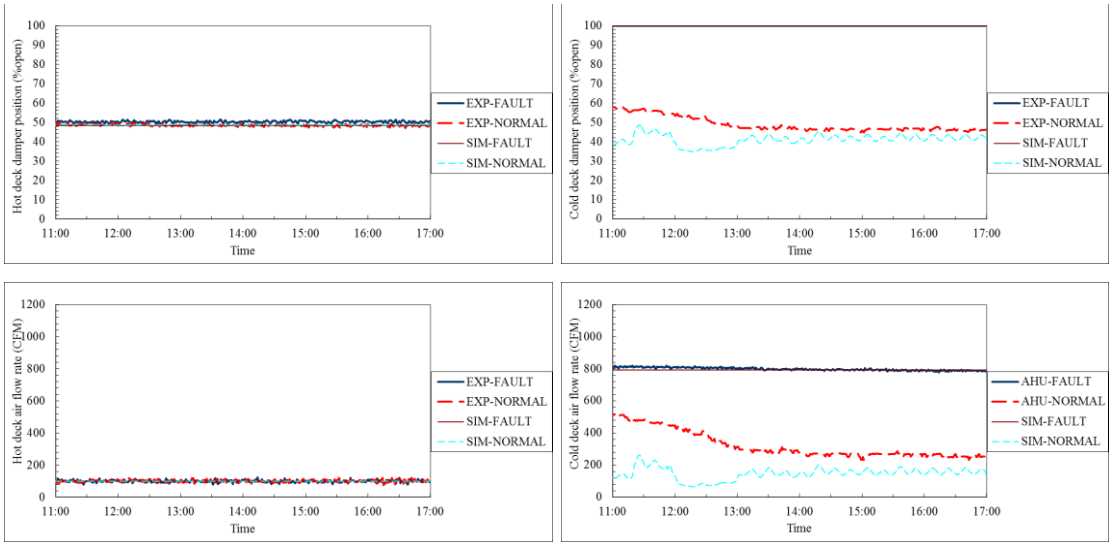

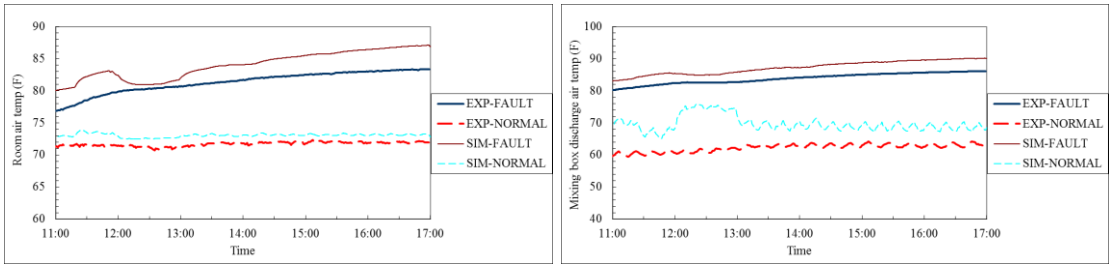

(d) East-B room results

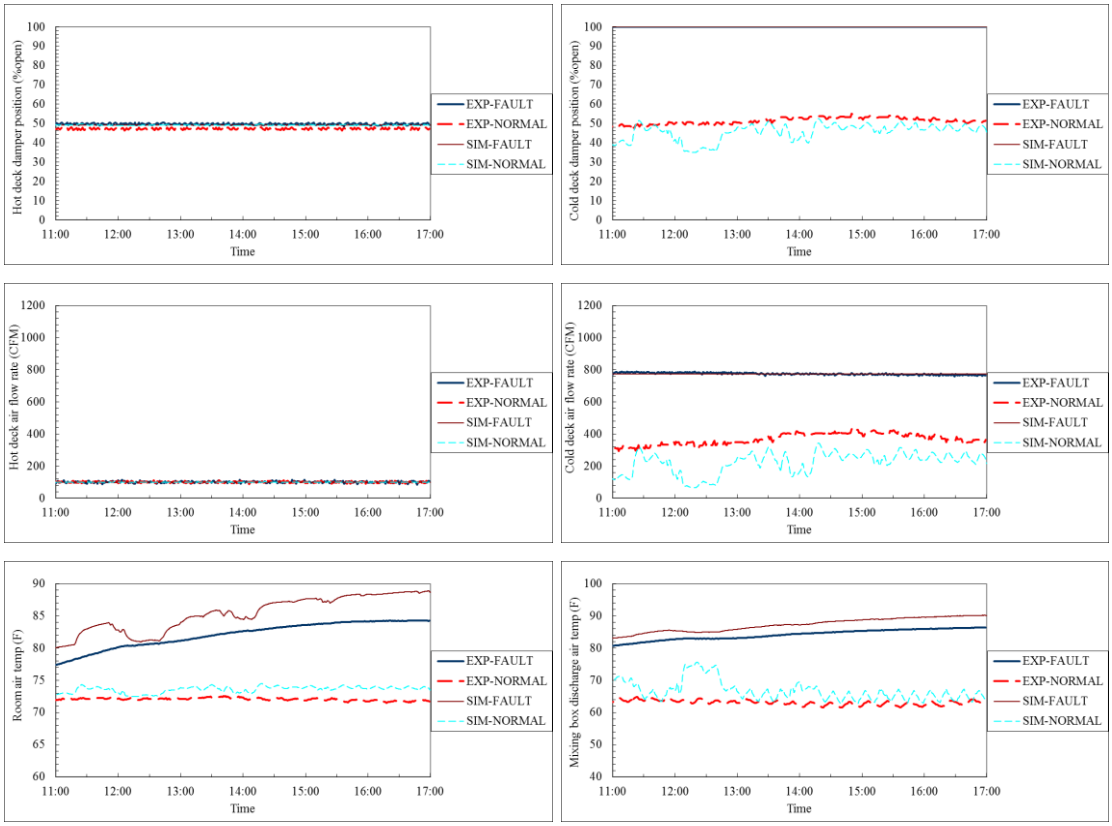

(e) South-A room results

Figure 3-27. Validation of chiller fault in dual duct double fan system (June 13th)

3.7 Conclusion and Summary

In this work, a dynamic numerical model of a dual duct double fan system has been developed and validated. Four new components models (TYPE) which three of them representing the air flow state and one of them representing the control sequence of VAV dual duct terminal units have been created for inclusion in the component

library of the HVACSIM+ simulation package. A model structure for the air flow states of dual duct systems that will result in robust dynamic simulations is introduced. Validation of the air flow model was in three steps, starting with component level validation, followed by system level validation itself in two separate steps. Validation of air flow subsystem including hot and cold deck splitters and ductwork all the way to rooms laid the groundwork for the entire air flow model validation. Similarly, the satisfactory validation results from the entire air flow model led us to the next steps of validation. Firstly, thermal network was added to the validated air flow model and at last all networks representing control, actuator, air flow, thermal and sensor states were validated all together. Full system experimental data from three seasons were used to validate the system at every step of validation. Experiments were conducted to investigate and determine key model parameters like dampers in dual duct terminal units. Real operational data provided by ERS served as a reference to which simulation results were compared. Under fault-free conditions, the dual duct model agreed well with reference data for several days in different seasons (summer, fall and winter) considering that the control sequence of the model is different from ERS. A fault flag system gives the model the flexibility to simulate various faults modes with differing severities without the need to develop additional TYPEs. That the model underwent a comprehensive fault matrix and validated well against experimental data establishes its validity to serve as a tool for evaluating dual duct systems fault detection and diagnostic methods.

4. CHAPTER FOUR: EFFICIENT AND ROBUST OPTIMIZATION FOR BUILDING ENERGY SIMULATION

4.1 Introduction

Efficiently, robustly and accurately solving large sets of structured, non-linear algebraic and differential equations is one of the most computationally expensive steps in the dynamic simulation of building energy systems. Here, the efficiency, robustness and accuracy of two commonly employed solution methods are compared. The comparison is conducted using the HVACSIM+ software package, a component based building system simulation tool. The HVACSIM+ software presently employs Powell's Hybrid method to solve systems of nonlinear algebraic equations that model the dynamics of energy states and interactions within buildings. It is shown here that the Powell's method does not always converge to a solution. Since a myriad of other numerical methods are available, the question arises as to which method is most appropriate for building energy simulation. This study finds considerable computational benefits result from replacing the Powell's Hybrid method solver in HVACSIM+ with a solver more appropriate for the challenges particular to numerical simulations of buildings. Evidence is provided that a variant of the Levenberg-Marquardt solver has superior accuracy and robustness compared to the Powell's Hybrid method presently used in HVACSIM+.

In this chapter, Section 4.2 summarizes the LM and PH methods while Section 4.3 describes the numerical study and implementation of both methods in HVACSIM+. The numerical results and comparison are also presented in this section. Finally, Section 4.4 provides conclusions and future research directions.

4.2 Simulation Description

The subroutine SNSQ in MODSIM implements PH, which seeks to find a zero of a system of N nonlinear, continuously differentiable functions in N variables. The N

variables are representative of state variables defined in the model and the N functions are the governing equations in the physical units. The system of nonlinear algebraic equations can be rewritten more generally in vector form as

$$F(x)=0 \tag{4-1}$$

where $F:\Re^N \rightarrow \Re^N$, $x \in \Re^N$ is the vector function of primal variables. It has been observed that in some cases like the FCU model, the PH method fails to converge to a solution in a reasonable number of steps even when a reasonable solution exists. The LM method appears to converge to this desirable solution efficiently. What follows is a short description of both the LM method and the PH method. The interested reader is referred to more thorough references on both the LM method (Levenberg, 1944; Marquardt, 1963) and the PH method (Powell, 1970).

4.2.1 Levenberg Marquardt method

In this section we summarize the LM algorithm; Table 1 presents pseudo-code for the method as implemented. The interested reader is referred to (Levenberg, 1944; Marquardt, 1963) for a more detailed description. The LM method has become a standard method for solving systems like Equation (4-1). Loosely speaking, LM can be thought of as a combination of both steepest descent and the Gauss-Newton methods in so far as the algorithm behaves like steepest descent when iterates are far from a local minimizer and when iterates draw closer to a local minimizer the method becomes the Gauss-Newton method. Making clear the distinction between being ‘close’ and ‘far’ from a local solution can be made more mathematically justified (see, for example (Yamashita, 2001; Kelley, 1999)). To help with a comparison, a short description of LM is presented here. In this implementation of LM, specific norms $\|.\|$ are not chosen because in this case, all norms are equivalent; the interested reader is referred to more extensive treatments presented in (Stewart et al., 1990). The LM

method is based on a linear approximation to F in a neighborhood of the point x. The Jacobian matrix J, which is comprised of the partial derivatives of F, $\partial F/\partial x$ can be approximated by a Taylor series with step size ∂x,

$$F(x+\delta_x) \approx F(x) + \frac{\partial F}{\partial x}\delta_x = F(x) + J\delta_x \tag{4-2}$$

and forms the basis of the iterative technique. In this way, the initial approximation x_0 produces iterates x_i, which seek to converge to the local minimizer x_*. Based on this formulation, the goal at each step is to minimize the residual,

$$\|b - F(x+\delta_x)\| \approx \|b - F(x) - J\delta_x\| = \|b - J\delta_x\|. \tag{4-3}$$

where b is defined by,

$$F(x_*) \approx b \tag{4-4}$$

In this case the step δ_x is a solution to a linear least squares problem and the solution occurs when $J\delta_x - r_x$ is orthogonal to the column space of J leading to the observation that $J^T(J\delta_x - r_x) = 0$. The Gauss-Newton step, δ_{gn}, solves the so-called normal equations,

$$J^T J\delta_{gn} = J^T\big(b - F(x)\big) = J^T r_x. \tag{4-5}$$

When higher order terms are neglected the matrix $J^T J$ approximates the Hessian matrix $r_x^T r_x$. In this case $J^T r_x$ is along the steepest descent direction as $-J^T r_x$ is the gradient of $\frac{1}{2}r_x^T r_x$. In practice the augmented normal equation is:

$$(J^T J + \mu I)\delta_x = J^T r_x \; where \; \mu > 0. \tag{4-6}$$

Here, I is the appropriately sized identity matrix. The process of adjusting μ is regulated by monitoring the updates in primal variables $x + \delta_x$. If this update results in a decrease in the squared residuals $r_x^T r_x$ then the change that resulted from the μ is

accepted and the algorithm continues to a new iteration. If not, the term μ can be increased and the system is solved again until a value of μ results in a sufficient decrease in the squared residuals $r_x^T r_x$. As Table 4-1 demonstrates, this adjustment takes place at every iteration of the LM algorithm. The larger the μ the more diagonally dominant the normal equations become and the closer the solution to these equations draw to the steepest descent, $J^T \delta_x$. The magnitude of the residual also decreases significantly with increasing μ. Clearly the smaller the steps the greater the robustness, but slower convergence follows. This regularization is also employed for rank deficient matrices J as it ensures the linear system being solved is always positive definite for positive μ. This method terminates, in most implementations, when at least one of the following conditions holds:

- The maximum number of iterations is reached,
- The norm of the gradient is sufficiently small,
- The norm of the step is sufficiently small.

Table 4-1. Levenberg Marquardt method algorithm

Input: A function $F: \Re^n \rightarrow \Re^n$ and initial estimate $x_0 \in \Re^n$ and output parameters b

Output: A vector $x^* \in \Re^n$ where $F(x^*) \approx b$

$k \coloneqq 0;\ \eta \coloneqq 2; x \coloneqq x_0$

$A \coloneqq J^T J;\ r_x \coloneqq b - F(x);\ g \coloneqq J^T r_x$

$\boldsymbol{converge} \coloneqq \left(\|g\| \leq \epsilon_g\right);\ \mu = \tau\ max_i\ A_{ii}$

$\boldsymbol{while}\ (k < k_{max}\ and\ \boldsymbol{converge} = \boldsymbol{false})\ \boldsymbol{do}$

    $k = k + 1$

    $\boldsymbol{Repeat}$

    $\boldsymbol{Solve}\ (A + \mu I)\delta_x = g$

    $\boldsymbol{if}\ (\|\delta_x\| \leq \epsilon_x \|x\|)\ \boldsymbol{then}$

9 $\boldsymbol{converge} \coloneqq \boldsymbol{true}$

10 $\boldsymbol{else}$

11 $x_+ = x + \delta_x;\ \rho = \frac{(\|r_x\|^2 - \|b - F(x_+)\|^2)}{(\delta)^T(\mu(\delta)+g)}$

12 $\boldsymbol{if}\ \rho > 0\ \boldsymbol{then}$

13 $x = x_+$

14 $A = J^T J;\ r_x = b - F(x);\ g = J^T r_x;\ \boldsymbol{converge} = (\|g\| \leq \epsilon_g)$

15 $\mu = \mu * \max(1/3\ , 1 - (2\rho - 1)^3);\ \nu = 2$

16 $\boldsymbol{else}$

17 $\mu = \mu * \nu;\ \nu = 2\nu$

18 $Until\ (\rho > 0)\ or\ stop\ x_+ = x$

4.2.2 Powell's Hybrid method

Similar to the LM method, the Powell's Hybrid method seeks to combine both Gauss-Newton and steepest descent, however, in this case the convergence is controlled through a trust-region. Trust-region methods have become a mainstay of nonlinear optimization strategies and are used in a wide variety of applications. Employing a trust-region formulation, the objective function F is used to construct a quadratic model function, H, so that in a neighborhood of a current iterate about which H is constructed, the functions H and F are similar. The function H is said to be trusted to accurately model F in a region with weighted radius Π that is centered at the current iterate. Using this strategy, a candidate step can be calculated by minimizing H over the trust-region. The model function is:

$$H(\delta) = (r_x^T r_x - 2(J^T r_x)^T \delta + \delta^T J^T J \delta) \quad (4\text{-}7)$$

and a candidate step can be attained by solving:

$$\min_{\delta} H(\delta) \ subject\ to\ \|\delta\| \leq \Pi. \tag{4-8}$$

In practice, the trust region radius is selected based on the ability of the model to 'fit' the objective function - strong agreement between the approximation and the original model suggest a strong value of Π. The solution to the trust-region in Equation (4-1) can be seen in Figure 4-1. In his seminal paper, Powell (Powell, 1970) used piecewise linear trajectories consisting of two line segments in order to approximate the solution curve. In other words, rather than solving the normal equations directly, which can be expensive, Powell approximated the solution using two less expensive calculations. The first segment emanates from the current approximation to the so-called Cauchy point which is the unconstrained minimum of the objective function along the steepest descent (or gradient) plane, $J^T r_x$ and is given by:

$$\delta_{sd} := \frac{g^T g}{g^T J^T J_g} g, \tag{4-9}$$

the second component runs from this δ_{sd} to the Gauss-Newton step. Table 4-2 summarizes the Powell's Hybrid algorithm.

Table 4-2. Powell's Hybrid method algorithm

Input: A function $F: \Re^n \rightarrow \Re^n$ and initial estimate $x_0 \in \Re^n$ and output parameters b

Output: A vector $x^* \in \Re^n$ where $F(x^*) \approx b$

1 $k := 0;\ \Pi := \Pi_0; x := x_0$

2 $A := J^T J;\ r_x := b - F(x);\ g := J^T r_x$

3 $\boldsymbol{converge} := \left(\|g\| \leq \epsilon_g\right)$

4 $\boldsymbol{while}\ (k < k_{max}\ and\ \boldsymbol{converge} = \boldsymbol{false})\ \boldsymbol{do}$

5 $\quad k = k + 1$

6 $\delta_{sd} = \frac{\|g\|^2}{\|Jg\|} g$

7 $\boldsymbol{Gauss\ Newton = false}$

8 ***Repeat***

9 $\boldsymbol{if}\ (\|\delta_{sd}\| \geq \Pi)\ \boldsymbol{then}$

10 $\delta_d \coloneqq \frac{\Pi}{\boldsymbol{\delta_{sd}}} \delta_{sd}$

11 ***else***

12 $\boldsymbol{if\ not\ Gauss\ Newton\ then}$

13 $\boldsymbol{Solve}\ A\delta_{gn} = g$

14 $\boldsymbol{Gauss\ Newton = true}$

15 $\boldsymbol{if}\ (\|\delta_{sd}\| \leq \Pi)\ \boldsymbol{then}$

16 $\delta_d = \delta_{gn}$

17 ***else***

18 $\delta_d = \delta_{sd} + \alpha(\delta_{gn} - \delta_{sd})$

19 $Choose\ \alpha\ so\ that\ \|\delta_d\| = \Pi$

20 $\boldsymbol{if}\ (\|\delta_d\| \leq \epsilon_\delta)\ \boldsymbol{then}$

21 $Converge = true$

22 ***else***

23 $x_+ = x + \delta_d;\ \rho = \frac{(\|r_x\|^2 - \|b - F(x_+)\|^2)}{H(0) - H(\delta_d)}$

24 $\boldsymbol{if}\ (\rho > 0)\ \boldsymbol{then}$

25 $x = x_+$

26 $A \coloneqq J^T J;\ r_x \coloneqq b - F(x);\ g \coloneqq J^T r_x$

27 $Converge \coloneqq (\|g\| \leq \epsilon_g)$

28 $\boldsymbol{Update}\ \Pi\ \boldsymbol{converge} \coloneqq (\Pi \leq \epsilon_x \|x\|)$

29 **Until** ρ > 0 or **converge**

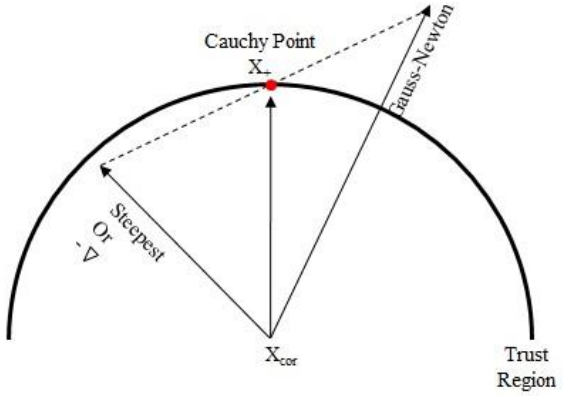

Figure 4-1. Visualization of the Cauchy Point for a system of nonlinear equations with trust-region

4.3 Numerical Case Study

The robust convergence capability and application of the LM and PH methods in the building energy simulation tool HVACSIM+ is examined in this numerical study. For this purpose a fan coil unit, an economical and simple secondary HVAC system used extensively in commercial, institutional and multifamily residential buildings, is modeled. The FCU model created in HVACSIM+ (Pourarian et. al, 2014) underwent simulation with both methods by keeping the model structure and architecture identical and substituting between the PH and LM algorithms. What follows are the physical and geometrical characteristics of the FCU under study and the control strategy of FCU operation. The specific FCU studied in this chapter is a vertical floor mounted four pipe hydronic system including three parallel fans run by two electric motors with three speeds: high, medium and low. The FCU modulates the amount of ventilation supplied to its zone by using a motorized damper in the outside air connection at the back of the unit. Figure 4-2 shows the configuration of the FCU with its components and their arrangements.

To simulate the FCU interacting with the corresponding zone in HVACSIM+, the components (units) models are grouped into five blocks and each block constitutes a superblock. The final model consists of five superblocks: control logic, actuators, air flow, thermal, and sensors. The superblocks are weakly coupled to each other. The solution of each superblock (obtained to some specified convergence tolerance) is the input for the next simulation time step and this process is repeated at every time step. The model of the FCU interacting with two exterior building zones, east and south facing, is simulated on a summer test day. These zones are referred to as rooms in the following discussion. In summer, the outdoor air damper is fully closed and the fan speed is normally set at high. When the FCU is operating properly, the controller compares room temperature to the cooling set-point (74F (23.33C)) and heating set-point (70F (21.11 C)). If the actual room temperature is greater than (cooling set-point −1F (0.56 C)), the FCU is in cooling mode and if it is less than (heating set-point +1F (0.56 C)), the FCU is in heating mode. A dedicated proportional integral derivative (PID) loop is enabled for each mode to control the cooling or heating valve position. A PID loop is a means of regulating a process quantity (room temperature) by compensating it with closed-loop feedback of its error (difference between the room temperature and set-point), with the compensation amount computed linearly using three gain coefficients.

As long as room temperature lies between the heating and cooling set-points, the PID loops are disabled and the corresponding valves are fully closed. The room air temperature signal is passed from the sensors superblock to the controls superblock, which calculates the required position of the heating and cooling coil valves. Valve positions as determined in the control superblock are passed to other superblocks as appropriate. Simultaneous solution of mass-pressure equations occurs in the air flow

superblock, while energy balance equations are solved simultaneously in the thermal superblock. As shown in Table 4-3, the total number of variables in the FCU simulation is 58. In this table the category and number of variables in those categories are listed. The Iowa Energy Center Energy Resource Station (ERS) provides weather condition and experimental data necessary for simulation and validation of the FCU model. Additional details of this model, including a discussion of model validation, can be found in (Pourarian et. al, 2014).

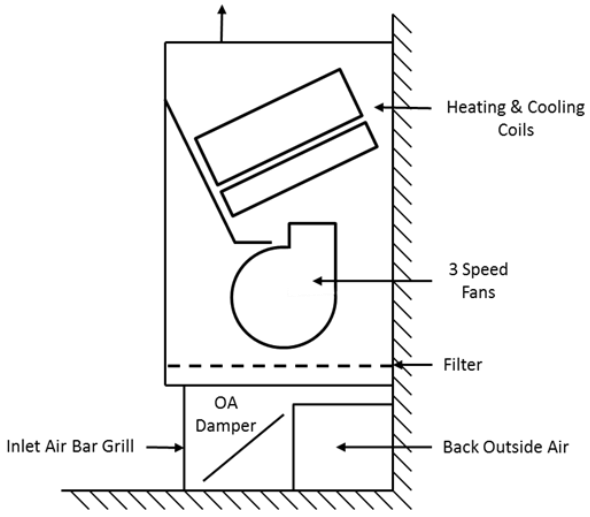

Figure 4-2. Fan coil unit configuration

Table 4-3. Category and number of state variables

Category	Pressure	Flow rate	Temperature	Control	Other (Fan rotational speed)	Power	Humidity
Number of state variables	7	8	16	14	1	8	4

In this section the simulation results of the FCU model as simulated with both methods are presented and compared. The FCU performance variables as well as the solver function variables are shown in order to compare the performance of the two methods. Room air temperature and cooling coil valve position are the FCU

performance variables. The number of function evaluations, number of iterations, cumulative number of iterations, and cumulative number of function evaluations are the performance variables of each solver method.

In Figure 4-3 and Figure 4-4 the FCU performance variables of simulations for east and south facing rooms using both the PH and LM methods are compared for identical initial conditions. The solid line represents experimental data, the dotted line represents the simulation result with the PH method and dashed line represents simulation results with the LM method. The FCU model parameters have been validated using experimental data which are reported in another publication (Pourarian et. al, 2014). Here, experimental data serve as a reference to compare the two solver methods.

As Figure 4-3 illustrates, the FCU in the east room is operated in cooling mode to maintain the cooling temperature set point. The cooling coil valve controls the water flow rate, which in part determines the heat transfer rate, and maintains the room temperature near the cooling set point. As the east room air temperature graph in Figure 4-3 shows, the results of the simulation for the PH and LM methods for room air temperature are identical except for the 10:00 to 11:10 and 13:30 to 15:40 time frames, in which the model using the PH method moves around the cooling temperature set point but is not able to capture it. When a nonlinear system does not converge at a given time step (i.e. the simulation fails to meet the termination criteria), the inaccurate solution is passed to later time steps. This can lead the simulation into non-physical state space (e.g., negative humidity) and/or an inaccurate solution. This can happen when residuals become small, but fail to vanish. Thus, while all but one superblock may reach convergence within a time step, the one superblock that failed to converge can cause the entire simulation to fail at that time

step. That scenario is avoided by the LM method, which successfully iterates all superblocks to desirable solutions within the simulation time window. For this reason, the simulation result for cooling coil valve position by the LM method is reasonable, whereas the solution provided by the PH method is not. The bump that occurs around 11:00 in the east room air temperature values calculated by the PH method shows that solver became trapped in an unsatisfactory region where it could not find the minimum of the sum of the squares of the functions.

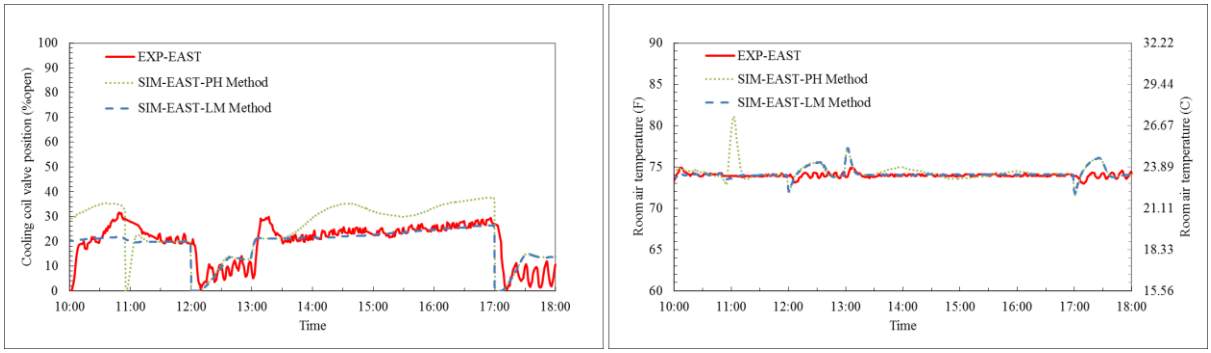

Figure 4-3. Simulation results of FCU operational variables in east room by PH and LM method

As Figure 4-4 shows, the FCU operation in the south room is consistent with the operation in the east room. The PH method did not solve the thermal superblock in the 10:00 to 11:10 and 13:10 to 15:45 time frames, having completed all iterations unsuccessfully. On the other hand, the LM method converged to a desirable solution for both the air flow and thermal superblocks. The simulation results predicting the FCU operation in the east and south rooms are acceptable when the solver returns a converged solution for all superblocks. As the south room air temperature graph in Figure 4-4 shows, the results of the simulation for the PH and LM methods for room air temperature are identical except for the 10:00 to 11:10, 13:10 to 14:00 and 14:30

to 16:00 time frames, in which the PH method moves around the cooling temperature set point but is not able to capture it. The cooling coil valve position based on the LM method, which successfully converged to a solution, gives more reasonable results.

The prior validation work (Pourarian et. al, 2014) revealed some weaknesses in the combined model of the FCU and room. The thermodynamic interaction between the modeled room and the ambient environment differs from the interaction that occurs in the real physical space. Thus, the cooling coil valve signals solved for in the control superblock do not completely agree with the experimental data. This weakness in the model is most clearly demonstrated by the decrease in cooling coil valve position shown near 14:00 in Figure 4-4 for both the PH and LM methods.

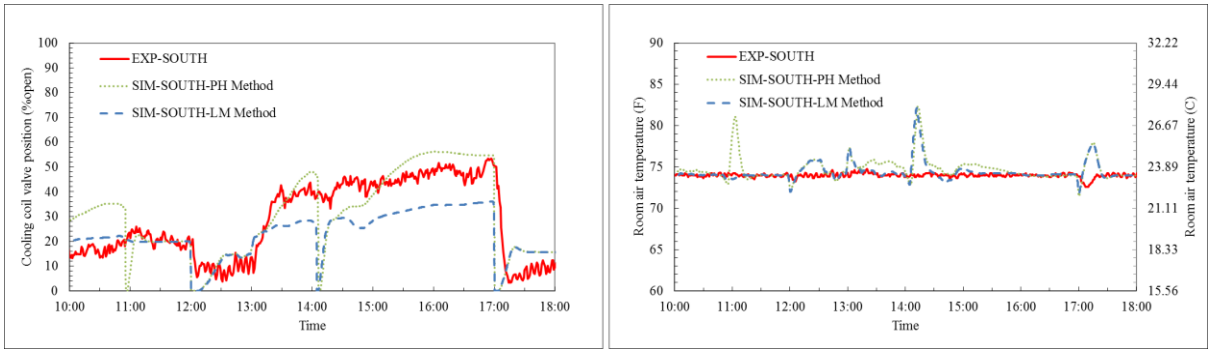

Figure 4-4. Simulation results of FCU operational variables in south room by PH and LM method

Figure 4-5- Figure 4-8 are a brief comparison of the PH and LM method performance variables obtained in solving the system of nonlinear equations that emerge in the FCU simulation. Figure 4-5 is a comparison of the PH and LM method cumulative number of iterations and the number of iterations at each time step in the air flow and thermal superblocks for the FCU in the east room. Similarly, Figure 4-6 displays the comparison of the PH and LM method cumulative number of function

evaluations and the number of function evaluations at each time step in the air flow and thermal superblocks for the FCU in the east room; Figure 4-7 and Figure 4-8 display the same data for the south room. According to the number of iterations at each time step for the thermal superblock of the FCU in the east and south room in Figure 4-5 and Figure 4-7, it is obvious that for the PH method, during the time frames with unsuccessful solutions, the number of iterations in the thermal superblock is greater. This implies that the PH method attempts to make good progress toward the solution by increasing the number of iterations. A close look at the number of function evaluations in Figure 4-6 and Figure 4-8 for the FCU thermal superblock in the east and south rooms leads us to the same conclusion. Note that in Figure 4-8, near 14:00 the number of function evaluations does not spike for either PH or LM because, as noted above, the deviation from the experimental data is not due to convergence failure.

Figure 4-6 and Figure 4-8show that the LM method requires more function evaluations than the PH method because, as discussed in Section 4.2, the LM method solves the normal equations directly rather than using the approximation employed in the PH method. Figure 4-5 and Figure 4-7 show that, for the airflow superblock, the LM method requires more iterations than the PH method; this is also a result of the direct solution of the normal equations. In Figure 4-7, for the thermal superblock, the LM method requires more iterations than the PH method, as expected, but in Figure 4-5, the thermal superblock requires more iteration for the PH method than for the LM method. This behavior demonstrates the difficulty that the PH method has converging to a solution in the thermal superblock for the east room as previously discussed in relation to Figure 4-3. If both methods are properly converging, the LM method should require more iterations than PH due to its greater complexity.

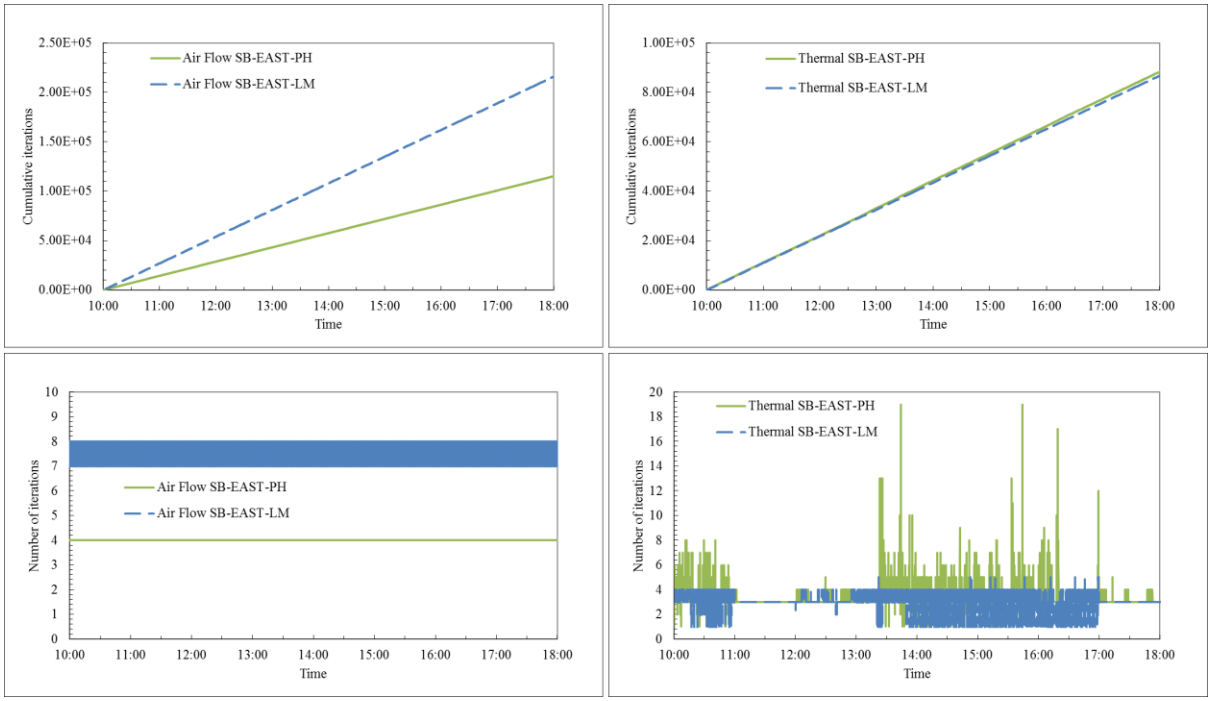

Figure 4-5. Comparison of the cumulative number of iterations and the number of iterations at each time step for the PH and LM methods in the air flow and thermal superblocks for the FCU in the east room. In the air flow superblock the LM method rapidly oscillates between seven and eight iterations, resulting in what appears to be a solid block.

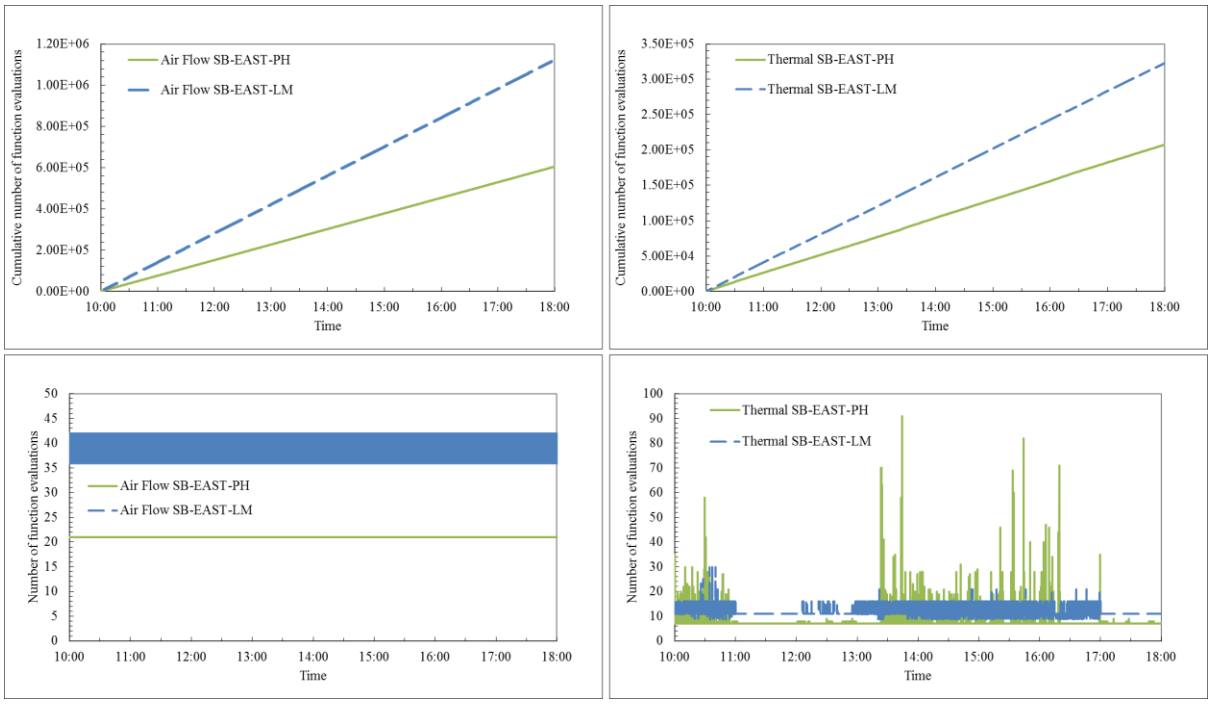

Figure 4-6. Comparison of the cumulative number of function evaluations and the number of function evaluations at each time step for the PH and LM methods in the air flow and thermal superblocks for the FCU in the east room. In the air flow superblock the LM method rapidly oscillates between seven and eight iterations, resulting in what appears to be a solid block.

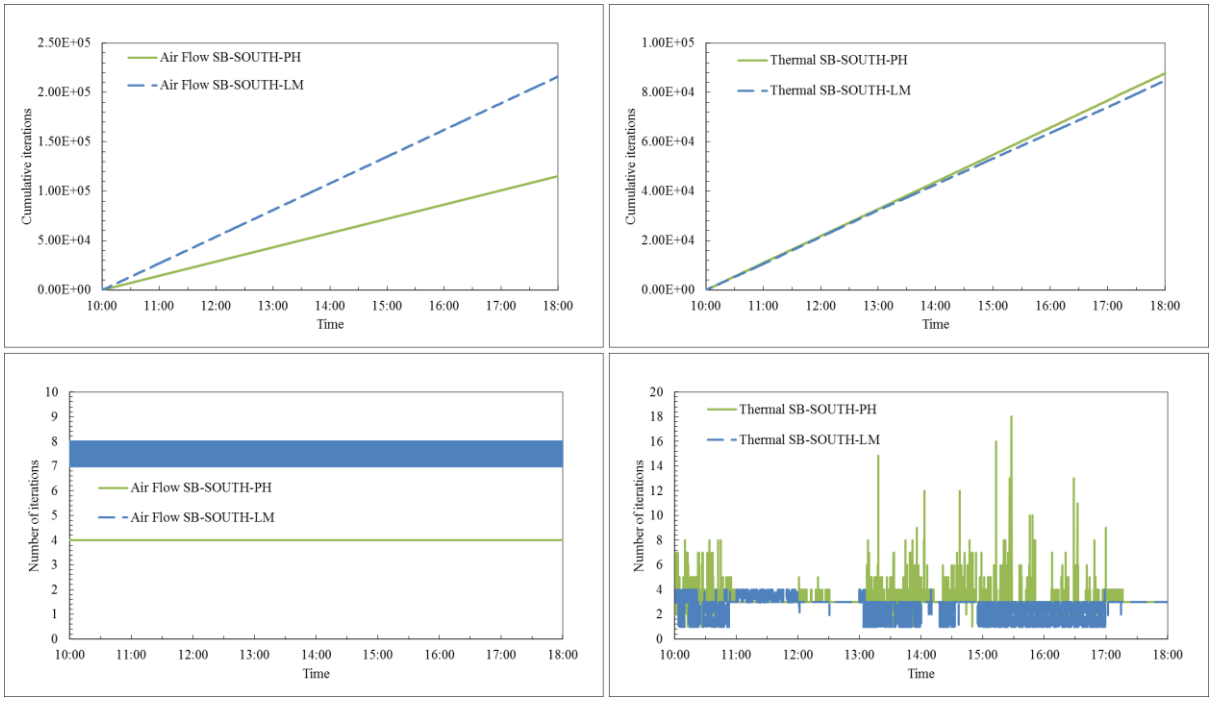

Figure 4-7. Comparison of the cumulative number of iterations and the number of iterations at each time step for the PH and LM methods in the air flow and thermal superblocks for the FCU in the south room. In the air flow superblock the LM method rapidly oscillates between seven and eight iterations, resulting in what appears to be a solid block.

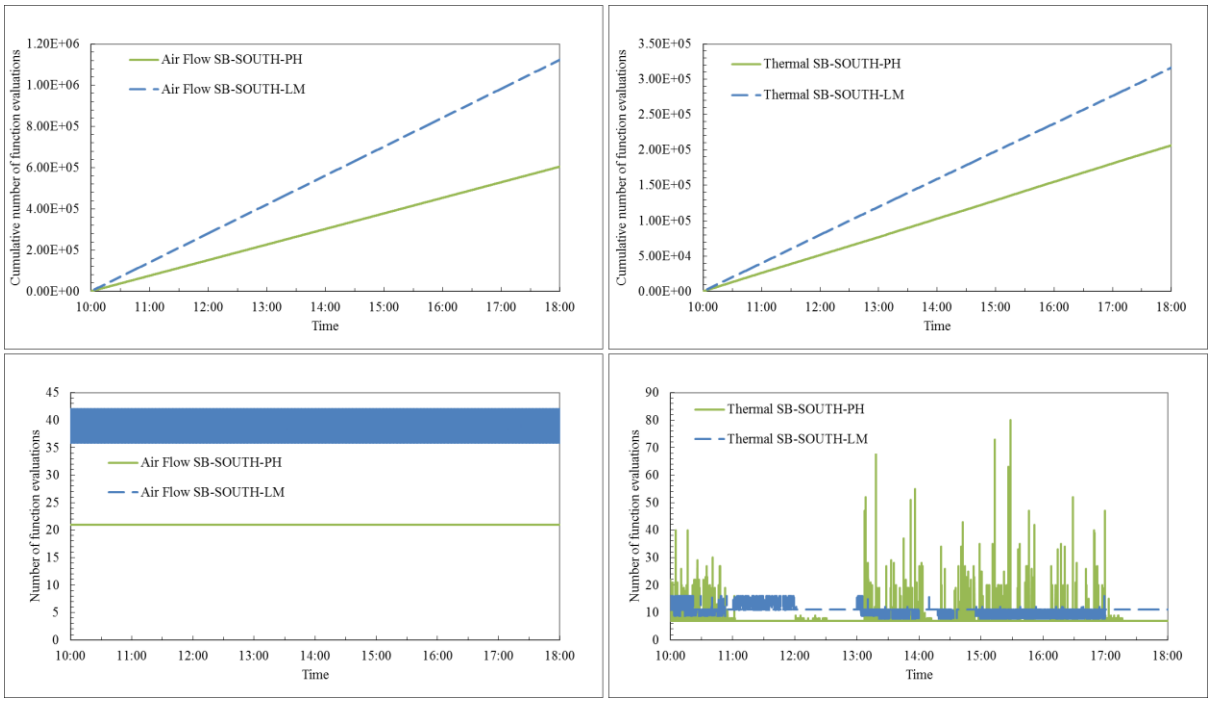

Figure 4-8. Comparison of the cumulative number of function evaluations and the number of function evaluations at each time step for the PH and LM methods in the air flow and thermal superblocks for the FCU in the south room. In the air flow superblock the LM method rapidly oscillates between seven and eight iterations, resulting in what appears to be a solid block.

4.4 Conclusion and summary

A qualitative difference between the LM and PH methods arises when a trial step fails to yield sufficient decrease in the residual of the nonlinear equations and the search direction must be altered. Many simple methods for solving nonlinear equations simply shorten the length of the search trial step in hopes that a shorter step will yield sufficient decrease of the residuals. Other more sophisticated techniques alter both the length and the direction of the trial step. In the case of LM, the μ parameter is increased and the resulting Eq. (4-6) is solved. This is the case even when a trial step with length less than that of the Cauchy step yields sufficient decrease in the residuals of the nonlinear equations and this trial step is an acceptable step. On the other hand, when PH computes a trial step, it is generated by augmenting or 'adding onto' the Gauss-Newton step. Once the Gauss-Newton step has been computed at a given point, the PH algorithm computes trial steps by changing the parameter Π. The PH algorithm, therefore, computes all trial steps, both successful steps and failed steps, without resolving the normal equations, (Eq. (4-7)). This is true even when a trial step with length less than the length of the Cauchy step is chosen to be the accepted step of PH. Where the LM method solves the normal equations, the PH method uses an approximation. This is the reason for the improvements in the LM method over the PH method, but it is also the reason why the LM method can be more computationally expensive.

An important computational issue that arises in the multiphysics framework of modelling buildings is that of preconditioning of nonlinear systems. This occurs when two or more component models are coupled with the goal of simulating events involving the output from these components. Many linear preconditoners exist for applications-specific linear systems; however, in the context of improving

HVACSIM+, greater improvement can be seen from considering directly the nonlinear system coupling components. Future research will focus on improving the problem formulation by developing and applying a preconditioner that is designed specifically for HVAC applications. This process will include creating a more uniform scaling across variables and ordering the solution of equations in a way that is numerically stable.

5. CHAPTER FIVE: MODIFICATION AND VALIDATION OF BUILDING ZONE MODEL

5.1 Introduction

The application of lumped parameter modelling methods to building dynamic thermal response is motivated by the desire to find simpler and, hence, computationally less expensive methods for the analysis building thermal energy response. Furthermore, this method simplicity and competence for full simulations including control system analysis and AFDD methods have been highlighted in the literature. Approaches broadly fall into two categories:

• Lumped parameter construction element models from which whole room models may be constructed (Gouda et al., 2002; Lorenz et al., 1982; Fraisse et al., 2002, Chaturvedi et al., 2002)

• Lumped parameter whole room models (Crabb et al., 1987; Tindale, 1993; Nielsen, 2005; Kampf et al., 2007; Antonopoulos et al., 2001)

Though the differences between the two approaches are rather subtle (since models of individual construction elements are almost always used as a basis for grouping or aggregating into whole room models), the treatment of individual elements usually provide greater detail in modelling information such as individual surface temperatures which can be important when dealing with radiant sources, etc.

Lorenz et al., 1982, were among the first to propose a simplified lumped parameter approach to building response modelling using a first-order model consisting of two resistances and one capacitor. Gouda et al., 2002, demonstrated improved accuracy using a second order model in which each construction element is described using three resistances and two capacitances. These approaches to modelling were often referred to as ‘analogue circuit’ models due to their similarity with electric circuits.

Fraisse et al., 2002, also compared first- and second-order element models (the latter referred to as a ‘3R2C’ model) and went further to propose a fourth-order ‘3R4C’ model with aggregated resistances. Like Lorenz et al. they propose an analytical method for deriving the parameters of the model (essentially, the distribution of resistance and capacitance values throughout the ‘circuit’) whereas Gouda et al. and Chaturvedi et al. used an optimization method to determine the parameters with reference to a rigorous reference model.

Crabb et al., Tindale, Nielsen et al. Kampf et al. and Antonopoulos et al. have applied the lumped parameter approach to the formulation of low-order whole room models by casting the capacitance parameter over the higher capacity elements of a room (external walls, solid floors, etc.) and using algebraic heat balances for the lower capacity room elements (demountable partitions, etc.). Tindale attempted this using a second-order room model but found that it provided unacceptable results for rooms with very high thermal capacity (i.e. ‘traditional’ construction). He corrected this by introducing a third ‘equivalent’ room capacitance which required an inconvenient method for its parameterization.

Though low-order whole room models offer very low computational demands and simplicity, there remain questions over the accuracy of these models particularly over long time horizons and they tend to provide less modelling information (i.e. individual and accurate element surface temperatures) essential in many lines of design enquiry. For this reason, it is argued that room models constructed from second-order (or higher) construction element descriptions provide greater accuracy and detail whilst retaining some of the key advantages of simplicity and low computational demand and are, therefore, to be preferred other than for approximate and early feasibility simulation studies. The key advantage of using lumped parameter

method to represent buildings is that they can be mathematically modelled by a set of first order differential equations; also called state-space systems. The integration of these systems provides the variables of the model (temperatures of building elements and zones) at a relatively low computational cost. The short computational times made these models popular during the 1970s when computational resources were limited. However they are still used when quick building simulators are needed to perform a large number of simulations (Coley et al., 2002; Kampf et al., 2009 and Kershaw et al., 2011). They are particularly suited to research-based building response modelling using either modular-graphical modelling tools or equation based methods and also to applications involving detailed systems, plant and control simulations requiring accurate short-term building model performance at minimum computer time.

5.2 Building Zone Thermal Model in HVACSIM+ Library of Component

Building zones characterized by a uniform temperature and a perfectly mixed volume (supposed to be thermally homogeneous) are modeled by TYPE 403 in HVACSIM+ library of components. In TYPE 403, each building zone is composed of two sets of Two-Capacitor–Three-Resistor (2C3R) LMP model (Norford and Haves, 1997, DeSimone, 1996). One set of 2C3R model represents the occupied space and the contents of the zone and the other set represents the corresponding plenum or unoccupied space and its contents (Figure 5-1). The two sets of 2C3R models are coupled together with a connecting resistance (R_{11}) which represents the ceiling separating the two spaces. As Figure 5-1 illustrates for each building zone, there are eleven parameters which need to be determined.

In Figure 5-1 the upper 2C3R network is representative of plenum and the lower one is room model the connecting resistance of the two networks (R_{11}) is

representative of ceiling. The constitutive resistances and capacitances of plenum 2C3R network are:

R_{21} represents light external wall and R_{22} and R_{23} are representative of proportioned structural resistances. C_{22} and C_{23} are internal and structural capacitance respectively.

Zone 2C3R network is composed of:

R_{01} represents light external wall and R_{02} and R_{03} are representative of proportioned structural resistances. C_{02} and C_{03} are internal and structural capacitance respectively.

Heat sources for zone directly added to the internal air node of zone network are lighting and equipment (Q_r) and occupant (Q_o) and HVAC heat gain (Q_v). Similarly heat gain in the plenum (Q_p) is added to the internal air node of the plenum network.

T_{pa} and T_{ra} are temperatures of the internal air and all light structures in the plenum and room model which are calculated in TYPE 403 as a weighted average, taking into account the influences of surrounding walls, the outside ambient air, leakage and infiltration from adjacent zones, and the supply air (Norford and Haves, 1997, DeSimone, 1996). T_p and T_r are plenum and zone structure temperature and T_{sa} is sol-air temperature.

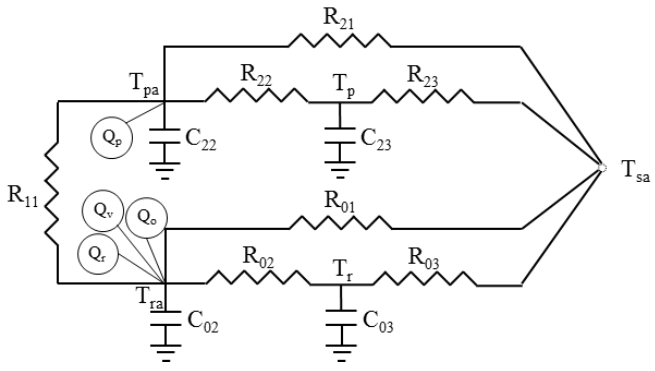

Figure 5-1. Illustration of a 2C3R model for a building zone (DeSimone,1996)

To determine the global parameters of 2C3R network, the resistances and capacitances of all individually identifiable walls, floor and ceiling components of the zone including internal, external and connecting walls are needed to be defined. The global model is an attempt to bring together a large number of individual systems in order to render a complex system into a simple network replicating the real behavior of the building zones. The details about the procedure and equations used to determine the resistance and capacitance of different constitutive components of the zone which consequently lead to determine the parameters for 2C3R global model are provided by DeSimone (1996) and are summarized here.

The individual walls are represented by two resistors and one capacitor. The thermal capacitance is located between the two thermal resistors at a location in the wall specified by a weighting factor θ_m. The walls are assumed to be comprised of "N" definable layers, each characterized by a resistive element and a capacitive element. Air boundary layers on both sides of the walls are accounted for as individual resistive elements, adding two additional resistors to the "N" wall layers combines for a total of "N+2" series resistors in each wall section. The "N+2" resistive elements are summed in series to obtain an overall resistance (Eq.(5-1)). The "N" capacitances are summed to obtain an overall capacitance (Eq.(5-2)), and the weighting factor is calculated by (Eq. (5-3)).

$$R_m = \sum_{n=0}^{N+1} R_{m,n} \tag{5-1}$$

$$C_m = \sum_{n=1}^{N} C_{m,n} \tag{5-2}$$

$$\theta_m = 1 - \sum_{n=1}^{N} \frac{\left(\sum_{p=0}^{n-1} R_{m,p} + \frac{R_{m,n}}{2}\right) C_{m,n}}{R_m C_m} \tag{5-3}$$

A time constant, expressed as a function of R_m, C_m and $\theta_{m.}$ in Eq. (5-4) is used to differentiate between light and heavy walls and sub-walls or structures.

$$\tau_m = \theta_m(1-\theta_m)R_m C_m \tag{5-4}$$

Where: $\tau_m \leq \tau_{limit} \rightarrow$light structure;

$\tau_m > \tau_{limit} \rightarrow$Heavy structure; and

the approximate limits for τ_{limit} are 1 hour $\leq \tau_{limit} \leq$ 2 hour.

Each of the resistive elements within the 2C3R zone model is defined as follows:

$$R_{01} = \frac{1}{K_{lite,ext}} \tag{5-5}$$

$$R_{02} = \frac{1}{K_{hvy,inner}}\theta_i \tag{5-6}$$

$$R_{03} = \frac{1}{K_{hvy,inner}}(1-\theta_i) \tag{5-7}$$

where $K_{lite,ext}$ is the conductance of internal structure directly to outside through light walls and $K_{hvy,inner}$ is the conductance of inner portion of heavy walls. The factor θ_i (global accessibility of structural capacitance) is expressed by,

$$\theta_i = \frac{K_{hvy,ext}}{K_{hvy,inner}} \tag{5-8}$$

where $K_{hvy,ext}$ is the conductance of heavy external wall. The conductance variables, $K_{lite,\ ext}$, $K_{hvy,\ inner}$, and $K_{hyy,ext}$ expressed in terms of composite resistance values are defined as follows:

$$K_{lit,ext} = \sum_m \frac{(1-H_m)E_m}{R_m} \tag{5-9}$$

$$K_{hvy,inner} = \sum_m \frac{H_m}{R_m \theta_m} \tag{5-10}$$

$$K_{hvy,ext} = K_{ext} - K_{lit,ext}; \text{ or} \tag{5-11}$$

$$K_{hvy,ext} = \sum_m \frac{E_m}{R_m} - \sum_m \frac{(1 - H_m)E_m}{R_m}$$

Where: E_m= 0 for each internal wall or connection sub-wall

E_m= 1 for each external wall

H_m= 0 for all wall or sub-walls with $\tau_m \leq \tau_{limit}$ (light walls)

H_m= 1 for all wall or sub-walls with $\tau_m > \tau_{limit}$ (heavy walls)

The time constant τ_i which characterizes the response to excitation for the zone system ascribed to each zone is expressed in the following equation:

$$\tau_i = \frac{1}{K_i} \sum_m (1 - \theta_m E_m) H_m C_m \quad (5\text{-}12)$$

The conductance K_i is defined as the overall loss coefficient and is expressed in terms of $C_{i,out}$ (the capacitive flow of infiltration in zone i based on the volumetric flow rate $V_{i,out}$ for infiltration) and K_{ext} (the overall loss coefficient for the heavy walls) in the following equations:

$$K_i = C_{i,out} + K_{ext} \text{ ; where} \quad (5\text{-}13)$$

$$C_{i,out} = \rho_a C_{pa} V_{i,out} \text{ ; and} \quad (5\text{-}14)$$

$$K_{ext} = \sum_m \frac{E_m}{R_m} \quad (5\text{-}15)$$

The infiltration volumetric flow rate $V_{i,out}$ is calculated by 0.37 CFM per feet of exterior window's sash crack (Pita, 2002).

The structural capacitance parameter $C_{03,i}$ represents the heavy structures in the zone model. It is expressed in terms of the overall heavy structure capacitance and a factor which characterizes the response of the 2C3R network to step changes in internal heat flux and outdoor temperature.

$$C_{03} = K_i \tau_i \frac{\left(1 - \frac{\xi_i K_i}{K_{eq,i}}\right)^2}{\left(1 - \frac{K_i}{K_{eq,i}}\right)} \tag{5-16}$$

The conductance $K_{eq,i}$ is described as the equivalent resistance for zone i and is expressed in the following equation:

$$K_{eq,i} = C_{i,out} + K_{lit,ext} + K_{hvy,inner} \tag{5-17}$$

and the term ξ_i is described as the ratio of heat loss through the light walls to the total heat loss to the outside:

$$\xi_i = \frac{C_{i,out} + K_{lit,ext}}{C_{i,out} + K_{ext}} \tag{5-18}$$

The internal capacitance parameter $C_{02,i}$ represents the light structures and the air contained within the zone. It is simply the sum of the represented thermal capacitance values:

$$C_{02} = C_{a,i} + \sum_m C_m (1 - \theta_m E_m)(1 - H_m) \tag{5-19}$$

The term $C_{a,i}$ represents the capacitance for the air within zone I ($\rho_{room\ air} C_{p,room\ air} V_{room\ air}$. The sum adds the entire contribution from the light, internal walls to a fractional contribution from the light, external walls.

In summary, for each building zone, there are eleven parameters (R_{01}, R_{02}, R_{03}, C_{02}, C_{03}, R_{11}, R_{21}, R_{22}, R_{23}, C_{22}, C_{23}) which need to be determined. To determine these eleven parameters, there are even more intermediate parameters that need to be calculated.

5.3 Solar Gains and Sky Radiation

Solar gains and sky radiation are expressed through the definition of an equivalent "sol-air" temperature $t_{sa,i}$. The overall, equivalent temperature represents an estimate of the energy flux across the external zone barriers. It is weighted average taking into account the effect of all incident radiation on all surfaces for each individual zone. Normally, weighting is derived from ratios of the conductance for the surfaces of similar optical characteristics and physical orientation within a given zone to the conductance for the entire external zone surface. The overall, equivalent sol-air temperature incorporating the effect of opaque surfaces, single pane windows and general barriers of any configuration is expressed in the following equation:

$$T_{sa,i} = \frac{\sum_m K_{ext,m}\, t_{sa,m,i,opaq}}{K_i} + \frac{\sum_m K_{ext,m}\, t_{sa,m,i,sing}}{K_i} \tag{5-20}$$

The conductance K_i and $K_{ext,m}$ are previously defined and the sol-air temperatures for the various barrier types are expressed as follows:

$$t_{sa,m,i,opaq} = t_{out} + \frac{1}{h_{out,m,i}}(\alpha_{m,i} I_{g,m,i} - \epsilon_{m,i} I_{r,m,i}) \tag{5-21}$$

$$t_{sa,m,i,sing} = t_{out} + \frac{1}{h_{out,m,i}}\left(\alpha_{m,i} I_{g,m,i} - \epsilon_{m,i} I_{r,m,i}\right) + \frac{\tau_{m,i} I_{g,m,i}}{U_{m,i}} \tag{5-22}$$

Where: $t_{sa,m,opaq}$= the sol-air temperature for an opaque wall

$t_{sa,m,sing}$ = the sol-air temperature for a single pane window

The coefficients included in Eqs. (5-21) and (5-22) are defined as follows:

$I_{r,m,i}$= the longwave heat transfer between the outer surface of wall m in zone i and the sky cover (W/m^2)

$I_{g,m,i}$= the shortwave solar gain on the outer surface of wall m in zone i (W/m^2)

$U_{m,i}$= the overall conductive heat transfer coefficient for wall m in zone i (W/°K m^2)

$\alpha_{m,i}$= the outer surface absorptance of wall m in zone i

$\varepsilon_{m,i}$= the emissivity of the outer surface of wall m in zone i

$\tau_{m,i}$= the transmittance of the outer surface of wall m in zone i

$h_{out,m,i}$= film coefficient for exterior surface of wall m in zone I (W/°K m^2)

t_{out}= outdoor air dry bulb temperature (°C)

5.3.1 Calculating the long-wave heat transfer

The heat flux $I_{r,m,i}$ across surface m can be expressed as a function of the long-wave (infrared) sky radiative transfer of a horizontal surface to the celestial surface and the angle s_m of surface m (measured from horizontal):

$$I_{r,m,i} = \frac{1 + \cos s_m}{2} I_{r,h} \qquad S_m < 90 \tag{5-23}$$

Where $I_{r,h}$ is defined as the long-wave sky radiative transfer of a horizontal surface. Typical values for $I_{r,h}$ range between 100 W/m^2 for clear sky condition to 45 W/m^2 for overcast conditions. When figuring what value to use, cloud cover data can provide a basis for factorization the difference between the two extremes. For $s_m = 90$ the value 0.5 $I_{r,h}$ is used.

5.3.2 Calculating the short-wave heat transfer

The total solar gain $I_{g,m,i}$ on the external surface of wall m is the sum of the direct solar radiation E_D, the total diffuse radiation E_d from the sky and ground and the solar radiation reflected from the surroundings E_r as follows:

$$I_{g,m,i} = E_D + E_d + E_r \tag{5-24}$$

where:

$$E_D = E_{DN} \cos \theta_v \quad (5\text{-}25)$$

And

$$E_d = E_{ds} + E_{dg} \quad (5\text{-}26)$$

With E_{DN} = the direct normal irradiance;

θ_v = the incident angle of the sun to the surface of wall m;

E_d = total diffuse radiation from the sky and ground;

E_{ds} = diffuse radiation from the sky;

E_{dg} = diffuse radiation from the ground;

5.3.3 Calculating the reflected solar radiation E_r

E_r is considered to be negligible for ERS building. Because, the building is open with an unobstructed view to all orientations.

5.3.4 Calculating the direct normal irradiance E_{DN}

For this project, direct normal irradiance is provided by the test facility and θ_v can be calculated following the procedure outlined in the next section.

5.3.5 Calculating the total diffuse radiation from sky and ground E_d

Here ASHREA handbook method is used to determine total diffuse radiation. Based on this method the diffuse sky radiation E_{ds} for vertical and horizontal surfaces can be expressed in terms of E_{DN}. some trigonometric relations relates to the orientation of the surface receiving the radiation, and a factor representing the degree of scatter introduced by the atmosphere as a function of the earth's relative position to the sun:

$E_{ds,vert} = C\ Y\ E_{DN}$; and (5-27)

$E_{ds,\sigma \neq 90} = C\ E_{DN} \frac{(1+\cos \sigma)}{2}$; where (5-28)

$$Y = 0.55 + 0.437\ \cos\theta + 0.313\cos^2\theta \quad \forall \cos\theta > -0.2; \tag{5-29}$$

Otherwise Y=0.45 (5-30)

And: C = Sky diffuse factor

The sky diffuse factor is a dimensionless ratio indicating the effect of the earth's relative position to the sun throughout the year, proportioning the effect of the direct normal irradiance as the season change. Values for C over the course of a year have been provided in ASHRAE fundamentals. It should be noted that this coefficient is affected by the local levels of smog, water vapor, and suspended dust in the atmosphere.

The diffuse radiation reflected from the ground is expressed as a function of the direct normal radiation:

$$E_{dg} = \frac{E_{DN}(C + \sin\beta)\rho_g(1 - \cos\sigma)}{2} \tag{5-31}$$

Where: C = Sky diffuse factor;

β = Solar altitude;

ρ_g = Ground reflectance; and

σ = receiving surface tilt angle from horizontal.

The coefficient C in this expression intensifies the effect of the direct normal irradiance as the season change. Again this effect is, in practice, subject to local variations in atmosphere conditions. The solar altitude β is calculated in Eq. (5-36). The ground reflectance is assumed to be 0.2. For this research, σ is equal to either 90 for vertical or 0 for horizontal surfaces.

5.3.6 Incident angle θ and solar altitude β

The incident angle θ_v can be expressed, in general for any surface orientation, as a function of the solar altitude β, the surface solar azimuth γ, and surface tilt angle σ as follows:

$$\cos\theta = \cos\beta\cos\gamma\sin\sigma + \sin\beta\cos\sigma \quad (5\text{-}32)$$

For vertical surfaces ($\sigma = 90$) and with γ expressed in terms of the solar azimuth ϕ and the surface azimuth ψ Eq. (5-32) becomes:

$$\cos\theta_v = \cos\beta\cos(\phi - \psi) \quad (5\text{-}33)$$

For horizontal surfaces ($\sigma = 90$) and with γ expressed in terms of ϕ and ψ Eq. (5-32) becomes:

$$\cos\theta_h = \sin\beta \quad (5\text{-}34)$$

The surface azimuth ψ is obtained from ASHRAE fundamentals, and the solar azimuth angle ϕ (a function of the solar altitude β, local latitude L, and the solar declination δ) can be calculated:

$$\cos\phi = \frac{\sin\beta\sin L - \sin\delta}{\cos\beta\cos L} \quad (5\text{-}35)$$

The solar altitude β is a function of local latitude L, solar declination δ and apparent solar time expressed as an hour angle H:

$$\sin\beta = \cos L\cos\delta\ \cos H + \sin L\sin\delta \quad (5\text{-}36)$$

$$H = 0.25 \times M_{number\ of\ minutes\ from\ local\ solar\ noon} \quad (5\text{-}37)$$

$$M_{number\ of\ minutes\ from\ local\ solar\ noon} = 720 - AST_{in\ minutes\ after\ midnight} \quad (5\text{-}38)$$

$$AST = LST + ET + 4(LSM - LON) \quad (5\text{-}39)$$

Where: LST = local standard time (minutes);

ET = the equation of time (minutes of time);

LSM= local standard time meridian (degrees of arc);

LON= local longitude (degree of arc);

4 = minutes of time required for 1.0 degree rotation of earth

5.4 The Issues Associated with the Zone Model in HVACSIM+ Library of Component

In order to investigate the zone model in HVACSIM+ library of component, TYPE 403 needs to undergo a close study as an isolated unit. For this reason, The inputs to the model which include supply air dry bulb temperature, humidity ratio and mass flow rate, ambient dry bulb temperature and humidity ratio, room and plenum sol-air temperatures as well as internal heat gain (occupant, light and equipment) need to be provided to the model from experimental data. The only output of the model which can be compared against experimental data is the room temperature which is also recorded at the test facility. A comprehensive study has been done to investigate the issues associated with the existing 2C3R model in HVACSIM+ component library. The outcome of this study is applied toward 2C3R zone model improvement.

5.4.1 Assumptions for zone model study

Originally in TYPE 403, all resistances and capacitances are assumed to be time invariant. Thus, the effect of varying wind velocity on external convection coefficients and room pressurization is not considered. Furthermore, TYPE 403 characterizes building zones by a uniform temperature and a perfectly mixed volume. In order to study the zone model as an independent unit some assumption has been made as following:

- No air leakage from/to outside
- No flow from/to adjacent zone 1 & 2
- No heat gain/loss from supply duct
- No heat gain/loss from return duct

5.4.2 Zone model comprehensive study

At the preliminary study the experimental data provided by ERS for fan coil unit in east, south and west facing rooms on a normal summer test day were picked to be fed to the model as inputs. Figure 5-2 illustrates the comparison of east, south and west facing rooms simulation result with experimental data on a summer test day (07.15.2012). The first graph at the top shows the ambient temperature and supply air temperature provided by FCU to each room. As this Figure demonstrates, there is a large deviation of the model results from experimental data for all rooms. While the provided supply air conditions and flow rate (0.421 kg/s (745 CFM)) to the rooms are the same as experiment, the modeled room is unable to keep room air temperature set point. Since fan coil unit is functioning in cooling mode, the room temperature is to be maintained at cooling set point temperature. In the legend of all following figures including this section and the next ones, CLGSTP and HTGSTP refer to cooling set-point and heating set-point respectively.

Figure 5-2 demonstrates that under the defined conditions based on the experimental data the simulated rooms get overcooled. The simulated room air temperature is representative of well mixed air within the room, but in reality the room temperature sensor may reflect a local temperature that is not necessarily reflective of a bulk room temperature. Furthermore, simulated zone is more sensitive to changes in internal load and fluctuations in supply air flow rate and temperature than the actual zone. As Figure 5-2 shows the simulated room temperature has

particularly sharp spikes in the absence and presence of equipment heat load at minutes 480 (presence), 720 (absence), 780 (presence) and 1020 (absence) (refer to Figure 5-3). The dynamics of the modeled zone display some deviation from the real one due in part to unavoidable simplification which needs to be thoroughly addressed.

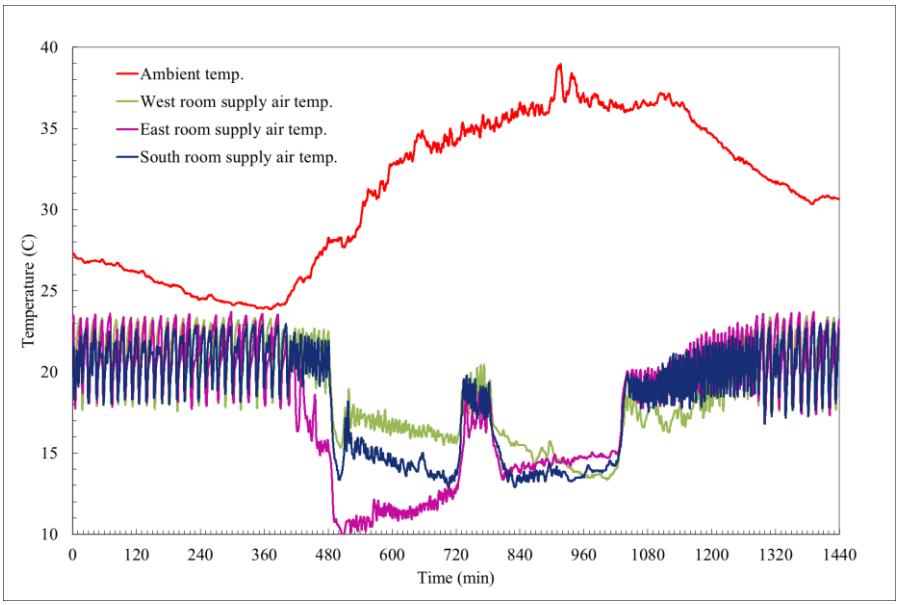

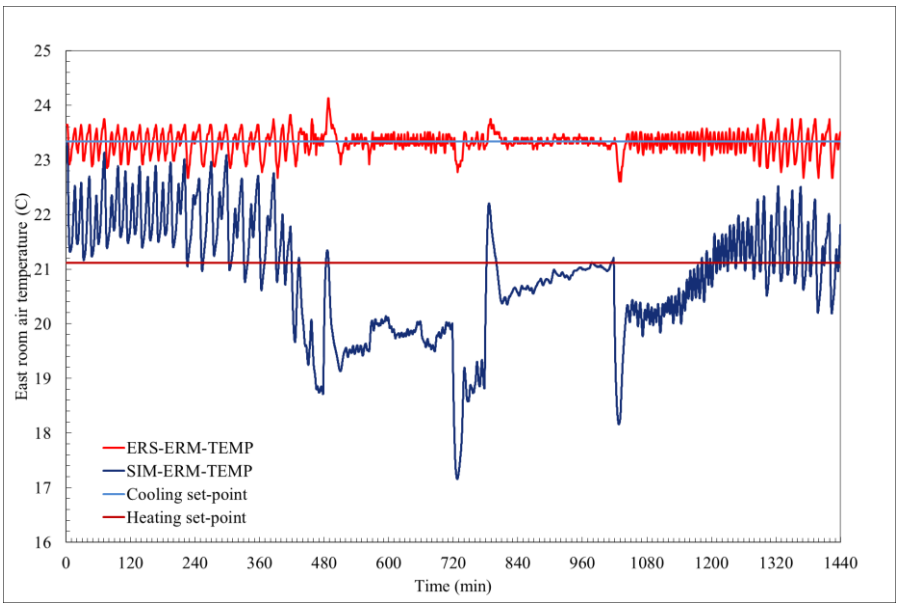

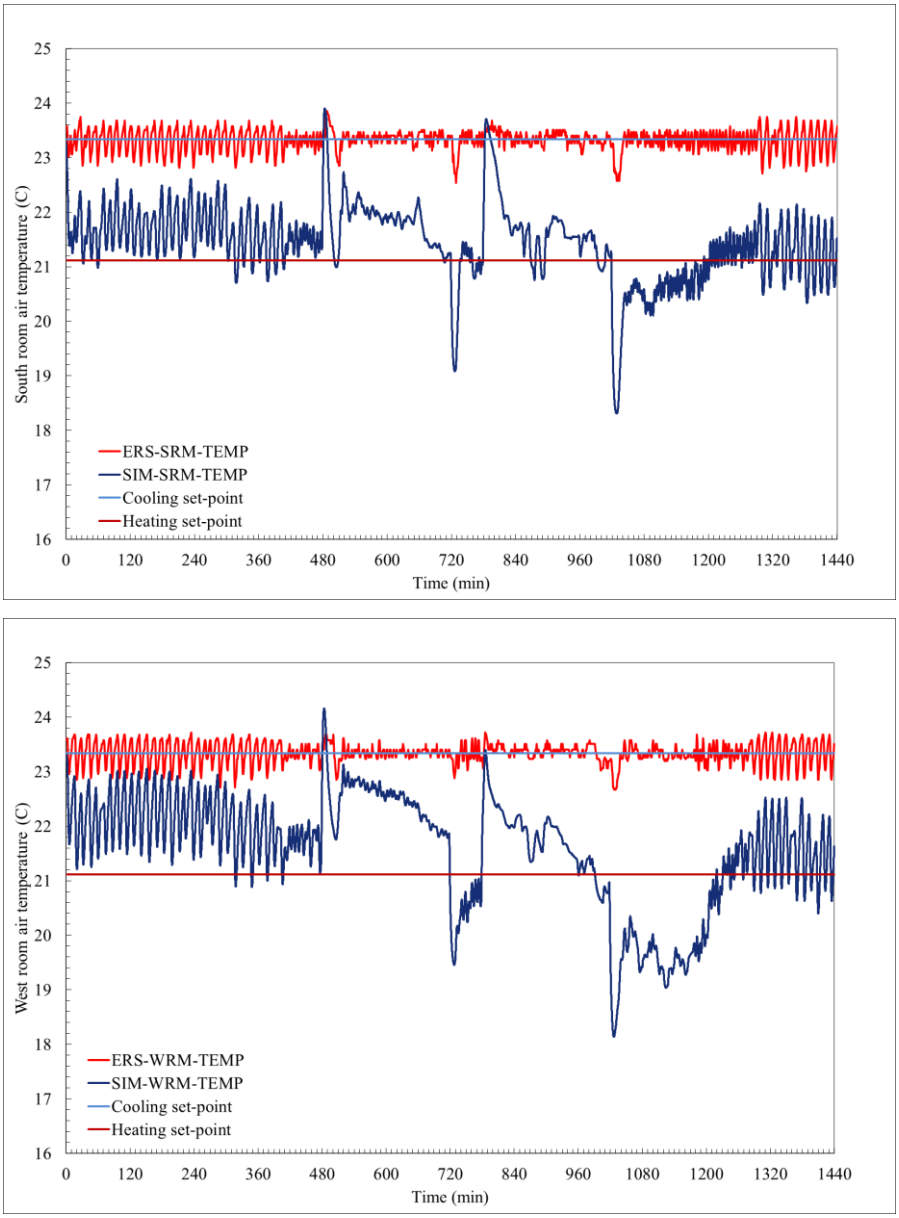

Figure 5-2. Comparison of simulation result with FCU experimental data for isolated zone model

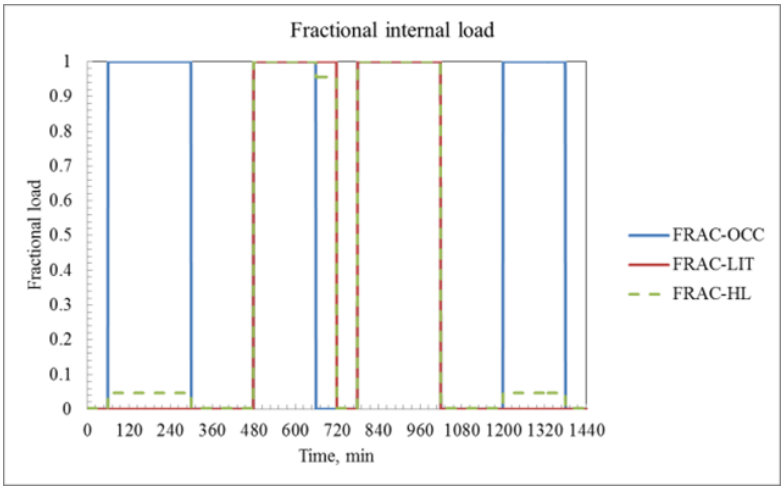

Figure 5-3. Fractional internal loads including occupant, lighting and equipment heating load as time dependent boundary conditions

Based on the comparison of the modeled zone results with real room temperature, a close observation in the following direction is needed:

1) Solar radiation through glazing: the existing 2C3R model does not consider the radiation received by the rooms through transparent surfaces
2) Optimizing the zone model physical parameters: as Figure 5-2 shows, the discrepancy of the zone model and experimental data at the beginning and late hours of the day cannot be related to the lack of the model in simulating the transmitted radiation. The main reason resides in the physical parameters of the zone model. It is partly due to the assumptions associated with the simulation and also the simplifications involved with the model to make it computationally efficient and feasible.
3) The uncertainty associated with the measured data: The uncertainty associated with sensors in collecting experimental data is unavoidable. As far as using experimental data as input to the model, this uncertainty propagates to the simulation as well as validation. For example, in the preliminary study the ERS experimental data collected for FCU has been used. The FCU supply

air temperature is recorded at one point. Obviously, in order to have a semi accurate supply air temperature the average of various point measurements at the outlet of FCU is needed.

5.4.2.1 Transmitted solar radiation through glazing

In the proposed 2C3R model for zone in TYPE 403 of HVACSIM+ the internal heat sources are confined to occupant, lighting and equipment heat loads which are directly added to the internal air node of zone network (refer to Figure 5-1). Most of the radiation heat received by the zone through the transparent surfaces is first absorbed by the internal surfaces, which include ceiling, floor, internal walls, furniture etc. Due to the large but finite thermal capacity of the roof, floor, walls etc., their temperature increases slowly due to absorption of radiant heat. The radiant portion introduces a time lag and also a decrement factor depending upon the dynamic characteristics of the surfaces. Due to the time lag, the effect of radiation will be felt even when the source of radiation, in this case the sun is removed. According to the literature using lumped parameter method particularly, Kampf et al., 2007; Xu et al., 2008; Braun et al., 2002; the transmitted solar radiation through the windows is considered as an internal heat source which is added to the internal air absorbed by space air and internal furniture. On the other hand, Chaturvedi et al., 2002, Cai et al. and Lee et al., 2008 denotes the transmitted solar radiation as a heat source added to the internal walls and floors. In the available model, sol-air temperature is calculated to represent exterior opaque surfaces heat exchange with the ambient. Sol-air temperature is the fictitious temperature of the outdoor air which, in the absence of radiative exchanges on the outer opaque surface of the roof or wall, would give the same rate of heat transfer through the façade as the actual combined heat transfer mechanism between the sun, the surface of exterior walls or roof, the outdoor air and

ambient. But the model lacks in incorporating the transmitted solar radiation through the glazing in zone model. Especially during the seasons with intense and longer exposure of the exterior rooms and windows to the sunshine, the role of transmitted radiation in the building zone load calculation cannot be ignored.

The objective is to incorporate the transmitted portion of solar radiation through transparent areas to the zone model as heat source. Two approaches are considered to treat transmitted solar radiation in the existing 2C3R model (refer to Figure 5-1):

1) As a direct heat source to the room node (Figure 5-4 (a))
2) As a direct heat source to the wall (structure) node (Figure 5-4 (b))

In Figure 5-4, Q_t is representing the transmitted solar radiation through glazing. For the first approach it is assumed that the total transmitted solar radiation is absorbed by room air (Eq. (5-40)) and for the second approach it is absorbed by the structure following Eq. (5-41) and then the stored heat is released to the room.

$$Q_t = \tau_{m,i} I_{g,m,i} * A_i \quad (5\text{-}40)$$

$$Q_t = \propto_i \tau_{m,i} I_{g,m,i} * A_i \quad (5\text{-}41)$$

Where

$\propto_i$= the effective solar absorptance of the zone i

$I_{g,m,i}$= the shortwave solar gain on the outer surface of wall m in zone i (W/m^2)

$\tau_{m,i}$= the transmittance of the outer surface of wall m in zone i

A_i= the surface area of window in zone i

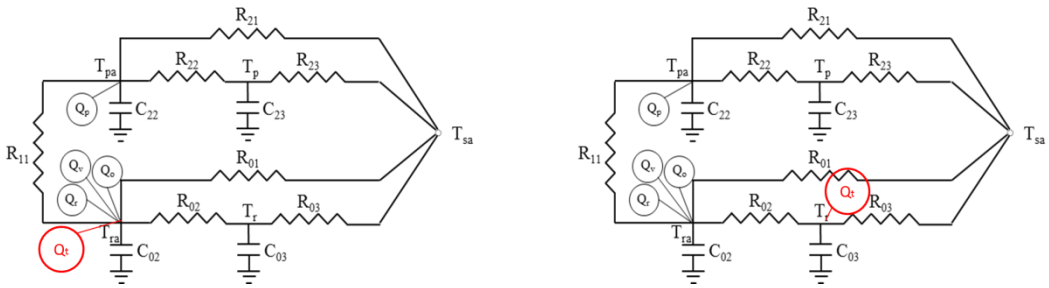

(a) Q_t as a heat source added to room air node

(b) Q_t as a heat source added to structure node

Figure 5-4. Two approaches to incorporate transmitted solar radiation through glazing to the 2C3R zone model

The results of modelling zone incorporating transmitted solar radiation utilizing both approaches are compared in Figure 5-5. As it shows adding the heat source to the room air node entails the instantaneous and sharp increase in the room air temperature. Whereas, by applying the transmitted solar radiation to the structure node the storage effect of building mass is also observable. As south and west facing rooms clearly show during their peak hours the added heat source causes a slow increase in room air temperature. Furthermore, the stored portion of radiation also plays a role in temperature increase after peak hours of solar radiation. It is what happened in reality even for light weight buildings so the second approach is followed here after.

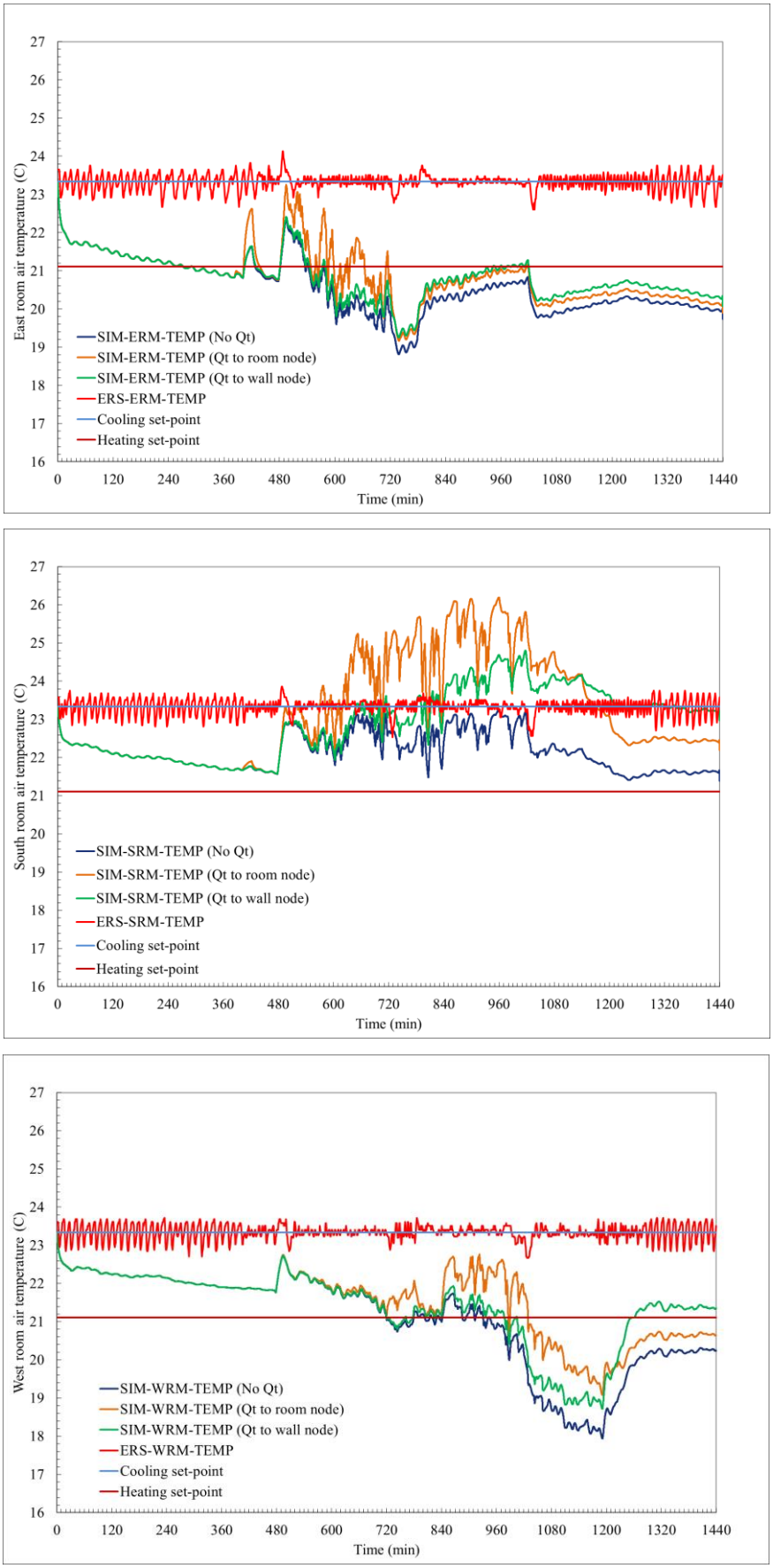

Figure 5-5. Zone simulation results comparison when transmitted heat is added to room air node and structure node

5.4.2.2 The uncertainty associated with the measured data

Uncertainty and inaccuracy associated with sensors in experimental data collection make its way into validation and especially for this case into simulation. In this case the inputs are directly fed to the zone model from experimental data. During the FCU model validation, we came up to the understanding that the measured supply air temperature is erroneous. On the other hand, supply air temperature as input plays a significant role in the prediction of zone model behavior. Therefore, dual duct system experimental data were found more reliable to be used for further detailed study although there are still some unavoidable inaccuracies in the sensor measurements. Table lists the accuracy of ERS measurements based on Lee et al., 2008.

Table 5-1. ERS measurements accuracy (Lee et al., 2008)

Name	Accuracy
Outdoor air temperature	± 0.1 ℃ (± 0.18°F)
Outdoor air humidity	$\pm 2\%$
Room temperature	± 0.14 ℃ (± 0.25°F)
Room supply air temperature	± 0.14 ℃ (± 0.25°F)
Room supply air flow rate (for exterior rooms)	$\pm 1.13\ {}^{m^3}/_{min}$ ($\pm 40\ CFM$)

There is also another source of inaccuracy regarding supply air temperature for dual duct VAV system measurements. In the VAV terminal unit, the proper proportions of hot and cold air streams are mixed before proceeding downstream to the space and the temperature sensor is right after the terminal unit. There is a hypothesis that due to inadequate space for the air streams to mix thoroughly, the supply air temperature sensor reading might be erroneous. The mixed air temperature

can be calculated given the air flow rate and temperature of each air stream, Eq. (5-42).

$$T_{mix} = (m_H * T_H + m_C * T_C)/(m_H + m_C) \quad (5\text{-}42)$$

Where, T_{mix} is the supply air temperature and m_H and T_H are flow rate and temperature of hot deck and similarly m_C and T_C are flow rate and temperature of cold deck.

In Figure 5-6, the calculated supply air temperature to east facing room on a summer test day is compared against the measured one. As it shows the supply air temperatures are not equal. Figure 5-7 compares zone model simulation results when the measured supply air temperature serves as input against feeding the simulation with the calculated supply air temperature as input. There is 0.8-1℃ difference between the results. In order to reduce the propagation of uncertainty in the simulation and validation the calculated supply air temperature is used to serve as input to the zone simulation.

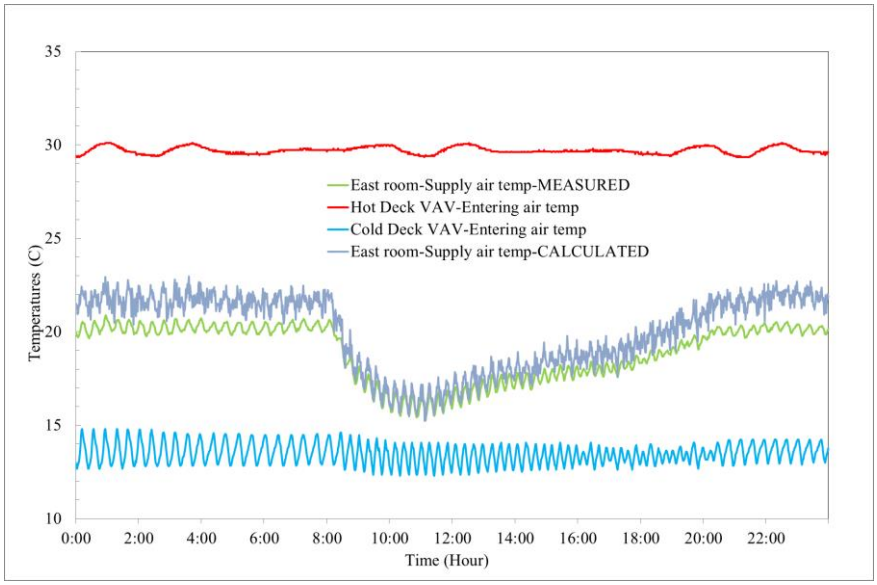

Figure 5-6. Comparison of measured and calculated supply air temperature to east room (06.02.2012)

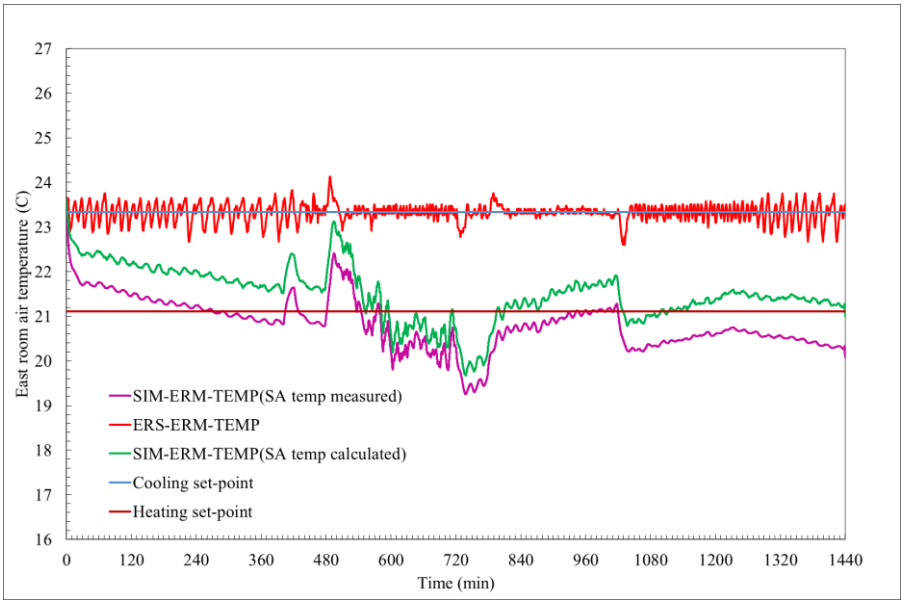

Figure 5-7. Simulation result comparison when the measured and calculated supply air temperatures serve as zone model input (06.02.2012)

5.4.2.3 Optimizing the zone model physical parameters

The early hours comparison of simulation results with experimental data strengthen the hypothesis of redefining the physical parameters describing the building zone dynamic. These parameters reflect the physical behavior and energy flows in the building structure. During the night hours when there is no solar radiation the discrepancy of the modeled room temperature and real one can be mostly due to the incorrect physical description of the building. Although the leakage and infiltration effects besides the other assumptions play a role here. In order to certify the necessity of redefining zone physical parameters through an optimization method; a sensitivity analysis is accomplished.

5.4.2.3.1 Sensitivity analysis

A brief sensitivity analysis was accomplished before concluding that the optimization is the last resort to modify the parameters of the zone which were borrowed from 1312 project. It is worth mentioning that the studies in this section are accomplished without treating the transmitted solar radiation. Figure 5-8 shows the

experimentally recorded supply air flow rate and temperature to the west-facing room and the calculated sol-air temperature on a summer test day (06.02.2012).

Figure 5-9 illustrates the west-facing room simulation results with the experimentally provided supply air flow rate and temperature. During the evening hours (minute 900-1260) when dual duct system provide ascending supply air flow rate with descending temperature to the room, simulated zone temperature is also descending. It implies that heat load of the zone during the evening hours and the HVAC system load are not in balance for the modeled zone. In another word, the modeled zone is mostly affected by the provided supply air flow rate and temperature rather than sol-air temperature. The same analysis was accomplished for other zones and various dates which led to the same conclusion. By these observations, a conclusion can be made that the conductivity of the modeled zone is higher than the real one so less responsive to sol-air temperature.

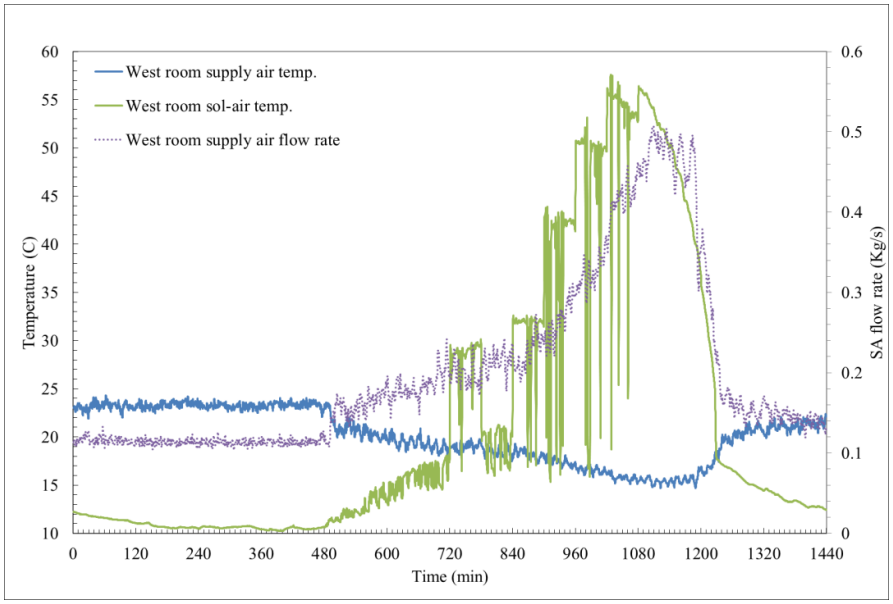

Figure 5-8. Supply air & sol-air temperature (left axis) and supply air flow rate (right axis) to west-facing room on 06.02.2012

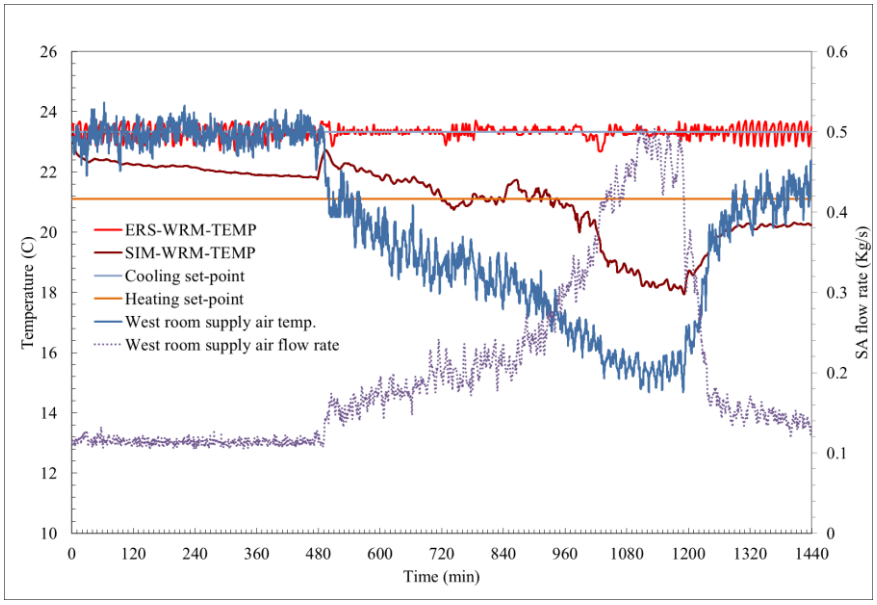

Figure 5-9. Sensitivity analysis of the modelled room temperature to the sol-air temperature and input experimental data (06.02.2012)

Further sensitivity analysis in the direction of improving zone model through physical parameter modification is to investigate the effect of R_{01} and C_{03} (refer to Figure 5-1). R_{01} directly reflects the effect of sol-air temperature fluctuations to the room air temperature. C_{03}, the capacitance of the zone mass, represents the thermal storage of the zone and the impact of stored heat in the room air temperature especially during and after the peak hours. Capacitance of the room mass node undergoes sensitivity analysis while the other parameters remain constant at the original values (based on 1312 project).

Figure 5-10 illustrates that effect of the capacitance of zone mass node (C_{03}) on the modeled room temperature. The navy blue line represents the west-facing room temperature with original parameters. Orange and light blue lines illustrate the modeled room temperature after increasing C_{03}. As C_{03} increases the room air temperature at the mid night and late in the afternoon gets closer to the real room temperature. The same sensitivity analysis was accomplished for the other zones (east

and south-facing) and another dates. All of them unanimously evidence that room mass capacitance is too low to reflect the thermal storage effect on room temperature. Increasing C_{03} alleviates the difference of the modeled and real room temperatures at the beginning and last hours of the day as well as dampening the temperature drop slope in 900-1200 minute. But the conductivity of the room is still too high to reflect the effect of intense solar radiation to the west-facing room on a summer evening test day. Now, a sensitivity analysis of the room temperature to R_{01} (direct resistance of the room air node to ambient) is needed to investigate the conductivity of the modeled room. Comparison of the simulated room temperature with varying R_{01} in Figure 5-11 while adjusting C_{03} to 1500000 demonstrates that the original zone model is highly isolated from ambient fluctuations. According to Figure 5-11 the more decrease in R_{01} the more dependency on sol-air temperature. By decreasing R_{01}, the room air temperature follow the trend of sol-air temperature (refer to Figure 5-8) and gets cooler in the mid night and warmer late in the evening.

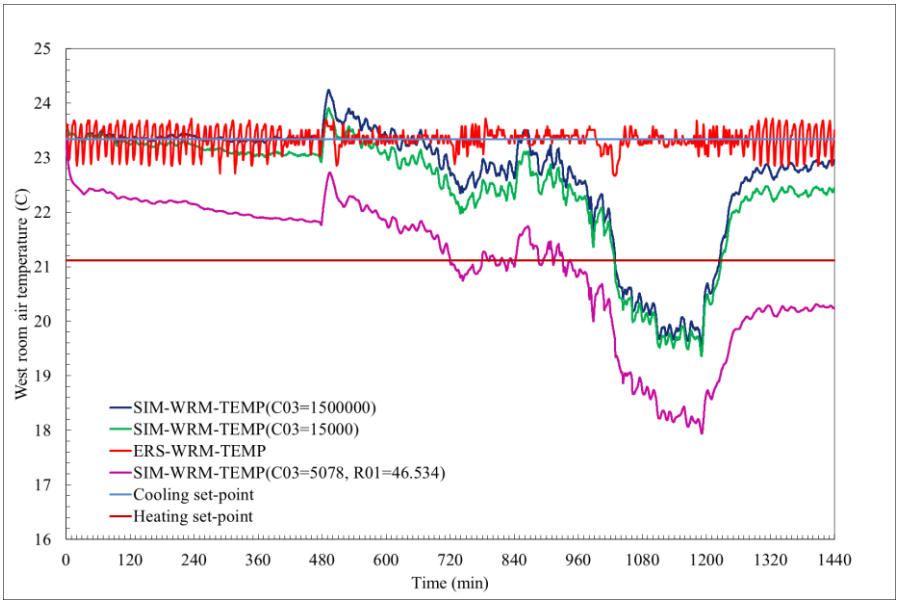

Figure 5-10. Sensitivity analysis of the modelled room temperature to the capacitance of room mass node (C_{03})

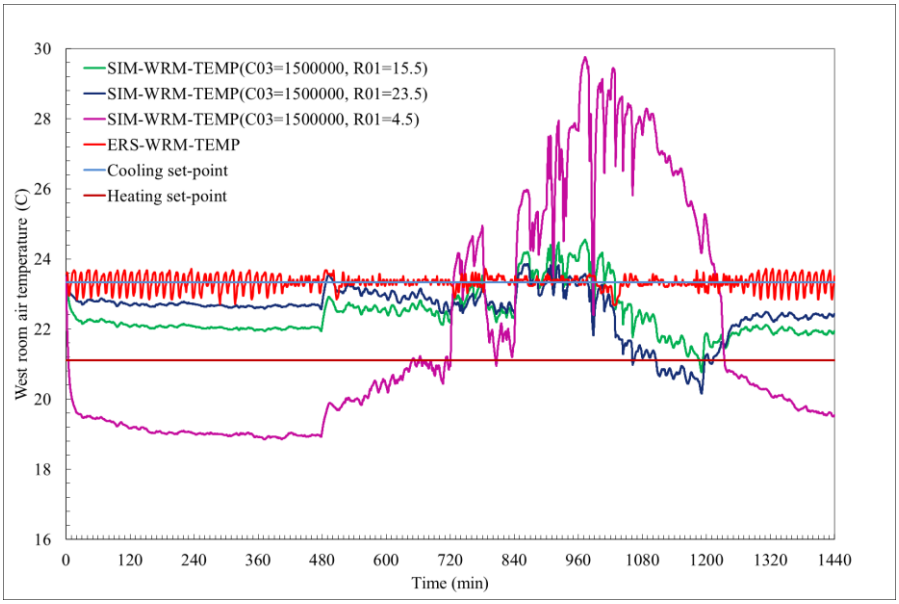

Figure 5-11. Sensitivity analysis of the modelled room temperature to the direct resistance of room air node to the ambient (R_{01})

5.4.2.3.2 Zone model physical parameters modification

The accomplished sensitivity analysis confirm that the adapted parameter from 1312 project do not properly reflect the building zone behavior and endorse their modification. In order to modify the parameters representing building zone dynamic pattern search algorithm is used. As Figure 5-1 shows four Cs and seven Rs need to be determined/ modified. The transfer functions representing the temperature of each node are derived as follows:

$$C_{02}\frac{dT_{ra}}{dt} = \frac{T_{pa} - T_{ra}}{R_{11}} + \frac{T_r - T_{ra}}{R_{02}} + \frac{T_{sa-r} - T_{ra}}{R_{01}} + Q_{HVAC} + Q_{sens-r} \quad (5\text{-}43)$$

$$C_{03}\frac{dT_r}{dt} = \frac{T_{sa-r} - T_r}{R_{03}} + \frac{T_{ra} - T_r}{R_{02}} \quad (5\text{-}44)$$

$$C_{22}\frac{dT_{pa}}{dt} = \frac{T_p - T_{pa}}{R_{22}} + \frac{T_{ra} - T_{pa}}{R_{11}} + \frac{T_{sa-p} - T_{pa}}{R_{21}} + Q_{sens-p} \quad (5\text{-}45)$$

$$C_{23}\frac{dT_p}{dt} = \frac{T_{sa-p} - T_p}{R_{23}} + \frac{T_{pa} - T_p}{R_{22}} \quad (5\text{-}46)$$

Where Q_{HVAC}, Q_{sens-r}, Q_{sens-p} are HVAC load, room and plenum sensible load and the window transmitted heat respectively. All of them are experimentally measures or calculated form experimentally recorded data.

Therefore, the thermal network of Figure 5-1 can be represented with a state-space model of the form of Eq. (5-47) with the following definition of state and input variables.

$$\frac{dX}{dt} = AX + BU \tag{5-47}$$

Where X is the state vector containing temperature of the nodes (room air and structure temperature as well as plenum air and structure temperature) and U is the input vector includes all of the important time varying driving conditions, such as zone and plenum sol-air temperature, room sensible load, HVAC load, plenum sensible load and solar radiation to the room through window.

$$X^T = \left[T_{ra}\ \ T_r\ \ T_{pa}\ \ T_p\right] \tag{5-48}$$

$$U^T = \left[T_{sa-r}\ \ T_{sa-p}\ \ Q_{sens-r}\ \ Q_{HVAC}\ \ Q_{sens-p}\right] \tag{5-49}$$

Matrices A and B are coefficient matrices calculated by the Rs and Cs. In this 2C3R model, A is a 4×4 matrix, B is a 4×5 matrix whose nonzero elements are determined as following:

$$\begin{aligned}
&A(1,1) = -\left(\frac{1}{C_{02}R_{01}} + \frac{1}{C_{02}R_{02}} + \frac{1}{C_{02}R_{11}}\right),\ A(1,2) = \frac{1}{C_{02}R_{02}},\\
&A(1,3) = \frac{1}{C_{02}R_{11}}\\
&A(2,1) = \frac{1}{C_{03}R_{02}},\ A(2,2) = -\left(\frac{1}{C_{03}R_{02}} + \frac{1}{C_{03}R_{03}}\right)\\
&A(3,1) = \frac{1}{C_{22}R_{11}},\ A(3,3) = -\left(\frac{1}{C_{22}R_{22}} + \frac{1}{C_{22}R_{21}} + \frac{1}{C_{22}R_{11}}\right),
\end{aligned} \tag{5-50}$$

$$A(3,4) = \frac{1}{C_{22}R_{22}}$$

$$A(4,3) = \frac{1}{C_{23}R_{22}}, A(4,4) = -(\frac{1}{C_{23}R_{22}} + \frac{1}{C_{23}R_{23}})$$

$$B(1,1) = \frac{1}{C_{02}R_{01}}, B(1,3) = \frac{1}{C_{02}}, B(1,4) = \frac{1}{C_{02}}$$

$$B(2,1) = \frac{1}{C_{03}R_{03}},$$

$$B(3,2) = \frac{1}{C_{22}R_{21}}, B(3,5) = \frac{1}{C_{22}} \quad (5\text{-}51)$$

$$B(4,2) = \frac{1}{C_{23}R_{23}}$$

Figure 5-12 shows the process for optimizing appropriate values for resistances (Rs) and capacitances (Cs) used for 2C3R zone model. These parameters are identified through the process of comparing the simulated zone temperature with the ERS measured zone temperature using a specific period of time. Initial guess values of the Rs and Cs are adopted from 1312 project. Physical description of the building including rough estimates of wall thicknesses, surface areas, and bounds on maximum and minimum thermal conductivity, specific heat, and density are required to set bounds on the Rs and Cs to establish a region within the parameter space for a global direct search. In addition, the orientations of external walls and windows are required, along with surface areas and transmittances of windows and solar absorptances for external surfaces. It is worth mentioning that transmittance of windows and absorbtances of external walls is considered constant in the calculation of room and plenum sol-air temperature and is not adjusted in the optimization duration. Zone temperature predicted by the model is defined by solving state-space equations (5-43)-(5-46). Here Pattern Searching optimization method is employed to update Rs

and Cs in order to minimize the integrated root-mean-square error defined as the objective function:

$$J = \sqrt{\frac{\sum_{j=1}^{N}\left(T_{calc,j} - T_{meas,j}\right)^2}{N-1}} \tag{5-52}$$

where N is the number of experimental data points or simulation time steps and the subscripts calc and meas denote simulated and measured temperature, respectively.

The evaluation of optimization is accomplished based on the following set up for pattern searching algorithm:

Maximum number of iteration: 500

Tolerance on mesh size: 1e-10

Tolerance on function: 1e-13 (Iterations stop if the change in function value is less than TolFun and the mesh size is less than TolX)

Tolerance on variables: 1e-7 (Iterations stop if both the change in position and the mesh size are less than TolX)

Maximum number of objective function evaluations: 1e10

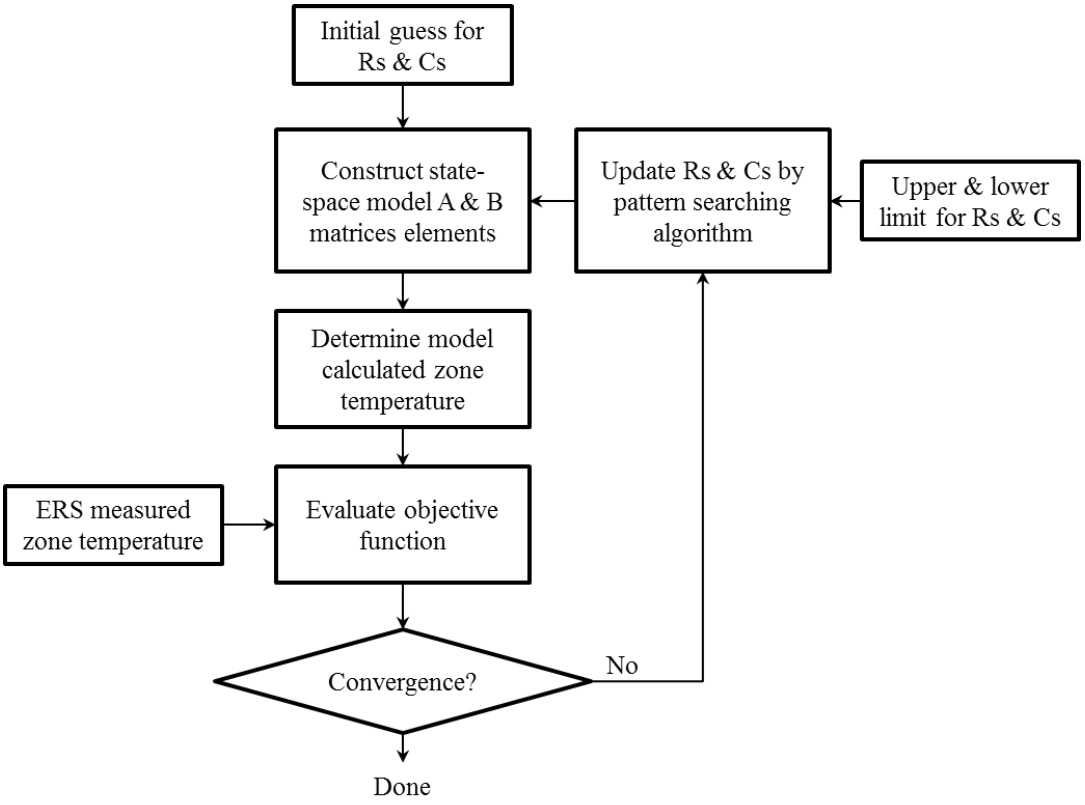

Figure 5-12. Algorithm for optimizing the 2C3R model parameters

Using experimental data for one test day in summer recorded every minute (1440 data points); the parameters of 2C3R model in HVASCIM+ library are modified. The performance of the 2C3R with the optimized parameters is evaluated using normalized root-mean-square (NRMS) errors as Eq. (5-53) and remodeling the zone with new parameters in HVACSIM+.

$$E_{rms} = \frac{100}{\left(T_{meas,max} - T_{meas,min}\right)} \sqrt{\frac{\sum_{j=1}^{N}\left(T_{calc,j} - T_{meas,j}\right)^2}{N-1}} \tag{5-53}$$

The modified parameters and NRMS for each east, south and west facing zones are summarized in Table 5-2.

Table 5-2. Modified parameters for 2C3R model

Zone	Resistances (K/KW)	Capacitances (Kj/K)	Error
East-facing zone	R_{01}=39.6094 R_{02}=2.3987 R_{03}=300.0581 R_{21}=1e+11 R_{22}=15.2225 R_{23}=100 R_{11}=4.9375	C_{02}=339.7012 C_{03}=35078 C_{22}=61.84 C_{23}=5000	NRMSE=5%
South-facing zone	R_{01}=45.4961 R_{02}=3.2425 R_{03}=500 R_{21}=1e+11 R_{22}=23.0428 R_{23}=200 R_{11}=9.5	C_{02}=241.3575 C_{03}=35078 C_{22}=23.3791 C_{23}=5000	NRMSE=2.7%
West-facing zone	R_{01}=15.5 R_{02}=3.4967 R_{03}=300 R_{21}=1e+11 R_{22}=21.3764 R_{23}=100 R_{11}=1.5	C_{02}=443.1354 C_{03}=35078 C_{22}=55.3595 C_{23}=4000	NRMSE=2.8%

Another summer test date (06.02.2012) is picked to run the zone model with employing the modified physical parameters. Figure 5-13 demonstrates the inputs provided to the zone model including zone and plenum sol-air temperatures, HVAC cooling load calculated by supply air flow rate and temperature and zones and plenum sensible heat load. Figure 5-14 compares the model predicted zone temperature when employing modified parameters and 1312 project adopted parameters against ERS measured zone temperature. The simulation results show a significant improvement toward predicting the building zone dynamic after optimizing the zone physical parameters. The NRMS for east, south and west facing rooms are 5%, 2.7% and 2.8% respectively.

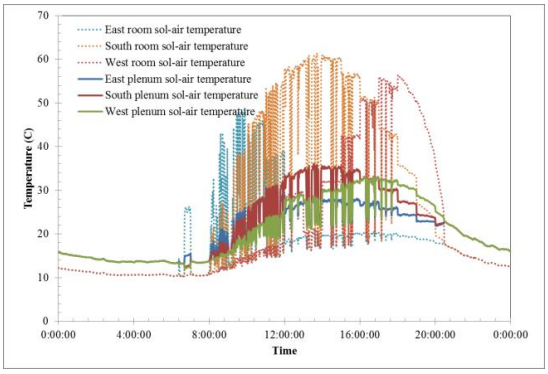

Exterior zones and plenums sol-air temperature

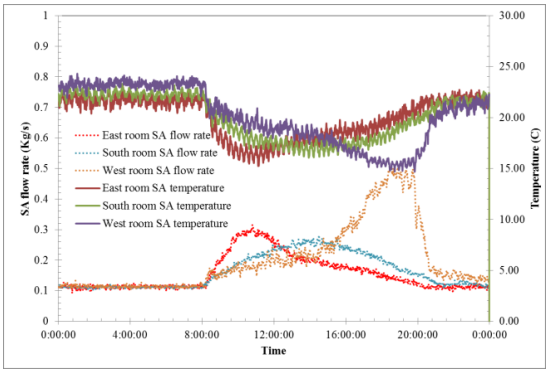

Exterior zones supply air flow rate and temperature

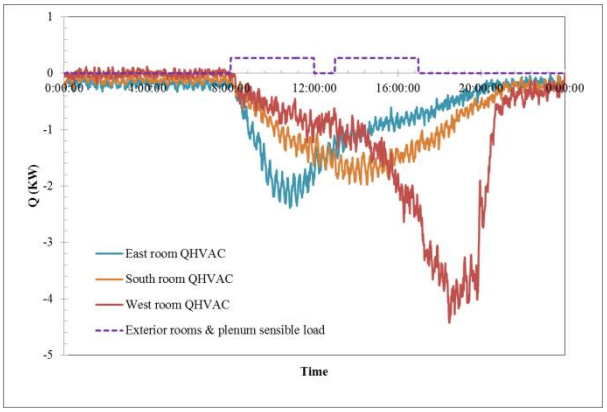

Exterior zones and plenums sensible load and the HVAC provided cooling load

Figure 5-13. The time-dependent input variables to the exterior zone models (06.02.2012)

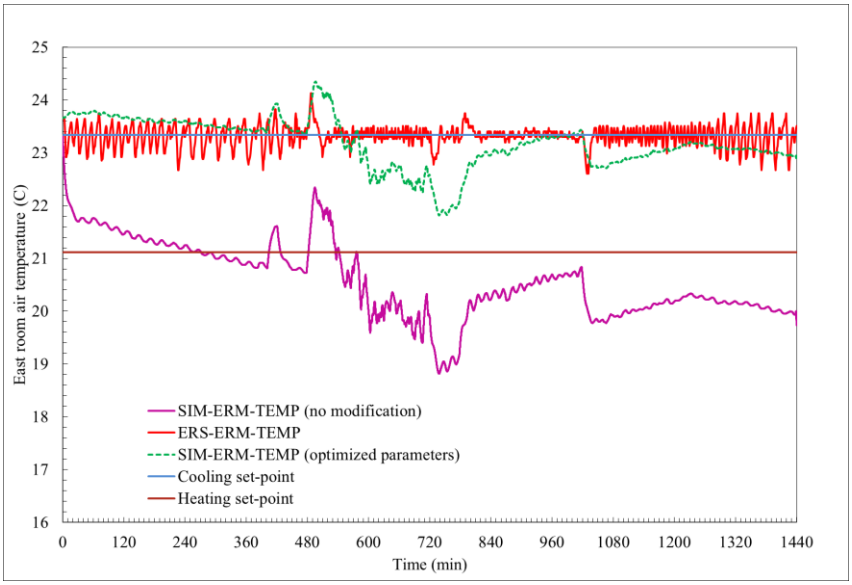

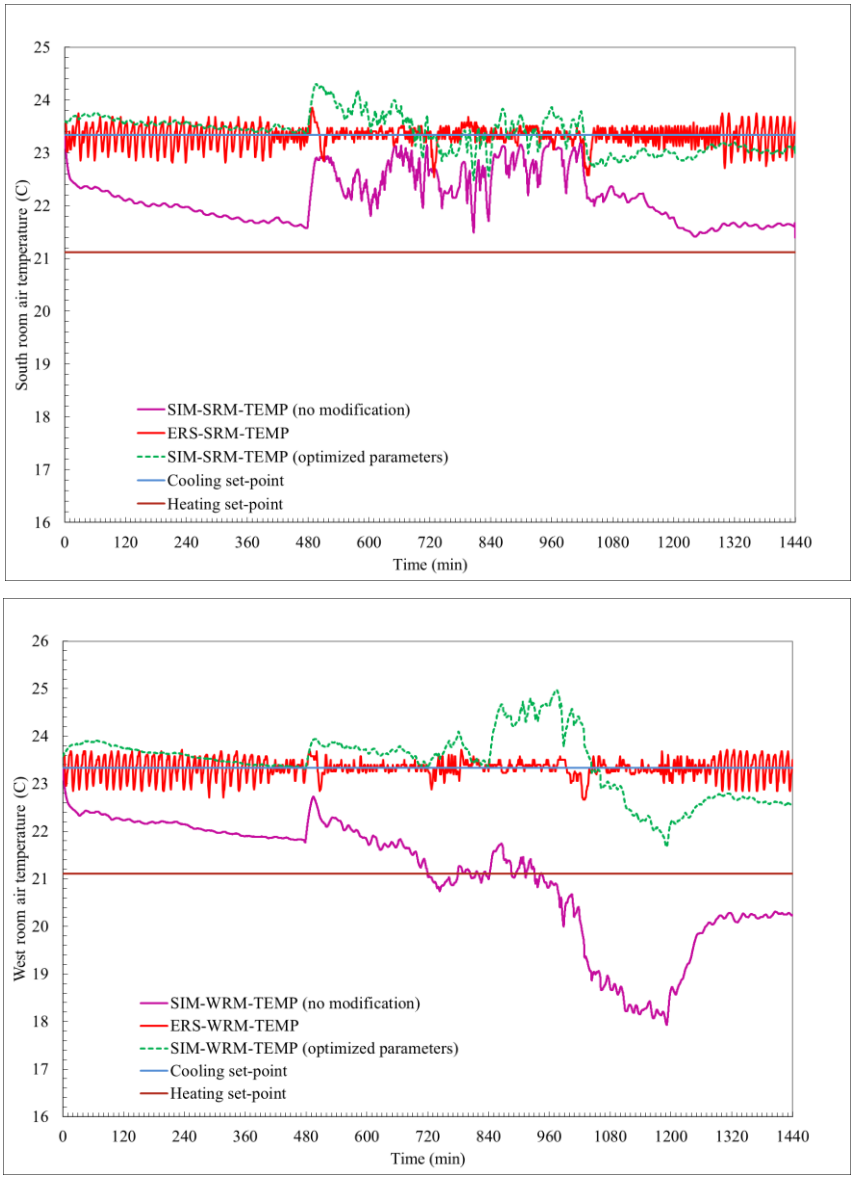

Figure 5-14. Simulation result comparison when physical parameters of the zone are modified with the unmodified parameters result (06.02.2012)

5.5 Results and Discussion

The final simulation regarding 2C3R model study is to model the zone with new parameters considering the transmitted solar radiation as a heat source to zone structure node. Figure 5-15 compares the modified zone model with new parameters and incorporated transmitted solar heat with the original one for a summer test day (06.02.2012). The modified model is still sensitive to internal load changes and also

the HVAC system load. But now it can balance between the internal changes and ambient fluctuations. The instantaneous and dampened effect of heat gain due to the solar radiation through glazing is observable from the results especially south-facing room temperature. Since the modified zone model has a high structural capacitance; time lag of heat gain is more obvious than its sudden effect. Especially south-facing room has a prolonged exposer with higher intensity to the sun. Therefore, the effect of load shifting to the evening hours gets more highlighted comparing with east and west facing rooms.

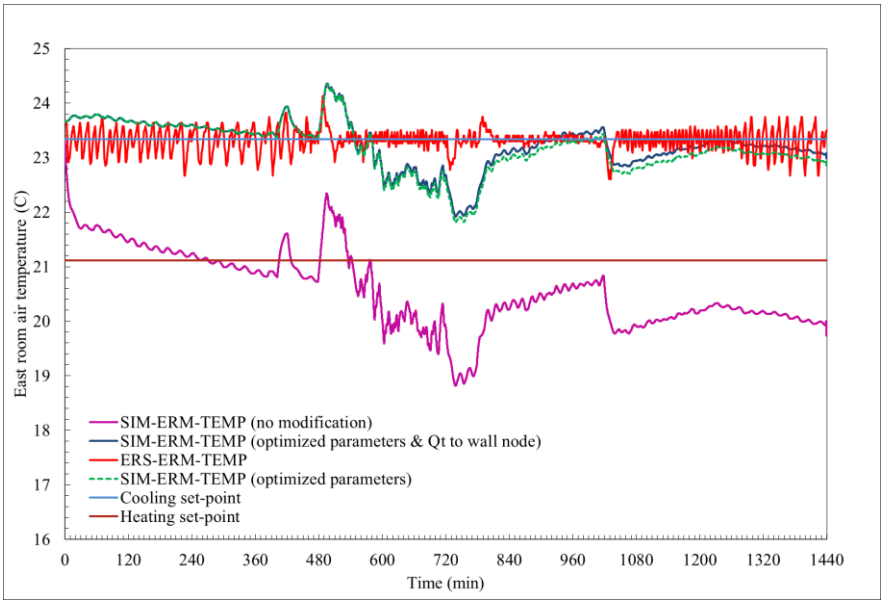

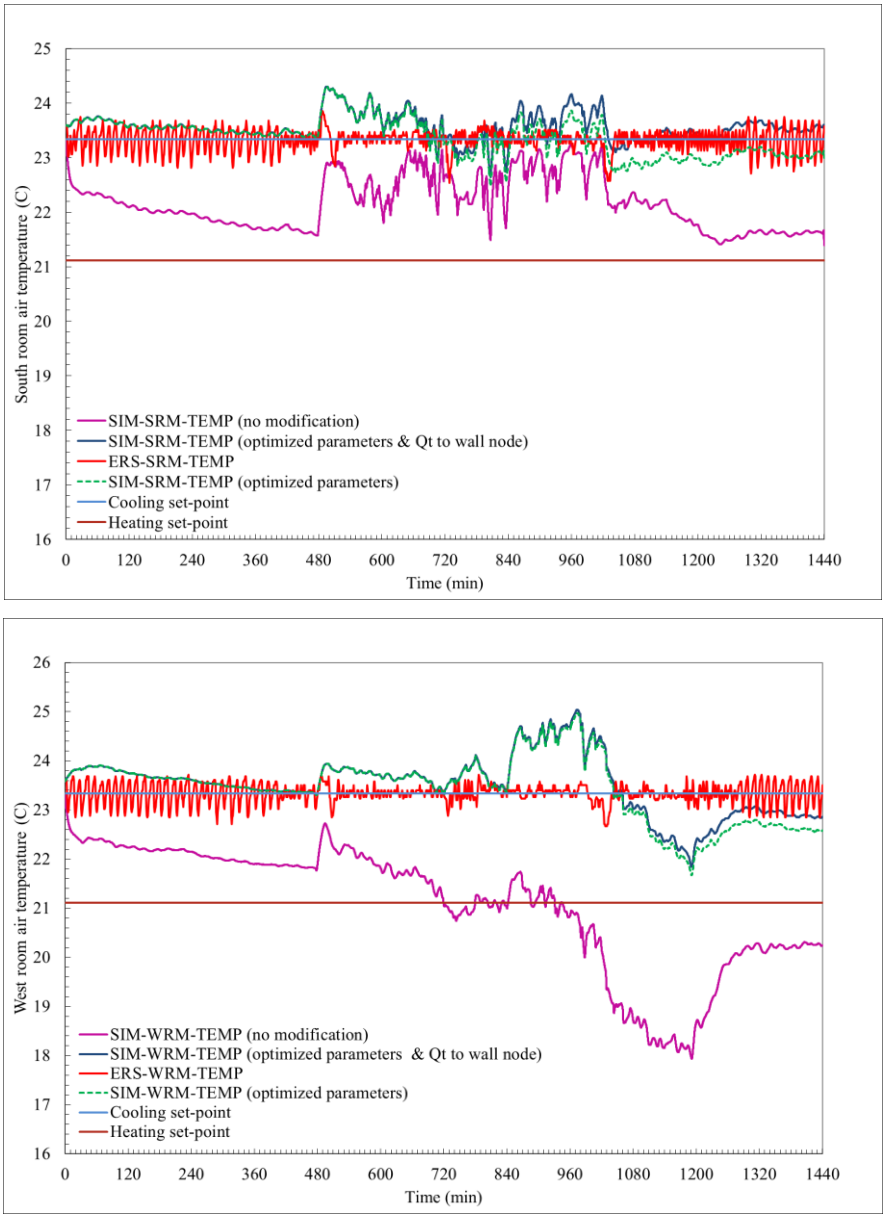

Figure 5-15. Zone model simulation results with new modifications for a summer test day

The parameters optimized based on a summer test day served as training data are used for modeling the zone on a winter test day (11.23.2012). The purpose of this simulation is to figure out whether the modified parameters also properly represent the building zone dynamic for a different weather condition. As Figure 5-16 demonstrates, although the modified model including the optimized parameters and incorporating the transmitted solar radiation enhance the simulation result accuracy; it

still deviates from the real zone dynamic. It should be reminded that the building zone model has some limitation in considering wind effect and room pressurization as well as considering Cs and Rs as time invariant. The wind plays a significant role in changing the air flow regime on the outer layer of the building as well as heat conduction coefficient. Therefore, the Rs and Cs obtained through training process by the applied optimization algorithm is unable to perfectly predict the building zone dynamic for all types of weather condition encountered in various seasons. To show these limitations associated with the available zone model (2C3R) a winter test day is demonstrated in Figure 5-16. Although the new model incorporating the modified parameters and transmitted solar radiation has been tested on a winter weather condition, the model is still unable to predict the dynamic of the zone accurately.

The accuracy of the modified 2C3R model has significantly improved in this study. Further improvement in the building zone model is required to make it capable of predicting the building zone dynamic for all weather conditions. Also, a more detailed lumped parameter method is required to cover the limitations associated with the current model as this model is just to approximate the building dynamic.

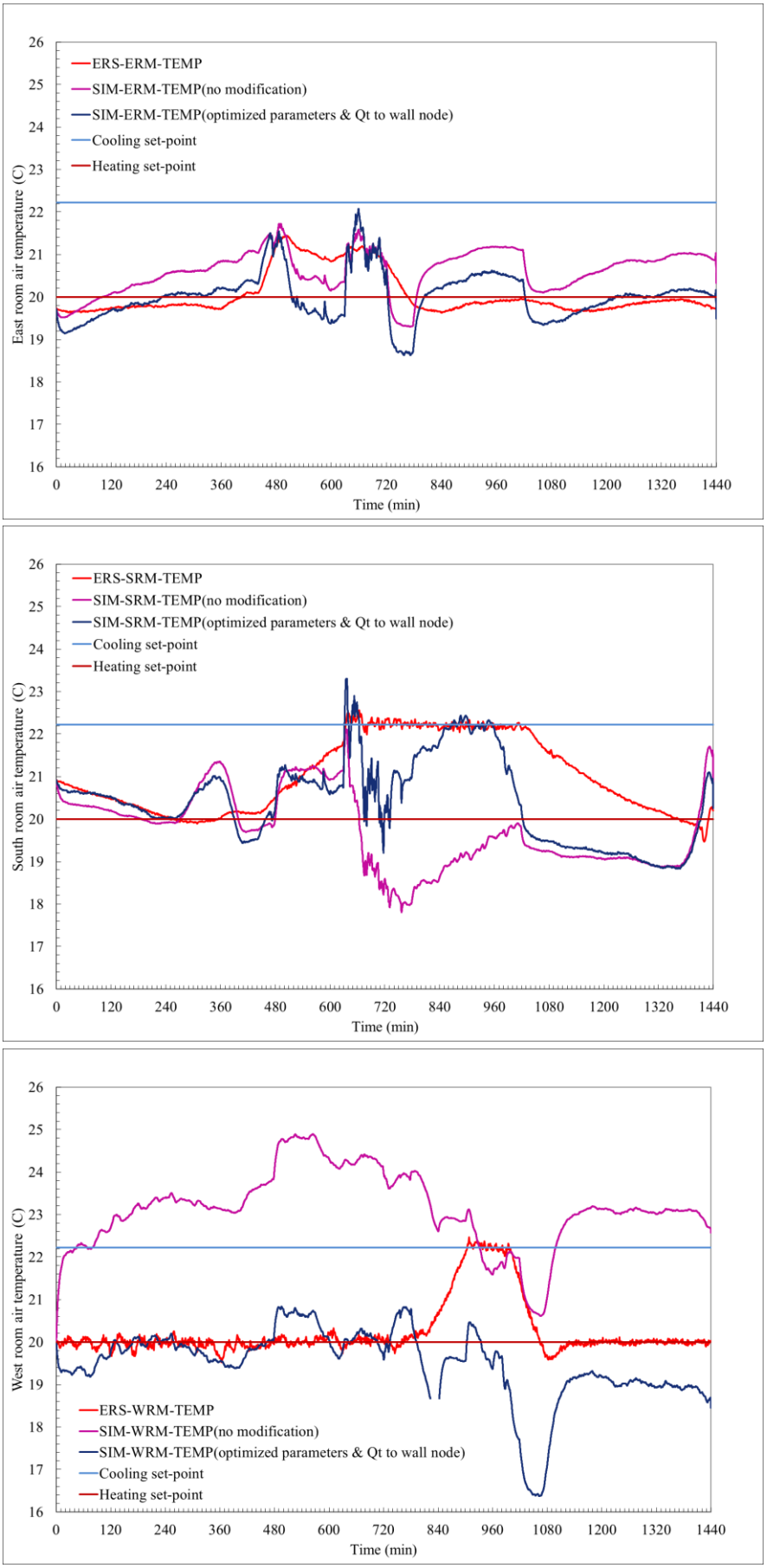

Figure 5-16. Zone model simulation results with new modifications for a winter test day

5.6 Conclusion and Summary

In this work the two time constant lumped parameter model employed in TYPE 403 of HVACSIM+ underwent a comprehensive study from different prospective to investigate the reasons of model results deviation from experiment. The inaccuracies associated with the model are partly due to the limitations of the model and partly due to the defined physical parameters for the building zone fabric, the uncertainty of the model inputs as well as the assumptions associated with the simulation. The accomplished sensitivity analysis indicated that the parameters representing the dynamic of zone envelope are highly insulating the zone from ambient air fluctuations and need to be redefined. Pattern searching algorithm employed for optimization of physical parameters with the objective function defined as minimizing the difference of model predicted zone temperature and the ERS measured one. Furthermore, the existing model lacks in considering transmitted solar radiation in load calculation. The final outcome of this study led to satisfactory results considering the limitations of the model which need to be addressed in future studies.

The 2C3R model with two time constants is computationally undemanding, but has limitations that may restrict its applicability to situations in which only an approximate treatment of the dynamics of the building envelope is required (ASHRAE RP 825). The approximations arise from combining the thermal capacity of high mass internal and external walls into a single node. The limitation of the model is the lack of a public domain computer-based procedure for calculating the resistance and capacitance parameters. If such a procedure were to become available, this extended model would be an attractive replacement for the basic two time constant model implemented here.

Therefore, a more accurate and also complicated zone model sacrificing the calculation time is required to capture the real dynamic behavior of the building reacting to ambient air with high frequency fluctuations. Furthermore, in the existing model the effect of fluctuating wind pressure on outside air flow rates and its convection coefficient and also room pressurization has not been considered. In the existing model, the internal heat gains due to lighting, occupant, equipment and etc. are considered as a convective component and their radiative portion is ignored. Another limitation of the existing model is to consider the windows transmittance time invariant while according to the literature it varies with incidence, Cai et al., 2012.

CONCLUSION

This thesis has developed testbeds in HVACSIM+ environment for two common secondary HVAC systems including fan coil unit and dual duct system. The prepared platform provides the user the possibility of dynamic simulation of these systems under fault-free and faulty condition. The generated operational data under fault-free and faulty conditions can be employed for the purpose of developing advanced control, operation, and fault detection and diagnosis techniques. The new approach adapted in this study for validation of large HVAC secondary systems has not taken hold in the existing literature and can emerge out as a new validation technique or procedure for researcher in the field. In the following the thesis is concluded with the summary of key achievements as well as a list of suggestions for future studies to enrich the work presented here.

Key Achievements:

1- A dynamic numerical model of a FCU has been developed as a single integrated component for inclusion in the component library of the HVACSIM+ simulation package by adding three new TYPEs to that library.

2- Validation of the FCU model started with component level validation, followed by validation of the model “installed” within an overall system. The experimental data provided by ERS in different seasons (summer, fall and winter) served as a reference to which simulation results were compared.

3- A fault flag system has been designed to give the model the flexibility to simulate various FCU faults modes with differing severities without the need to develop additional TYPEs.

4- A dynamic numerical model of a dual duct double fan system in a step by step approach has been developed. Four new components models (TYPE) which three of them representing the air flow state and one of them representing the control sequence of VAV dual duct terminal units have been created for inclusion in the component library of the HVACSIM+ simulation package.

5- Due to the complexity of air flow network of dual duct system, this secondary system model development started with creating a model structure for the air flow states of dual duct systems that would result in robust dynamic simulations.

6- Validation of dual duct double fan system has been accomplished in three independent steps: Air flow network validation, air flow and thermal network validation and the entire system validation. The required time dependent boundary variables for each step of validation have been fed to the model using experimental data provided by ERS. The key components in each network also underwent component level validation employing experimental data provided by ERS.

7- The designed fault flag system has been extended to include the potential faults of dual duct double fan system. System model underwent a comprehensive fault matrix and validated well against experimental data establishes its validity to serve as a tool for evaluating dual duct double fan system fault detection and diagnostic methods.

8- A numerical study has been performed to compare two solution techniques: Powell's Hybrid (PH) and Levenberg-Marquardt (LM) in terms of their robustness and accuracy. In this study, the PH algorithm, as implemented in

SNSQ, is replaced by the LM algorithm to solve the identical problem. In this numerical study, the developed dynamic model for FCU interacting with a building zone underwent investigation. We found out that the LM method outperform PH in robustness and accuracy in the expense of more computational efforts.

9- In order to adapt an accurate, robust and reliable solution method to solve the system of nonlinear algebraic equations emerged from the developed testbed two numerical methods underwent a thorough study. For this purpose, a numerical study has been performed to compare two solution techniques: Powell's Hybrid (PH) and Levenberg-Marquardt (LM). This study finds considerable computational benefits result from replacing the Powell's Hybrid method solver in HVACSIM+ with a solver more appropriate for the challenges particular to numerical simulations of buildings. Evidence has been provided that a variant of the Levenberg-Marquardt solver has superior accuracy and robustness compared to the Powell's Hybrid method presently used in HVACSIM+.

10- Dynamic simulation of the secondary HVAC systems unavoidably requires an interacting zone model, including systemic interactions with the building's surroundings. Since the zone model and its dynamic directly affect the performance of HVAC systems, the deficiencies of the available building zone model in HVACSIM+ library of components need to be addressed. The work presented here has thoroughly investigated the 2C3R method used in HVACSIM+ in order to modify the building zone model accuracy.

Future Works:

1 Improve the solver robustness and accuracy:

An important computational issue that arises in the multiphysics framework of modelling buildings is that of preconditioning of nonlinear systems. This occurs when two or more component models are coupled with the goal of simulating events involving the output from these components. Many linear preconditoners exist for applications-specific linear systems; however, in the context of improving HVACSIM+, greater improvement can be seen from considering directly the nonlinear system coupling components. Future research will focus on improving the problem formulation by developing and applying a preconditioner that is designed specifically for HVAC applications. This process will include creating a more uniform scaling across variables and ordering the solution of equations in a way that is numerically stable.

2 Improve the validation procedure for HVAC system components:

For some components the provided experimental data are scarce, sparse and inadequate to entirely and accurately cover the operational conditions of the devise /component. Even, for some cases collecting experimental data due to inaccessibility of the component is challenging. Given enough experimental data for training the component model under different operational conditions along with employing an optimization method would help to improve the accuracy of parameter determination process for the constituent components of a HVAC secondary system. Further accuracy in parameter estimation for detailed modeling such as the work documented here lead to more accurate and reliable simulation results.

3 Replacement or improvement the 2C3R zone model:

The model used in HVACSIM+ is just for approximating the dynamic response of the building to the ambient. Aggregating the entire building mass and envelope in two nodes would definitely cause to lose the accuracy of the model in responding to the surrounding with high frequency in fluctuating and variation. A more complicated model with further degree of freedoms is needed to capture the building behavior.

The existing model considers constant resistances for all seasons and weather condition for the zone envelope. The wind and room pressurization affect the inside and outside flow rate and consequently the convection coefficients of inside and outside. The existing model needs to be revised as these effects have considerable impact on the simulation results accuracy.

4 Creating a data base for the fault symptoms:

The symptoms associated with various faults simulated in this work and the previous projects can be collected in a data base for the fault diagnosis purposes.

LIST OF REFERENCES

Antonopoulos, K.A., E.P. Koronaki, 2001. On the dynamic thermal behavior of indoor spaces, Applied Thermal Engineering 21: 929–940.

Ardehali, M.M., T.F. Smith, J.M. House, and C.J. Klaassen. 2003. "Building Energy Use and Control Problems: An Assessment of Case Studies," ASHRAE Transactions, Vol. 109, Pt. 2.

ASHRAE. 2008. ASHRAE Handbook-Systems & Equipment, Chapter 12. Atlanta: American Society of Heating Refrigeration and Air Conditioning Engineers, Inc.

ASEAM 3.0, 1991. A Simplified Energy Analysis Method, U.S. Department of Energy, Washington, D.C.

Ayres, J. M., and E. Stamper. 1995. "Historical Development of Building Energy Calculations," ASHRAE Transactions, 101(1), pp. 31 – 38.

Bunn R. (ed.), 1995. Main feature—dynamic thermal simulation. Building Services; 17(1): 23–8.

Bendapudi, S., and J. E. Braun, 2002. Development and Validation of a Mechanistic, Dynamic Model for a Vapor Compression Centrifugal Liquid Chiller, Report #4036-4, Deliverable for Research Project 1043-RP, ASHRAE, Atlanta, GA.

Bloomfield, D.P. 1999. "Overview of Validation Methods for Energy and Environmental software," ASHRAE Transactions, 105, pp. 685-693.

Bourdouxhe, J. P., M. Grodent and J. Lebrun, 1998. Reference Guide for Dynamic Models of HVAC Equipment, ASHRAE, Atlanta, GA.

Brandemuehl, M., 1993. HVAC 2: Toolkit for Secondary HVAC System Energy Calculations, ASHRAE, Atlanta, GA.

Braun, J. E., and X. Zhou, 2004. A Dynamic Forward Model for Chilled Water Cooling Coils, Interim Report, ASHRAE Research Project 1194 – RP, ASHRAE, Atlanta, GA.

Broderick, C. R., and Q. Chen, 2001. "A Simple Interface to CFD Codes for Building Environment Simulations," Seventh International IBPSA Conference, pp. 577 – 584, August, Rio de Janeiro, Brazil.

BSL, 1999. BLAST 3.0 Users' Manual, Building Systems Laboratory, Department of Mechanical and Industrial Engineering, University of Illinois, Urbana-Champaign, IL.

Bushby, S. T., N. Castro, M. A. Galler, and C. Park, 2001. "Using the Virtual Cybernetic Building Testbed and AFDD Test Shell for AFDD Tool Development," NISTIR 6818, National Institute of Standards and Technology, Gaithersburg, MD.

Cai, J. and Braun, J.E., 2012. "An Efficient and Robust Training Methodology for Inverse Building Modeling", SimBuild 2012.

Castro, N. S., Schein, J., Park, C., Galler, M. A., Bushby, S. T., and J. M. House. 2003. Results from simulation and laboratory testing of air handling unit and variable air volume box diagnostic tools, NISTIR 6964, National Institute of Standards and Technology, Washington, DC.

CEC, 1999, Performance Assessment and Adoption Processes of an Information Monitoring and Diagnostic System Prototype, Contract 500-97-013 Final Report, California Energy Commission.

Chaturvedi N, JE. Braun, 2002. An inverse grey-box model for transient building load prediction. International Journal of HVAC&R Research, 8(1): 73–100.

Chu, C. M., Jong, T. L., and Y. W. Huang. 2005. Thermal comfort control on multi-room fan coil unit system using LEE-based fuzzy logic. Energy Conversion & Management, 46: 1579-1593.

Clark, D. R. and May, W. R, Jr. HVACSIM+ Building Systems and Equipment Simulation Program Users Guide. NBSIR 85-3243. National Bureau of Standards, September, 1985.

Clark, D. R. HVACSIM+ Building Systems and Equipment Simulation Program Reference Manual. NBSIR 84-2996. NIST, January, 1985.

Clarke, J.A., 1985. Energy Simulation in Building Design. Bristol: Adam Hilger.

Clarke, J. and D. McLean, 1988. ESP – A Building and Plant Energy Simulation System, version 6, Release 8, University of Strathclyde, Glasgow, UK.

Coley, D.A. and S. Schukat, 2002. Low-energy design: combining computer-based optimization and human judgment, Building and Environment 37: 1241–1247.

Comstock, M. C. and J. E. Braun. 1999a. “Experimental Data from Fault Detection and Diagnostic Studies on a Centrifugal Chiller,” Ray W. Herrick Laboratories, HL 99-18: Purdue University, West Lafayette, IN.

Comstock, M. C. and J. E. Braun. 1999b. “Development of Analysis Tools for the Evaluation of Fault Detection and Diagnostics in Chillers,” Ray W. Herrick Laboratories, HL 99-20: Purdue University, West Lafayette, IN.

Crabb, J.A., N. Murdoch, J.M. Penman, 1987. A Simplified Thermal Response Model. Building Services Engineering Research& Technology; 8: 13–19.

Crawley, D.B., J.W. Hand, M. Kurnmert, B.T. Griffith. 2008. Contrasting the capabilities of building energy performance simulation programs, Building Environment, 43: 661–673.

Crawley, D. B, L. K. Lawrie, C. O. Pedersen, F. C. Winkelmann, M. J. Witte, R. K. Strand, R. J. Liesen, W. F. Buhl, Y. J. Huang, R. H. Henninger, J. G., D. E. Fisher, D. B. Shirey III, B. T. Griffith, P. G. Ellis, and L. Gu. 2004. "EnergyPlus: New, Capable, and Linked," Journal of Architectural and Planning Research, 21 (4).

DeSimone, M. 1996. A Standard Simulation Testbed for the Evaluation of Control Algorithms and Strategies Related to Variable Air Volume HVAC System. Massachusetts Institute of Technology, Cambridge, MA, M.S. Thesis.

Dexter, A.L., D., Ngo, 2001. "Fault diagnosis in air-conditioning systems: a multi-step fuzzy model-based approach," HVAC & R Research, 7(1), pp. 83-102.

Dexter, A. L., M. M. Eftekhari, P. Haves, and J. G. Jota, 1987. "The Use of Dynamic Simulation Models to Evaluate Algorithms for Building Energy Control: Experience with HVASIM+", Proceedings of ICBEM'87, International Congress on Building Energy Management, October, Lausanne, Switzerland.

DOE, Building Energy Software Tools Directory, U.S. Department of energy, 2009, Available at: http://www.eere.energy.gov/ [Accessed: August, 2009].

Devore, J.L., *Probability and Statistics for Engineering and the Sciences*, ed. 6. 2004: Brooks/Cole Publishing Co.

EnergyPlus, 2005. EnergyPlus Energy Simulation Software, U. S. Department of Energy, http://www.eere.energy.gov/buildings/energyplus.

EnergyPlus, 2014. The reference to EnergyPlus calculations, U. S. Department of Energy.

Furr, J. C.; O'Neal, D. L.; Davis, M. A.; Bryant, J. A.; Cramlet, A., "Performance of VAV parallel fan-powered terminal units: Experimental results and models," ASHRAE Transactions, v 114 PART 1, p 83-90, 2008a.

Furr, J. C., O'Neal, D. L.; Davis, M. A.; Bryant, J. A., Cramlet, A., "Performance of VAV fan-powered terminal units: Experimental setup and methodology," ASHRAE Transactions, v 114 PART 2, 2008.

Fraisse, G., C. Viardot, O. Lafabrie, G. Achard, 2002. Development of a simplified and accurate building model based on electrical analogy, Energy and Buildings 34: 1017–1031.

Frtitzson, P. Principals of object-oriented modeling and simulation with MODELICA 2.1. IEEE press, 667-677, 2004.

Ghiaus, C. 2001. Fuzzy model and control of a fan-coil. Energy and Building, 33: 545-551.

Gouda, M.M., S. Danaher, C.P. Underwood, 2002.Building thermal model reduction using nonlinear constrained optimization, Building and Environment 37: 1255–1265.

Haves, P., 1997. "Fault Modeling in Component-Based HVAC Simulation," Proceedings of Building Simulation 97, IBPSA, pp. 119 – 126.

Hensen, J. Simulation Tools for Energy Efficient Building Design, 2009, Available at: http://www.bwk.tue.nl/bps/hensen/courseware [Accessed: August, 2009].

House, J. M., W. Y. Lee, and D. R. Shin, 1999. "Classification Techniques for Fault Detection and Diagnosis of an Air-Handling Unit," ASHRAE Transactions, 105 (1).

Joo, I., and Liu, M.S., "Performance Analysis of Dual-fan, Dual-duct Constant Volume Air-handling Units," ASHRAE Transactions, V. 108, Part 2, pp. 39-46, 2002.

Judkoff, R. D., J. S. Neymark, 1999. "Adaptation of the BESTEST Intermodel Comparison Method for Proposed ASHRAE Standard 140P: Method of Test for Building Energy Simulation Programs," ASHRAE Transactions, 105, pp. 721-736.

Kämpf, J.H., D. Robinson, 2007. A simplified thermal model to support analysis of urban resource flows, Energy and Buildings 39: 445–453.

Kämpf, J.H. and D. Robinson, 2009. A hybrid CMA-ES and HDE optimization algorithm with application to solar energy potential, Applied Soft Computing 9: 738–745.

Katipamula, S. R. G. Pratt, and J. Braun, 2001. "Building System Diagnostics and Preventive Maintenance," Section 7.2, Handbook of Heating, Ventilation, and Air Conditioning, CRC Press, Boca Raton, FL.

Katipamula, S. and M.R. Brambley, 2005a,b. Methods for fault detection, diagnostics, and prognostics for building systems, Part I and II, HVAC&R Research Journal, Jan, April.

Kelley, C.T., 1999, Iterative Methods for Optimization. Frontiers in Applied Mathematics, 18, SIAM, Philadelphia, PA.

Kershaw, T., M. Eames, D. Coley, 2011. Assessing the risk of climate change for buildings: a comparison between multi-year and probabilistic year simulations, Building and Environment 46: 1303–1308.

Knebel, D. 1983. Simplified Energy Analysis Method, ASHRAE, Atlanta, GA.

Kreider, J. F., Curitis, P. S., and A. Rabl. 2002. Heating and Cooling of Buildings (2nd Ed.). McGraw-Hill.

Kusuda, T., 1999. "Early History and Future Prospects of Building Systems Simulation," Proceedings of the Sixth International IBPSA Conference, Kyoto, Japan.

Kusuda, T., 2001. "Building Environment Simulation Before Desktop Computers in the USA through a Personal Memory," Energy and Buildings, 33, pp. 291 – 302.

LBNL, 2011, Modelica Library for Building Energy and Control Systems, Lawrence Berkeley National Laboratory, https://gaia.lbl.gov/bir.

Lebrun J., M. Jokela, A. Karola, P. Andre, U. Willan, Annex 30: Bringing Simulation to Application- Final report. International Energy Agency, University of Liege, Belgium, April 1999.

Lebrun J., SW. Wang, Evaluation and Emulation of Building Energy Management Systems-Synthesis Report, IEA (BCS) Annex 17 Final report, University of Liege, Belgium, 1993.

Lee, K.H., J.E Braun, 2008. Model-based demand-limiting control of building thermal mass. Building and Environment 43 (10), 1633–1646.

Legg, R. C., 1986. Characteristics of single and multi-blade dampers for ducted air systems. Building Services Engineering Research and Technology, 7(4), 1986.

Levenberg, K., A Method for the Solution of Certain Non-linear Problems in Least Squares. Quarterly of Applied Mathematics, 2(2); 164-168, 1944.

Li, S. and J. Wen, 2010. “Development and Validation of a Dynamic Air Handling Unit Model - Part I (RP 1312)”, ASHRAE Transactions, Vol. 116, Pt. 1, pp. 45–56.

Li, S., J. Wen, X. Zhou, and C. J. Klaassen, 2010. “Development and Validation of a Dynamic Air Handling Unit Model - Part II (RP 1312) ”, ASHRAE Transactions, Vol. 116, Pt 1, pp. 57 – 73.

Loughborough University and Massachusetts Institute of Technology, 1997, “A Standard Simulation Testbed for the Evaluation of Control Algorithms and Strategies”, ASHRAE 825 Final Report.

Marquardt, D., An Algorithm for the Least-Squares Estimation of Nonlinear Parameters. SIAM Journal of Applied Mathematics, 11(2); 431-441, 1963.

Mitalas, G. P. and D.G. Stephenson, 1967. Room Thermal Response Factors. ASHRAE Transactions, Vol. 73, Pt. 2, pp. 1–10.

Magnier, L. and F. Haghighat, 2010. Multiobjective optimization of building design using TRNSYS simulations, genetic algorithm, and artificial neural network, Building and Environment 45: 739–746.

Nielsen, T.R. 2005. Simple tool to evaluate energy demand and indoor environment in the early design stages, Solar Energy 78: 73–83.

Norford, L. K. and P. Haves. 1997. A Standard Simulation Testbed for the Evaluation of Control Algorithms and Strategies. Final Report of ASRAE 825-RP. American Society of Heating, Refrigerating, and Air-Conditioning Engineers, Inc.: Atlanta, Georgia.

Norford, L. K., Wright, J. A., Buswell, R. A., and D. Luo. 2000. Demonstration of fault detection and diagnosis methods in a real building. Final Report of ASHRAE 1020RP. Atlanta: American Society of Heating, Refrigerating, and Air-Conditioning Engineers, Inc.

Park, C., D. R. Clark, and G. E. Kelly, 1985. "An Overview of HVACSIM+, A Dynamic Building/ HVAC/ Control System Simulation Program," the 1st Annual Building Energy Simulation Conference, Seattle, WA, August 21-22.

Park, C., D.R. Clark, and G.E. Kelly, 1986. HVACSIM+ Building Systems and Equipment Simulation Program Building Loads Calculation, NBSIR 86-3331, NIST.

PECI, 1998. Model Commissioning Plan and guide Commissioning Specifications, U.S. Department of Energy, version 2.05, Portland, OR.

Peitsman, H. C., and L.L. Soethout. 1997. ARX models and real-time model-based diagnosis. ASHRAE Transactions, 103 (1): 657-671.

Pita, E.G. 2002. Air conditioning principles and system (4th Ed.). Prentice Hall.

Powell M. J. D., 1970. A Hybrid Method for Nonlinear Equations. In P. Rabinowitz, editor, Numerical Methods for Nonlinear Algebraic Equations, pages 87-144. Gordon and Breach Science, London.

Powell M. J. D., 1970. A new algorithm for unconstrained optimization, In Nonlinear Programming J. B. Rosen, Ol. L. Mangasarian and K. Ritter (eds.), Academic Press, New York.

Price, B. A., and T. F. Smith. 2003. Development and validation of optimal strategies for building HVAC systems. Technical Report: ME-TEF-03-001, Department of Mechanical Engineering, The University of Iowa, Iowa City, Iowa.

Pourarian, S., J. Win, D. Veronica, X. Zhou, R. Lui, A Tool for Evaluating Fault Detection and Diagnostic Methods for Fan Coil Units. Annual ASHRAE Conference, Seattle, Washington, June 28-July 2, 2014.

Reddy, T.A. and al. 2005. Literature review on calibration of building energy simulation programs: uses, problems, procedures, uncertainty and tools, accepted for publication by ASHRAE Trans.

Salsbury, T., and R. Diamond. 2000. Performance validation and energy analysis of HVAC systems using simulation. Energy and Buildings, 32: 5–17.

Schein, J. and S. Bushby, 2005. "A Simulation Study of a Hierarchical, Rule-Based Method for System-Level Fault Detection and Diagnostics in HVAC Systems", Technical Report, NISTIR 7216, U.S DEPARTMENT OF COMMERCE, National Institute of Standard and Technology, Building Environment Division, Building and Fire Research Laboratory, Gaithersburg, MD 20899-8631.

Schein, J, 2006. "Results from Field Testing of Embedded Air Handling Unit and Variable Air Volume Box Fault Detection Tools", Technical Report, NISTIR 7365, U.S DEPARTMENT

OF COMMERCE, National Institute of Standard and Technology, Building Environment Division, Building and Fire Research Laboratory, Gaithersburg, MD 20899-8631.

SEL, 2000. TRNSYS Version 15 User Manual and Documentation, Solar Energy Laboratory, Mechanical Engineering Department, University of Wisconsin, Madison.

SEL, 2007. TRNSYS Version 16 programmer's guide, Volume 8, Solar Energy Laboratory, Mechanical Engineering Department, University of Wisconsin, Madison.

Shah, D. J., 2001. "Generalized Engineering Modeling and Simulation (GEMS)," Seventh International IBPSA Conference, pp. 723 – 730, August, Rio de Janeiro, Brazil.

Shavit, G., 1995. "Short-time Step Analysis and Simulation of Homes and Buildings during the last 100 years," ASHRAE Transactions, 101 (1).

Shterenlikht A., N.A. Alexander, Levenberg-Marquardt vs Powell's Dogleg Method for Gurson-Tvergaard-Needleman Plasticity Model. Comput. Methods Appl. Mech. Engrg, 237-240, 2012.

SPARK 2003. Simulation Problem Analysis and Research Kernel. Lawrence Berkeley National Laboratory and Ayres Sowell Associates, Inc.

SPARK, 2003. Simulation Problem Analysis and Research Kernel. Lawrence Berkeley National Laboratory and Ayres Sowell Associates, Inc.

Stewart, G.W. and Sun, J.G., 1990. Matrix Perturbation Theory. San Diego, Academic Press.

Tindale, A. 1993. Third-order lumped-parameter simulation method, Building Services Engineering Research and Technology 14 (3): 87–97.

Trcka, M. & Hensen, J. L. M. 2010. Overview of HVAC system simulation, Automation in Construction, vol. 19, no. 2, pp. 93-99.

Waltz, J. P., 2000. Computerized Building Energy Simulation Handbook, Fairmont Press, Liburn, GA.

Wang S.W., 1999. Dynamic simulation of a building VAV air-conditioning system and evaluation of EMCS online control strategies, Build. Environ. 34: 681-705.

Wang, F., Yoshida, H., and Miyata, M., 2004. "Total Energy Consumption Model of Fan Subsystem Suitable for Continuous Commissioning," ASHRAE Transactions, 110(1).

Wen, 2010, "Tools for Evaluating Fault Detection and Diagnostic Methods for Air-Handling Units", ASHRAE 1312 Final Report.

Winkelmann, F. C., B. E. Birdsall, W. F. Buhl, K. L. Ellington, A. E. Erdem, J. J. Hirsch, and S. Gates, 1993. DOE-2 Supplement Version 2.1 E, Lawrence Berkeley National Laboratory, November.

Wright, A.J., D. Bloomfield, T.J. Wiltshire, 1992. Building Simulation and Building Representation: Overview of Current Developments. Building Services Engineering Research& Technology; 13(1): 1–11.

Yamashita, N. and Fukushima, M., 2001. On the Rate of Convergence of the Levenberg-Marquardt Method. Computing (suppl. 15), 237-249.

APPENDIX A: FAN COIL UNIT CONTROL SEQUENCE

A.1 OBJECTIVE

The purpose of this document is to describe the Energy Resource Station Fan Coil Units (FCU) sequence of operations and operation control modes.

A.2 INTRODUCTION AND POINT NAMES:

There are currently four FCUs in ERS, one in each of the four B test rooms. Each FCU has a three-speed fan, a mixed air damper, a heating coil and a cooling coil. FCU controls are fully automated via ERSTEST system DDC controller (Johnson Control DX-9100). Chilled water and heating water supply are controlled by ERSTEST system Network Control Unit (NCU). The related FCU control and chilled water / heating water supply control point names are listed below:

Room Temperature Points

RM-TEMP	Room Temperature	Deg F
RMCLGSPT	Room Cooling Setpoint	Deg F
RMHTGSPT	Room Heating Setpoint	Deg F

FCU Points

FCU-CTRL	Fan Coil Unit Control Modes	Occ/Unocc
FCUOAMIN	Fan Coil Unit Outside Air Min. Damper Position Setpoint	%Open
FCUMATSP	Fan Coil Unit Mixed Air Temperature Setpoint	Deg F
FCU-MAT	Fan Coil Unit Mixed Air Temperature	Deg F
FCU-DAT	Fan Coil Unit Discharge Air Temperature	Deg F
FCU-CVLV	Fan Coil Unit Cooling Coil Valve Position	%Open
FCU-HVLV	Fan Coil Unit Heating Coil Valve Position	%Open
FCU-DMPR	Fan Coil Unit Mixed Air Damper Position	%Open to O.A.
FAN-CTRL	Fan Coil Unit Fan Operation Mode	Auto/Cycle/ON
FAN-SPD	Fan Coil Unit Fan Cycle/ON Mode Preset Speed	Low/Med/High
FCU-AMPS	Fan Coil Unit Fan Current	Amps
FCU-LOW	Fan Coil Unit Fan Low Speed	On/Off
FCU-MED	Fan Coil Unit Medium Speed	On/Off
FCU-HI	Fan Coil Unit High Speed	On/Off
FCU_MAT	Calibrated Fan Coil Unit Mixed Air Temperature	Deg F
FCU_DAT	Calibrated Fan Coil Unit Discharge Air Temperature	Deg F
FCU-MAT0	True Mixed Air Temperature (not biased from fault testing)	Deg F
RM-TEMP0	True Room Temperature (not biased from fault testing)	Deg F

FCU-TEST	Fan Coil Unit Test Mode	0=setup/1=norm/2=fault
VAVHCGPM	Fan Coil Unit Heating Water Flow Rate	GPM

Heating Water Supply Points

LBP-GPM	Heating Water LB Water Flow Rate	GPM
LB-SWT	Heating Water LB Supply Water Temperature	Deg F
LB-RWT	Heating Water LB Return Water Temperature	Deg F
LB-DP	Heating Water LB Differential Pressure	PSI
LB_DPSPT	Heating Water LB Differential Pressure Setpoint	PSI
LBP-SPD	Heating Water Pump LB Speed	%Speed
LBP-SST	Heating Water Pump LB Start/Stop	On/Off
LBP-STS	Heating Water Pump LB Status	On/Off
LBP-ALM	Heating Water Pump LB Alarm	Normal/Alarm
LBP-WAT	Heating Water Pump LB Power	Watts

Chilled Water Supply Points

LCP-GPM	Chilled Water LC Water Flow Rate	GPM
LC-SWT	Chilled Water LC Supply Water Temperature	Deg F
LC-RWT	Chilled Water LC Return Water Temperature	Deg F
LCP-SST	Chilled Water Pump LC Start/Stop	Start/Stop
LCP-SPD	Chilled Water Pump LC Speed	%Speed
LCP-WAT	Chilled Water Pump LC Power	Watts
LC-HP	Chilled Water LC Discharge Head Pressure	PSI
LC_HPSPT	Chilled Water LC Discharge Head Pressure Setpoint	PSI

A.3 FCU CONTROL SEQUENCE:

A.3.1 FCU CONTROL MODES

Fan coil unit control modes (“FCU-CTRL”) can be selected either “Unoccupied” or “Occupied” mode. In “Unoccupied” mode, the fan is positively off. The mixed air damper is fully closed. FCU cooling coil valve and heating coil valve are also fully closed. Test Room temperatures float. In “Occupied” mode, the fan coil unit is controlled to maintain test room heating and cooling temperature setpoint. Fan control operates in one of three modes: Auto/Cycle/On. Mixed damper adjust to maintain minimum damper position setpoint set by “FCUOAMIN”. When cooling is needed, damper will also be adjusted to maintain a mixed air temperature setpoint set by

“FCUMATSP”. When heating is needed, the damper will maintain the minimum damper position.

A.3.2 FCU COOLING VALVE CONTROL

In each test room, there is a room cooling setpoint (“RMCLGSPT”) that can be scheduled or adjusted. When FCU is in “Occupied” mode, the controller will compare room temperature “RM-TEMP“ with the cooling setpoint. If the actual room temperature is within 1 Deg F of the cooling setpoint, the FCU is in the “cooling” mode, and the controller cooling PID loop is enabled and the cooling valve position will be controlled by the cooling PID output. When the room temperature falls below more than 1 Deg F compared to the cooling setpoint, the cooling PID is disabled and valve fully closed.

A.3.3 FCU HEATING VALVE CONTROL

In each test room, there is a room heating setpoint (“RMHTGSPT”) that can be scheduled or adjusted. When FCU is in “Occupied” mode, the controller will compare room temperature “RM-TEMP“ with the heating setpoint. If the actual room temperature is within 1 Deg F of the heating setpoint, the FCU is in the “heating” mode, and the controller heating PID loop is enabled and the heating valve position will be controlled by the heating PID output. When the room temperature rises above more than 1 Deg F compared to the heating setpoint, the heating PID is disabled and valve fully closed.

A.3.4 FCU MIXED AIR DAMPER CONTROL

The mixed air damper is controlled by a separate PID loop in the controller. When FCU is in “Unoccupied” mode, this damper will be fully closed. When FCU is in “Occupied” mode and the room demand calls for cooling, the mixed air damper will be adjusted automatically to meet the mixed air temperature setpoint for mixed

air temperature (“FCU-MAT”), with a minimum damper position set by “FCUOAMIN”. When FCU is in “Occupied” mode and the room does not require heating or cooling, the mixed air damper will be at the minimum position.

A.3.5 FCU FAN OPERATION MODES AND SPEED CONTROL

The FCU fan can operate in three speeds: Low, Medium, or High. The On/Off and fan speed change can be based on three different modes of operations in point “FAN-CTRL” selection: Auto, Cycle, and ON.

Auto Mode:

In “Auto” mode, the fan on/off and speed change is based on the cooling PID output / heating PID output values. If PID outputs (thus valve position) are greater than 0%open but smaller than 40%, the fan is running in “Low” speed. If PID outputs are greater than 40%open but smaller than 80%, the fan is running in “Medium” speed. If PID outputs are greater than 80%open, the fan is running in “High” speed. There is 10% dead band at each switchover level to minimize the fan speed changeover. The fan will be off when there is not a demand for heating or cooling, or FCU is in “Unoccupied” mode.

Cycle Mode:

In “Cycle” mode, the fan on/off and speed change are based on the preset speed value set at “FAN-SPD”: Low, Medium, or High. Whenever the FCU demands for cooling or heating, the fan will run at the specified speed. The fan will be off when there is not a demand for heating or cooling, or FCU is in “Unoccupied” mode.

On Mode:

In “On” mode, the fan will always run at preset speed set by “FAN-SPD” (Low, Medium, or High), regardless the cooling or heating PID output. The fan will be off only when FCU is in “Unoccupied” mode.

A.3.6 HEATING WATER SUPPLY PUMP CONTROL

The heating water to B test room fan coil units runs through heating loop B. If all four B test room FCUs are in “Unoccupied” mode for “FCU-CTRL” The heating water loop B pump “LBP-SST” will be automatically stopped.

If all four B test room FCUs are in “Occupied” mode for “FCU-CTRL”, but the maximum heating valve position for the four FCUs is less than 15% (with 5% dead band), the heating water loop B pump “LBP-SST” will also be automatically stopped.

If all four B test room FCUs are in “Occupied” mode for “FCU-CTRL”, but the maximum heating valve position for the four FCUs is greater than 15% (with 5% dead band), the heating water loop B pump “LBP-SST” will be automatically started. The pump speed “LBP-SPD” will be controlled to maintain the loop differential pressure “LB-DP” at the preset setpoint by “LB_DPSPT”.

A.3.7 COOLING WATER SUPPLY PUMP CONTROL

The cooling water to B test room fan coil units runs through chilled water loop C. If all four B test room FCUs are in “Unoccupied” mode for “FCU-CTRL” The chilled water loop C pump “LCP-SST” will be automatically stopped.

If all four B test room FCUs are in “Occupied” mode for “FCU-CTRL”, but the maximum cooling valve position for the four FCUs is less than 15% (with 5% dead band), the chilled water loop C pump “LBP-SST” will also be automatically stopped.

If all four B test room FCUs are in “Occupied” mode for “FCU-CTRL”, but the maximum cooling valve position for the four FCUs is greater than 15% (with 5% dead band), the heating water loop B pump “LCP-SST” will be automatically started. The pump speed “LCP-SPD” will be controlled to maintain the loop head pressure “LC-HP” at the preset setpoint by “LC_HPSPT”. Figure A1 shows the algorithm of FCU control sequence used as the basis for TYPE 479 coding. PID1 is a PID loop that

compares zone temperature with zone cooling set point, PID2 is a PID loop that compares zone temperature with zone heating set point and PID3 is a PID loop that compares mixed air temperature with mixed air temperature set point.

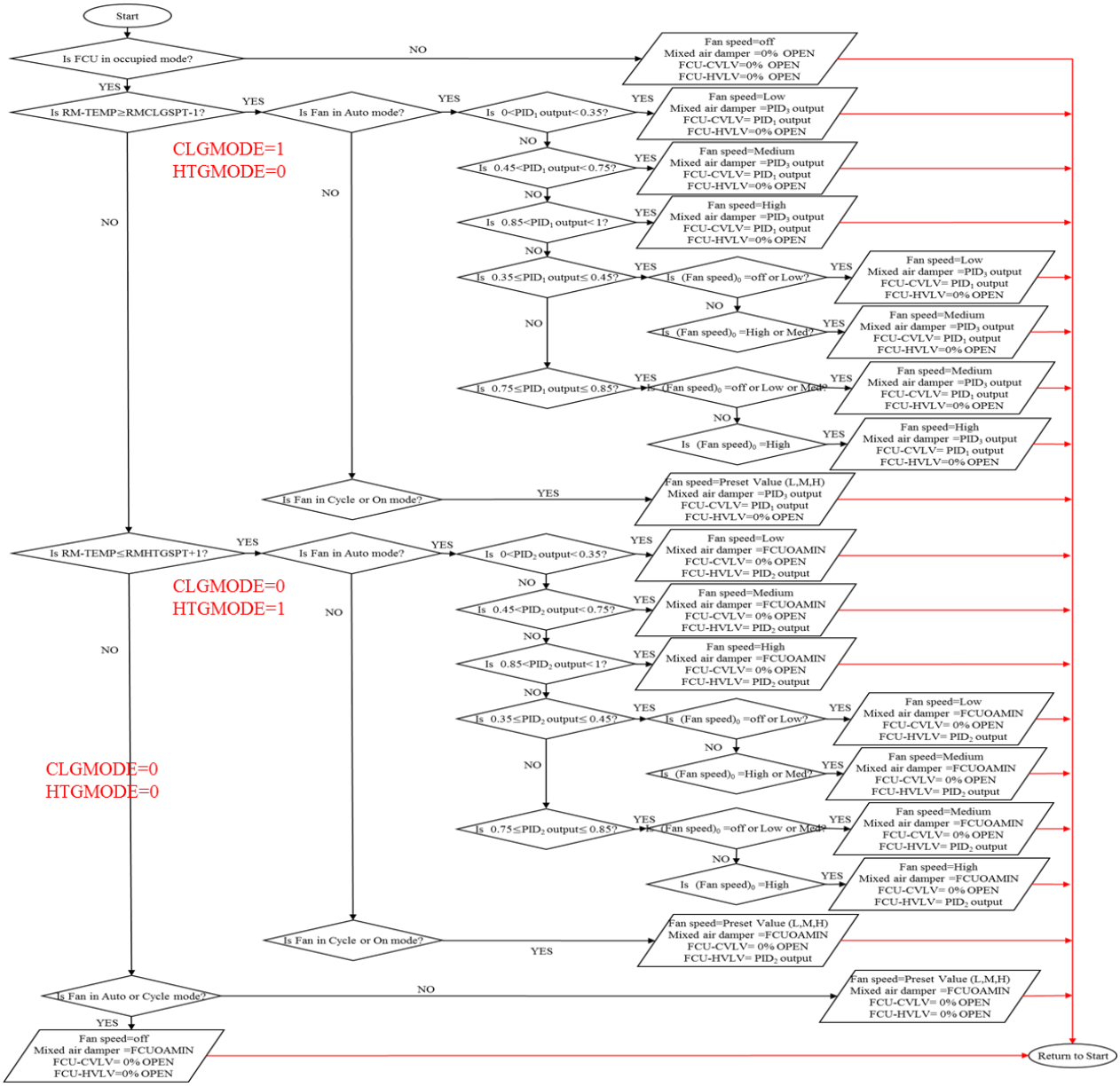

Figure A1. Control sequence algorithm for ERS fan coil units

APPENDIX B: LIST OF PARAMETERS AND THEIR VALUE FOR FCU SIMULATION IN HVACSIM+

Table B1 Required parameters for Fan coil Unit simulation in HVACSIM+

TYPEs	PARAMETER	VALUE
TYPE 479 (Fan coil unit supply air temperature control)	heating set point for zone (C)	21.11
	cooling set point for zone (C)	23.33
	mixed air temperature set point(C)	37.78
	outdoor air minimum damper position (0-1)	0
	fan speed in cycle or on mode (0=off, 1=low, 2=medium, 3=high)	3
	fan rotational speed in low speed (rev/s)	9.75
	fan rotational speed in medium speed (rev/s)	13.083
	fan rotational speed in high speed (rev/s)	18.083
	proportional band for PID1 (K)(cooling)	10*1.8=18
	integral time for PID1 (s) (cooling)	0.3
	derivative time for PID1 (s) (cooling)	0
	proportional band for PID2 (K)(heating)	-30*1.8=-54
	integral time for PID2 (s)(heating)	0.3
	derivative time for PID2 (s)(heating)	0
	proportional band for PID3 (K) (damper)	60
	integral time for PID3 (s) (damper)	1
	derivative time for PID3 (s) (damper)	0
	control mode (0=open loop, 1=closed loop) (-)	1
	open loop outdoor air damper position (0-1) (-)	0.3
	open loop cooling coil valve demand (0-1) (-)	0.5
	open loop heating coil valve demand (0-1) (-)	0.5
	sampling interval (s)	1
	controller number (parameters in file contN.par) (-)	
TYPE 321 (Motor-driven actuator) (OA DAMPER)	direction: 1=forward, -1=reverse, 0=stuck	1
	starting position (0-1)	0
	travel time (lim-lim) (s)	150
	minimum change in demanded position for movement (-)	0
	hysteresis (-)	0
	crank travel angle (0 for linear) (deg)	0
	Upper limit of control element range on actuator scale	1
	Lower limit of control element range on actuator scale	0
TYPE 321 (Motor-driven actuator) (COOLING VALVE)	direction: 1=forward, -1=reverse, 0=stuck	1
	starting position (0-1)	0
	travel time (lim-lim) (s)	90
	minimum change in demanded position for movement (-)	0
	hysteresis (-)	0
	crank travel angle (0 for linear) (deg)	0
	Upper limit of control element range on actuator scale	1
	Lower limit of control element range on actuator scale	0
TYPE 321 (Motor-driven actuator) (HEATING VALVE)	direction: 1=forward, -1=reverse, 0=stuck	1
	starting position (0-1)	0
	travel time (lim-lim) (s)	90
	minimum change in demanded position for movement (-)	0
	hysteresis (-)	0
	crank travel angle (0 for linear) (deg)	0
	Upper limit of control element range on actuator scale	1
	Lower limit of control element range on actuator scale	0
TYPE 307 (Fan coil unit air flow network)	number of the fans in fan coil unit	3
	1st pressure coefficient	11.609, 0.277660E+03
	2nd pressure coefficient	-6.4299,

		-0.693570E+02
	3rd pressure coefficient	0
	4th pressure coefficient	0
	5th pressure coefficient	0
	1st efficiency coefficient	0.9, -0.185000E+00
	2nd efficiency coefficient	0,0.770590E+01
	3rd efficiency coefficient	0
	4th efficiency coefficient	0
	5th efficiency coefficient	0
	diameter (m)	0.160274
	lowest valid normalized flow (-)	0.832, 0.422607E+00
	highest valid normalized flow (-)	1.782, 0.211304E+01
	total resistance of fan coil components (1000/kg.m)	0.07,9.6
	face area of outside air damper (m2)	0.14429464403
	face area of return air damper (m2)	0.14429464403*
TYPE 341 (Fluid resistance) (FCU OUTLET GRILL RESISTANCE)	flow resistance (1000/kg.m)	0.0018
TYPE 349 (Room air mass balance)	resistance to 1st adjacent zone [1000/(kg m)]	100000
	leakage resistance [1000/(kg m)]	1.93700
	local extract fan mass flow rate [kg/s]	0
TYPE 314 Four pipes Fan coil unit (THERMAL NETWORK)	method : 0 = steady state, 1 = dynamic	1
	fault : 0 for no faults, 1 = parallel flow (cooling co	0
	psycho : 0 = no psychrometric output calcs, 1 = calcs	0
	number of rows of tubes in cooling coil	3
	number of tubes per row in cooling coil	8
	number of parallel water circuits in cooling coil	4
	length of cooling coil finned section in direction of f	0.0635
	number of rows of tubes in heating coil	1
	number of tubes per row in heating coil	6
	number of parallel water circuits in heating coil	1
	length of heating coil finned section in direction of f	0.0254
	height of finned section (m)	0.2032
	width of finned section (m)	1.2446
	tube outside diameter (m)	0.009525
	tube wall thickness (m)	0.00079375
	tube material (Al=1,Cu=2,Fe=3,CaCO3=4)	2
	fin spacing (pitch) (m)	0.00213
	fin thickness (m)	0.0001905
	fin material (Al=1,Cu=2,Fe=3)	1
	cooling coil water flow resistance (1000/kg.m)	334.85
	cooling coil valve capacity (Kv) (m3/hr @ 1 bar)	4.042
	cooling coil valve curvature parameter (0=linear) (-)	2
	cooling coil valve rangability (-)	34
	cooling coil valve leakage (fractional flow) (-)	0.0001
	heating coil water flow resistance (1000/kg.m)	13298
	heating coil valve capacity (Kv) (m3/hr @ 1 bar)	1.634
	heating coil valve curvature parameter (0=linear) (-)	2
	heating coil valve rangability (-)	22
	heating coil valve leakage (fractional flow) (-)	0.0001
	time constant (s)	30
TYPE 403 Room with plenum and ducted return and interzone flows	room air capacity multiplier (-)	1
	direct resistance room air node <-> ambient (K/kW)	46.5340
	resistance room air node <-> room mass node (K/kW)	4.43000
	resistance ambient <-> room mass node (K/kW)	308.730

	direct resistance plenum air node <-> ambient (K/kW)	0.100000E+12
	resistance plenum air node <-> plenum mass node (K/kW)	21.6600
	resistance ambient <-> plenum mass node (K/kW)	192.000
	resistance room air node <-> plenum air node (K/kW)	9.50600
	capacitance of room mass node (kJ/K)	5078.28
	capacitance of room air node (unmodified) (kJ/K)	145.920
	capacitance of plenum mass node (kJ/K)	4569.91
	capacitance of plenum air node (kJ/K)	47.3400
	volume of room (m3)	48.0000
	volume of plenum (m3)	13.0000
	number of occupants (-)	0
	lighting heat gain (kW)	0.54
	fraction of lighting heat gain to extract air (-)	0
	equipment heat gain (kW)	1.8
	zone number (parameter file=zoneN.par, n > 0) (-)	0
TYPE 301 Room temperature sensor	offset: input for zero output (C)	0
	gain: change in input for 0->1 output (K)	1
	time constant (s)	30
	upper limit of output range (-)	40
	lower limit of output range (-)	-10
TYPE 301 Room temperature sensor	offset: input for zero output (C)	0
	gain: change in input for 0->1 output (K)	1
	time constant (s)	30
	upper limit of output range (-)	121.11
	lower limit of output range (-)	-38.89

APPENDIX C: CARRIER DUAL DUCT VAV TERMINAL UNITS CONTROL STRATEGY

C.1 OBJECTIVE

The purpose of this document is to describe the Energy Resource Station dual-duct dual fan system sequence of operations and control modes.

C.2 INTRODUCTION AND POINT NAMES

Four dual duct VAV terminal units were tested in East B, South A, South B, and West A rooms. They were automatically controlled by Johnson Controls VMA-1420 controllers. The dual-duct VAV system was served by a double fan, single return AHU described in Section 3.2. The related dual duct control point names are listed below:

Room Temperature Points

RM-TEMPD	Room Temperature for Dual-duct System Test	Deg F
RMCLGSPT	Room Cooling Setpoint	Deg F
RMHTGSPT	Room Heating Setpoint	Deg F

Dual-Duct Terminal Unit Points

VAV-DATD	Dual-duct Mixing Box Discharge Air Temperature	Deg F
VAV-DP1	Dual-duct Mixing Box Cold-deck Velocity Pressure	in. WG
VAV-DP2	Dual-duct Mixing Box Hot-deck Velocity Pressure	in. WG
VAV-DMPR1	Dual-duct Mixing Box Cold-deck Damper Command	%Open
VAV-DMPR2	Dual-duct Mixing Box Hot-deck Damper Command	%Open
VAVCFM-C	Dual-duct Mixing Box Cold-deck Air Flow Rate	CFM
VAVCFM-H	Dual-duct Mixing Box Hot-deck Air Flow Rate	CFM
VAVCFM-T	Dual-duct Mixing Box Total Air Flow Rate	CFM
VAV-EAT1	Dual-duct Mixing Box Cold Deck Entering Air Temp.	Deg F
VAV-EAT2	Dual-duct Mixing Box Hot Deck Entering Air Temp.	Deg F

AHU-A (Hot Deck) Points

SYS-CTL	Occupied/Unoccupied/StartUp/SetBack Control Mode	
HWC-DAT	Heating Water Coil Discharge Air Temperature	Deg F
HWC-EWT	Heating Water Coil Entering Water Temperature	Deg F
HWC-LWT	Heating Water Coil Leaving Water Temperature	Deg F
HWC-MWT	Heating Water Coil Mixed Water Temperature	Deg F
HWC-VLV	Heating Water Coil Valve Position	%Closed
HWP-DP	Heating Water Pump Differential Pressure	PSI
HWP-GPM	Heating Water Pump HWP Water Flow Rate	GPM
HWP-SST	Heating Water Pump HWP Start/Stop	On/Off
HWP-WAT	Heating Water Pump HWP Power	Watts

SA_SPSPT	Supply Air Duct Static Pressure Setpoint	in. WG
SA-CFM	Supply Air Flow Rate	CFM
SA-HUMD	Supply Air Humidity	%RH
SA-SP	Supply Air Duct Static Pressure	in. WG
SAT_SPT	AHU Supply Air Temperature Setpoint	Deg F
SA-TEMP	AHU Supply Air Temperature	Deg F
SF-ALM	Supply Fan Alarm	Normal/Alarm
SF-CS	Supply Fan Current Status	On/Off
SF-DP	Supply Fan Differential Pressure	in. WG
SF-SPD	Supply Fan VFD Speed	%Speed
SF-SST	Supply Fan Start/Stop	On/Off
SF-STS	Supply Fan Status	On/Off
SF-WAT	Supply Fan Power	Watts

AHU-B (Cold Deck) Points

SYS-CTL	Occupied/Unoccupied/StartUp/SetBack Control Mode	
CHWC-DAT	Chilled Water Coil Discharge Air Temperature	Deg F
CHWC-EAH	Chilled Water Coil Entering Air Relative Humidity - AHU A Only	%RH
CHWC-EAT	Chilled Water Coil Entering Air Temperature - AHU A Only	Deg F
CHWC-EWT	Chilled Water Coil Entering Water Temperature	Deg F
CHWC-LAT	Chilled Water Coil Leaving Air Temperature - AHU A Only	Deg F
CHWC-LWT	Chilled Water Coil Leaving Water Temperature	Deg F
CHWC-MWT	Chilled Water Coil Mixed Water Temperature	Deg F
CHWC-VLV	Chilled Water Coil Valve Position	%Open
CHWP-GPM	Chilled Water Pump CHWP Water Flow Rate	GPM
CHWP-SST	Chilled Water Pump CHWP Start/Stop	On/Off
CHWP-WAT	Chilled Water Pump CHWP Power	Watts
EA-DMPR	Exhaust Air Damper	%Open
EADPRALM	Exhaust Air Damper Alarm	Normal/Alarm
EA-FDBK	EA Damper Feedback	%Open
ECONCTRL	Economizer Control Options	See Note 3.
ECONHSPT	Economizer Humidity Setpoint	%RH
ECONTSPT	Economizer Temperature Setpoint	Deg F
MA_LLSPT	MA Low Limit Setpoint	Deg F
MA-LL	MA Low Limit Freezestat Status	Normal/Alarm
MA-TEMP	Mixed Air Temperature	Deg F
OA-CFM	Outside Air Flow Rate	CFM
OACFMSPT	Outside Air CFM Setpoint	CFM
OA-CTRL	Min Outside Air Control Mode Select	%Open
OA-DMPR	Outside Air Damper	%Open
OADPRALM	Outside Air Damper Alarm	Normal/Alarm
OAD-TEMP	OA Duct Temperature	Deg F
OAENTHPY	Outside Air Enthalpy	BTU/LB
OA-FDBK	OA Damper Feedback	%Open
OAF-SST	OA Fan Start/Stop	Stop/Start
OA-HUMD	Outside Air Humidity	Deg F
OAMINSPT	Outside Air Minimum Damper Position Setpoint	%Open
OA-TEMP	Outside Air Temperature	Deg F
RA-CFM	Return Air Flow Rate	CFM
RA-DMPR	Recirculated Air Damper	%Closed
RADPRALM	Return Air Damper Alarm	Normal/Alarm
RAENTHPY	Return Air Enthalpy	BTU/LB
RA-FDBK	RA Damper Feedback	%Closed
RA-HUMD	Return Air Humidity	%RH
RA-TEMP	Return Air Temperature	Deg F
RF%SFSPD	Return Fan % of Supply Fan Speed	%
RFCFMLAG	Return Fan CFM Lag	CFM

RFCFMSPT	Return Fan Calculated CFM Setpoint	CFM
RF-CTRL	Return Fan Control Mode Select	CFM
RF-DP	Return Fan Differential Pressure	in. WG
RF-SPD	Return Fan VFD Speed	%Speed
RF-SST	Return Fan Start/Stop	On/Off
RF-STS	Return Fan Status	On/Off
RF-WAT	Return Fan Power	Watts
RMT-CFM	Sum of Room Supply Air Flow Rates	CFM
SA_SPSPT	Supply Air Duct Static Pressure Setpoint	in. WG
SA-CFM	Supply Air Flow Rate	CFM
SA-HUMD	Supply Air Humidity	%RH
SA-SP	Supply Air Duct Static Pressure	in. WG
SAT_SPT	AHU Supply Air Temperature Setpoint	Deg F
SA-TEMP	AHU Supply Air Temperature	Deg F
SF-ALM	Supply Fan Alarm	Normal/Alarm
SF-CS	Supply Fan Current Status	On/Off
SF-DP	Supply Fan Differential Pressure	in. WG
SF-SPD	Supply Fan VFD Speed	%Speed
SF-SST	Supply Fan Start/Stop	On/Off
SF-STS	Supply Fan Status	On/Off
SF-WAT	Supply Fan Power	Watts

C.3 DUAL DUCT CONTROL MODE

The controller determines the control mode, heating, deadband, or cooling by comparing the zone temperature to the active heating temperature setpoint and active cooling temperature setpoint.

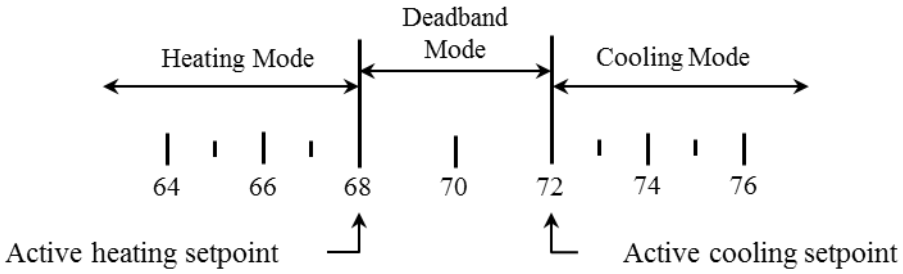

The controller enters the cooling control mode when the zone temperature equals or is greater than the active cooling temperature setpoint. The hot deck damper will modulate to maintain the minimum flow setpoint (100 cfm) and the cold deck damper will modulate open to maintain calculated cooling airflow setpoint. The control reenters the deadband mode, when the zone temperature is below the active cooling temperature setpoint and the calculated cooling requirement is equal to zero. The control enters the heating mode when the zone temperature is equal to or less than the

active Heating temperature setpoint. The cold deck damper will modulate to maintain the minimum flow setpoint (100 cfm) and the hot deck damper will modulate open to maintain calculated heating airflow setpoint. The control reenters the deadband mode when the zone temperature is greater than the active heating temperature setpoint and the calculated heating requirement is equal to zero. The controller maintains the zone temperature between active cooling and heating temperature setpoints.

The dampers modulate from a minimum CFM set point of 100 CFM to a maximum CFM set point of 1000 and 400 for the cold and hot decks, respectively. The cold deck supply air temperature set point is 55°F and the hot deck supply air temperature is 90°F. Figure C.1 shows the dual duct flow schedule.

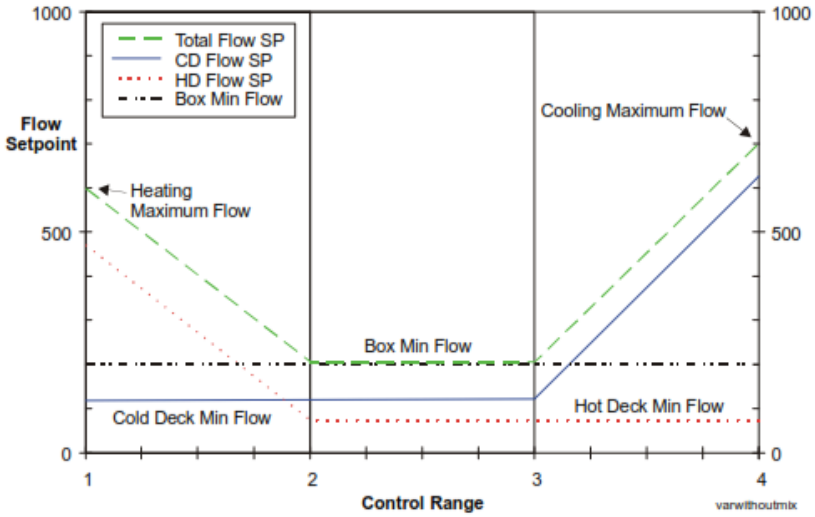

Figure C-1. Dual duct VAV system control sequence

C.4 COOLING AND HEATING REQUIREMENT

In deadband control mode, the heating and cooling requirements are zero. In the cooling or heating control mode, the cooling or heating requirement is calculated using a PI control loop. The change in heating or cooling requirement is calculated.

In heating: Error = Active HTG SP - Zone Temp

$$\Delta\text{Error} = \text{Previous Zone Temp} - \text{Zone Temp}$$

or in cooling: Error = Zone Temp - Active CLG SP

ΔError = Zone Temp - Previous Zone Temp.

ΔRequirement = (100%/ThrottleRange)*[Error*(CalcTime/Int Time) + Δ Error]

The factory setting for throttle range is 4.0 degrees, and for integral time is 2.5 minutes.

C.5 AHU FLOW AND TEMPERATURE CONTROL

The dual-duct dual-fan AHU modulate dampers, fan speeds and valve positions to maintain desired airflow rates and supply air temperature. Supply fans in both hot deck and cold deck are controlled by separate variable frequency drives (VFDs), which vary the fan speeds to maintain the supply air pressure setpoints (1.6 in.wc for both decks). The return fan also adjusts the speed to maintain a return airflow rate which equals to the summation of supply air flow rates in both the hot deck and the cold deck. In the hot deck, heating PID loop controls the valve position on the heating water coil to maintain the hot deck supply air temperature at 90 °F. In the cold deck, cooling PID loop controls the valve position on the chilled water coil to maintain the cold deck supply air temperature at 55 °F, if the economizer is not enabled. In dual-duct summer test, the economizer is disabled and the minimum outside air (OA) damper is 0% open. In fall and winter tests, the economizer is enabled and the minimum outside air damper is 45% open. 45% open minimum OA damper is maintained to meet the minimum ventilation requirements based on ASHRAE Standard 62.1 (2010), which is 0.06 cfm/ft^2 plus 5 cfm/person (assuming 2 people in each test room) for office building. When the OA temperature is below 60 °F, the economizer starts to operate. The outside air and exhaust air (EA) dampers will modulate to open and the return air (RA) damper will modulate to close. The cold deck will use the outside air preferentially to maintain the cold deck supply air

temperature setpoint. OA, EA, and RA dampers will modulate accordingly. If the economizer cannot maintain the cold deck supply air temperature setpoint, the chilled water valve will open to provide more cooling capacity.

APPENDIX D: LIST OF PARAMETERS AND THEIR VALUE FOR DUAL DUCT DOUBL FAN SIMULATION IN HVACSIM+

Table D1 Required parameters for dual duct double fan simulation in HVACSIM+

Module	Value
Air Flow Network	
Mixing box (U21 T325)	
1- Outside air damper: opposed (0) or parallel (1)	0
2- Recirc air damper: opposed (0) or parallel (1)	0
3- Exhaust air damper: opposed (0) or parallel (1)	0
4- Open resist. for outside air damper (0.001/k.m)	0.530000E-01
5- Open resist. for recirc air damper (0.001/k.m)	0.530000E-02
6- Open resist. for exhaust air damper (0.001/k.m)	0.140000E-01
7- Face area of outside air damper (m2	0.2713
8- Face area of recirc air damper (m2)	0.2713
9- Face area of exhaust air damper (m2)	0.3475
10- Leakage for outside air damper	0.930000E-02
11- Leakage for recirc air damper	0.910000E-02
12- Leakage for exhaust air damper	0.930000E-02
13- Fixed resistance in outside air branch (0.001/k.m)	0.100000
14- Fixed resistance in recirc air branch (0.001/k.m)	0.117700
15- Fixed resistance in exhaust air branch (0.001/k.m)	0.480000E-02
16- 0=invert return air damper, 1=not inverted	1.0
Duct between mixing box and main splitter (U22 T341)	
1- flow resistance (0.001/kg.m)	0.100000E-11
Flow split (main duct flow splitter) (U23 T345)	
1- inlet resistance (0.001/kg.m)	0.100000E-04
2- resistance of outlet 1 (0.001/kg.m)	0.168000E-04
3- resistance of outlet 2 (0.001/kg.m)	0.405000E-01
Fluid resistance (U24 T343)	
1- coefficient of PN**0 in resistance curve	1.00210
2- coefficient of PN**1 in resistance curve	-2.30280
3- coefficient of PN**2 in resistance curve	2.35960
4- coefficient of PN**3 in resistance curve	-1.08520
5- coefficient of PN**4 in resistance curve	0.185100
6- location: 1-hot deck, 2-cold deck	1.00000
Hot deck supply air fan (U25 T355)	
1- 1st pressure coefficient	9.80000
2- 2nd pressure coefficient	-6.69960
3- 3rd pressure coefficient	9.14630
4- 4th pressure coefficient	-3.85990
5- 5th pressure coefficient	0.495900
6- 1st efficiency coefficient	-0.191000E-01
7- 2nd efficiency coefficient	0.595700
8- 3rd efficiency coefficient	-0.391900
9- 4th efficiency coefficient	0.192300
10- 5th efficiency coefficient	-0.400000E-01
11- diameter (m)	0.2667
12- mode: air=1, water=2	1
13- lowest valid normalized flow	0.2
14- highest valid normalized flow	2.5
15- location: 1-SA hot deck (or SA for single deck AHUs),2-SA cold deck, 3- return fan	1.0
Asymmetric flow split (U26 T346)	
1- inlet resistance (0.001/kg.m)	0.917000E-01
2- resistance of main outlet (0.001/kg.m)	0.610000E-02
3- resistance of branch outlet (0.001/kg.m)	4.15250
Asymmetric flow split (U27 T346)	
1- inlet resistance (0.001/kg.m)	0.610000E-02
2- resistance of main outlet (0.001/kg.m)	0.260000E-02
3- resistance of branch outlet (0.001/kg.m)	4.81400
Asymmetric flow split (U28 T346)	
1- inlet resistance (0.001/kg.m)	0.260000E-02
2- resistance of main outlet (0.001/kg.m)	0.537100

3- resistance of branch outlet (0.001/kg.m)	6.45850
Fluid resistance (U29 T343)	
1- coefficient of PN**0 in resistance curve	1.00210
2- coefficient of PN**1 in resistance curve	-2.30280
3- coefficient of PN**2 in resistance curve	2.35960
4- coefficient of PN**3 in resistance curve	-1.08520
5- coefficient of PN**4 in resistance curve	0.185100
6- location: 1-hot deck, 2-cold deck	2.00000
Cold deck supply air fan (U30 T355)	
1- 1st pressure coefficient	10.6500
2- 2nd pressure coefficient	-6.69960
3- 3rd pressure coefficient	9.14630
4- 4th pressure coefficient	-3.85990
5- 5th pressure coefficient	0.495900
6- 1st efficiency coefficient	-0.500000E-01
7- 2nd efficiency coefficient	0.595700
8- 3rd efficiency coefficient	-0.391900
9- 4th efficiency coefficient	0.192300
10- 5th efficiency coefficient	-0.400000E-01
11- diameter (m)	0.266700
12- mode: air=1, water=2	1.00000
13- lowest valid normalized flow	0.400000
14- highest valid normalized flow	2.50000
15- location: 1-SA hot deck (or SA for single deck AHUs),2-SA cold deck, 3- return fan	2.00000
Asymmetric flow split (U31 T346)	
1- Inlet resistance (0.001/kg.m)	0.200000E-01
2- Resistance of main outlet (0.001/kg.m)	0.620000E-02
3- Resistance of branch outlet (0.001/kg.m)	0.687500
Asymmetric flow split (U32 T346)	
1- Inlet resistance (0.001/kg.m)	0.620000E-02
2- Resistance of main outlet (0.001/kg.m)	0.230000E-02
3- Resistance of branch outlet (0.001/kg.m)	0.478700
Asymmetric flow split (U33 T346)	
1- Inlet resistance (0.001/kg.m)	0.230000E-02
2- Resistance of main outlet (0.001/kg.m)	0.198800
3- Resistance of branch outlet (0.001/kg.m)	0.464300
Motorized pressure-independent dual duct VAV box 1 (U34 T531)	
1- nominal volumetric flow rate of cold deck (m3/s)	0.471947
2- nominal volumetric flow rate of hot deck (m3/s)	0.188779
3- face area of damper of cold deck (m2)	0.410430E-01
4- face area of damper of hot deck (m2)	0.182400E-01
5- cold deck dual duct box resistnace (1/1000kg.m)	0.149000E-01
6- hot deck dual duct box resistnace (1/1000kg.m)	0.819200E-01
7- actuator travel time (0-90 deg) of cold deck (s)	150.000
8- actuator travel time (0-90 deg) of hot deck (s)	150.000
9- minimum fractional motor speed cold deck	0.00000
10- minimum fractional motor speed hot deck	0.00000
11- hysteresis of cold deck (-)	0.00000
12- hysteresis of hot deck (-)	0.00000
13- controller gain (frac speed/frac error) of cold deck (-)	19.9900
14- controller gain (frac speed/frac error) of hot deck (-)	3.99000
Motorized pressure-independent dual duct VAV box 2 (U35 T532)	
1- nominal volumetric flow rate of cold deck (m3/s)	0.471947
2- nominal volumetric flow rate of hot deck (m3/s)	0.188779
3- face area of damper of cold deck (m2)	0.410430E-01
4- face area of damper of hot deck (m2)	0.182400E-01
5- cold deck dual duct box resistnace (1/1000kg.m)	0.149000E-01
6- hot deck dual duct box resistnace (1/1000kg.m)	0.819200E-01
7- actuator travel time (0-90 deg) of cold deck (s)	150.000
8- actuator travel time (0-90 deg) of hot deck (s)	150.000
9- minimum fractional motor speed cold deck	0.00000
10- minimum fractional motor speed hot deck	0.00000
11- hysteresis of cold deck (-)	0.00000
12- hysteresis of hot deck (-)	0.00000
13- controller gain (frac speed/frac error) of cold deck (-)	19.9900

14- controller gain (frac speed/frac error) of hot deck (-)	3.99000
15- location: 1- SA room, 2- SB room (-)	2.00000
Motorized pressure-independent dual duct VAV box 2 (U36 T532)	
1- nominal volumetric flow rate of cold deck (m3/s)	0.471947
2- nominal volumetric flow rate of hot deck (m3/s)	0.188779
3- face area of damper of cold deck (m2)	0.410430E-01
4- face area of damper of hot deck (m2)	0.182400E-01
5- cold deck dual duct box resistnace (1/1000kg.m)	0.149000E-01
6- hot deck dual duct box resistnace (1/1000kg.m)	0.819200E-01
7- actuator travel time (0-90 deg) of cold deck (s)	150.000
8- actuator travel time (0-90 deg) of hot deck (s)	150.000
9- minimum fractional motor speed cold deck	0.00000
10- minimum fractional motor speed hot deck	0.00000
11- hysteresis of cold deck (-)	0.00000
12- hysteresis of hot deck (-)	0.00000
13- controller gain (frac speed/frac error) of cold deck (-)	19.9900
14- controller gain (frac speed/frac error) of hot deck (-)	3.99000
15- location: 1- SA room, 2- SB room (-)	1.00000
Motorized pressure-independent dual duct VAV box 3 (U37 T534)	
1- nominal volumetric flow rate of cold deck (m3/s)	0.471947
2- nominal volumetric flow rate of hot deck (m3/s)	0.188779
3- face area of damper of cold deck (m2)	0.410430E-01
4- face area of damper of hot deck (m2)	0.182400E-01
5- cold deck dual duct box resistnace (1/1000kg.m)	0.149000E-01
6- hot deck dual duct box resistnace (1/1000kg.m)	0.819200E-01
7- actuator travel time (0-90 deg) of cold deck (s)	150.000
8- actuator travel time (0-90 deg) of hot deck (s)	150.000
9- minimum fractional motor speed cold deck	0.00000
10- minimum fractional motor speed hot deck	0.00000
11- hysteresis of cold deck (-)	0.00000
12- hysteresis of hot deck (-)	0.00000
13- controller gain (frac speed/frac error) of cold deck (-)	19.9900
14- controller gain (frac speed/frac error) of hot deck (-)	3.99000
Fluid resistance (U38 -U41 T341)	
1- flow resistance (0.001/kg.m)	0.500000E-01
Room air mass balance (U42 – U45 T349)	
1- Resistance to 1st adjacent zone [0.001/(kg m)]	100000
2- Leakage resistance [0.001/(kg m)]	193.7
3- Local extract fan mass flow rate [kg/s]	0
Flow merge (U46 T348)	
1- Inlet resistance 1 (0.001/kg.m)	0.196700
2- Inlet resistance 2 (0.001/kg.m)	0.273700
3- Resistance of outlet (0.001/kg.m)	0.100000E-04
Flow merge (U47 T348)	
1- Inlet resistance 1 (0.001/kg.m)	0.100000E-04
2- Inlet resistance 2 (0.001/kg.m)	0.100000E-01
3- Resistance of outlet (0.001/kg.m)	0.144000E-01
Flow merge (U48 T348)	
1- Inlet resistance 1 (0.001/kg.m)	0.600000E-03
2- Inlet resistance 2 (0.001/kg.m)	0.500000E-02
3- Resistance of outlet (0.001/kg.m)	0.148000E-01
Return air fan (U49 T355)	
1- 1st pressure coefficient	-1069.00
2- 2nd pressure coefficient	1676.80
3- 3rd pressure coefficient	-974.130
4- 4th pressure coefficient	249.490
5- 5th pressure coefficient	-23.7510
6- 1st efficiency coefficient	949.170
7- 2nd efficiency coefficient	-1174.60
8- 3rd efficiency coefficient	543.530
9- 4th efficiency coefficient	-111.430
10- 5th efficiency coefficient	8.53990
11- diameter (m)	0.311150
12- mode: air=1, water=2	1.00000
13- lowest valid normalized flow	2.30000

14- highest valid normalized flow	3.25000
15- location: 1-SA hot deck (or SA for single deck AHUs),2-SA cold deck, 3- return fan	1.0
Duct between mixing box and return fan (U50 T341)	
1- flow resistance (0.001/kg.m)	0
Thermal Network	
Mixing box (U51 T367)	
1- (dummy)	0
Hot deck supply fan heating (U52 T366)	
1- fluid: 1 = air, any other value = water (-)	1.00000
2- time constant (s)	30.0000
Heating coil (U53 T533)	
1- Method : 0- steady state, 1- dynamic	1
2- Fault: 0 - for no faults, 1 - parallel flow	0
3- Psycho : 0 - no psychrometric output calcs, 1 - calcs	0
4- Number of rows of tubes	2
5- Number of tubes per row	18
6- Number of parallel water circuits	18
7- Length of finned section in direction of flow (m)	0.165100
8- Height of finned section (m)	0.609600
9- Width of finned section (m)	0.914400
10- Tube outside diameter (m)	0.127E-01
11- Tube wall thickness (m)	0.4064E-03
12- Tube material (Al=1,Cu=2,Fe=3,CaCO3=4)	2
13- Fin spacing (pitch) (m)	0.265043E-02
14- Fin thickness (m)	0.190500E-03
15- Fin material (Al=1,Cu=2,Fe=3)	1
16- Flow resistance on air side (0.001 kg.m)	0.155270E-01
17- Coil water flow resistance (0.001 kg.m)	10
18- By-pass water flow resistance (0.001 kg.m)	10
19- Valve type: 0=lin/lin, 1=eq%(flow)/lin(byp), 2=lin/eq%	0
20- Valve capacity (Kv) (m3/hr @ 1 bar)	1.28000
21- Valve curvature parameter (0=linear)	0
22- Valve rangability-ratio of highest to lowest controllable flow	1
23- Valve leakage (flow fraction at second segment start position)	0.1E-01
24- stem position at which second segment starts (-)	0.200000
25- Third segment start position (No wearoff -- 1) (-)	0.800000
26- Flow fraction at third segment start position (-)	0.970660
27- Bypass valve capacity (Kv) (m3/hr @ 1 bar)	1.33500
28- Bypass valve leakage (Flow fraction at second segment start position)	0.120000
29- Bypass Flow fraction at third segment start position (-)	0.990000
30- coil : 1- heating coil, 2- cooling coil (-)	1.00000
Cold deck supply fan heating (U54 T366)	
1- fluid: 1 - air, any other value = water	1
2- time constant (s)	30
Cooling coil (U55 T533)	
1- Method : 0- steady state, 1- dynamic	1
2- Fault: 0 - for no faults, 1 - parallel flow	0
3- Psycho : 0 - no psychrometric output calcs, 1 - calcs	0
4- Number of rows of tubes	6
5- Number of tubes per row	18
6- Number of parallel water circuits	18
7- Length of finned section in direction of flow (m)	0.317500
8- Height of finned section (m)	0.609600
9- Width of finned section (m)	0.914400
10- Tube outside diameter (m)	0.127000E-01
11- Tube wall thickness (m)	0.406400E-03
12- Tube material (Al=1,Cu=2,Fe=3,CaCO3=4)	2.00000
13- Fin spacing (pitch) (m)	0.264200E-02
14- Fin thickness (m)	0.190500E-03
15- Fin material (Al=1,Cu=2,Fe=3)	1.00000
16- Flow resistance on air side (0.001 kg.m)	0.465810E-01
17- Coil water flow resistance (0.001 kg.m)	0.100000E-02
18- By-pass water flow resistance (0.001 kg.m)	0.100000E-02
19- Valve type: 0=lin/lin, 1=eq%(flow)/lin(byp), 2=lin/eq%	0.00000
20- Valve capacity (Kv) (m3/hr @ 1 bar)	3.65000

21- Valve curvature parameter (0=linear)	0.00000
22- Valve rangability-ratio of highest to lowest controllable flow	1.00000
23- Valve leakage (flow fraction at second segment start position)	0.123000E-01
24- stem position at which second segment starts (-)	0.200000
25- Third segment start position (No wearoff -- 1) (-)	0.800000
26- Flow fraction at third segment start position (-)	0.970660
27- Bypass valve capacity (Kv) (m3/hr @ 1 bar)	4.00000
28- Bypass valve leakage (Flow fraction at second segment start position)	0.123000E-01
29- Bypass Flow fraction at third segment start position (-)	0.950000
30- coil : 1- heating coil, 2- cooling coil (-)	2.00000
Mixing of two moist air streams (U56- U59 T367)	
1- dummy	0
Z1 – Z4 Room with plenum (U60 – U63 T403)	
1- room air capacity multiplier (-)	1
2- direct resistance room air node <-> ambient (K/kW)	46.5340
3- resistance room air node <-> room mass node (K/kW)	4.43000
4- resistance ambient <-> room mass node (K/kW)	308.730
5- direct resistance plenum air node <-> ambient (K/kW)	0.1E+12
6- resistance plenum air node <-> plenum mass node (K/kW)	21.6600
7- resistance ambient <-> plenum mass node (K/kW)	192.000
8- resistance room air node <-> plenum air node (K/kW)	9.50600
9- capacitance of room mass node (kJ/K)	5078.28
10- capacitance of room air node (unmodified) (kJ/K)	145.920
11- capacitance of plenum mass node (kJ/K)	4569.91
12- capacitance of plenum air node (kJ/K)	47.3400
13- volume of room (m3)	48.0000
14- volume of plenum (m3)	13.0000
15- number of occupants (-)	0.00000
16- lighting heat gain (kW)	0.540000
17- fraction of lighting heat gain to extract air (-)	0.00000
18- equipment heat gain (kW)	1.80000
19- zone number (parameter file=zoneN.par, n > 0) (-)	0.00000
Mixing of four moist air streams (U64 T368)	
1- (dummy)	0
Return fan heating (U65 T366)	
1- fluid: 1 = air, any other value = water	1
2- time constant (s)	30
Control Network	
Read inputs from a file (U1 T554)	
1- file number (FILE=inputN.par, N > 0)	1
2- sample time (interval between reads) (s)	5
3- real time scaling factor (0=no wait, 1=real time)	0
4- text output to screen (0=no, 1=yes)	0
5- number of values to read	3
6- room heating temperature setpoint (C)	21.6667
7- room cooling temperature setpoint (C)	22.22
Hot deck supply fan static pressure control (U2 T481)	
1- proportional band (kPa)	5
2- integral time (s)	50
3- derivative time (s)	0
4- deadband (KPa)	0.33E-01
5- high limit override proportional band (kPa)	0.125
6- high limit override setpoint (KPa)	0.623
7- control mode (0=open loop, 1=closed loop)	1
8- open loop supply fan speed (0-1)	1
9- sampling interval (s)	5
10- controller number (parameters in file contN.par)	0
11- location (1=SA hot deck, 2=SA cold deck) (-)	1
Cold deck supply fan static pressure control (U3 T481)	
1- proportional band (kPa)	5
2- integral time (s)	50
3- derivative time (s)	0
4- deadband (KPa)	0.33E-01
5- high limit override proportional band (kPa)	0.125
6- high limit override setpoint (KPa)	0.623

7- control mode (0=open loop, 1=closed loop)	1
8- open loop supply fan speed (0-1)	1
9- sampling interval (s)	5
10- controller number (parameters in file contN.par)	0
11- location (1=SA hot deck, 2=SA cold deck) (-)	2
Flow difference control of return fan (U4 T482)	
1- proportional band (m3/s)	-25
2- integral time (s)	30
3- derivative time (s)	0
4- deadband (m3/s)	0.236E-01
5- control mode (0=open loop, 1=closed loop)	1
6- open loop return fan speed (0-1)	1
7- sampling interval (s)	5
8- controller number (parameters in file contN.par)	0
ERS economizer control (U5 T587)	
1- sampling interval (s)	5
2- economizer air temperature setpoint (C)	15.556
Low temperature control (U6 T488)	
1- supply air temperature limit (C)	-44.44
2- outdoor air temperature limit (C)	-66.66
3- sampling interval (s)	5
4- controller number (parameters in file contN.par)	0
ERS dual duct system HD & CD supply air temperature (U7 T586)	
1- cold deck proportional band (K)	-45.7000
2- cold deck integral time (s)	2.00000
3- cold deck derivative time (s)	0.00000
4- breakpoint between damper and cooling coil demand (0-2)	1.00000
5- cold deck deadband (K)	0.00000
6- cold deck control mode (0=open loop, 1=closed loop) (-)	1.00000
7- cold deck supply air temperature setpoint (C)	12.7780
8- hot deck proportional band (K)	45.7000
9- hot deck integral time (s)	0.500000
10- hot deck derivative time (s)	0.00000
11- hot deck deadband (K)	0.00000
12- hot deck control mode (0=open loop, 1=closed loop) (-)	1.00000
13- hot deck supply air temperature setpoint (C)	32.2200
14- manual cooling coil demand (0-1) (-)	0.00000
15- manual heating coil demand (0-1) (-)	0.00000
16- sampling interval (s)	5.00000
17- controller number (parameters in file contN.par) (-)	0.00000
ERS modulated mixed air damper control (U8 T585)	
1- mixed air temperature setpoint (C)	12.7780
2- proportional band (K)	-3.89000
3- integral time (s)	0.00000
4- derivative time (s)	0.00000
5- deadband (K)	0.00000
6- control mode (0=open loop, 1=closed loop) (-)	1.00000
7- open loop outside air damper position (-)	1.00000
8- open loop return air damper position (-)	0.00000
9- open loop exhaust air damper position (-)	1.00000
10- OA damper minimum position (0-1) (-)	0.00000
11- sampling interval (s)	5.00000
12- controller number (parameters in file contN.par) (-)	0.00000
Dual duct VAV room temperature control (U9- U12 T477)	
1- cooling setpoint for zone (C)	22.2200
2- heating setpoint for zone (C)	20.0000
3- minimum normalized volumetric cold flow demand (0-1) (-)	0.100000
4- minimum normalized volumetric hot flow demand (0-1) (-)	0.250000
5- proportional band (K)	4.00000
6- integral time (s)	2.50000
7- derivative time (s)	0.00000
8- deadband (K)	0.00000
9- control mode (0=open loop, 1=closed loop) (-)	1.00000
10- open loop demanded normalized volumetric cold flow rate	0.00000
11- open loop demanded normalized volumetric hot flow rate	0.00000

12- sampling interval (s)	5.00000
13- controller number (parameters in file contN.par) (-)	0.00000
Variable speed drive (U13 and U14 T333)	
1- maximum rotation speed (rev/s)	35.667
2- travel time (lim-lim) (s)	90
Variable speed drive (U15 T333)	
1- maximum rotation speed (rev/s)	16.35
2- travel time (lim-lim) (s)	90
Motor-driven actuator (U16 – U20 T321)	
1- direction: 1=forward, -1=reverse, 0=stuck	1
2- starting position (0-1)	0
3- travel time (lim-lim) (s)	125
4- minimum change in demanded position for movement (-)	0
5- hysteresis (-)	0
6- crank travel angle (0 for linear) (deg)	0
7- Upper limit of control element range on actuator scale	1
8- Lower limit of control element range on actuator scale	0
Static pressure sensor (U66 T305)	
1- air = 1, water = 2 (-)	1
2- cross-sectional area of duct or pipe (m2)	0.2477
3- offset: input for zero output (kpa)	0
4- gain: change in input for 0->1 output (kpa)	1
5- time constant (s)	1
6- upper limit of output range (-)	5
7- lower limit of output range (-)	-5
8- location: 1-SA hot deck, 2-SA cold deck (-)	1
Static pressure sensor (U67 T305)	
1- air = 1, water = 2 (-)	1
2- cross-sectional area of duct or pipe (m2)	0.2477
3- offset: input for zero output (kpa)	0
4- gain: change in input for 0->1 output (kpa)	1
5- time constant (s)	1
6- upper limit of output range (-)	5
7- lower limit of output range (-)	-5
8- location: 1-SA hot deck, 2-SA cold deck (-)	2
Flow rate sensor (U68 T303)	
1- mass flow=1, vol flow=2, vel=3, vel pres=4 (-)	2
2- air = 1, water = 2 (-)	1
3- cross-sectional area of duct or pipe (m2)	0.2477
4- offset: input for zero output (sensed quantity)	0
5- gain: change in input for 0->1 output (sensed quantity)	1
6- time constant (s)	1
7- upper limit of output range (-)	20
8- lower limit of output range (-)	-10
Flow rate sensor (U69 T303)	
1- mass flow=1, vol flow=2, vel=3, vel pres=4 (-)	2
2- air = 1, water = 2 (-)	1
3- cross-sectional area of duct or pipe (m2)	0.3097
4- offset: input for zero output (sensed quantity)	0
5- gain: change in input for 0->1 output (sensed quantity)	1
6- time constant (s)	1
7- upper limit of output range (-)	20
8- lower limit of output range (-)	-10
Temperature sensor (U70 T311)	
1- offset: input for zero output (C)	0
2- gain: change in input for 0->1 output (K)	1
3- time constant (s)	30
4- upper limit of output range (-)	40
5- lower limit of output range (-)	-10
6- location: 1-RA, 2-MA, 3-OA, 4-SA hot deck, 5-SA cold deck	2
Temperature sensor (U71 T311)	
1- offset: input for zero output (C)	0
2- gain: change in input for 0->1 output (K)	1
3- time constant (s)	30
4- upper limit of output range (-)	40

5- lower limit of output range (-)	-10
6- location: 1-RA, 2-MA, 3-OA, 4-SA hot deck, 5-SA cold deck	4
Temperature sensor (U72 T311)	
1- offset: input for zero output (C)	0
2- gain: change in input for 0->1 output (K)	1
3- time constant (s)	30
4- upper limit of output range (-)	40
5- lower limit of output range (-)	-10
6- location: 1-RA, 2-MA, 3-OA, 4-SA hot deck, 5-SA cold deck	5
Temperature sensor (U73-76 T311)	
1- offset: input for zero output (C)	0
2- gain: change in input for 0->1 output (K)	1
3- time constant (s)	30
4- upper limit of output range (-)	40
5- lower limit of output range (-)	-10
6- location: 1-RA, 2-MA, 3-OA, 4-SA hot deck, 5-SA cold deck	1
Temperature sensor (U77 T311)	
1- offset: input for zero output (C)	0
2- gain: change in input for 0->1 output (K)	1
3- time constant (s)	30
4- upper limit of output range (-)	40
5- lower limit of output range (-)	-10
6- location: 1-RA, 2-MA, 3-OA, 4-SA hot deck, 5-SA cold deck	3

APPENDIX E: FLOW RESISTANCE FOR DUCT SYSTEM

Section	Item	Flow rate (CFM)	Duct size (inch)	Equivalent round (inch)	V (FPM)	Friction loss/100 ft (in.w.)	Length (ft)	Loss coefficient, C	Pressure loss (in.w.)	Note (Ptia, 2002)
Hot deck supply air section (AHU-A)										
AHU-A	Supply fan inlet	1600							0.2000	T 8.10
	Supply fan outlet								0.0800	T 8.10
A1	Duct		24*16	21	600.00	0.03	26.6		0.0090	Fig 8.21
A1-A2	Converging Transition	1600	24*14					0.06	0.0018	T 8.6 θ=60
A1-A2	Duct		24*14	20	685.71	0.04	28.5		0.0114	Fig 8.21
A2-A3	Converging Transition	1200	16*14					0.06	0.0022	T 8.6 θ=60
A2-A3	Elbow		16*14		771.43			0.18	0.0067	T 8.4 E R/W=1.5
A2-A3	Duct		16*14	16	771.43	0.07	20		0.0136	Fig 8.21
A2-A3	Duct	800	16*14	16	514.29	0.03	12.5		0.0043	Fig 8.21
A3-A4	Converging Transition	400	10*14					0.06	0.0006	T 8.6 θ=60
A3-A4	Elbow		10*14		411.43			0.154	0.0016	T 8.4 E R/W=1.5
A3-A4	Duct		10*14	13	411.43	0.03	34		0.0085	Fig 8.21
Cold deck supply air section (AHU-B)										
AHU-B	Supply fan inlet	4000							0.2000	T 8.10
	Supply fan outlet								0.0800	T 8.10
B1	Duct		24*16	21	1500.00	0.19	26.6		0.0505	Fig 8.21
B1-B2	Converging Transition	4000	24*14					0.06	0.0110	T 8.6 θ=60
B1-B2	Duct		24*14	20	1714.29	0.25	28.5		0.0713	Fig 8.21
B2-B3	Converging Transition	3000	16*14			0.04		0.06	0.0139	T 8.6 θ=60
B2-B3	Elbow		16*14		1928.57			0.18	0.0418	T 8.4 E R/W=1.5
B2-B3	Duct		16*14	16	1928.57	0.44	20		0.0880	Fig 8.21
B2-B3	Duct	2000	16*14	16	1285.71	0.19	12.5		0.0238	Fig 8.21
B3-B4	Converging Transition	1000	10*14					0.06	0.0040	T 8.6 θ=60
B3-B4	Elbow		10*14		1028.57			0.154	0.0102	T 8.4 E R/W=1.5
B3-B4	Duct		10*14	13	1028.57	0.15	34		0.0510	Fig 8.21
Return air duct										
AHU-B	Return fan inlet	5600							0.2000	T 8.10
	Return fan outlet								0.0800	T 8.10
R1	Elbow		30*16		1680.00			0.17	0.0300	T 8.4 E R/W=1.5
R1	Duct		30*16	23.5	1680.00	0.22	16		0.0352	Fig 8.21
R1-R2	Diverging Transition							0.31	0.0675	T 8.5 B θ=60
R1-R2	Elbow		24*18		1866.67			0.17	0.0370	T 8.4 E R/W=1.5
R1-R2	Elbow		24*18		1866.67			0.17	0.0370	T 8.4 E R/W=1.5
R1-R2	Duct		24*18	22.5	1866.67	0.26	51.5		0.1339	Fig 8.21
R2-R3	Diverging Transition	4200						0.31	0.0380	T 8.5 B θ=60
R2-R3	Elbow		18*16		2100.00			0.17	0.0469	T 8.4 E R/W=1.5
R2-R3	Duct		18*16	18		0.44	55		0.2420	
R2-R3	Duct	2800	18*16	18	1400.0	0.18	15		0.0270	Fig 8.21

					0					
R3-R4	Diverging Transition	1400						0.31	0.0243	T 8.5 B θ=60
R3-R4	Elbow		18*10		1120.00			0.17	0.0133	T 8.4 E R/W=1.5
R3-R4	Duct		18*10	14	1120.00	0.18	70		0.1260	Fig 8.21
Supply air branch duct sections into dual duct box										
Supply A (WA)	Duct	400		6	2038.22	1.30	5		0.0650	Fig 8.21
Supply B (WA)	Duct	1000		9	2264.69	0.90	6		0.0540	Fig 8.21
Supply A (SB)	Duct	400		6	2038.22	1.30	6		0.0780	Fig 8.21
Supply B (SB)	Duct	1000		9	2264.69	0.90	5		0.0450	Fig 8.21
Supply A (SA)	Duct	400		6	2038.22	1.30	5		0.0650	Fig 8.21
Supply B (SA)	Duct	1000		9	2264.69	0.90	6		0.0540	Fig 8.21
Supply A (EB)	Duct	400		6	2038.22	1.30	6		0.0780	Fig 8.21
Supply B (EB)	Duct	1000		9	2264.69	0.90	5		0.0450	Fig 8.21
Return air branch duct sections to the plenume										
R (WA)	Duct	1400		16	1003.18	0.10	6		0.0057	Fig 8.21
R (SB)	Duct	1400		16	1003.18	0.10	5		0.0048	Fig 8.21
R (SA)	Duct	1400		16	1003.18	0.10	6		0.0057	Fig 8.21
R (EB)	Duct	1400		16	1003.18	0.10	5		0.0048	Fig 8.21

Section	Item	Flow rate (CFM)	Duct size (inch)	Equivalent round (inch)	V (FPM)	Vb/Vc	Qb/Qc	Loss coefficient, C	Pressure loss (in.w.)	Note (Ptia, 2002)
Supply air Tee sections										
Supply A (WA)	Tee	400		10	733.76	1.07	0.25	1.29	0.0379	T 8.8 F
Supply B (WA)	Tee	1000		10	1834.39	1.78	1	2.07	0.1369	T 8.8 F
Supply A (SB)	Tee	400		10	733.76	0.95	0.3333333333	1.18	0.0439	T 8.8 F
Supply B (SB)	Tee	1000		10	1834.39	1.43	0.5	1.57	0.1622	T 8.8 F
Supply A (SA)	Tee	400		10	733.76	1.43	0.5	1.57	0.0260	T 8.8 F
Supply B (SA)	Tee	1000		10	1834.39	0.95	0.3333333333	1.18	0.2743	T 8.8 F
Supply A (EB)	Tee	400		10	733.76	1.78	1	2.07	0.0219	T 8.8 F
Supply B (EB)	Tee	1000		10	1834.39	1.07	0.25	1.29	0.2369	T 8.8 F
Supply A (WA)	Converging Transition	400			2038.22			0.065	0.0169	T 8.6 A θ=60
Supply B (WA)	Converging Transition	1000			2264.69			0.06	0.0192	T 8.6 A θ=60
Supply A (SB)	Converging Transition	400			2038.22			0.065	0.0169	T 8.6 A θ=60
Supply B (SB)	Converging Transition	1000			2264.69			0.06	0.0192	T 8.6 A θ=60
Supply A (SA)	Converging Transition	400			2038.22			0.065	0.0169	T 8.6 A θ=60

Supply B (SA)	Converging Transition	1000			2264.69			0.06	0.0192	T 8.6 A θ=60
Supply A (EB)	Converging Transition	400			2038.22			0.065	0.0169	T 8.6 A θ=60
Supply B (EB)	Converging Transition	1000			2264.69			0.06	0.0192	T 8.6 A θ=60
Return air Tee sections										
Return (WA)	Tee	1400		16	1003.18	0.90	1	5.6	0.4390	T 8.7 A
Return (SB)	Tee	1400		16	1003.18	0.72	0.5	1.27	0.1556	T 8.7 A
Return (SA)	Tee	1400		16	1003.18	0.48	0.333333333	0.23	0.0634	T 8.7 A
Return (EB)	Tee	1400		16	1003.18	0.54	0.25	0.01	0.0022	T 8.7 A

VITA

Shokouh Pourarian
E-mail: shpoorarian@gmail.com
Tel: 678.882.9098

EDUCATION

2010- 2015 **Drexel University** Philadelphia, PA
Doctor of Engineering, College of Engineering (Advisor: Dr. Jin Wen)

Dissertation Title: Tools for Evaluation Fault Detection and Diagnostic Methods for HVAC secondary systems

2003-2005 **Sharif University of Technology** Tehran, Iran
Master of energy systems engineering, College of Engineering

Thesis Title: Development of a CFD model for heat transfer in a pelletizing furnace

1998-2002 **Isfahan University if Technology** Isfahan, Iran
Bachelor of Mechanical Engineering, College of Engineering

Project: Mechanical analysis of hydraulic lifters and a software development for their design and analysis

RESEARCH EXPERIENCE

2010-2015 **Tools for Evaluation Fault Detection and Diagnostic Methods for HVAC secondary systems of a Net Zero Building**
Drexel University, Philadelphia, PA

Funding Source: U.S. National Institute of Standard and Technology

Description: The purpose of this project are to develop and validate necessary tools for building control, operation and automated fault detection and diagnosis (AFDD) technologies for secondary HVAC systems which has been less studied in the literature. However, secondary systems such as fan coil units, fan powered VAV boxes and dual duct systems, although widely used in commercial, industrial and multifamily residential buildings, have received very little attention. The developed dynamic models are able to generate operational data under fault-free condition and replicate faulty symptoms under wide variety of faults and different fault severities for the mentioned secondary HVAC systems.

2011-2013 **Efficient and Robust Optimization for Building Energy Simulation**
Drexel University, Philadelphia, PA

Funding Source: U.S. National Institute of Standard and Technology

Description: Efficiently, robustly and accurately solving large sets of

structured, non-linear algebraic and differential equations is one of the most computationally expensive steps in the dynamic simulation of building energy systems. This project aims at applying various mathematical methods to solve the system of nonlinear algebraic equations whose solution leads to dynamic energy simulation of buildings.

PUBLICATIONS & PRESENTATIONS

Peer-Reviewed Journal Publications (Under review or In Preparation)

2015

Pourarian Sh, Kearsley A, Wen J, Pertzborn A. Efficient and Robust Optimization for building energy simulation. (Submitted)

Pourarian Sh, Wen J, Li X, Veronica D, Zhou X, Liu R. Tools for evaluating air flow & thermal network of dual duct double fan systems. (In preparation)

Pourarian Sh, Wen J, Veronica D, Zhou X, Liu R. A tool for evaluating fault detection and diagnostic methods for fan coil units. (Submitted)

Pourarian Sh, Wen J, Veronica D, Zhou X, Liu R. A tool for evaluating fault detection and diagnostic methods for dual duct double fan systems. (In preparation)

Pourarian Sh, Jang B, Wen J, Veronica D, Zhou X, Liu R. A tool for evaluating fault detection and diagnostic methods for fan powered VAV units. (In preparation)

DavazdahEmami M and **Pourarian Sh**. Text book of "Heat exchanger design. (In preparation)

Peer-Reviewed Conference Proceedings

2014

Pourarian Sh, Wen J, Veronica D, Zhou X, Liu R A tool for evaluating fault detection and diagnostic methods for fan coil units. Presented at: ASHRAE Annual Conference 2014; June 27-July 02, 2014; Seattle, WA.

Pourarian Sh, Wen J, Li X, Veronica D, Zhou X, Liu R. Tools for evaluating air flow network of dual duct double fan systems. Paper accepted to: 2014 ASHRAE/IBPSA-USA Building Simulation Conference; September 12-14, 2014; Atlanta, GA.

2006

Pourarian Sh, Saboohi Y. A CFD 3-D model for gas-fired furnace of pelletizing unit. Presented at: ISME 2006; May 16-18, 2006; Isfahan, Iran.

2008

DavazdahEmami M and **Pourarian Sh.** Numerical simulation of a 200 MW industrial boiler. Presented at: the 12th Asian Congress of Fluid Mechanics; Aug 18-21, 2008; Daejeon, Korea.

INDEPENDENT PROJECTS

2006-2009 **Isfahan Science and Technology Town** Isfahan, Iran
Aerodynamic and thermal analysis of combustion flow in the boiler of Montazeri Power Plant.

2003-2006 **Sharif Energy Research Institute** Tehran, Iran
Active & passive cooling and heating of buildings

Load calculation of two residential buildings and design their HVAC systems

Optimization of heat recovery in steam generators of power plants

Performance comparison of various types of tube inserts in shell & tube heat exchangers

Techno-economic analysis of co-fired biomass integrated gasification/combined cycle systems with inclusion of economies of scale

PROFESSIONAL EXPERIENCE

2007-2009 **Nargan Company, Mechanical Department** Tehran, Iran
Senior engineer of Fixed equipment (especially Heat Exchanger design and analysis)

2006-2007 **Saman Energy Company, Isfahan Science and Technology Town** Isfahan, Iran
Senior Engineer of "preliminary energy auditing of Isfahan Steel Co." project

Senior Engineer of "preliminary and detailed energy auditing in 5 main Iranian steel companies" project

Senior Engineer of "detailed energy auditing in Mobarakeh steel company" project

2003-2006 **Sharif University of Technology**....Tehran, Iran
Computer Administrator in dormitory

2002-2003 **Isfahan Science and Technology Town** Isfahan, Iran
Coordinator of Energy and environment Committee

Parsayesh Company, Isfahan Science and Technology Town Isfahan, Iran
Design the components of Tribotester

1999-2002 **Isfahan University of Technology, Mechanical Engineering Department** Isfahan, Iran
Editor in chief of department science magazine (TAKIN)

TEACHING & MENTORING EXPERIENCE

2006-2007 **Adjunct faculty** ….Material Science Engineering Department, Najaf Abad Azad University, Isfahan, Iran

Adjunct faculty ….Mechanical Engineering Department, Khomeini Shahr Azad University, Isfahan, Iran

Courses:
Strength of Materials
Fluid Mechanics

2007-2008 **Mathematics & Physics** Tehran, Iran
Private tutor of high school students

2009-2010 **Thermal Science Lab (MIME 3470)** The University of Toledo, Toledo, OH
Teaching Assistant for undergraduate-level lab (Instructor: Dr. Terry Ng)

03.2013-06.2013 **Control Systems for HVAC (AE 430)** Drexel University, Philadelphia, PA
Teaching Assistant for undergraduate-level course (Instructor: Dr. Jin Wen)

10.2013-01-2014 **HVAC load (MEM 413)** Drexel University, Philadelphia, PA
Teaching Assistant for undergraduate-level course (Instructor: Dr. Jin Wen)

01.2014-04.2014 **HVAC Equipment (MEM 414)** Drexel University, Philadelphia, PA
Teaching Assistant for undergraduate-level course (Instructor: Dr. Jin Wen)

PROFESSIONAL MEMBERSHIPS

American Society of Heating, Refrigerating, and Air-Conditioning Engineers (ASHRAE)

SKILLS

Proficient

Fortran, MATLAB, C++, Basic, HVACSIM+, Carrier, CATIA, Tecplot, Fluent, Ansys, Nisa, Pipe Flow, PvElite, Aspen BJac, SPSS, MS Office Suite (PowerPoint, Word, Excell),

Familiar

AutoCAD, EnergyPlus, Trnsys

REFERENCES

Jin Wen, Ph.D. Associate Professor, Department of Civil, Architectural and Environmental Engineering, Drexel University, 3141 Chestnut St., Philadelphia, PA 19104, (215) 895-4911, jinwen@drexel.edu

Daniel A. Veronica, Ph.D. Mechanical Engineer, Energy and Environment Division, National Institute of Standards and Technology (NIST), Gaithersburg, MD 20899, (301) 975-5874, daniel.veronica@nist.gov

Anthony J. Kearsley, Ph.D. Research Mathematician, Mathematical and Computational Science Division, National Institute of Standards and Technology, Gaithersburg, MD 20899, (301) 975-6103, ajk@cam.nist.gov

Patrick L. Gurian, Ph.D. Associate Professor, Department of Civil, Architectural and
Environmental Engineering, Drexel University, 3141 Chestnut St., Philadelphia, PA 19104, (215) 895-2889, plg28@drexel.edu